Investigations into the effects of berry flavonoids on nutrient transport processes in Caco-2 enterocytes

Alzaid, Fawaz

Awarding institution:
King's College London

Title: Investigations into the effects of berry flavonoids on nutrient transport processes in Caco-2 enterocytes

Author: Fawaz Alzaid

Investigations into the effects of berry flavonoids on nutrient transport processes in Caco-2 enterocytes

Fawaz Alzaid

A thesis submitted to the University of London for the degree of Doctor of Philosophy in the Faculty of Science

Diabetes and Nutritional Sciences Division

King's College London

University of London

October 2012

Dedicated to my family

Publications and presentations

Abstract publications

Alzaid F, Pourvali K, Lin CI, Arno M, Astarloa EA-O, Sharp PA, Hogstrand C, Emery PW, Bagchi D, Preedy VR & Wiseman H. (2010). Flavonoid-rich-berry-extract treatment decreases the expression of DMT1 and functionally-similar metal transporter genes in human intestinal Caco-2 cells. *Proceedings of the Nutrition Society*. **69**.

Alzaid F, Pourvali K, Sharp PA, Bagchi D, Preedy VR & Wiseman H. (2010). Anthocyanin-rich berry-extract treatment decreases expression of dietary glucose transporter genes in human intestinal Caco-2 cells. *Proceedings of the Nutrition Society*. **69**.

Alzaid F, Pourvali K, Sekhon G, Sharp PA, Preedy VR & Wiseman H. (2010). Flavonoid-rich berry-extract influences expression of genes in the iron-uptake pathway in human intestinal Caco-2 cells. *Proceedings of the Nutrition Society.* **69**.

Alzaid F, Robotham A, Pourvali K, Sharp PA, Preedy VR & Wiseman H. (2010). Flavonoid-rich berry-extract treatment influences expression of genes in the copper-uptake pathway in human intestinal Caco-2 cells. *Proceedings of the Nutrition Society*.**69**.

Alzaid F, Cheung HM, Sharp PA, Preedy VR & Wiseman H. (2011). Flavonoid-rich berry-extract treatment decreases glucose uptake in human intestinal Caco-2 cells. *Proceedings of the Nutrition Society*. **70**.

Poster presentations

2009 Poster presentation at Nutrition Society summer meeting, University of Surrey, UK. Title of the poster: Flavonoid-rich-berry-extract treatment decreases the expression of DMT1 and functionally-similar metal transporter genes in human intestinal Caco-2 cells.

2009 Poster presentation at Nutrition Society winter meeting, University of Reading, Surrey, UK. Title of the poster: Anthocyanin-rich berry-extract treatment decreases expression of dietary glucose transporter genes in human intestinal Caco-2 cells.

2010 Poster presentation at Nutrition Society summer meeting, Heriot-Watt University, Edinburgh, Scotland. Title of the poster: Flavonoid-rich berry-extract influences expression of genes in the iron-uptake pathway in human intestinal Caco-2 cells.

2010 Poster presentation at Nutrition Society winter meeting, Royal Institute of British Architects, London, UK. Title of the poster: Flavonoid-rich berry-extract treatment influences expression of genes in the copper-uptake pathway in human intestinal Caco-2 cells.

2011 Poster presentation at Nutrition Society winter meeting, University of Reading, Surrey, UK. Title of the poster: Flavonoid-rich berry-extract treatment decreases glucose uptake in human intestinal Caco-2 cells.

Achievements

2008 Postgraduate research scholarship award from the Ministry of Higher Education of the State of Kuwait.

2010 Research support grant from the Arab-British Chamber of Commerce Charitable Foundation.

Abstract

Flavonoids are known to interact with a number of membrane transporters, influencing the rate of intestinal nutrient absorption. The transcriptional effects and consequences of such interactions remained to be fully elucidated. To address this we carried out gene expression microarray analysis on intestinal Caco-2 cells treated with a flavonoid-rich berry extract (0.125 % w/v for 16 h). This microarray analysis identified alterations in numerous specific nutrient pathways, three of which were selected for further study, namely: 1) glucose, 2) iron and 3) copper. We then determined the effects of berry flavonoids on the expression and function of these transport pathways using qRT-PCR, Western blotting and functional assays.

We found: 1) Chronic treatment (16 h) with flavonoids decreased the expression of glucose transporter genes (GLUT2 and SGLT1) and induced an acute (15 min) inhibitory effect on enterocytic glucose uptake. 2) Chronic treatment (16 h) with berry extract modulated the expression of genes that regulate iron uptake (down-regulation of DMT1, DCYTB and HFE; up-regulation of TfR1). Iron transepithelial transport was decreased by both acute (15 min) and chronic (16 h) berry extract treatment. 3) Chronic berry extract treatment (16 h) decreased the expression of genes that coordinate copper uptake (CTR1, HAH1, ATP7A and ATP7B). However, copper uptake was increased by both acute (15 min) and chronic (16 h) berry extract treatment.

Thus overall, there is a clear effect of flavonoids on the pathways of glucose, iron and copper and a possible interactive effect between these nutrients themselves. Further research into the functional and physiological relevance of our findings will aid in optimising the dietary management of conditions such as diabetes and disturbances in copper or iron homeostasis.

Acknowledgments

I would like to thank the following for guidance and support throughout this work:

My Supervisors Dr. Helen Wiseman and Prof. Victor R. Preedy.

Dr. Paul A. Sharp, his guidance, support, knowledge and limitless patience throughout this work has been invaluable.

Dr. Matthew Arno, Dr. Estibalez Aldecoa-Otalora Astarloa, Professor Peter Emery, Ms. Rukshana Hoque, Dr. Katayoun Pourvali and Ms. Abigail Robotham.

And my family.

Statement of work performed by author

I was involved in the planning and performing of all the projects detailed in chapters 3 to 6. This involved planning, sample maintenance, treatments, isolation and purification of sample material, assay design and optimisation, quality controls, statistical analysis and interpretation of data.

Assay design and optimisation was carried out in collaboration with Dr. Katayoun Pourvali. In Chapter 3, microarray sample preparation, hybridisation and running was carried out by Dr. Matthew Arno and Dr. Estibalez Aldecoa-Otalora Astarloa.

Planning, data interpretation and statistical analysis were carried out under consultation and guidance of Professor Peter Emery, Professor Victor R. Preedy, Dr. Paul A. Sharp, and Dr. Helen Wiseman.

I am extremely grateful to all of the above named colleagues for their helpful advice, input and discussions throughout this work.

Table of contents

List of tables

List of figures

Abbreviations

18S	18S ribosomal RNA
28S	28S ribosomal RNA
3T3L1	Adipocyte cell line
ABC	ATP-binding cassette
ADP	Adenosine diphosphate
APS	Ammonium persulfate
AQP3	Aquaporin 3
ATP	Adenosine triphosphate
ATP7A	Copper transporting ATPase α-polypeptide
ATP7B	Copper transporting ATPase β-polypeptide
β_2m	β-2-microglobulin
BACE1	Beta-secretase 1
BSA	Bovine serum albumin
BUB1	Budding uninhibited by benzimidazoles 1
C2C12	Mouse myoblast cell line
C57BL/6J	Common strain of laboratory mice
Caco-2	Human epithelial colorectal adenocarcinoma cells
$Ca_v1.3$	Calcium channel, voltage-dependent, L type, alpha 1D subunit
CACNA1D	Calcium channel, voltage-dependent, L type, alpha 1D subunit
CCS	Copper chaperone for superoxide dismutase
CDKN1A	Cyclin-dependent kinase inhibitor 1
cDNA	Complementary DNA
CHRNA1	Acetylcholine receptor subunit α
CLCN2	Chloride channel protein 2
C_t	Threshold cycle
CTR1	High affinity copper uptake protein 1
CYB561	Cytochrome b561
CYB5A	Cytochrome b5, form A
DAVID	Database for Annotation, Visualisation and Integrated Discovery
DCYTB	Duodenal cytochrome B reductase
DMEM	Dulbecco's modified Eagle medium
DMSO	Dimethyl sulfoxide
DMT1	Divalent metal ion transporter 1
DMT1+IRE	DMT1with IRE region in transcript
DMT1-IRE	DMT1without IRE region in transcript
DNA	Deoxyribonucleic acid
dNTP	Deoxyribonucleotide
ECL	Electrochemiluminescence
FBS	Foetal bovine serum
FPN	Ferroportin/ iron-regulated transporter 1
FU	Fluorescence units
GAE	Gallic acid equivalence

GAPDH	Glyceraldehyde 3-phosphate dehydrogenase
GCOS	GeneChip Operating Software
GLUT	Family of facilitative glucose transporters
GLUT1	Glucose transporter 1
GLUT2	Glucose transporter 2
GLUT3	Glucose transporter 3
GLUT4	Glucose transporter 4
GMNN	Geminin, DNA replication inhibitor
GO	Gene ontology
GOI	Gene of interest
GPRC5A	Retinoic acid-induced protein 3
HAH1	Human antioxidant protein 1 homolog
HbA_{1c}	Glycosylated haemoglobin
HBSS	HEPES buffered salt solution
HDL	High-density lipoprotein
HEPES	4-(2-hydroxyethyl)-1-piperazineethanesulfonic acid
HEPH	Hephaestin
HFE	Human haemochromatosis protein
HIF	Hypoxia-inducible factors
HIF2α	Endothelial PAS domain-containing protein 1
HKG	Housekeeping gene
ICP-OES	Inductively coupled plasma atomic emission spectroscopy
IPA	Ingenuity® Pathway analysis
IRE	Iron-responsive element
IRP	Iron regulatory proteins
KCNJ8	K^+ inwardly-rectifying channel, subfamily J, member 8
KCNMB3	Calcium-activated potassium channel subunit beta-3
LDL	Low-density lipoprotein
MBSS	MES buffered salt solution
MES	2-(N-morpholino)ethanesulfonic acid
mRNA	Messenger RNA
MRS2	Magnesium transporter MRS2 homolog, mitochondrial
MSR1	Macrophage scavenger receptor 1
MT	Metallothinein
NCLN	Nicalin
NEAA	Non-essential amino acids
NOX1	NADPH oxidase 1
nt	Nucleotides
ORAC	Oxygen radical absorbance capacity
PBS	Phosphate buffered saline
PCR	Polymerase chain reaction
PODXL	Podocalyxin-like protein 1
PROCR	Endothelial protein C receptor
PRRG1	Proline-rich gamma-carboxyglutamic acid protein 1

qRT-PCR	Quantitative real-time polymerase chain reaction
RHBG	Rh family, B glycoprotein
RIN	RNA integrity number
RNA	Ribonucleic acid
RNase	Ribonuclease
ROS	Reactive oxygen species
RT	Room temperature
RT buffer	Reverse transcription buffer
SDS	Sodium dodecyl sulfate
SDS software	Sequence detection system software
SEM	Standard error of the mean
SFXN3	Sideroflexin 3
SGLT1	Sodium/glucose cotransporter 1
SLC	Solute carrier family
SLC10A2	Ileal sodium/bile acid cotransporter
SLC12A2	Sodium/potassium/chloride transporters
SLC24A1	Sodium/potassium/calcium exchanger
SLC25A37	Mitoferrin-1
SLC26A2	Sulfate transporter
SLC33A1	Acetyl-CoA transporter
SLC36A1	Proton/amino acid symporter
SLC3A1	Cystine, dibasic and neutral amino acid transporters
SLC4A7	Sodium bicarbonate cotransporter
SLC6A20	Proline IMINO transporter
SLC6A4	Neurotransmitter transporter, serotonin
SLC6A8	Neurotransmitter transporter, creatine
SVCT1	Human vitamin C (L-ascorbic acid) transporter
SYNGR1	Synaptogyrin 1
TE	Trolox equivalents
TEMED	Tetramethylethylenediamine
Tf	Transferrin
TfR1	Transferrin receptor protein 1
TfR2	Transferrin receptor protein 2
TGN	Trans-Golgi network
TM4SF1	Transmembrane 4 L six family member 1
TPCN1	Two pore segment channel 1
TR	Sweet taste receptor
TRPV1	Transient receptor potential cation channel subfamily V member 1
TSPAN7	Tetraspanin-7
U937	Human monocyte cell line
ZIP2	Zinc transporter 2
ZNT10	Zinc transporter 10

CHAPTER ONE

Introduction

1 Introduction

1.1 Dietary flavonoids

1.1.1 Flavonoid biochemistry

The flavonoids are low-molecular weight polyphenolic compounds that are formed in plants by combining synthesised derivatives of phenylalanine and acetic acid. The shikimic acid pathway is the main route by which flavonoids are synthesised, alongside many other products such as tryptophan and tyrosine (Knaggs, 2003). In this pathway phenylalanine is synthesised from phenylpyruvate which is transformed into trans-cinammic acid and hydrolysed to *p*-coumaric acid. Then, *p*-coumaric acid is condensed with 3 units of malonyl-Coenzyme A to form a chalcone. Subsequent hydration and ring closure of *p*-coumaric acid and malonyl-Coenzyme A leads to the formation of flavonoid compounds (Aherne & O'Brien, 2002; Knaggs, 2003).

The structure of flavonoids is based on a nucleus which is composed of three 6-member carbon rings. As illustrated in **Figure 1.1**, the benzene A-ring is condensed to the C-ring which can be either a pyran ring (anthocyanidins, catechins and flavanols) or pyrone ring (flavones, flavonols and flavanones). The C-ring carries the phenyl benzene B-ring at the 2 position, which contains functional groups that can dictate species and biochemical properties of flavonoids (Prior & Wu, 2006; Xiao *et al*, 2011). See **Figure 1.2** for functional groups that dictate structural classification of flavonoid species that are important in this work.

The basic structure of flavonoids allows for conformational flexibility and a variety of chemical interactions and structural substitutions. Thus, the biochemical nature and biological activities of flavonoid compounds will typically depend on structural class, hydroxylations, substitutions, the structure and positions of sugar moieties and their metabolites (Chen *et al*, 1996; Hollman *et al*, 1999; Prior & Wu, 2006). The

basis of dividing flavonoids into structural classes is mainly on the degree of oxidation of the C-ring (**Figure 1.3**). The main substitutions that flavonoids undergo during their synthesis include glycosylation, hydroxylation and hydrogenation at several positions. One of the major effects of the conjugation patterns in the C- or B-rings is on the hydrophillicity or hydrophobicity of the flavonoid molecule (i.e. glycosylation increases hydrophillicity) (Sivakumar *et al*, 2009; Xiao *et al*, 2011).

It is common for flavonoids to be found in nature as glycosylated compounds, often at the C-3 or C-7 positions, with *D*-glucose. Glycosylation increases flavonoid hydrophillicity as the polarity of the flavonoid molecules increases. This property is necessary for storage of flavonoids in plant cell vacuoles. Whilst stored in plants, flavonoids are relatively resistant to heat, dryness and oxidation, although they are still photosensitive (Aherne & O'Brien, 2002; Sadilova *et al*, 2007).

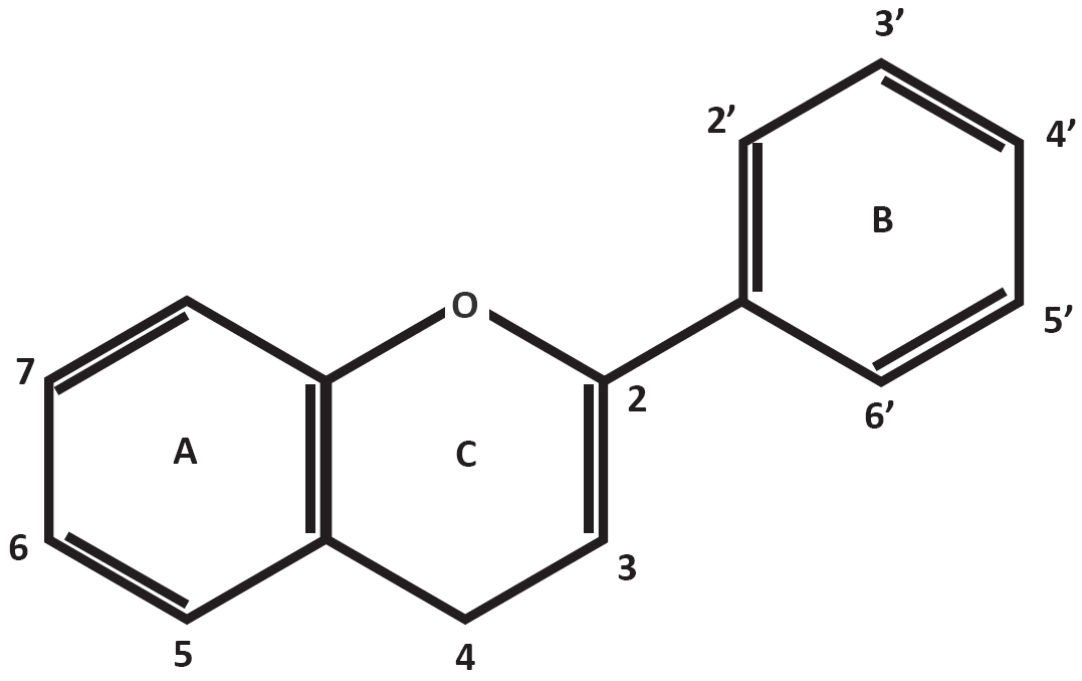

Figure 1.1. The basic flavonoid nucleus. Flavonoids consist of three 6-member carbon rings, identified as A, B and C. The benzene A-ring is condensed to the C-ring. The C-ring can be a pyran or a pyrone ring and is also the common site for moieties. At position 2, the C-ring is conjugated to the B-ring. These rings carry functional groups that dictate flavonoid classification and properties. (adapted from Aherne & O'Brien, 2002).

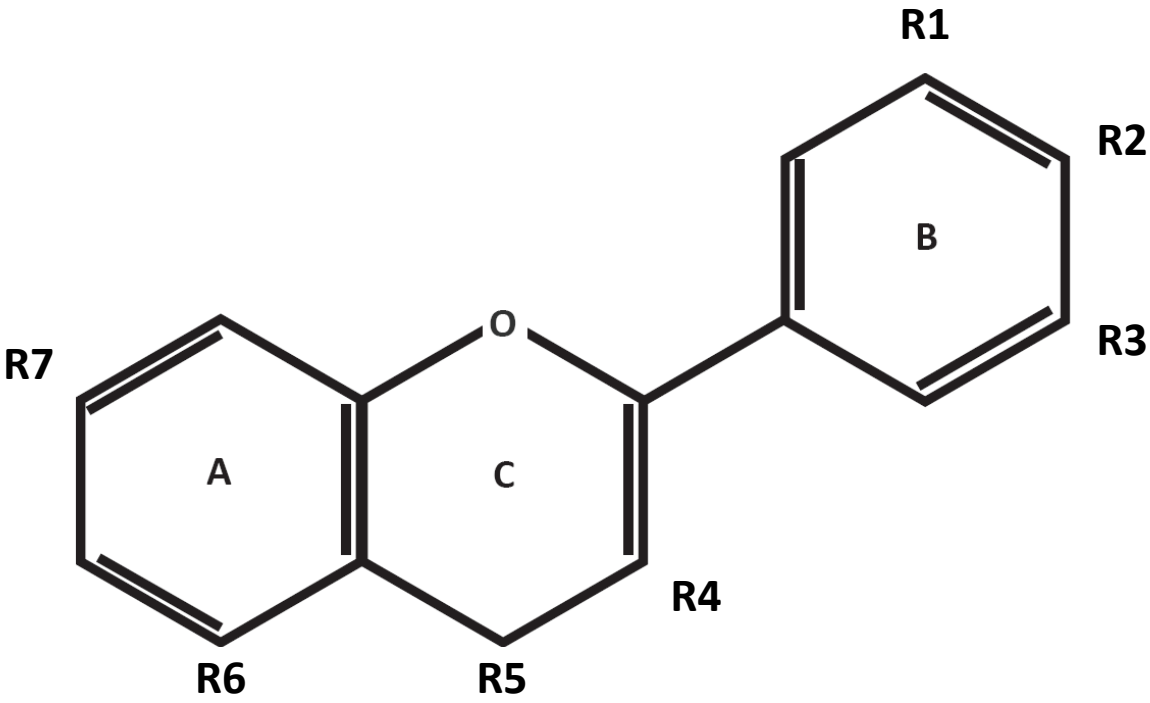

	R1	R2	R3	R4	R5	R6	R7
Flavonol				**-OH**	**=O**		
Quercetin	-OH	-OH	-H	-OH	=O	-OH	-OH
Chalcone*					**=O**		
Phloretin	-H	-OH	-H	-H	=O	-OH	-OH
Phloridzin	-H	-OH	-H	-H	=O	-*O*-glucose	-OH
Anthocyanidin†		**-OH**		**-OH**		**-OH**	**-OH**
Delphinidin	-OH	-OH	-OH	-OH	-H	-OH	-OH
Malvidin	$-OCH_3$	-OH	$-OCH_3$	-OH	-H	-OH	-OH
Cyanidin	-OH	-OH	-H	-OH	-H	-OH	-OH
Petunidin	-OH	-OH	$-OCH_3$	-OH	-H	-OH	-OH

Figure 1.2. Functional groups that distinguish the structural characteristics of important flavonoid species. Flavonols are characterised by presence of a hydroxyl group at C-3 and a pyrone C ring. *Chalcones are characterised by a pyrone C-ring, with an open configuration between C-9 and C-2, ring closure of a chalcone during biosynthesis leads to formation of other flavonoid species. †Anthocyanidins are characterised by 4 hydroxyl groups at C-4', C-2, C-5 and C-7 and a pyran C-ring; anthocyanidins are also functionally distinguished with a positive charge on the C-ring oxygen.

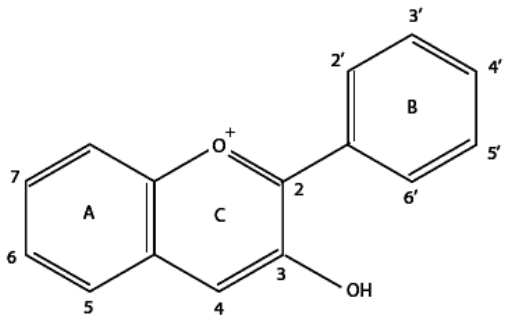

Anthocyanidins

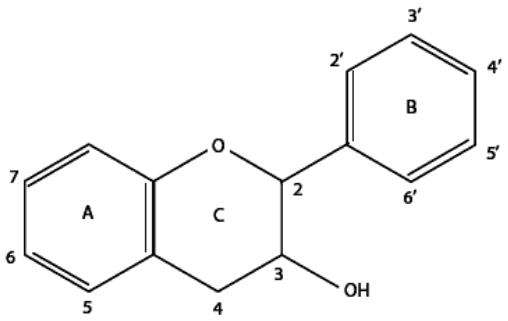

Catechins

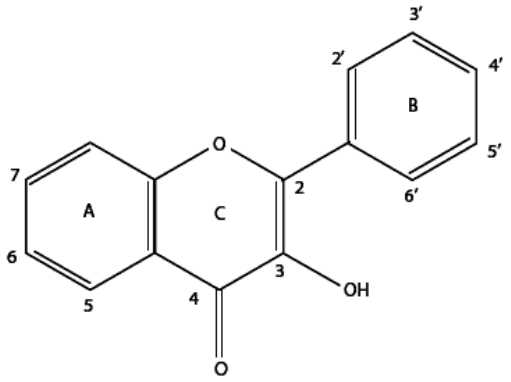

Flavonols

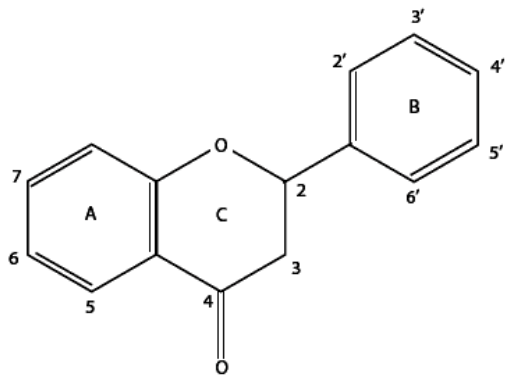

Flavanones

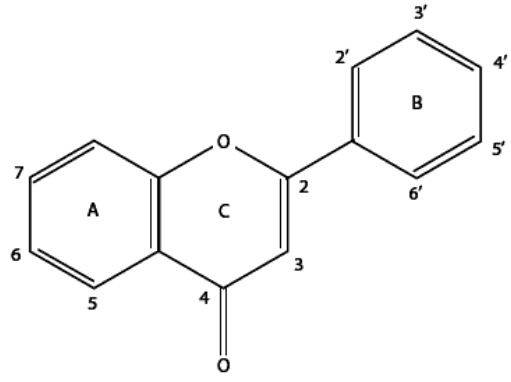

Flavones

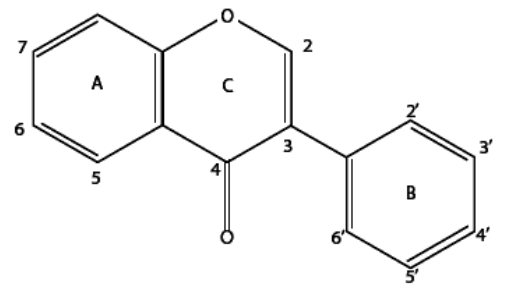

Isoflavones

Figure 1.3. Major flavonoid structural classes. The structural classification of a flavonoid will depend largely on the degree of hydroxylation of the C-ring. Note the pyrone C-ring configuration for flavones, flavonols, flavanones and isoflavones, whilst for anthocyanidins and catechins the C-ring is a pyran (adapted from Aherne & O'Brien, 2002).

1.1.2 Flavonoid intake

The main dietary sources of flavonoids in the western world are fruits, vegetables, red wine and tea (Hertog *et al*, 1993; Johannot & Somerset, 2006; Song & Chun, 2008). The flavonoid content of fruits and vegetables will depend very much on cultivar, skin to volume ratio of the fruit and other factors (Nyman & Kumpulainen, 2001; Chira *et al*, 2009).

Nutritional data regarding the intake of flavonoids is mainly based on quantifying the flavonols quercitin, myrictin and kaempferol and the flavones apigenin and luteolin. As flavonoid species consumed in the diet are much more diverse than those typically measured it can be assumed that the reported intakes may be underestimates (Aherne & O'Brien, 2002). There have been numerous studies estimating varied levels of intake in several countries; see **Table 1.1** for a brief summary.

Table 1.1 demonstrates the very high variability in flavonoid intakes, both between and within countries and over time. Variations have been attributed to the multiple quantification approaches that can be applied. Quantification of flavonoid intake will start with estimating consumption using food frequency questionnaires, diet records or food balance sheets; which may give different results (Mullie *et al*, 2008). Following this, the determination of flavonoid content in food is problematic. This is because different standards are used as estimates of flavonoid content (e.g. United States Department of Agriculture, Food and Agricultural Organisation).Furthermore; very few flavonoid species are included for quantification. Typically 5-10 flavonoids are included in intake estimates; these include flavonols (quercetin, myricetin, kaempferol) and flavones (apigenin, luteolin). However there are more than 5000 species of flavonoids that are ubiquitously distributed in the human diet.

Table 1.1. Summary of studies investigating flavonoid intake.

Country/ countries	Population	Flavonoid intake (mg/day)	Major sources	Authors, Year
Australia	M & F	454	Apples, onions, wine, tea	Johannot & Somerset, 2006
Belgium	F	166-203	-	Mullie *et al*, 2008
Fiji	M & F	18	-	Lako *et al*, 2006
Finland	M	131	-	Mursu *et al*, 2008
Greece	M	16	Vegetables, fruits, tea, wine	Hertog *et al*, 1995
Holland	M & F	23	Tea, onions	Hertog *et al*, 1993
Ireland		177	-	Beking & Vieira, 2011
Italy	M	23-34	Vegetables, fruits, tea, wine	Hertog *et al*, 1995
Italy	M & F	134	-	Tavani *et al*, 2006
Italy	M	153	-	Bosetti *et al*, 2009
Spain	M & F	313	Fruits, red wine	Zamore-Ros *et al*, 2010
UK	M & F	182	-	Beking & Vieira, 2011
USA	M	13	Vegetables, fruits, tea, wine	Hertog *et al*, 1995
USA	F (post-menopause)	14	Tea, apples, broccoli	Yochum *et al*, 1999
USA	M & F	190	Tea, wine	Song & Chun, 2008
USA	M & F	60	-	Cui *et al*, 2008
USA	M & F	190	Tea, citrus fruit juices, wine	Chun *et al*, 2007
USA	M & F (13-15 y)	15	-	Holt *et al*, 2009

1.1.3 Flavonoid bioavailability and intestinal metabolism

The metabolism of flavonoids has been extensively studied both *in-vivo* and *in-vitro*. Flavonoid absorption through the intestinal epithelium has been demonstrated by several lines of evidence, however there is still confusion regarding whether there is preferential absorption of aglycone or glycosidic forms (Aziz *et al*, 1998; Manach *et al*, 1998; Hollman *et al*, 1999; Arts *et al*, 2002). With respect to glycosidic forms, Hollman *et al* (1995, 1999), demonstrated that the absorption of flavonoid glycosides was largely dependent on the nature of the sugar moiety. For example, quercitin rutinoside has only 20% of the bioavailability of quercitin glucoside. Thus conjugation to a glucose molecule enhances absorption of flavonoids (Hollman *et al*, 1995; Hollman *et al*, 1999). Conjugation to a monosaccharide (i.e. to glucose, not to a disaccharide such as rutinose as is the case with rutin) implies the recruitment of active glucose transporters in the transport or cotransport of flavonoid glycosides (Johnston *et al*, 2005). Conversely, aglycones can be absorbed by facilitative diffusion, whereas conjugation to disaccharides will require further metabolism (e.g. deglycosylation, glucuronidation) prior to complete absorption. Therefore the bioavailability of flavonoids that are conjugated in a complex manner may be hindered due to further steps in preabsorptive metabolism (Hollman *et al*, 1999; Spencer *et al*, 1999; Johnston *et al*, 2005).

It has been speculated that absorption of glycosides or aglycones will occur through different pathways, i.e. by active or diffusive mechanisms, respectively. The hydrophobic nature of flavonoid aglycones allows them to be absorbed passively by diffusion or facilitated diffusion across cell membranes. Conversely, for the more polar glycosylated flavonoids an active transporter is required. The sodium/glucose cotransporter (SGLT1) and bilitransclocase have been implicated in the cotransport

or transport of flavonoid glycosides; and aglycones are suggested to diffuse through the facilitative glucose transporter (GLUT2) (Walgren *et al*, 2000; Passamonti *et al*, 2002). In light of this, aglycone forms of flavonoids are made readily available by intestinal enzymatic action (Day *et al*, 1998; Day *et al*, 2000). Therefore, the effects of glycosylation on flavonoid absorption may be negligible.

For a schematic overview of the intestinal cellular metabolism of flavonoids see **Figure 1.4a**. Typically the first stage in flavonoid intestinal metabolism is the deglycosylation of the flavonoid glycosidic forms. Lactase-phlorizin hydrolase and 1-β-glucosidase are two enzymes localised in the intestinal brush border that have been shown to deglycosylate flavonoids within the gut lumen (Day *et al*, 1998; Day *et al*, 2000). Parent compounds may also be absorbed unaltered, cellular metabolism involved several other reactions including: hydroxylation, methylation and conjugation (Spencer *et al*, 1999). Following these reactions flavonoids can be effluxed back into the lumen or are released into circulation. For the estimated proportions of flavonoids that undergo metabolism or are directly release into the lumen or into circulation see **Figure 1.4b**.

Jejunal tissues have been found to have the highest transport efficiencies for flavonoids (Talavera *et al*, 2004; Matuschek *et al*, 2006). Flavonoids that have not been metabolised by luminal enzymes nor absorbed in the small intestine undergo bacterial degradation in the colon. Colonic microbacter metabolise flavonoid glycosides to aglycones and phenolic acids which are easily reabsorbed (Bokkenheuser *et al*, 1987; Hollman *et al*, 1995; Walle *et al*, 2000). The final step in flavonoid metabolism is the excretory pathway. When in polar forms flavonoids are excreted in urine or secreted in bile. Flavonoids secreted in bile will undergo further intestinal metabolism (Das & Sothy, 1971; Prior *et al*, 2006) (**Figure 1.5**).

ABBREVIATIONS

LPH
Lactase-phloridzin hydrolase

GBA3
β-glucosidase

GLUTs
Facilitative glucose transporters

SGLT1
Sodium/glucose cotransporter

P-gp
P-glycoprotein

MRP
Multidrug resistance associated protein 2/3

CYP
Cytochrome P450

UGT
UDP-glucuronosyltransferase

SULT
Sulfotransferase

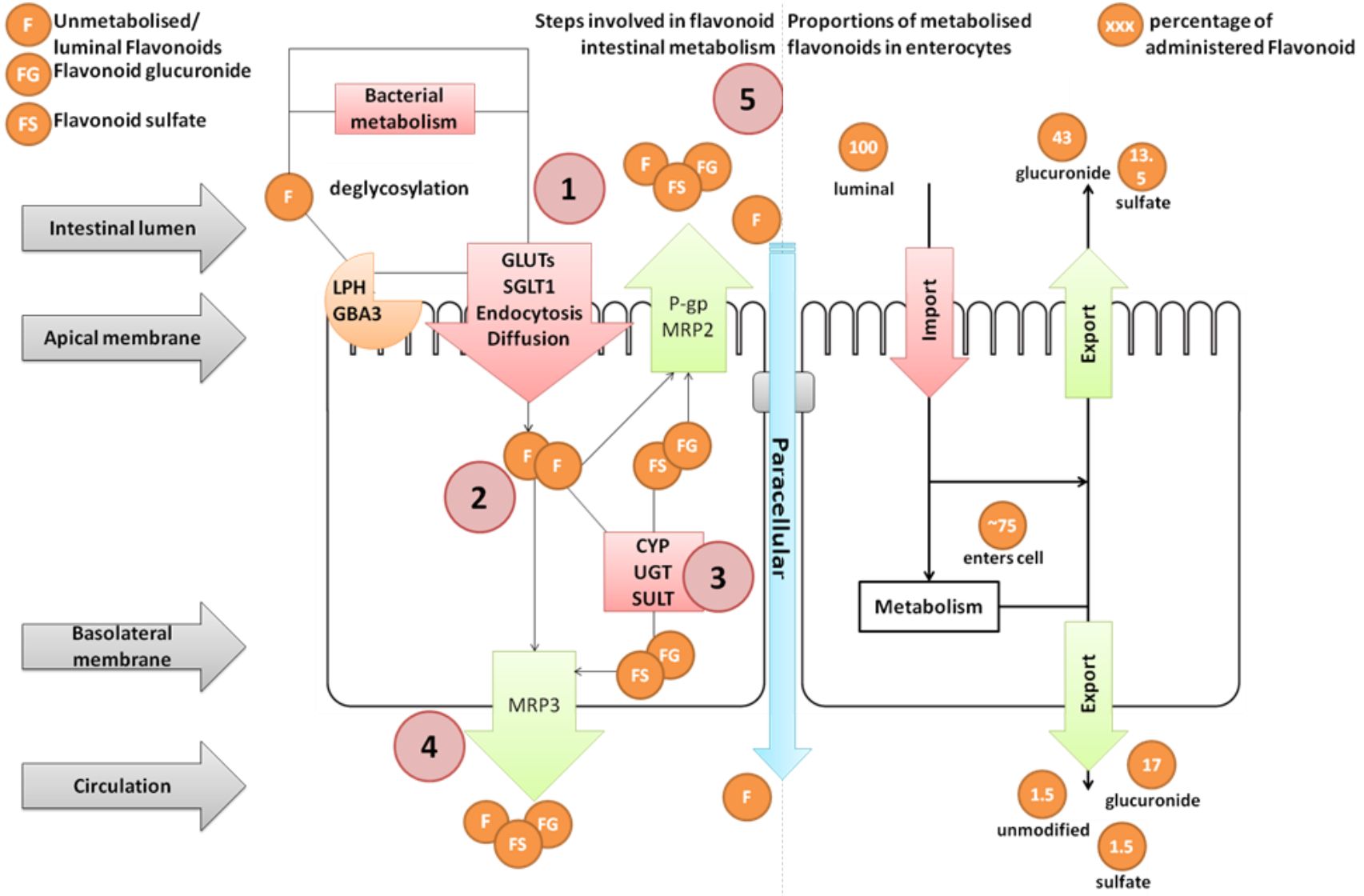

Figure 1.4a. Enterocyte flavonoid metabolism. 1) Luminal flavonoids enter cells unaltered or undergo deglycosylation by bacterial or endogenous enzymes, influx will be either carrier mediated or by endocytosis **2)** intracellular flavonoids are destined for immediate efflux or for downstream metabolism prior to efflux **3)** metabolism involves hydroxylation, sulfonylation or glucuronidation **4)** flavonoids can reach circulation by transporter mediated basolateral release or by paracellular diffusion **5)** flavonoids can also be release back into the lumen by apical transporters. Various sources, e.g. Walle, 2004; Planas *et al*, 2012

Figure 1.4b. Proportions of flavonoids that undergo metabolism. ~ 75% of luminal flavonoids will be absorbed, the majority undergoing cellular metabolism. > 50% of the initial dose will be metabolised and rereleased back into the lumen. ~ 20% will be glucuronidated or sulfonated and released into circulation. ~ 1.5% of the parent compound reaches circulation. Various sources, e.g. Spencer, 2003; Walle, 2004; Lotito *et al*, 2011

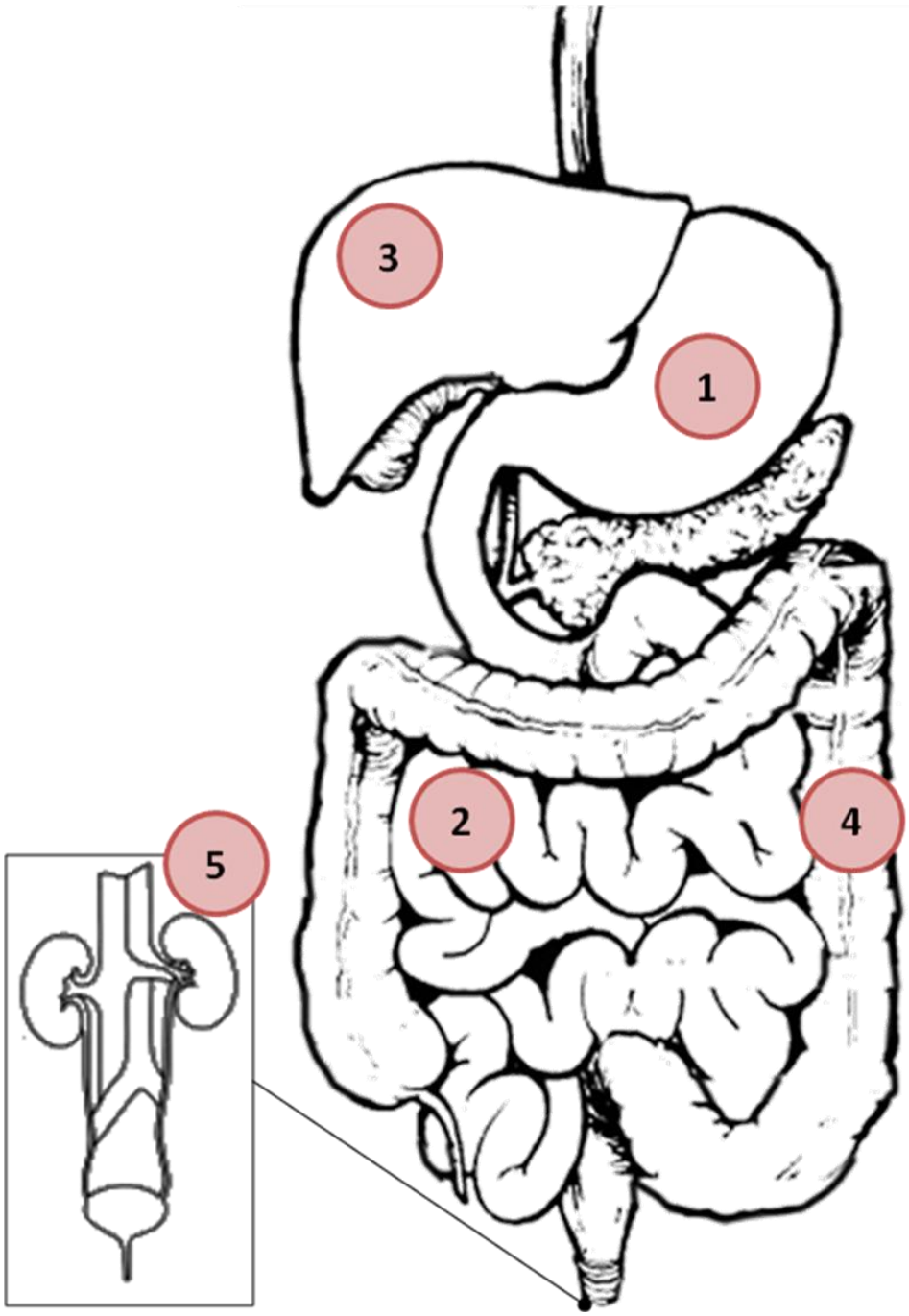

Figure 1.5. Schematic overview of flavonoid digestion & absorption. 1) Flavonoids enter the stomach mainly as glycosylated compounds from dietary sources. **2)** In the small intestine is the highest efficiency of flavonoid absorption, in the digestive tract flavonoids will undergo deglycosylation, glucuronidation, oxidation among other enzymatic reactions. **3)** After systemic distribution flavonoids are metabolised by the liver, undergoing hepatic phase 2 metabolism, flavonoids can be secreted in bile. **4)** Flavonoids that are not absorbed/ metabolised in the small intestine, as well as flavonoids that are secreted in bile will undergo bacterial degradation in the large intestine to a final product of easily absorbable aglycones or phenolic acids. **5)** Polar flavonoids can also be excreted in urine following metabolism. Various sources, e.g. Das & Sothy, 1971; Bokkenheuser *et al*, 1987; Hollman *et al*, 1995

1.1.4 Health effects of flavonoids

There have been numerous reports on the health promoting and protective effects of flavonoids on lipid metabolism, neurodegenerative decline, cancer cell proliferation, nutrient bioavailability, cardiovascular health and glycaemic control among many other effects (Vuorela *et al*, 2005; Mursu *et al*, 2008; Renis *et al*, 2008). This section will briefly review some of the current research into the health promoting and protective effects of flavonoids *in-vitro* and *in-vivo*. Further sections will specifically discuss the effects of flavonoids on intestinal tissues and nutrient interactions which pertain to the subject of this thesis.

1.1.4.1 In-vitro studies on the health effects of flavonoids

The flavonoids have a number of mechanisms that can lead to their antioxidant effects; namely these are the chelation of metal ions and the direct interaction with reactive oxygen species (ROS). When chelating metal ions, flavonoids decrease the abundance of reactive metals which catalyse Haber-Weiss-Fenton reactions. When interacting directly with ROS, flavonoids are capable of donating hydrogen from a hydroxyl group, thus decreasing ROS reactivity (Nijveldt *et al*, 2001). The above mechanisms are examples of these reactions:

1) $^{\cdot}O_2^{(e-)} + H_2O_2 \rightarrow O_2 + OH^{(e)} + {}^{\cdot}OH$

Presence of a metal ion will provide a destination for the electron to be donated from the $^{\cdot}O_2^{(e-)}$; which is then donated from the metal to catalyse H_2O_2 degradation. Flavonoids will chelate metal ions, preventing the electron exchange.

2) $\text{Flavonoid–OH} + R^{-} \rightarrow \text{Flavonoid–O}^{-} + RH$

In the above reaction flavonoids will donate a hydrogen from reactive hydroxyl groups to an ROS (annotated R above) forming more stable products. This

antioxidant effect is physiologically important in preventing the oxidation of biological substrates which are potentially damaging; e.g. low-density lipoprotein (LDL) oxidation (Nijveldt *et al*, 2001). The *in-vitro* investigations on flavonoids have generally focused on these antioxidant properties and the molecular reactions they can induce; this is discussed in the ensuing section.

A series of preclinical studies using extracts from raspberry, rapeseed and pinebark found multiple properties that were of putative benefit for health (Vuorela *et al*, 2005). For example, rapeseed and pinebark phenolic compounds and raspberry anthocyanins had antioxidant properties towards liposomal membranes (Vuorela *et al*, 2005). Rapeseed phenolic compounds are effective free radical scavengers in diphenylpicryl-hydrazyl tests (Vuorela *et al*, 2005). Furthermore, raspberry and pinebark phenolic compounds are effective inhibitors of LDL oxidation (Vuorela *et al*, 2005). These phenolic compounds also inhibited the formation of pro-inflammatory mediators and the growth of some bacterial strains (Vuorela *et al*, 2005).

A study by Renis *et al* (2008) investigated the molecular effects of anthocyanin glycosides and aglycones on cell growth, formation of ROS, cell-cycle/stress protein modifications and DNA fragmentation in Caco-2 cells. Aglycone anthocyanins decreased ROS formation at all concentrations (25, 50, 100 and 200 µmol/l), whilst the glycosides had the same effect only at the lower concentration tested (25 µmol/l) (Renis *et al*, 2008). The studies by Renis *et al* (2008) showed that both aglycone and glycosides counteract oxidative stress, with the latter being more effective. It was concluded that anthocyanin aglycones exert their chemoprotective effects by a ROS-dependent mechanism. Conversely, when anthocyanins are conjugated to a sugar moiety the interaction is ROS-independent (Renis *et al*, 2008).

Renis *et al* (2008) suggested that flavonoids will mediate their antioxidant effects through separate mechanisms, depending on their glycosylation. The aglycone mediates a cytoprotective effect by directly modulating ROS levels and through the induction of DNA-repair pathways (e.g. P53, Ataxia telangiectasia mutated genes). Whereas the glycoside derivative was cytoprotective without modulating ROS levels, and had a more direct protective effect on DNA. This was observed after inducing stress to naked DNA and observing a protective effect against fragmentation. This can be attributed to intercalation capabilities of flavonoids, providing direct protection from radicals, as well as increased stability and cross-linking of DNA structures (Renis *et al*, 2008; Kanakis *et al*, 2007).

1.1.4.2 In-vivo animal studies of the health effects of flavonoids

The *in-vivo* animal studies with flavonoids are commonly focused on investigating the metabolic and systemic potential of flavonoids, such as the cardiovascular and glycaemic effects. This section presents a few recent studies that investigated such related themes.

Studies have compared the effects of berry anthocyanins on markers of metabolic syndrome in experimental C57BL/6J mouse models (Prior *et al*, 2008; Hsu *et al*, 2009). Prior *et al* (2008) used a murine model of obesity based on high-fat feeding. They showed that the addition of purified anthocyanins to the high-fat diets reduced weight gain, body fat and fasting plasma glucose relative to high-fat fed controls (Prior *et al*, 2008). The aforementioned study did not address the mechanisms behind their findings; however another study in adipocyte cell lines found that anthocyanins induce adiponectin expression (Tsuda *et al*, 2006). High adiponectin expression prevents adipocyte differentiation and increases energy expenditure thus contributing to the decreased weight gain (Bauche *et al*, 2007).

Similar effects were reported by Hsu *et al* (2009), where mice were fed a high-fat diet with or without rutin and *o*-coumaric acid. Supplementation with the phenolic compounds resulted in less weight gain and decreased serum lipid profiles, insulin and leptin concentrations (Hsu *et al*, 2009). In addition, hepatic biomarkers and antioxidant capacity were beneficially altered, i.e. decreased malondialdehyde from lipid peroxidation, trolox equivalent antioxidant capacity was increased, increased glutathione, with increased ratio to glutathione disulfide, increased activity of hepatic antioxidant enzymes glutathione peroxidase, glutathione S-transferase and superoxide dismutase (Hsu *et al*, 2009). Thus, the results indicated anthocyanin suppression of dyslipideamia, hepatosteatosis and oxidative stress induced by a high-fat diet (Hsu *et al*, 2009). Other studies investigating the cardiovascular effects of flavonoids in diabetic conditions found proanthocyanidins reduced markers of glycation damage (advanced glycation end products and their receptors) and decrease the number of degenerated mitochondria whilst maintaining myocardium fine structure (Cheng *et al*, 2007). The general metabolic effects associated with flavonoid intake were attributed to their abilities to act as antioxidants and to their involvement in pathway activation. The above studies have demonstrated the modulation of antioxidant enzyme levels, adipocytokine expression, glycation, glycation products and receptors; all of which had a measurable and physiologically relevant response in animal models.

1.1.4.3 In-vivo human studies of the health effects of flavonoids

Similarly to the *in-vivo* animal studies on the effects of flavonoids, experiments in humans tend to focus on the metabolic and systemic effects of flavonoids. Such studies have included a variety of tissues and conditions, e.g. cardiovascular disease,

osteoporosis, oxidative stress, inflammation, diabetes and cancer (Scheiber *et al*, 2001; Chambers & Camire, 2003; Di Giacomo *et al*, 2009; Holt *et al*, 2009).

Flavonoids have been beneficially linked to oxidative capacity both in athletes who are expected to encounter oxidative stress, and in normal subjects (Di Giacomo *et al*, 2009; Holt *et al*, 2009). Consumption of fruits and vegetables, rich in antioxidants such as isoflavones and lycopene, is correlated with decreased markers of inflammation and oxidative stress (Holt *et al*, 2009). In athletes, supplementation with lycopene and isoflavonoids increases plasma antioxidant capacity, decreases lipid peroxidation and improves plasma non-proteic antioxidant defence (Di Giacomo *et al*, 2009).

Beneficial effects of flavonoids on the cardiovascular and skeletal systems have been reported in a prospective clinical trial involving a twelve week supplementation with isoflavone-rich soy (Scheiber *et al*, 2001). Mean lag time of LDL oxidation increased and correlated with serum phytoestrogen concentrations (Scheiber *et al*, 2001). In the same study, plasma high-density lipoprotein (HDL) cholesterol and serum osteocalcin were both significantly increased. The ratio of total cholesterol to HDL cholesterol was decreased and negatively correlated with the urinary excretion of isoflavones (Scheiber *et al*, 2001).

Although numerous *in-vitro* studies have found evidence of flavonoid and dietary sugar interactions, few studies in humans have investigated the effects of flavonoids on glycaemic regulation. For example, a small study by Chambers & Camire (2003) investigated the effects of cranberry-extract in patients with type-II diabetes who have good control of their blood sugar with diet alone. No differences were observed in fasting serum glucose, HbA_{1c}, fructosamine or blood lipids after 6 or 12 weeks of supplementation. However, insulin levels in the cranberry supplemented

group were significantly decreased. Differences in some biomarkers may not have been significant due to small sample size (control n=13 and treated n=14), low dosage and an already good level of glycaemic control among subjects prior to participation (Chambers & Camire, 2003). Prospective studies with interventions at different stages of the disease, such as during insulin resistance rather than after the development of diabetes, may yield more significant or meaningful results.

1.2 Dietary glucose

1.2.1 The roles of SGLT1 and GLUT2

Intestinal glucose transport is the primary step in glucose metabolism. It is adaptable to luminal and systemic factors *in-vivo*, thus maintaining the metabolic milieu of the tissue and thus the whole organism (Gouyon *et al*, 2003; Tobin *et al*, 2008). Classical mechanisms of intestinal glucose transport state that apical uptake is initially by the sodium/glucose cotransporter member 1, SGLT1. This occurs through a downhill sodium ion gradient which is maintained by a sodium-potassium ATPase at the basolateral membrane of enterocytes. SGLT1 is capable of transporting glucose against its concentration gradient when luminal glucose concentrations are higher than blood glucose concentrations (Debnam & Levin, 1975; Díez-Sampedro *et al*, 2004). Following entry into the enterocyte, glucose undergoes basolateral release at the high-capacity low-affinity facilitative glucose transporter member 2 (GLUT2). GLUT2 transports glucose, as well as fructose and galactose (Cheeseman, 1993; Helliwell *et al*, 2000) (reviewed by Kellet *et al*, 2008).

The apical SGLT1 uptake pathway is saturable and phloridzin-sensitive. A diffusive component of apical glucose uptake also exists which has been attributed to apically localised GLUT2 (Kellet & Helliwell, 2000). Current models suggest that GLUT2 translocates to the apical membrane under conditions of high luminal glucose to increase uptake by up to 3-fold more than SGLT1-mediated transport alone (Corpe *et al*, 1996; Kellet & Helliwell, 2000; Gouyon *et al*, 2003). Under healthy conditions, GLUT2 is retracted from the apical membrane in response to insulin signaling after plasma glucose increases (Tobin *et al*, 2008). However, in insulin-resistant states, GLUT2 is permanently localised at the apical membrane and does not respond to

insulin signaling. Therefore glucose influx is greatly increased with the permanent apical localisation of GLUT2 (Corpe *et al*, 1996; Tobin *et al*, 2008). In fact, this permanent apical presence of GLUT2 is popularly used as an experimental model of insulin resistance in mice (reviewed by Kellet *et al*, 2008; Tobin *et al*, 2008; Ait-Omar *et al*, 2011).

Typically, low concentrations of glucose are absorbed efficiently by SGLT1. When luminal concentrations of monosacharides are above the saturation limits of SGLT1, then any GLUT2 that is not saturated is recruited to the apical membrane to aid in uptake (Kellet & Helliwell, 2000; Gouyon *et al*, 2003; Chaudhry *et al*, 2012). The translocation of GLUT2 occurs rapidly, within 1-2 minutes of sugar sensing. This occurs following a signaling cascade from sweet taste receptors and the voltage gated calcium channel, ($Ca_v1.3$). $Ca_v1.3$ induces an accessible cytoskeleton for the trafficking of proteins (Mace *et al*, 2007; Mace *et al*, 2009). After the uptake of sugar, GLUT2 is internalised by insulin-dependent mechanisms (Kellet *et al*, 2008; Tobin *et al*, 2008). The ability of GLUT2 to translocate and the kinetics involved with the apical GLUT2 pathway are factors that make it a candidate for the previously unexplained diffusive component of glucose uptake (Kellet & Helliwell, 2000; Kellet *et al*, 2008).

1.2.2 Importance and regulation of the GLUT2 transporter

As well as the intestine, GLUT2 is localised to several other tissues including the liver, pancreas, kidney and brain (Gould & Holman, 1993; Goestemeyer *et al*, 2007). In these aforementioned tissues, GLUT2 has similar capabilities to process high concentrations of glucose in a bidirectional flux owing to its high-capacity, low-affinity, and translocation properties. The regulation of GLUT2 is complex; it

responds to calcium, sweet-taste receptors, glycaemia, insulineamia, and paracrine and endocrine signaling (reviewed by Kellet *et al*, 2008; Leturque *et al*, 2009).

The capability of GLUT2 to traffic between membranes facilitates a considerable bidirectional flux of glucose. The importance of this transporter protein and its influx and efflux capabilities is demonstrated by its redundancy in Fanconi-Bickel syndrome. Fanconi-Bickel syndrome results in sugar intolerance, growth retardation, hepatomegaly and nephropathy, among other effects (Santer *et al*, 1997; Leturque *et al*, 2009). Furthermore, the deletion of the GLUT2 gene in mouse models is fatal (Guillam *et al*, 1997).

The initial phases of enterocytic glucose uptake occur through SGLT1 (**Figure 1.6**). When SGLT1 activity increases, under conditions of high glucose (also detected by apically localised sweet taste receptors) there is an increased intracellular ATP: ADP ratio. This increase causes closure of the basolateral ATPase, which initially maintains SGLT1 activity, and depolarisation of the apical membrane. This depolarisation activates $Ca_v1.3$, in-turn causing an influx of calcium ions into the cell. The increased intracellular calcium content causes a rearrangement of the cytoskeleton, making it accessible to protein trafficking, and a terminal web that is available for GLUT2 insertion (Mace *et al*, 2007; Morgan *et al*, 2007; Mace *et al*, 2009). This rearrangement allows for GLUT2 to attain its apical localisation when stimulated (**Figure 1.7**). Following translocation, flux of dietary glucose greatly increases and this in turn increases plasma glucose which activates insulin signaling. Under normal conditions, GLUT2 is retracted from the apical membrane in response to insulin signaling (Tobin *et al*, 2008) (**Figure 1.8**).

The response of GLUT2 is an example of the molecular adaptability of enterocytes to the local environment (i.e. the luminal contents). When GLUT2 is apically

localised, the enhanced glucose accumulation affects downstream molecular events (Uyeda & Repa, 2006). These include the transcription rates of genes with carbohydrate response elements, such as L-type pyruvate kinase (Yamashita *et al*, 2001). These regions associate with carbohydrate response element-binding proteins (Noordeen *et al*, 2010).

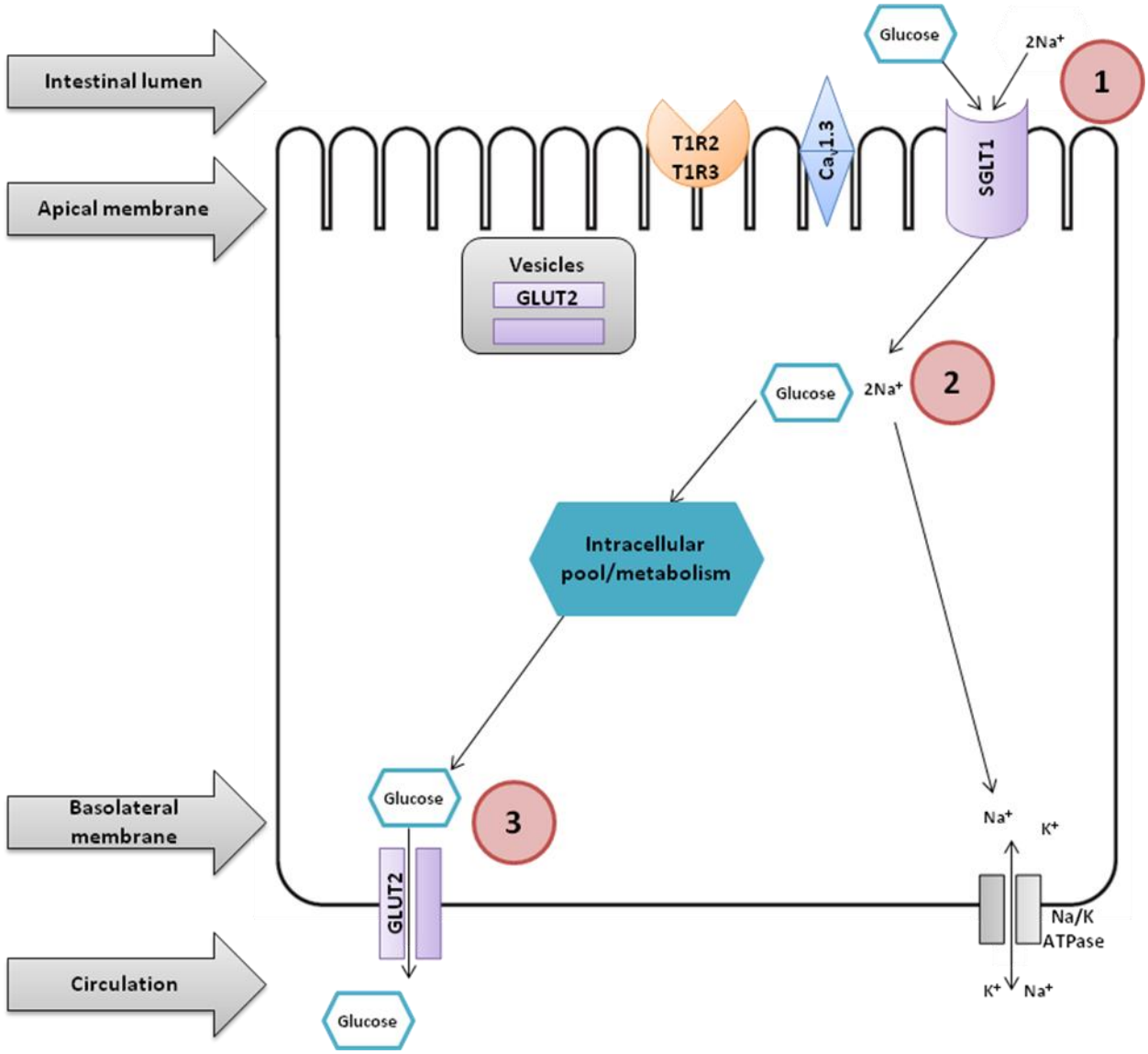

Figure 1.6. SGLT1 and GLUT2 mediated glucose transport under normal conditions of low luminal glucose. **1)** Under states of low luminal glucose (e.g. between meals) SGLT1 adequately co-transports glucose and 2 sodium ions along a downhill sodium gradient. **2)** The downhill sodium gradient is maintained by a sodium/potassium ATPase at the basolateral membrane of enterocytes. **3)** Intracellular glucose can be utilised for cellular metabolism or is effluxed via basolateral GLUT2. Under these conditions, apical GLUT2 is localised to subapical vesicles and does not function to influx glucose. SGLT1: sodium/glucose cotransporter; GLUT2: facilitative glucose transporter 2; $Ca_v1.3$: voltage dependent calcium channel; T1R2/T1R3: taste receptors 2 & 3. Adapted from various sources (e.g. Debnam & Levin, 1975; Díez-Sampedro *et al*, 2004)

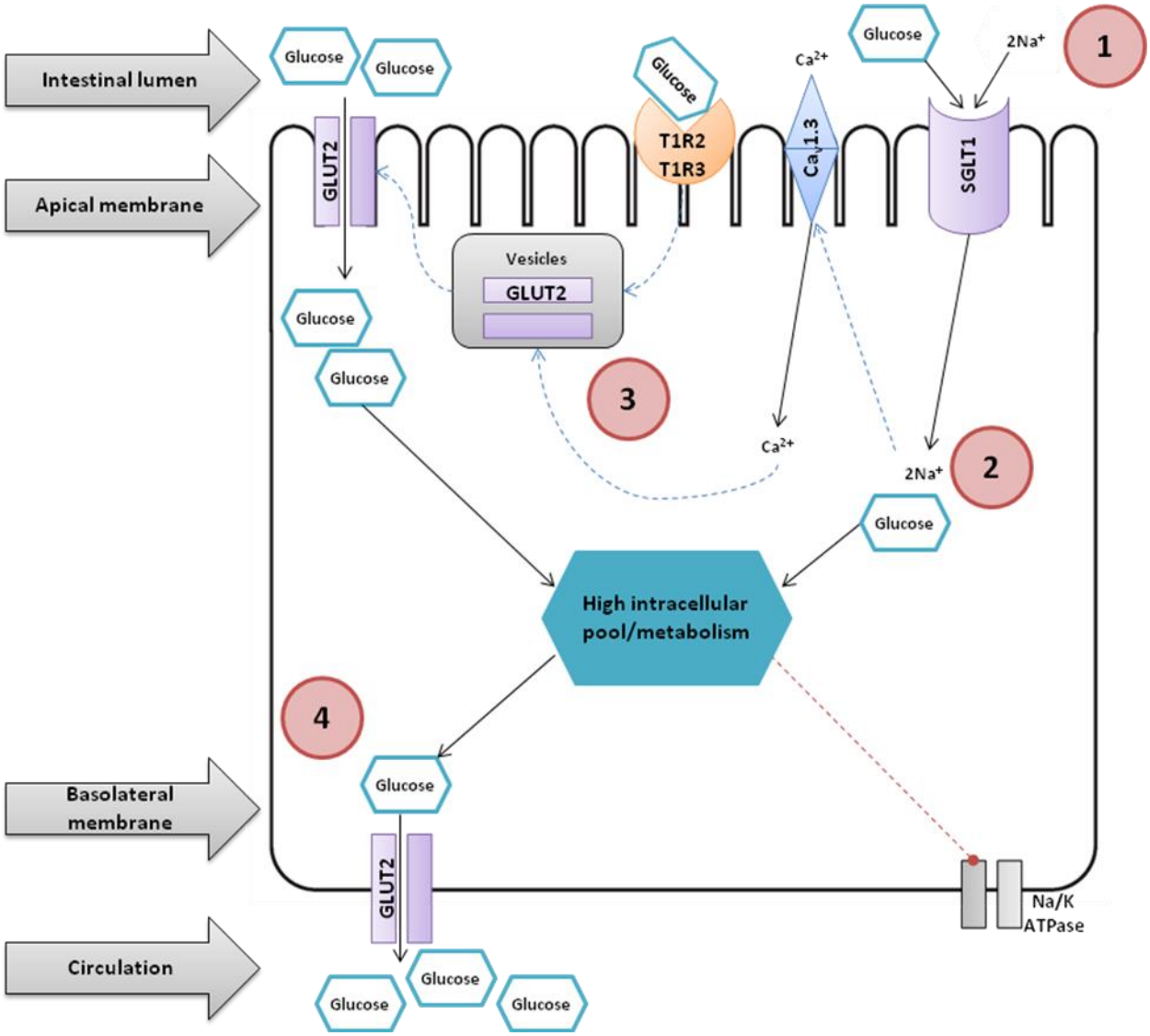

Figure 1.7. Activation of the apical GLUT2 pathway of glucose transport across enterocytes. **1)** A high luminal glucose concentration (e.g. following a sugary meal) will increase SGLT1–mediated glucose and sodium influx. **2)** The resulting high intracellular glucose and sodium content closes the basolateral sodium/potassium ATPase, in turn activating the $Ca_v1.3$. **3)** High intracellular calcium and sodium cause the cytoskeleton to rearrange, allowing protein trafficking. The apical membrane depolarises and is prepared for GLUT2 insertion from the subapical vesicles, insertion of GLUT2 is signaled by apical sweet taste receptors. **4)** High influx of glucose results from apical GLUT2 recruitment and therefore there is a higher rate of glucose release into circulation from basolateral GLUT2. SGLT1: sodium/glucose cotransporter; GLUT2: facilitative glucose transporter 2; $Ca_v1.3$: voltage dependent calcium channel; T1R2/T1R3: taste receptors 2 & 3. Blue dashed lines represent activation; red dashed lines represent inhibition. Adapted from various sources. (e.g. Goestemeyer *et al*, 2007; Mace *et al*, 2007)

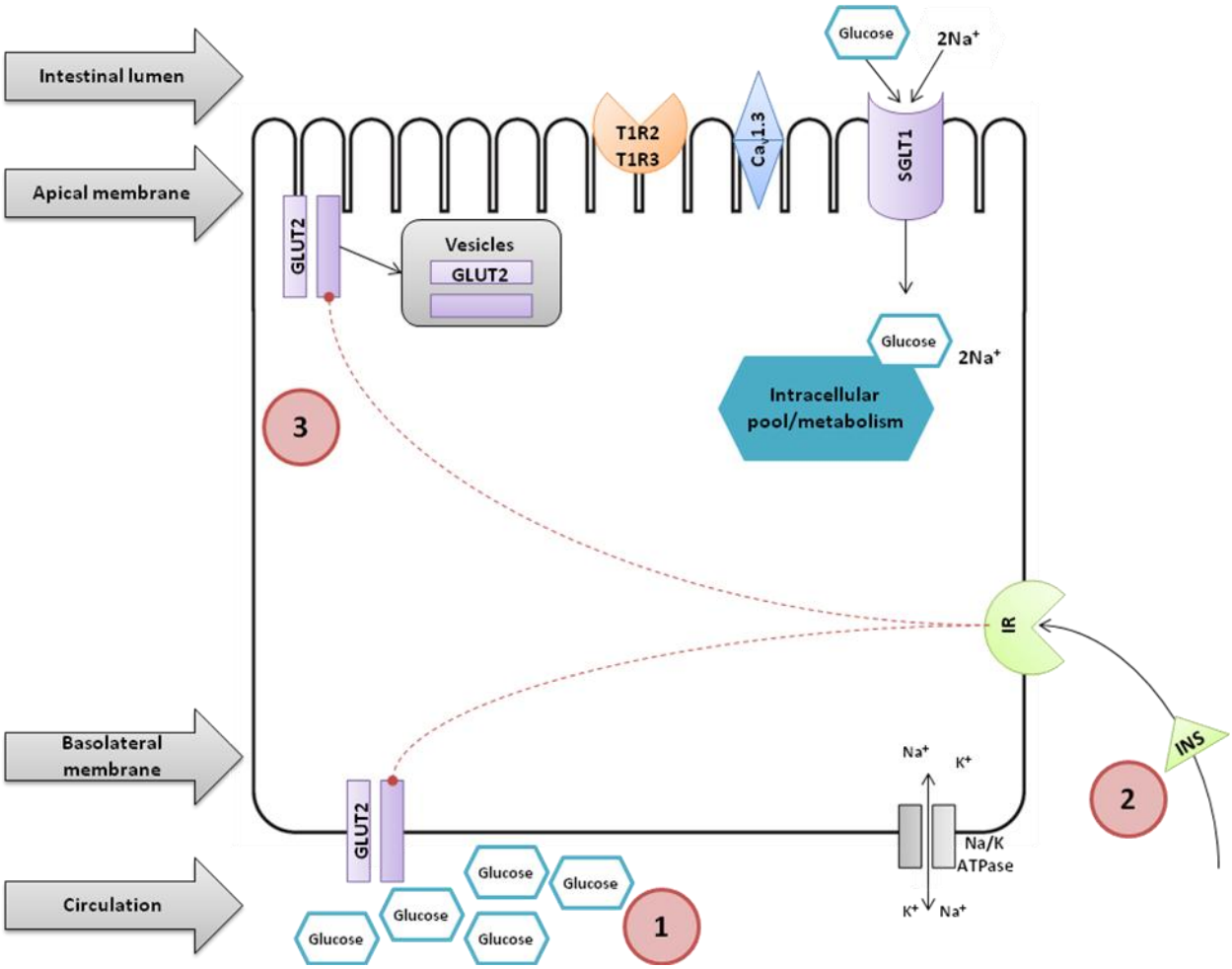

Figure 1.8. Retraction of the apical GLUT2 pathway of glucose transport across enterocytes. **1)** Following the apical recruitment of GLUT2, the increased circulating glucose stimulates the secretion of insulin from the pancreas. **2)** Secreted insulin acts on insulin receptors in enterocytes. **3)** Insulin causes the retraction of GLUT2 from the apical membrane back to subapical vesicles, GLUT2 can undergo degradation. SGLT1: sodium/glucose cotransporter; GLUT2: facilitative glucose transporter 2; $Ca_v1.3$: voltage dependent calcium channel; T1R2/T1R3: taste receptors 2 & 3; IR: insulin receptor; INS: insulin. Blue dashed lines represent activation; red dashed lines represent inhibition. Adapted from various sources. (e.g. Tobin *et al*, 2008)

1.3 Dietary iron

Iron is an essential element in the human body as it is an integral component of several enzymes and proteins. These include, most importantly, the role of iron in haemoglobin as the oxygen carrying protein in blood. Iron deficiency causes anaemia and insufficient oxygen delivery to cells and tissues, whereas iron excess can cause haemochromatosis. The latter can lead to several conditions such as cirrhosis and cardiomyopathy. The uptake of iron from the human intestine is mediated by complex interactions between several proteins localised in cells of the intestinal epithelium. The uptake mechanisms of dietary *haem* iron are different from those of dietary ionic iron (i.e. *non-haem* iron) (reviewed by Wang & Pantopoulos, 2011). Our focus is on the intestinal uptake of non-haem iron and the ensuing discussion reflects this.

1.3.1 Iron uptake and transepithelial transport

A number of important genes and proteins are involved in transepithelial transport of ionic iron in enterocytes. These include the apically localised uptake proteins duodenal cytochrome B reductase (DCYTB) and the divalent metal ion transporter (DMT1) (Canonne-Hergaux *et al*, 1999; McKie *et al*, 2001). Localised basolaterally is the regulatory complex denoted as HFE-β2m-TfR1 (**Figure 1.9**). This complex is comprised of the haemochromatosis protein (HFE), transferrin receptor 1 (TfR1) and β-2-microglobulin (β2m), it is typically expressed in crypt enterocytes and in mature enterocyte cell lines. This complex is a putative regulator for DMT1-mediated iron uptake and for the interaction between transferrin (Tf) and its receptors (TfR1/TfR2) (Feder *et al*, 1998; Arredondo *et al*, 2001; Arredondo *et al*, 2006). The proteins responsible for basolateral efflux of iron are the iron channel ferroportin (FPN) and the ferroxidase hephaestin (HEPH) (McKie *et al*, 2000; Anderson *et al*, 2002a).

When dietary ferric iron (Fe^{3+}) enters the intestine it is reduced to ferrous iron (Fe^{2+}) by DCYTB at the apical membrane of enterocytes (McKie *et al*, 2001). Iron can then be easily imported into the cell by DMT1 (Han *et al*, 1995). A transcytotic step is necessary prior to the transfer of iron across the basolateral membrane. FPN is the exporter of intracellular ferrous iron at the enterocyte basolateral membrane. HEPH oxidises ferrous iron to its ferric form before iron is bound to Tf and then circulated systemically (De Domenico *et al*, 2007a). A schematic representation of the overall transport pathway of iron through enterocytes is detailed in **Figure 1.10**.

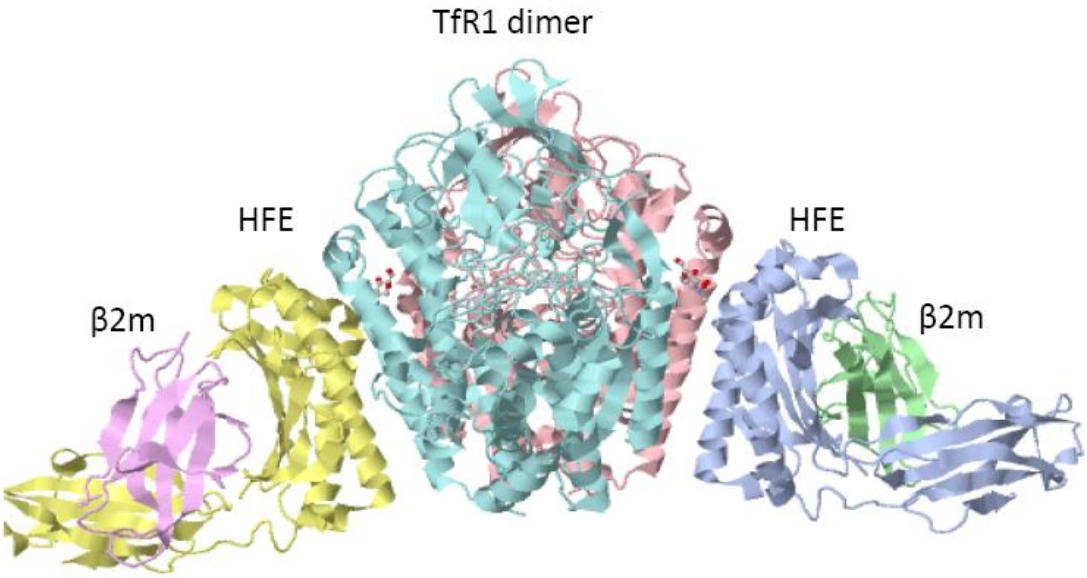

Figure 1.9. Structure of the regulatory HFE-β2m-TfR1 complex. TfR1: transferrin receptor 1; HFE; haemochromatosis protein; β2m: β-2-microglobulin. Structure elucidated by Lebrón *et al* (1998). Image generated with Jmol (Herráez, 2006).

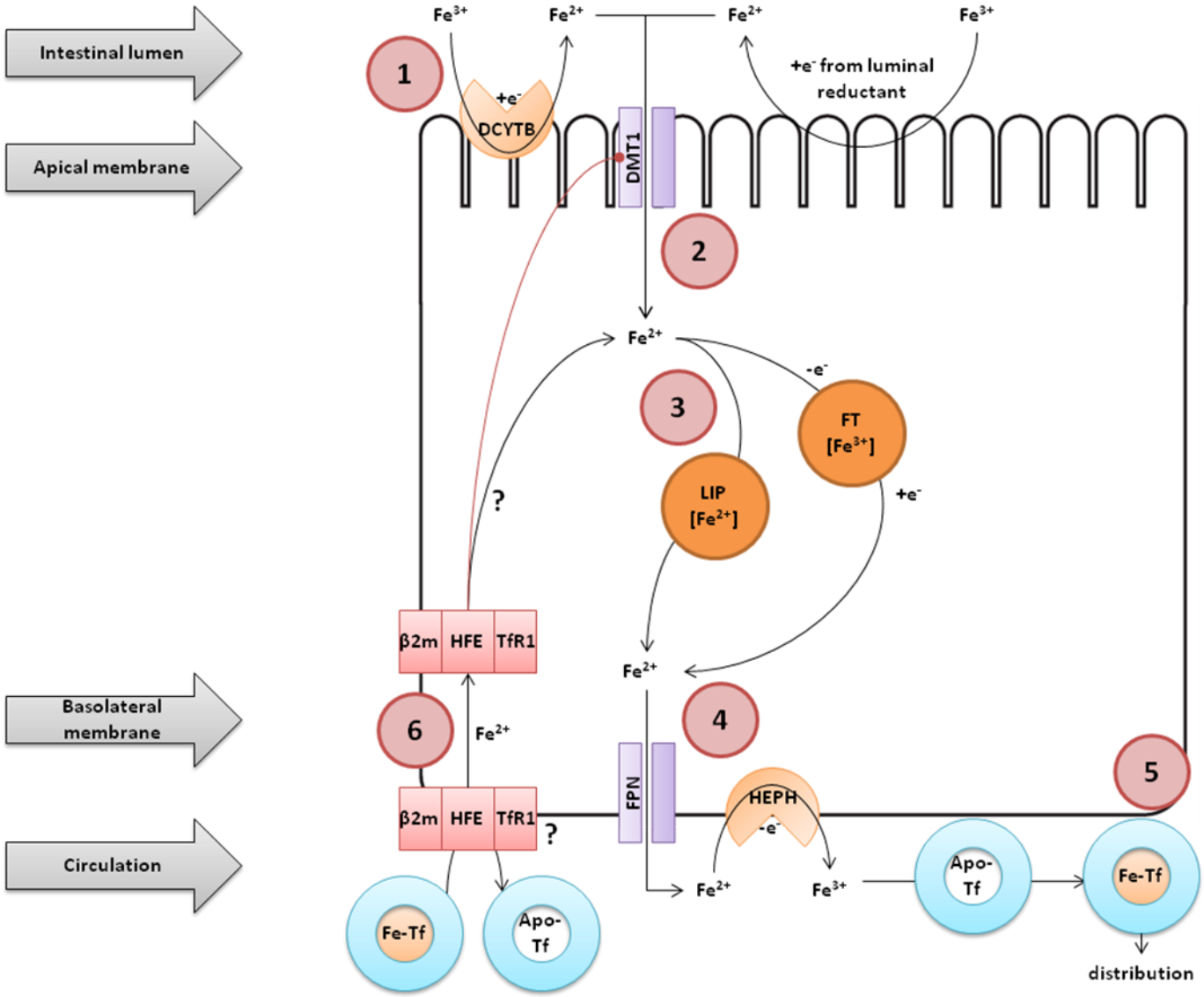

Figure 1.10. Transepithelial transport of dietary non-haem iron across enterocytes. **1)** Luminal Fe^{3+} is reduced by luminal reductants or by apical reductase DCYTB. **2)** Fe^{2+} is influxed as a substrate for DMT1. **3)** Fe^{2+} will become part of the intracellular pool of iron. **4)** Fe^{2+} is effluxed via FPN and oxidised by HEPH. **5)** Fe^{3+} is bound to Tf for systemic distribution. **6)** The HFE−TfR1-β2m complex is thought to inhibit Fe absorption by re-routing Fe from Tf or by inhibiting apical DMT1-mediated uptake. DCYTB: duodenal cytochrome B reductase; DMT1: divalent metal ion transporter 1; HFE: haemochromatosis protein; FPN: ferroportin; HEPH: hephaestin; Tf: transferrin; TfR: transferrin receptor; FT: ferritin; LIP: labile iron pool. Adapted from various sources (e.g. Han *et al*, 1995; McKie *et al*, 2001; De Domenico *et al*, 2007a).

1.3.2 Maintaining iron homeostasis

Several factors are involved in the regulation of iron uptake, such as the interaction with other metals, vitamins and flavonoids. Molecular factors such as protein interactions and systemic factors such as feedback signals from body iron stores also contribute to this homeostatic control. The effects of ascorbate and flavonoids on iron uptake are discussed in **Section 1.5.2** and in **Chapter 5**. This section reviews briefly the systemic and molecular factors that influence iron homeostasis to maintain body levels and distribution as in **Figure 1.11**.

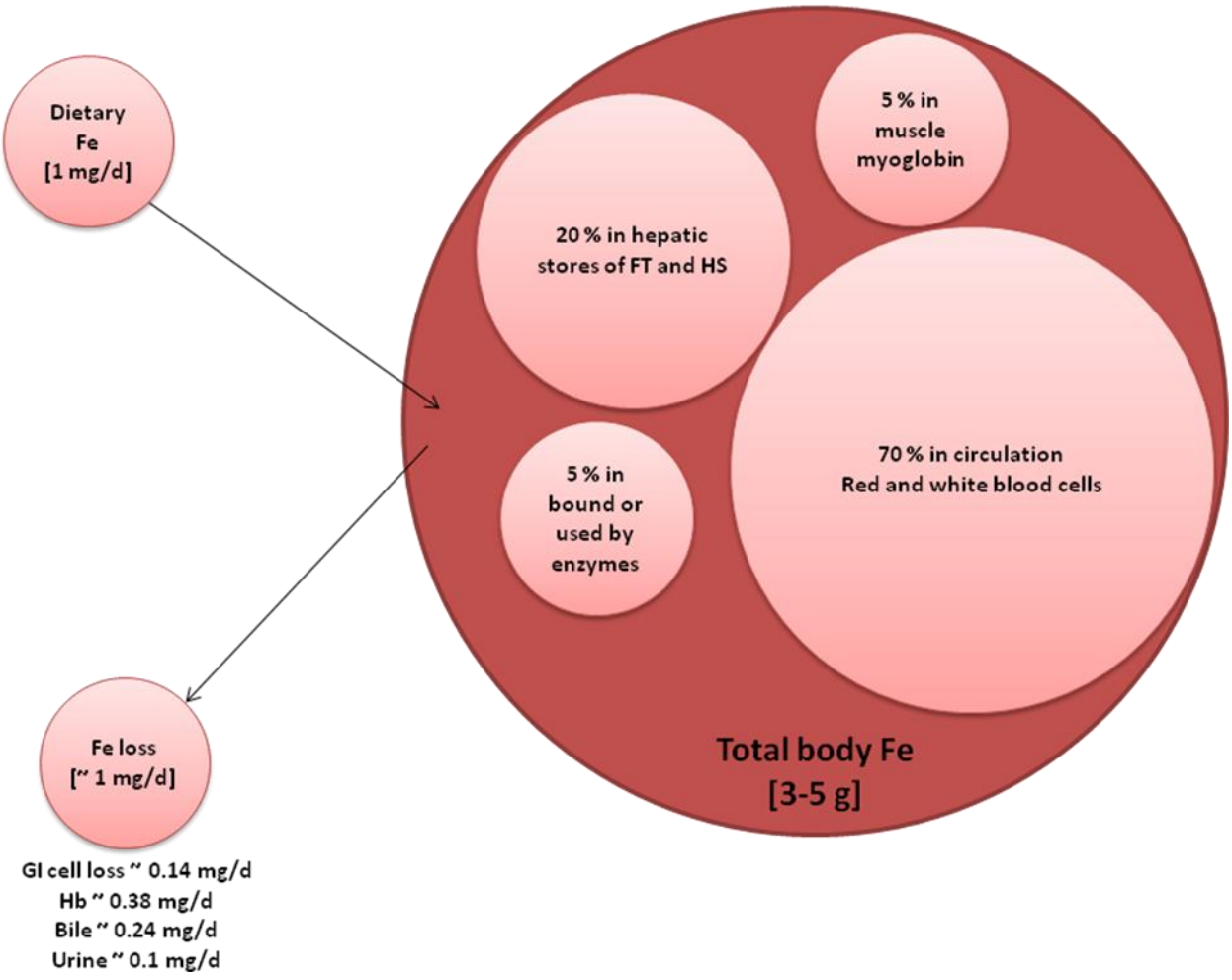

Figure 1.11. Typical distribution and use of total body iron. FT: ferritin; HS: haemosiderin (Geissler & Powers, 2005).

The systemic regulation of iron is very much dependent on increasing or restricting iron uptake and absorption (Yamaji *et al*, 2004; Wang & Pantopoulos, 2011). Hepcidin, a hepatically expressed peptide, negatively regulates enterocytic iron transport into the body by inhibition of DMT1-mediated uptake or by inducing the internalisation and degradation of FPN (Nemeth *et al*; 2004; De Domenico *et al*, 2007b). Hepcidin also acts on macrophages. When levels of hepcidin are high macrophages retain iron, as FPN is not available to release cellular iron. Low hepcidin levels will cause macrophages to readily release iron (Chaston *et al*, 2008). Hepcidin is abundantly expressed following iron intake and during inflammation. In contrast, hepcidin levels decrease in states of iron deficiency, anaemia and hypoxia (Wang & Pantopoulos, 2011). HFE and TfR2 are proteins also thought to be necessary for the iron dependent activation of hepcidin. However, their mode of action remains unclear (reviewed by Lee & Beutler, 2009). See **Figure 1.12** for a summary of the systemic regulation of body iron and the involvement of hepcidin.

Other molecules involved in the cellular regulation of enterocytic iron uptake include HFE and TfR1; both of these are highly expressed in crypt cells (Anderson *et al*, 1990; Parkkila *et al*, 1997). The precise mechanism through which HFE regulates iron absorption has not been thoroughly characterised. However, it is thought to be mediated through formation of the HFE-β_2m-TfR1 complex. Formation of this complex either decreases the affinity of Tf for TfR1, or reduces TfR1 cycling-time (Feder *et al*, 1998; Ikuta *et al*, 2000). The formation of the HFE-β2m-TfR1 complex is sensitive to the whole body iron pool in a feedback loop between hepatic hepcidin and the intestinal epithelium (Brissot *et al*, 2004).

HFE may also be a direct negative regulator of DMT1, by a hypothesised interaction between DMT1 and the HFE-β_2m-TfR1 complex causing decreases in apical iron

uptake (Arredondo *et al*, 2001; Arredondo *et al*, 2006). It has been found that HFE transfected Caco-2 cells have a decreased labile iron pool and cellular iron content, whilst apical iron uptake is decreased independently of DMT1 expression. Furthermore, DMT1 expression increases in Caco-2 cells transfected with HFE, therefore making HFE as a primary rate-limiting protein of iron uptake (Arredondo *et al*, 2001).

Transcriptome analysis of differentiating Caco-2 cells indicates variability in several of the genes mentioned above during stages of differentiation (Bédrine-Ferran *et al*, 2004). As HFE is expressed in crypt cells, which are undifferentiated epithelial tissue, it was hypothesised that HFE expression (among other genes) will be responsive to body iron stores throughout the differentiation process (Bédrine-Ferran *et al*, 2004). Indeed in the study by Bédrine-Ferran *et al* (2004), HEPH, DMT1, FPN, and Tf were all up-regulated during differentiation. It is possible therefore that HFE may be part of a signal transduction cascade that will dictate the iron uptake capacity of mature villi enterocytes (Bédrine-Ferran *et al*, 2004).

Given the regulatory mechanisms in place for the absorption of iron, there are no known mechanisms for the regulated disposal of excess body stores of iron. The only known processes are the unregulated exfoliation of cells, such as intestinal epithelial cells, and through menstrual bleeding. Therefore, regulating the iron absorption process is the most important aspect in maintaining body iron stores within normal levels.

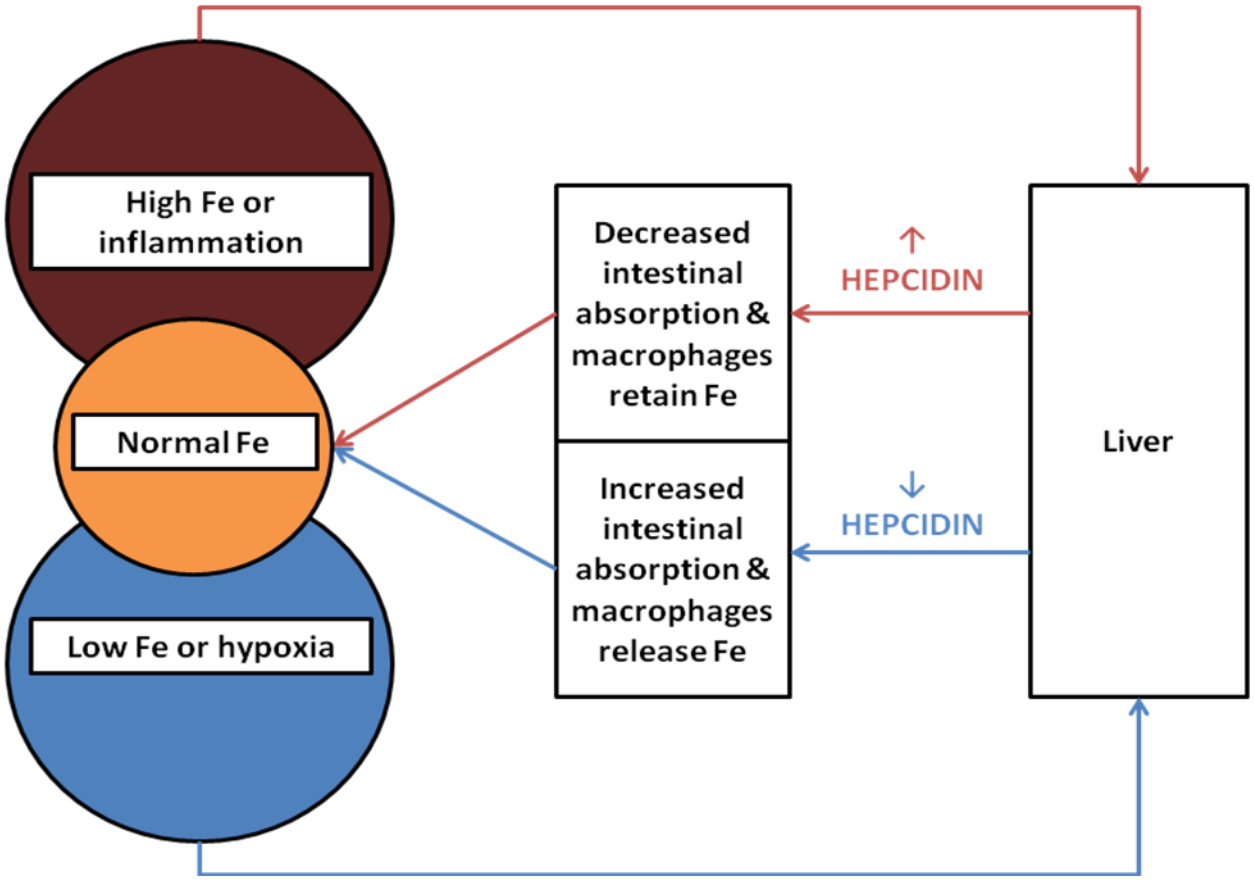

Figure 1.12. The systemic regulation of iron homeostasis. Hepcidin is a key regulator of iron homeostasis. During states of high iron, hepcidin levels increase; this signals the degradation of macrophage ferroportin and limits the intestinal release of iron from what is absorbed from the diet. When sates of iron are low this signals a decrease in hepcidin levels thus increasing intestinal release of iron into the body and allowing macrophages to readily release iron.

1.4 Dietary copper

Copper is an essential trace element in the human body and has multiple functions for example forming parts of proteins and enzymes (e.g. Cu-Zn superoxide dismutase, ceruloplasmin, hephaestin). Copper deficiency can have detrimental effects including iron anaemia, impaired growth and osteoporosis. Copper overload can be toxic and is often a consequence of genetic abnormalities such as Wilson's or Menke's disease. Both uptake and excretion of copper is tightly regulated, mainly through the hepatointestinal pathways. This section discusses the enterocytic role in copper uptake and the main regulatory mechanisms in maintaining body copper levels. Dietary copper can also interact with other nutrient such as flavonoids; this is discussed in more detail in **Section 1.5.2** and in **Chapter 6**.

1.4.1 Copper uptake and transepithelial transport

Copper can be apically absorbed into enterocytes via copper transporter1 (CTR1) in its reduced form. Alternatively, both cupric and cuprous copper might be substrates for DMT1 (Gunshin *et al*, 1997, Lee *et al*, 2002; Arredondo *et al*, 2003). Copper is reduced through interaction with the Steap proteins, DCYTB or other reducing agents (Wyman *et al*, 2008; Ohgami *et al*, 2006). Cellular copper must then be bound to a chaperone molecule, such as antioxidant protein 1 (HAH1) (Walker *et al*, 2002). HAH1 delivers copper to the copper transporting ATPase ATP7A which can export copper or utilise it in the trans-Golgi network, the site of enzyme cupration (Petris & Mercer, 1999; Hamza *et al*, 2003). Another copper transporting ATPase found in enterocytes is ATP7B (Yamaguchi *et al*, 1996). The role of ATP7B in intestinal cells is unclear, though it is thought to be involved in copper delivery to HEPH, cupration of other metalloenzymes and copper efflux (Walker *et al*, 2002; Lörinczi *et al*, 2008). A schematic representation of the transport pathway of copper through enterocytes is detailed in **Figure 1.13**.

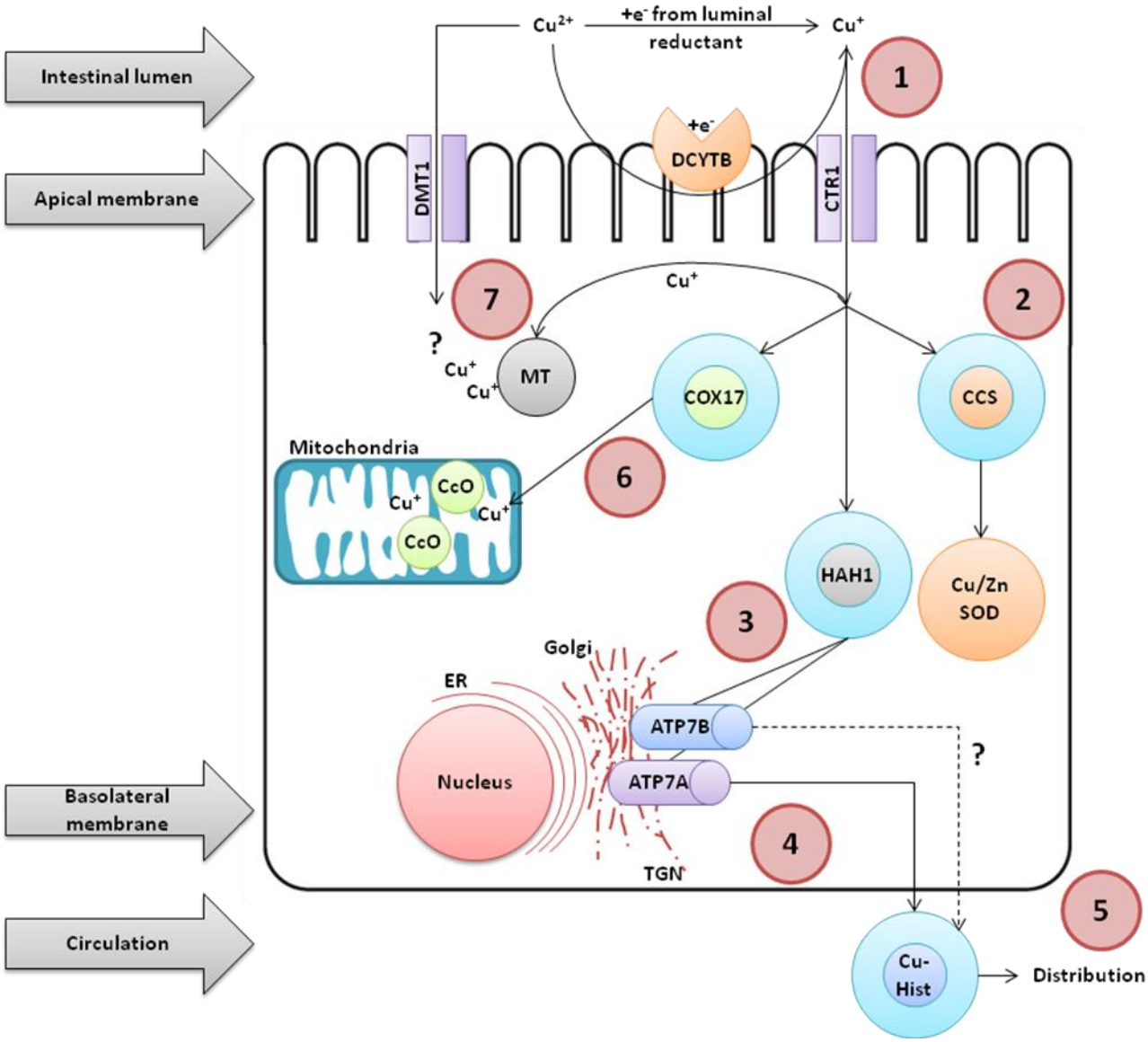

Figure 1.13. Intestinal transport of dietary copper through enterocytes. **1)** Cu^{2+} is reduced by luminal reductants or by apical reductase activity (e.g. DCYTB) and influxed by CTR1 and bound to an intracellular chaperone. **2)** Copper bound to CCS is delivered to Cu/Zn-SOD. **3)** Copper bound to HAH1 is delivered to ATP7A or ATP7B which will function to cuprate metalloenzymes in the TGN. **4)** ATP7A (and possibly ATP7B) will efflux copper at the basolateral membrane. **5)** Effluxed copper is bound to histidine (Hist) for systemic distribution. **6)** Copper that is bound to COX17 will enter the mitochondria and is incorporated into CcO. **7)** DMT1 has been shown to influx copper, however with an unknown destination; such excess copper can be reversibly bound by MT. DMT1: divalent metal ion transporter 1; CTR1: copper transporter 1; HAH1: antioxidant protein 1; ATP7A and ATP7B: copper transporting ATPases, α and β polypeptides, respectively. TGN: trans-Golgi network. ER: Endoplasmic reticulum; Cu/Zn-SOD: Copper/Zinc-superoxide dismutase; CCS: Copper chaperone for superoxide dismutase. CcO: cytochrome C oxidase; COX17: CcO copper chaperone; Cu-Hist: copper histidine; MT: metallothionein. Adapted from various sources. (e.g. Yamaguchi *et al*, 1996; Gunshin *et al*, 1997; Lee *et al*, 2002)

1.4.2 Maintaining copper homeostasis

The general homeostatic regulation of copper balance is well known, for example intestinal copper absorption is not only influenced by total body copper status but also by the copper content of the meal. For example, *in-vitro* copper depletion of Caco-2 enterocytes resulted in higher transport, whereas high oral doses in rat pups result in decreased absorption and increased intestinal retention (Zerounian *et al*, 2003; Bauerly *et al*, 2005; Lönnerdal, 2008). The more molecular events and mechanisms that coordinate copper balance are complex and are described below.

1.4.2.1 Copper uptake, storage and toxicity

The enterocytic regulation of copper uptake is the first step in limiting dietary copper availability. Important regulatory proteins include CTR1, ATP7A, ATP7B and HAH1 (Lönnerdal, 2008). For example, CTR1 knockout mice exhibit neonatal defects with peripheral tissue copper accumulation, cardiac hypertrophy; impaired growth and hepatic iron overload (Nose *et al*, 2006). Hepatic iron overload is a consequence of CTR1 knockout because ferroxidases (hephaestin or ceruloplasmin) are cuproenzymes necessary for iron efflux; thus a cellular deficiency in copper will impede the formation and function of these ferroxidases. In CTR1 knock-out mice there is still some accumulation of copper, which indicates alternative uptake pathways. These pathways include DMT1-mediated uptake, paracellular uptake and pinocytosis (Arredondo *et al*, 2003; Nose *et al*, 2006). HAH1 knockout mice show poor survival, growth failure and high levels of intracellular copper, indicating defects in copper efflux and impaired delivery to secretory pathways (Hamza *et al*, 2001).

Copper loading in Caco-2 cells causes no change in the expression of CTR1. CTR1 is however endocytosed whilst metallothionein (MT) expression is increased. MT is

a metal-binding protein heavily involved in the regulation of metal-induced oxidative stress. Although the regulation of MT can be independent of copper status, the increased expression at higher levels of copper treatment is a mechanism of enterocytic copper retention, thus preventing systemic copper toxicity (reviewed by Lönnerdal, 2008).

1.4.2.2 Copper handling and efflux: the copper transporting ATPases

Other essential genes in the cellular metabolism of copper are ATP7A and ATP7B; both of which encode the copper transporting ATPases. They are particularly important for the cupration of membrane bound and/or secreted proteins. ATPases utilise energy from ATP hydrolysis to carry out their role in transporting copper from the cytosol to the lumen of intracellular compartments such as the endoplasmic reticulum or Golgi network. It is within these compartments that cupration of enzymes occur (reviewed by Lutsenko *et al*, 2007).

Copper transporting ATPases are found mainly within the apical membranes of polarised cells or in the trans-Golgi network. However, they are also localised in small amounts along the secretory pathway for subsequent remetallation and phosphorylation of secreted enzymes (Veldhuis *et al*, 2009; White *et al*, 2009). Some cells will contain both ATP7A and ATP7B, indicating another level of homeostatic regulation. It is not known whether the same biochemical factors regulate both ATPases, or whether different forms of copper will bind preferentially to either one. Some studies have suggested that ATP7B is a slower transporter of copper than ATP7A (reviewed by Lutsenko *et al*, 2007).

ATP7A is required for the formation of numerous enzymes including tyrosinase, peptidyl-α-monooxygenase, superoxide dismutase and lysyl oxidase (Petris *et al*, 2000; Tchaparian *et al*, 2000; Qin *et al*, 2006). ATP7B is required for the formation

of the copper-dependant ferroxidase holoceruloplasmin (Terada *et al*, 1998). ATP7B expression is tissue specific to some degree. For example, the main role of ATP7B in hepatocytes is to facilitate the export of copper. This function of ATP7B is of crucial importance as the liver is the primary organ responsible for copper homeostasis, for example transporting excess copper into bile for subsequent faecal excretion (Tao *et al*, 2003).

Studies into the cellular responses to copper depletion have found that the copper transporting ATPases will relocalise to the site of enzyme metallation (Petris *et al*, 1996). Indeed expression of these ATPases will increase, decrease or relocalise in response to copper supply, hormonal signaling or other unknown events (Schlief *et al*, 2005; Kelleher & Lönnerdal, 2006). Very little is known regarding the molecular regulation of the proteins and genes involved in the copper uptake pathway. However, it is known that degradation of some of these proteins is copper dependent whereas their mRNA expression appears to be copper independent (Bertinato & L'Abbé, 2004; Nose *et al*, 2010).

1.5 Flavonoids and nutrient interactions

As flavonoids are abundant in the human diet and are known to interact with nutrients, the modulatory effects of flavonoids on nutrient availability are proposed to be a major physiological consequence of their consumption (Park, 1999; Cermak *et al*, 2004; Ma *et al*, 2010). The following sections will briefly discuss the interaction of polyphenolic flavonoids with the nutrients that are the focus of this thesis, namely glucose, iron and copper.

1.5.1 Dietary glucose and flavonoid interactions

In diabetic states pharmacologic interventions to modulate glucose homeostasis are mainly used in conjunction with optimised lifestyle and dietary management. Regarding the latter, establishing the therapeutic properties of naturally occurring flavonoids will potentially reduce the reliance on pharmacological interventions which are often characterised by unwanted side effects (Cheng & Fantus, 2005; Martinuea *et al*, 2006).

The glycosylated flavonoid phloridzin, abundantly found in apples, is the classic and specific inhibitor of SGLT1-mediated glucose uptake (Alvarado & Crane, 1962; Alvarado, 1967). Studies using Caco-2 cells have found that other glycosylated flavonoids such as neohesperidin and quercitin glucosides also elicit a similar and SGLT1-specific inhibition of glucose uptake (Gee *et al*, 1998; Wolffram *et al*, 2002; Johnston *et al*, 2005). In contrast, aglycone flavonoids are known to selectively inhibit GLUT-mediated transport of glucose. The classical inhibitor of GLUT2 is phloretin, the aglycone counterpart of phloridzin (Johnston *et al*, 2005; Kwon *et al*, 2007). Flavonols, flavones, isoflavones and anthocyanidins (e.g. quercetin, apigenin, daidzein and cyanidin, respectively) have all also been shown to modulate glucose uptake in U937 monocytes (Park, 1999).

Through numerous studies, the structural characteristics of flavonoids that potently inhibit glucose uptake have been identified. These appear to be flavones or flavonols with hydroxylation of the C-5 and/or C-7 positions. Furthermore, there have been attempts to distinguish mechanisms of inhibition. Inhibition of glucose uptake in a U937 model was shown to be mainly sodium-independent and competitive for GLUT-mediated transport (Park, 1999). Inhibition of GLUT2-mediated glucose uptake has been shown to be specific, reversible and non-competitive in other studies investigating the effects of quercetin and isoquercetin (Kwon *et al*, 2007). These aforementioned studies investigated glucose uptake in transfected *Xenopus laevis* oocytes, GLUT2 over-expressing pituitary cells and Caco-2 cells (Kwon *et al*, 2007). In adipocytes and myoblasts, blueberry root and fruit, stem and leaf extracts were shown to enhance basal and insulin-stimulated glucose uptake. Interestingly, the fruit extract from blueberries was the only part of the plant to contain anthocyanins, which had specific inhibitory properties on glucose uptake (Martineau *et al*, 2006).

Several mechanisms have been proposed to explain the inhibitory effects of flavonoids on glucose uptake. These include, for example, competitive inhibition and steric hindrance due to the structural similarities between monosacharides and flavonoid functional groups. For example, glucose moieties on flavonoids may bind to hexose binding sites on glucose transporters thus inhibiting monosaccharide influx. Conversely, a separate binding site for flavonoids may be present on a glucose transporter, preventing glucose binding due to steric hindrance. Alternatively, there may be molecular interactions of flavonoids directly with cell membranes, affecting transporter function (Nakayama *et al*, 2000). Furthermore, flavonoids may influence the redox state of certain nutrients such as copper and iron; the latter of which influences glucose uptake (Ren *et al*, 2008; Lekka *et al*, 2009). It

is well known that flavonoids are powerful reducing agents, this will reduce iron and copper, and these reduced forms of the metals are preferentially absorbed due to their solubility. In light of this, solubility of iron, and therefore its absorption, can be dependent on the proportion of monosacharides present in the diet, e.g. fructose lowers the solubility of dietary iron relative to glucose (Brouwer *et al*, 1993). Finally, interactions between flavonoids and metals, may initiate the competitive inhibition of glucose transporters. The formation of metal polyphenol complexes have been shown to initiate the use of a GLUT-type transporter for metal shuttling out of epithelial cells (Vlachodimitropoulou *et al*, 2010b). There is also the possibility that flavonoids may cause transcriptional and/or translational effects that influence glucose transport, though this has not been investigated in detail (Miyamoto *et al*, 1993; Oliveira *et al*, 2008). Given these numerous interactions between dietary flavonoids, metals and glucose it is not surprising to assume a much more important role of flavonoids may be in modifying the absorption of nutrients, rather than a main role strictly as a systemic antioxidant.

1.5.2 Interactions of flavonoids, iron and copper

There have been numerous studies investigating the interaction between dietary metal bioavailability, cellular metabolism and interactions with polyphenols. These studies have included epidemiological data, *in-vivo* and *in-vitro* investigations in both man and animals. For example, dietary iron is significantly influenced by vitamin C, flavonoids and presence of other dietary metals such as zinc, manganese, lead and, of relevance to this thesis, copper (Mira *et al*, 2002; Teucher *et al*, 2004; Reeves *et al*, 2005; Thumser *et al*, 2010).

With regards to vitamin C, this reducing agent increases iron uptake by forming transportable iron-ascorbate complexes (Thumser *et al*, 2010). Flavonoids will also

influence the bioavailability of iron through the formation of polyphenol-metal complexes (Kim *et al*, 2008; Ren *et al*, 2008*;* Vlachodimitropoulo *et al*, 2010b). Specifically, green tea flavonoids have been shown to decrease enterocyte transepithelial iron transport by limiting basolateral release (Kim *et al*, 2008).

Dietary factors that affect copper status are similar to those for iron, such as the presence of vitamin C (Kuo *et al*, 2004). Furthermore, copper can form a complex with flavonoids, similar to that formed by iron (Lekka *et al*, 2009). In light of this, it cannot be ruled out that these interactions will induce similar effects on the transport of copper as they do to iron, if inhibitory mechanisms are to be based on the structural interactions. Whilst numerous studies have investigated the physiological basis of copper transport, many molecular mechanisms remain to be elucidated.

Copper and iron metabolism are also known to be intertwined. The genes that are integral to copper transport are not overtly regulated by their substrate (Tennant *et al*, 2002; Nose *et al*, 2010). Their transcription is more sensitive to the presence of iron (Collins, 2006; Collins *et al*, 2009). However, copper is able to induce post-translational modifications of the proteins involved in its uptake (Tallkvist *et al*, 2000; Bertinato & L'Abbé, 2004).

Furthermore, iron homeostasis can essentially be regulated by copper in three ways. Firstly, copper is a constituent of key iron regulatory proteins such as HEPH and ceruloplasmin (Eisentstein, 2000). Thus copper deficiency can lead to iron deficiency anaemia. Secondly, copper presents competition for iron at the DMT1 iron binding site (Tennant *et al*, 2002, Arredondo *et al*, 2003). Thirdly, copper loading is known to influence expression of DMT1 and FPN, proteins that coordinate iron uptake and release, respectively (Tennant *et al*, 2002).

1.6 Hypothesis and aims of this thesis

We hypothesised that dietary berry flavonoids are capable of modulating intestinal transport of glucose, iron and copper via functional, transcriptional and translational mechanisms.

To address this we investigated the effects of dietary flavonoids in the form a flavonoid-rich berry extract on intestinal epithelial Caco-2 cells.

This thesis is divided into four parts with the following aims:

1. To evaluate the effects of dietary berry flavonoids on the global gene expression profile of enterocytes. From this study we identified areas of interest for further investigation.

2. To characterise the transcriptional, translational and functional effects of dietary berry flavonoids on glucose uptake processes in human intestinal epithelial Caco-2 cells.

3. To characterise the transcriptional, translational and functional effects of dietary berry flavonoids on iron transport processes in human intestinal epithelial Caco-2 cells.

4. To characterise the transcriptional, translational and functional effects of dietary berry flavonoids on copper uptake processes in human intestinal epithelial Caco-2 cells.

CHAPTER TWO

Materials and methods

2 Materials and methods

2.1 Materials

The following sections will list the reagents, equipment, software and commercial suppliers.

2.1.1 Materials used in Caco-2 cell culturing and flavonoid treatments

The Caco-2 TC7 cell line expresses the necessary proteins for transport of glucose, iron and copper, has been previously characterised and applied as a successful model of the intestinal epithelium (Mahraoui *et al*, 1994; Bédrine-Ferran et al, 2004; Sun *et al*, 2008). The Caco-2 cells and many of the ensuing protocols were provided by the laboratory of Dr. Paul Sharp (Diabetes and Nutritional Sciences Division, King's College London, UK). For reagents and composition of cell culture media see **Table 2.1**. For reagents and composition of treatments see **Table 2.2**. For reagents used in cell subculturing and viability testing see **Table 2.3**. For consumables and equipment used in cell culture see **Table 2.4**.

Table 2.1. Reagents, composition and suppliers of Caco-2 cell culture media.

Reagent	Concentration in complete media (% v/v)	Concentration in serum- free media (% v/v)	Product details/ Supplier
Antibiotics	1	1	15140122, Invitrogen Life Technologies, Paisley UK
DMEM	86.8	97	41965062, Invitrogen Life Technologies, Paisley UK
FBS	10	-	F9665-500ML, Sigma, Dorset, UK
L-glutamine	1	1	25030024, Invitrogen Life Technologies, Paisley UK
NEAA	1	1	11140035, Invitrogen Life Technologies, Paisley UK
Plasmocin™	0.2	-	Source BioScience LifeSciences, Nottingham, UK

DMEM: Dulbecco's modified Eagle medium; FBS: Foetal bovine serum; NEAA: non-essential amino acids

Table 2.2. Reagents, composition and suppliers for Caco-2 cell treatments.

Reagent	Final concentration	Product details/ Supplier
Berry extract	0.125 % (w/v)	Optiberry®, InterHealth Nutraceuticals, USA
Quercetin	100 µM	Q4951-10G, Sigma, Dorset, UK
Phloretin	100 µM	P7912-250MG, Sigma, Dorset, UK
Phloridzin	100 µM	274313-5G, Sigma, Dorset, UK
DMSO	0.05 % (v/v)	D1435-500ML, Sigma, Dorset, UK

All reagents were diluted in DMEM for gene expression, or protein abundance analysis, or were diluted into relevant buffers for functional investigations. DMSO: dimethyl sulfoxide. DMEM: Dulbecco's modified Eagle medium.

Table 2.3. Reagents used for Caco-2 cell subculturing and viability testing.

Reagent	Product details/ Supplier
Trypan blue dye	T6146-100G, Sigma, Dorset, UK
PBS	BR0014G, Oxoid, Hants, UK
TrypLE™	0040090DG, Invitrogen Life technologies, Paisley UK

PBS: phosphate buffered saline.

Table 2.4. Consumables and equipment used in Caco-2 cell culture.

Consumables/Equipment	Product details/Supplier
Air cabinet	Airtech Class2, Howorth, Bolton, UK
Glass pipettes (5-10 ml)	CLS4487, CLS4488, Sigma, Dorset, UK
Cell scraper	CLS3010, Sigma, Dorset, UK
Centrifuge	5810R, Eppendorf, Cambridge, UK
CO_2 incubator	MCO-36AC, Sanyo, CA, USA
Cover slips	631-1566, VWR, PA, USA
Disposable filters (0.2 µM)	Minisart®, Sartorius Stedim Biotech, France
Falcon tubes (15-50 ml)	210261, Grenier Bio One, Gloucestershire, UK
Flasks (T-25/T-75)	690/658175, Grenier Bio One, Gloucestershire, UK
Haemocytometer	CM175-20, Sigma, Dorset, UK
Needles	305115, BD, NJ, USA
Pipette controller	E4866-0021, Starlab UK Ltd, Milton Keynes, UK
Plates (6-12 well)	CLS3516, Sigma, Dorset, UK
Syringes (20-50 ml)	309628, BD, NJ, USA
Upright light microscope	Eclipse TS100, Nikon Instruments Inc., NY, USA
Waterbath	W14, Grant, Cambridgeshire, UK
Transwell® inserts	TKT-526-010M, Fisher Scientific, Leicestershire, UK

2.1.2 Materials used in Caco-2 cell RNA isolation and quantification

This section lists materials used for RNA isolation, integrity analysis and quantification protocols. For reagents used in RNA isolation see **Table 2.5**. RNA was quantified using a NanoDrop spectrophotometer (Thermo Fisher Scientific, Leicestershire, UK). RNA integrity was quantified using the 2100 BioAnalyzer (Agilent, Cheshire, UK) with the RNA 6000 Nano Kit (Agilent, Cheshire, UK). For consumables and equipment used in RNA integrity and quantification see **Table 2.6**.

Table 2.5. Reagents, consumables and equipment for Caco-2 cell RNA isolation, quantification and integrity analysis.

Reagents/Consumables	Product details/Supplier
Ethanol	34963-2.5L, Sigma, Dorset, UK
Chloroform	25668, Sigma, Dorset, UK
Nuclease-free water	AM9937, Applied Biosystems, Cheshire, UK
Propan-2-ol	P/7509/17, Fisher Scientific, Leicestershire, UK
TRIzol® reagent	15596026, Invitrogen Life Technologies, Paisley UK

Table 2.6. Consumables and equipment for RNA isolation and integrity analysis.

Consumables/Equipment	Product details/Supplier
Temperature controlled centrifuge	Microlite RF, ThermoFisher, Hampshire, UK
Nuclease-free, extended-length, filtered tips	I1402-4300, Starlab UK Ltd, Milton Keynes, UK
Nuclease-free tubes (1.5-2 ml)	S1615-5510, Starlab UK Ltd, Milton Keynes, UK

2.1.3 Materials used in gene expression experiments

This section lists materials used for gene expression analysis. RNA was reverse transcribed using a high-capacity reverse transcription kit (Applied Biosystems, Cheshire, UK) in a thermal cycler (DNA Engine Tetrad PTC-225, Bio-Rad, Hertfordshire, UK). Global gene expression was quantified using Affymetrix HGU-133A GeneChip arrays (Affymetrix Inc., CA, USA). Affymetrix GeneChip arrays are a high-throughput platform for the analysis of global gene expression or transcriptome variation in samples. They are constructed of thousands of hybridised oligonucleotide probes and labeled with fluorescent tags. Such arrays allow the quantification of gene expression through template cDNA adherence to the probes and the concomitant detection of fluorescence. The specific expression of genes was quantified using quantitative real-time polymerase chain reaction (qRT-PCR). For qRT-PCR analysis, SYBR green was used as a DNA-binding dye with sequence specific primers. For reagents used in specific gene expression analysis and their suppliers see **Table 2.7**. For consumables and equipment used in gene expression analysis see **Table 2.8**.

Table 2.7. Reagents used for gene expression analysis

Reagent	Product details/Supplier
SYBR green DNA binding dye	4367659, Applied Biosystems, Cheshire, UK
Sequence specific primers	MWG Eurofins, London, UK
Nuclease-free water	AM9937, Applied Biosystems, Cheshire, UK
High Capacity Reverse Transcription Kit	4368814, Applied Biosystems, Cheshire, UK

Table 2.8. Consumables and equipment used in gene expression analysis

Consumables/Equipment	Product details/Supplier
96-well PCR plates	N8010560, Applied Biosystems, Cheshire, UK
Adhesive film applicator	4313663, Applied Biosystems, Cheshire, UK
Optical adhesive film	4360954, Applied Biosystems, Cheshire, UK
Optical compression pads	4313663, Applied Biosystems, Cheshire, UK
96-well plate-adaptable centrifuge	5804R, Eppendorf, Cambridge, UK
Nuclease-free, extended-length, filtered tips	3810, Starlab UK Ltd, Milton Keynes, UK
Nuclease-free microtubes (0.2 ml)	I1402-4300, Starlab UK Ltd, Milton Keynes, UK
Nuclease free tubes (1.5-2.0 ml)	S1615-5510, Starlab UK Ltd, Milton Keynes, UK
Sequence detection system	ABI Prism® 7700 sequence detection system, Applied Biosystems, Cheshire, UK
Thermal cycler	DNA engine tetrad PTC-225, Bio-Rad, Hertfordshire, UK

2.1.4 Materials used in Caco-2 cell protein isolation and quantification

This section lists materials used in protein isolation and quantification. For a list of the reagents used, see **Table 2.9**. For the composition of the cell lysis buffer and sample loading buffer, see **Table 2.10** and **Table 2.11**, respectively. For sodium dodecyl sulphate-polyacrylamide gel electrophoresis (SDS-PAGE) running buffer, see **Table 2.12** and for the nitrocellulose membrane semi-dry transfer buffer, see **Table 2.13**. For the polyacrylamide gel composition, see **Table 2.14**. For the composition of washing, blocking and stripping solutions, see **Table 2.15**, **Table 2.16** and **Table 2.17**, respectively. For the consumables and equipment used in protein isolation and quantification, see **Table 2.18**. Western blot membranes were excited using the Novex® ECL chemiluminescent substrate reagent kit (WP20005, Invitrogen life technologies, Paisley, UK) then developed on Kodak light film (Z370398-50EA, Sigma, Dorset, UK) with standard developing and fixing reagents (product numbers P7042 and P7167, Sigma, Dorset, UK).

Table 2.9. Reagents used in Caco-2 cell protein isolation and quantification

Reagent	Product details/Supplier
Acrylamide	A4058-100ML, Sigma, Dorset, UK
APS	215589-500G, Sigma, Dorset, UK
Bromophenol blue	B0126-25G, Sigma, Dorset, UK
Chemiluminescence agent	WP20005, Invitrogen Life Technologies, Paisley, UK
Developer	P7042, Sigma, Dorset, UK
Fixer	P7167, Sigma, Dorset, UK
Glycerol	G9012-100ML, Sigma, Dorset, UK
Glycine	94119-10G, Sigma, Dorset, UK
Non-fat powdered milk	Premier Foods, Windsor, UK
PBS	BR0014G, Oxoid, Hants, UK
Protease inhibitor	P8340-1ML, Sigma, Dorset, UK
Protein weight marker	SM0441, Fermentas Life Sciences, North Yorkshire, UK
SDS	ELR-428-010N, Fisher Scientific, Leicestershire, UK
TEMED	T9281-50ML, Sigma, Dorset, UK
Tris-base	648310-500GM, Merck chemicals Ltd. Nottingham, UK
Tween 20	P5927-500ML, Sigma, Dorset, UK
β-mercaptoethanol	436024C, VWR international Ltd. Leicestershire, UK

PBS: phosphate buffered saline; SDS: sodium dodecyl sulphate; APS: ammonium persulphate; TEMED: tetramethylethylenediamine.

Table 2.10. Composition of Caco-2 cell lysis buffer

Reagent	Concentration
PBS	50 mM
Protease inhibitor	1% (v/v)
SDS*	0.1% (w/v)

*SDS was excluded from cell lysis buffer when isolating membrane bound protein.
PBS: phosphate buffered saline; SDS: sodium dodecyl sulphate.

Table 2.11. Composition of 5X protein sample loading buffer

Reagent	Concentration
Bromophenol blue	0.1% (v/v)
Glycerol	25% (w/v)
SDS	2% (v/v)
β-mercaptoethanol	5% (v/v)

SDS: sodium dodecyl sulphate.

Table 2.12. Composition of 10X SDS-PAGE running buffer

Reagent	Concentration (g/L)
Glycine	142.00
SDS	10.00
Tris-base	30.28

SDS: sodium dodecyl sulphate; SDS-PAGE: sodium dodecyl sulphate-polyacrylamide gel electrophoresis.

Table 2.13. Composition of 10X SDS-PAGE-membrane semi-dry transfer buffer*

Reagent	Concentration (g/L)
Glycine	36.25
SDS	4.63
Tris-base	72.50

*10X transfer buffer in Table 2.13 was diluted into a 20% (v/v) methanol solution to make the 1X transfer buffer. SDS: sodium dodecyl sulphate; SDS-PAGE: sodium dodecyl sulphate-polyacrylamide gel electrophoresis.

Table 2.14. Composition of polyacrylamide gels for protein electrophoresis

Reagent	Volume per gel		
	8% (v/v) acrylamide	10% (v/v) acrylamide	12% (v/v) acrylamide
Distilled water	4.40 ml	3.75 ml	3.10 ml
Tris (pH 8.8)	2.15 ml	2.15 ml	2.15 ml
40 % (w/v) acrylamide	1.65 ml	2.25 ml	2.85 ml
10 % (w/v) APS	82.5 µl	82.5 µl	82.5 µl
10 % (w/v) SDS	82.5 µl	82.5 µl	82.5 µl
TEMED	11.0 µl	11.0 µl	11.0 µl

APS: ammonium persulphate; SDS: sodium dodecyl sulphate; TEMED: tetramethylethylenediamine.

Table 2.15. Composition of washing solution and antibody incubation solution.

Reagent	Concentration
Non-fat powdered milk	1% (w/v)
PBS	1X
Tween 20	0.1 % (v/v)

PBS: Phosphate buffered saline.

Table 2.16. Composition of nitrocellulose membrane blocking solution.

Reagent	Concentration
Non-fat powdered milk	5% (w/v)
PBS	1X
Tween 20	0.1 % (v/v)

PBS: Phosphate buffered saline.

Table 2.17. Composition of nitrocellulose membrane stripping buffer.

Reagent	Concentration (% v/v)
10% (w/v) SDS	20
Distilled water	69.22
Tris (pH 6.8)	10
β-mercaptoethanol	0.78

SDS: sodium dodecyl sulphate.

Table 2.18. Consumables and equipment for protein isolation and quantification.

Consumables/Equipment	Product details/Supplier
Disposable gel cassettes	NC2015, Invitrogen Life Technologies, Paisley, UK
Exposure cassette	Molecular Dynamics, Fisher Scientific, Leicestershire, UK
Falcon tubes (50 ml)	210261, Grenier Bio One, Gloucestershire, UK
Homogeniser	Ultra Turrax T8, Sartorius Mechatronics Ltd., Epsom, UK
Light film	Z370398-50EA, Sigma, Dorset, UK
Needles	305115, BD, NJ, USA
Platform shaker	Innova 2100, 444-0541, VWR, PA, USA
Powerpack	Labosi Power 300, Fisher Scientific, Leicestershire, UK
Roller-mixer	Mixer SRT2, MIX1990, SLS, Nottingham, UK
Calibrated densitometer	GS-800™, BioRad Laboratories, Hertfordshire, UK
Semi-dry transfer blotter	TE77PWR, GE Healthcare, Buckinghamshire, UK
Syringes (1 ml)	309628, BD, NJ, USA
Well-combs	NC3510, Invitrogen Life Technologies, Paisley, UK
Microplate reader	Synergy HT, PJB-290-040A, Fisher Scientific, Leicestershire, UK
Safelight	Photax A safelight, Paterson photographic limited, West Midlands, UK
Electrophoresis tank	XCell Surelock™ Mini-cell, Invitrogen Life Technologies, Paisley, UK
Membrane-filter paper sandwiches	LC2001, Invitrogen Life Technologies, Paisley, UK

2.1.5 Materials used in nutrient uptake and transport studies

This section lists materials used in uptake and transport studies. For a list of reagents used, see **Table 2.19**. For the radionuclides and their suppliers, see **Table 2.20.** For the composition of the HEPES-buffered salt solution (HBSS) used for the glucose uptake experiments, see **Table 2.21**; this was made glucose-free and supplemented with D-glucose to initiate uptake. A sodium-free HBSS was also prepared with equimolar potassium salts for D-glucose uptake studies of sodium-independent glucose uptake pathways. For the composition of MES-buffered salt solution (MBSS) and HBSS used in iron transport experiments see **Table 2.22** and **Table 2.23**, respectively. The same HBSS buffer used for iron transport experiments was used for our copper uptake experiments. For consumables and equipment used in uptake and transport studies see **Table 2.24**.

Table 2.19. Reagents used in substrate uptake and transport studies.

Reagent	Product details/Supplier
Sodium chloride	424290010, Acros Organics, Geel, Belgium
Potassium chloride	P4504-500G, Sigma, Dorset, UK
Sodium phosphate	342483-500G, Sigma, Dorset, UK
Calcium chloride	06991-1KG-F, Sigma, Dorset, UK
Magnesium chloride	M8266-100G, Sigma, Dorset, UK
HEPES-salt	S11-001, Fisher Scientific, Leicestershire, UK
BSA	B6917-5X100MG, Sigma, Dorset, UK
D-glucose	15023021, Invitrogen Life Technologies, Paisley UK
Ascorbate	A4034-500G, Sigma, Dorset, UK
Ferrous sulphate	F8048-500G, Sigma, Dorset, UK
Copper chloride	203149, Sigma, Dorset, UK
Nitric acid 68 % (w/v)	225711, Sigma, Dorset, UK
Nitric acid (1 M)	35315, Sigma, Dorset, UK
MES-salt	M3058-100G, Sigma, Dorset, UK

HEPES: 4-(2-hydroxyethyl)-1-piperazineethanesulfonic acid; BSA: bovine serum albumin; MES: 2-(*N*-morpholino) ethanesulfonic acid.

Table 2.20. Radionuclides used in uptake and transport studies.

Radioisotopes	Chemical form	Product details/Supplier
^{55}Fe*	Ferric Chloride	NEZ043001MC, Perkin-Elmer, Bucks, UK
^{3}H†	D-glucose	NET100C001MC, Perkin-Elmer, Bucks, UK

*Diluted into $FeSO_4$: Ascorbate in a 1:10 molar ratio to give a final concentration of 1 µM:10 µM and activity of ~500,000 DPM/well. †Diluted into 20 mM D-glucose to give a final concentration of 1 mM glucose and activity of ~500,000 DPM/well.

Table 2.21. Composition of glucose free HEPES-buffered salt solution (HBSS) used in glucose uptake studies.

Reagent	Concentration (mM)
Sodium chloride*	140
Potassium chloride	5
Sodium phosphate*	1
Calcium chloride	1
Magnesium chloride	0.5
HEPES-salt	10
BSA	0.2% (w/v)

*Sodium-free buffer was made by replacing sodium salts with equimolar potassium salts. Buffered to pH 7.5; HEPES: 4-(2-hydroxyethyl)-1-piperazineethanesulfonic acid; BSA: bovine serum albumin.

Table 2.22. Composition of MES-buffered salt solution (MBSS) used in copper uptake and iron transport studies.

Reagent	Concentration (mM)
Sodium chloride	140
Potassium chloride	5
Sodium phosphate	1
Calcium chloride	1
Magnesium chloride	0.5
MES-salt	10
D-glucose	5

Buffered to pH 6.5; MES: 2-(*N*-morpholino) ethanesulfonic acid; BSA: bovine serum albumin.

Table 2.23. Composition of HEPES-buffered salt solution (HBSS) used in iron uptake and transport studies.

Reagent	Concentration (mM)
Sodium chloride	140
Potassium chloride	5
Sodium phosphate	1
Calcium chloride	1
Magnesium chloride	0.5
HBSS-salt	10
D-glucose	5
BSA	0.2 % (w/v)

Buffered to pH 7.5; HEPES: 4-(2-hydroxyethyl)-1-piperazineethanesulfonic acid; BSA: bovine serum albumin.

Table 2.24. Consumables and equipment used in radiolabelled substrate uptake and transport studies.

Consumables/Equipment	Product details/Supplier
Cell scraper	CLS3010, Sigma, Dorset, UK
Falcon tubes (15-50 ml)	210261, Grenier Bio One, Gloucestershire, UK
Needles	305115, BD, NJ, USA
Plate reader	Optima, Promega, CA, USA
Scintillation counter	LS6500, Beckman-Coulter, High Wycombe, UK
Scintillation vials	BOT15, KCL Central Stores, London, UK
Syringes (1 ml)	309628, BD, NJ, USA
Transwell® inserts	TKT-526-010M, Fisher Scientific, Leicestershire, UK
Tubes (1.5-2.0 ml)	S1615-5510, Starlab UK Ltd, Milton Keynes, UK

2.1.6 Analysis software

This section lists the software used for the experiments in this thesis **Table 2.25**.

Table 2.25. Software applied in research.

Software	Application/s	Source/references
GCOS	Microarray normalisation and filtering	Affymetrix Inc. CA, USA
GraphPad Prism® 5	Data analysis and figures	GraphPad software, CA, USA
Primer3	Primer design	Rozen & Skaletsky, 2000
IPA	Pathway analysis	Maaser & Borlak, 2008; Ingenuity® systems Inc. CA, USA
DAVID	Clustering and gene ontology	Huang da *et al*, 2009; Dennis *et al*, 2003
QuantityOne®	Densitometry	BioRad Laboratories, Hertfordshire, UK
SDS software	Gene expression analysis	Applied Biosystems, Cheshire, UK
Microsoft office package	Word processing, data analysis and formatting	Microsoft corporation, WA, USA

DAVID: Database for annotation, visualisation and integrated discovery; GCOS: GeneChip operating software; IPA: Ingenuity® pathway analysis; SDS: sequence detection system.

2.2 Methods

2.2.1 General study design

Global gene expression microarray analysis was initially carried out to identify genes and pathways of interest for further investigation. Two groups (i.e. control and treated) were used to identify effects of a flavonoid-rich berry extract on transcriptome variation in Caco-2 cells. Six RNA samples from each of the separate groups were pooled for use on two separate microarray chips (**Figure 2.1**).

Following microarray analysis, target genes and pathways of interest were selected for further investigation by qRT-PCR and Western blotting. Finally, functional effects were quantified with nutrient uptake and transport assays (**Figure 2.2**).

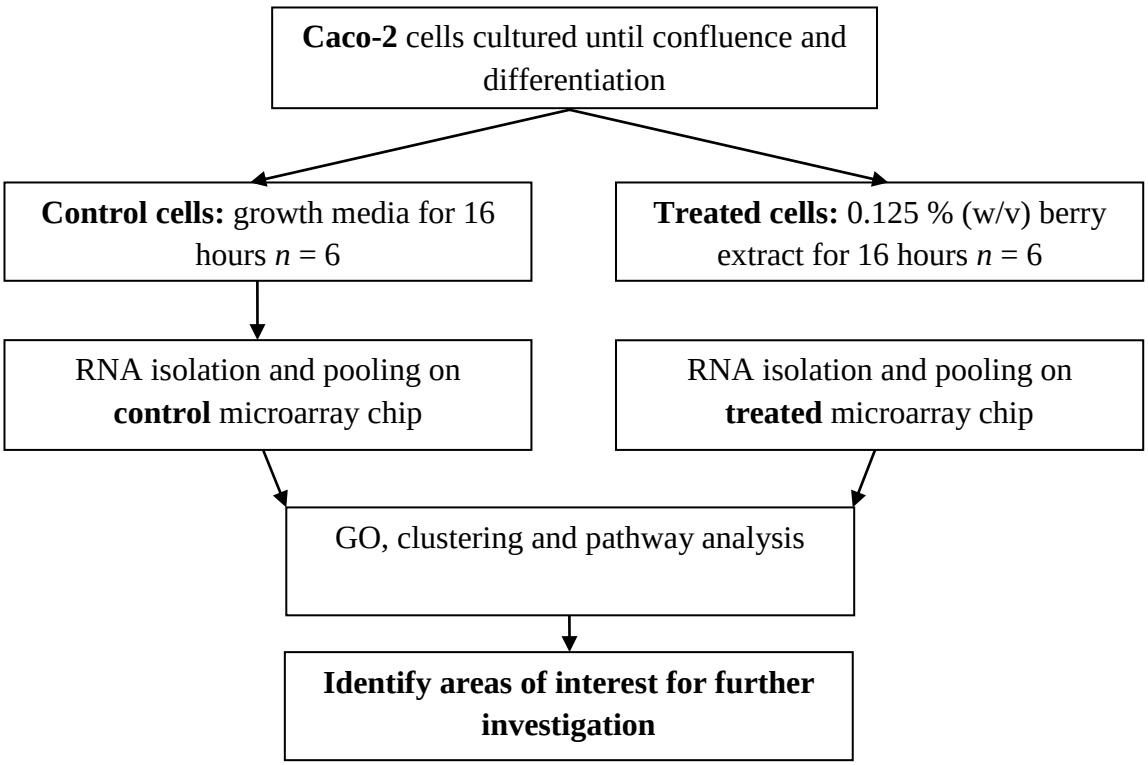

Figure 2.1. Study design. Caco-2 cells were treated with a flavonoid-rich berry extract at 0.125 % (w/v) for 16 h. Following treatment, RNA was isolated, pooled per group, and applied to microarray chips. Informatic analysis of microarray data identified areas of interest for subsequent validation and further investigation. GO: gene ontology.

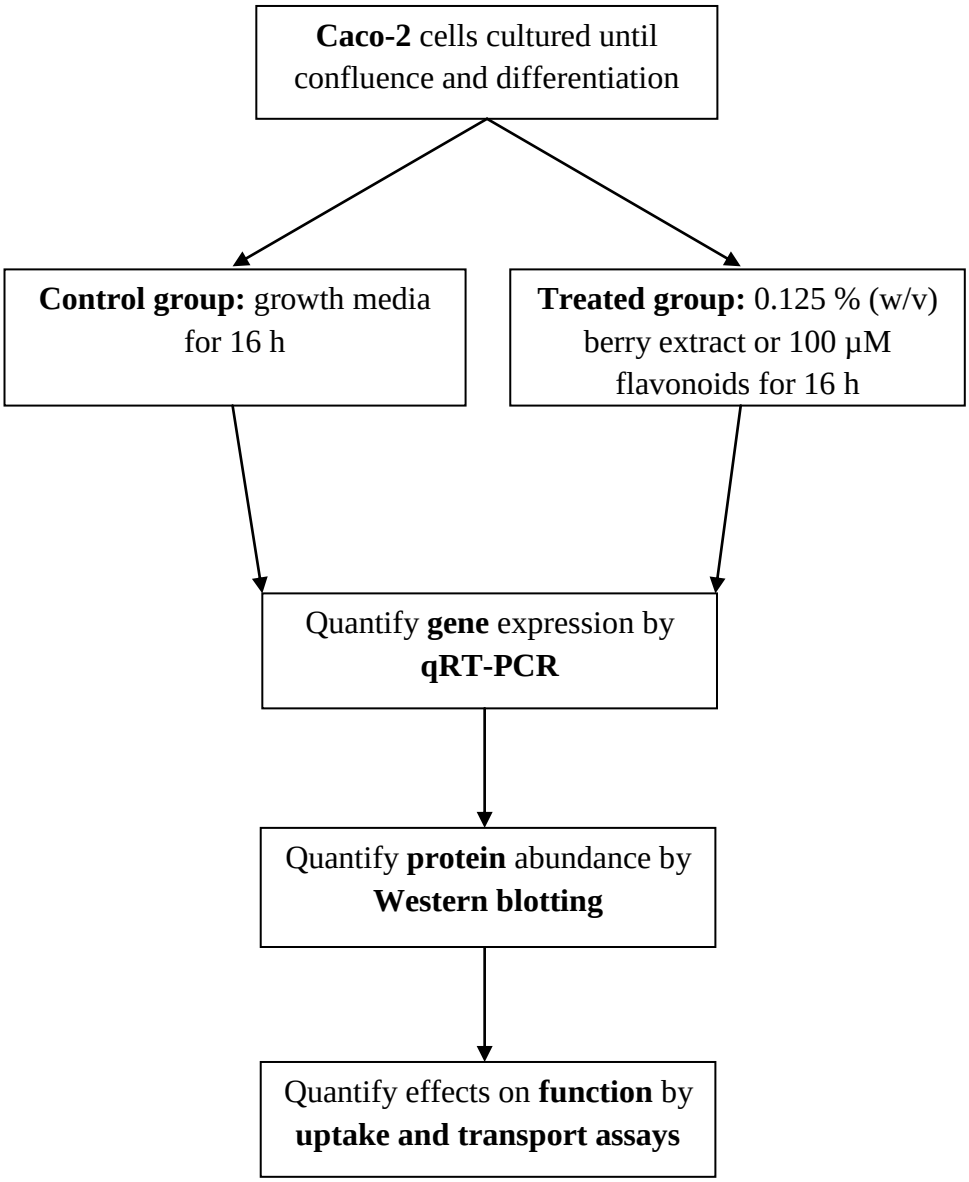

Figure 2.2. Validation of gene expression and further investigations. Following microarray analysis areas of interest were further investigated through gene expression analysis, protein abundance analysis and functional assays. qRT-PCR: quantitative real-time polymerase chain reaction.

2.2.2 Human intestinal Caco-2 cell cultures and treatments

The human intestinal Caco-2 cell line TC-7 strain was used in all of the following studies. This cell line has been previously used as an adequate model of the human intestinal epithelium (Mahraoui *et al*, 1994). Caco-2 cells were cultured until confluence (i.e. adhered to at least 90% of the growth surface) and differentiation (i.e. exhibited morphological characteristics of mature enterocytes such as thickened membranes) (**Figure 2.3**). Cells were only treated once differentiated, this typically occurred during the third week of growth. For cell seeding densities and media volumes used see **Table 2.26**.

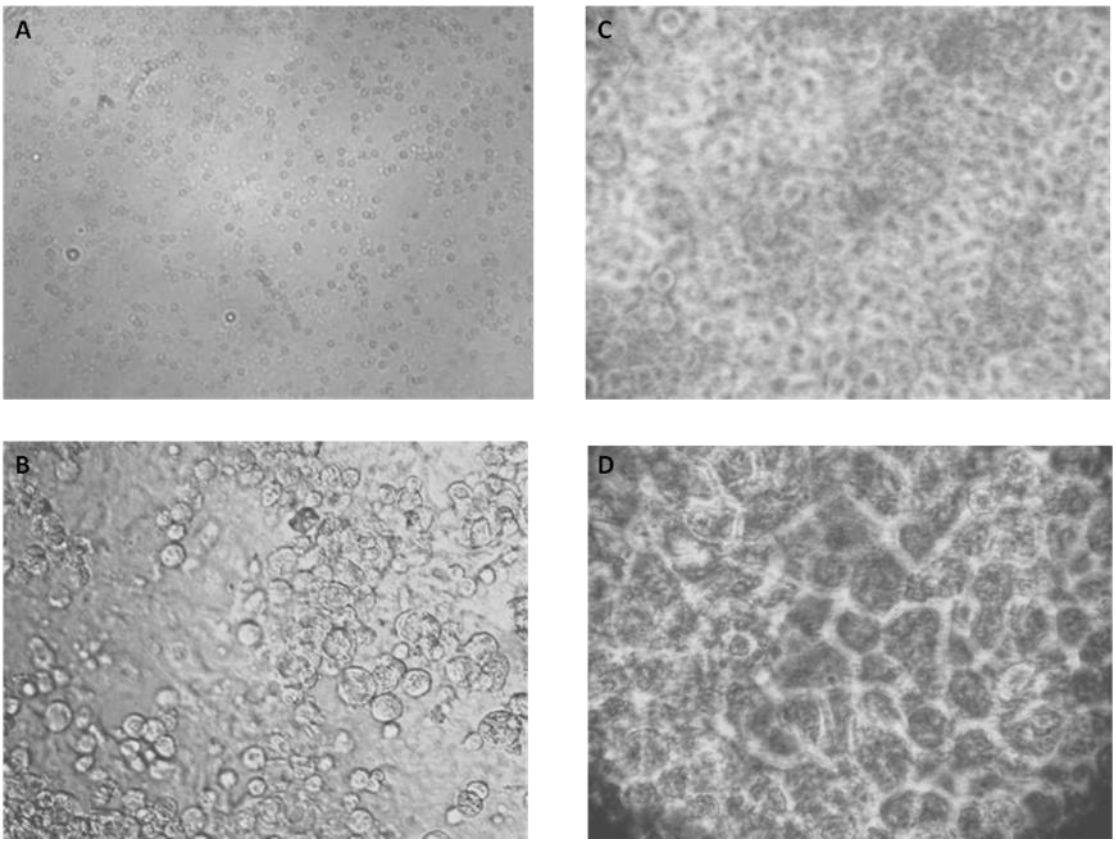

Figure 2.3. Newly seeded and fully differentiated Caco-2 cells. A. Newly seeded Caco-2 cells at X10 magnification and **B.** Newly seeded Caco-2 cells at X100 magnification; **C.** Confluent and differentiated Caco-2 cells at X10 magnification; **D.** Confluent and differentiated Caco-2 cells at X100. Note in panels **A** and **B** Caco-2 cells are not adherent and do not resemble enterocytic cells. In panels **C** and **D** note a monolayer has developed of tightly packed cells with thickened membranes, at this stage Caco-2 cells are ready for treatment.

Table 2.26. Standard conditions for Caco-2 cell seeding and culture.

Plate/flask size	Growth area (cm^2)	Approximate number of cells	Volume of media used (ml)
6-well plates	9.6	40,000	2
12-well plates	3.8	20,000	1
T-25 flasks	25.0	150,000	4
T-75 flasks	75.0	450,000	12
6-well plates with Transwell® inserts	4.7	50,000	2.5 (basolateral) 1.5 (apical)

The *complete* cell growth media consisted of Dulbecco's modified Eagle media supplemented with 10 % (v/v) foetal bovine serum filtered through a 0.2 µm pore filter, with 1 % (v/v) non-essential amino acids, 1 % (v/v) penicillin-streptomycin antibiotic solution, 1 % (v/v) L-glutamine and 0.2 % (v/v) plasmocin micoplasma inhibitor. *Serum-free* media was prepared with the same components, with the exclusion of foetal bovine serum and Plasmocin™ micoplasma inhibitor. Serum-free media was used 24 h prior to cell treatment in order to arrest cell growth, synchronising cells at the G0/G1 *restriction point* (Pardee, 1974; Pardee, 1989; Cooper; 2003). For suppliers of cell culture media components see **Section 2.1.1**.

2.2.2.1 Caco-2 cell passaging and viability testing

Caco-2 cells were subcultured for 40-43 passages and then experiments were performed on passages 44-47. Caco-2 cells were seeded in T-25 or T-75 cell culture flasks, allowed to reach confluence after approximately one week of growth and then detached using TrypLE™, a trypsin-like enzyme. Monolayers in each T-25 or T-75 flask were gently washed once with 3-5 ml PBS. TrypLE™ was then applied; 1.5 ml was added into the T-25 flasks (or 4.5 ml in T-75 flasks) and allowed to act on the monolayers at 37°C for 5-10 min. After detaching the cells, a suspension was made up to a volume of 10-15 ml with complete cell growth media and centrifuged at 600 rpm for 5 min at room temperature. The media was discarded and the cell

pellet was dispersed by gentle tapping. The cells were then resuspended in 10-15 ml of complete cell growth media. From the resulting cell suspension 15 µl was used for haemocytometry in order to determine the volume required to seed experimental plates and further flasks for passaging.

Cell viability was routinely tested during passaging and during the optimisation of treatment conditions using the trypan blue dye-exclusion method (Thanou *et al*, 2000). After detaching the Caco-2 cell monolayer, centrifugation and resuspension of the pellet, 10 µl of the cell suspension was mixed with 10 µl of 2 X trypan blue dye. Then 15 µl of this cell suspension was used for counting and determination of cell viability.

2.2.2.2 Caco-2 cell treatments

To investigate the response of Caco-2 cells, our primary treatments used a flavonoid-rich berry extract at a final concentration of 0.125 % (w/v). Our further studies included the following synthetic flavonoids: quercetin (marker flavonol, most abundant flavonoids in the human diet), phloridzin (specific SGLT1 inhibitor) and phloretin (specific GLUT2 inhibitor) at final concentrations of 100 µM dissolved in DMSO, the final concentration of DMSO in treatment media was 0.05 % (w/v). Berry extract treatments and synthetic flavonoid treatments had separate flavonoid-free controls. Thus, controls for the berry extract treated cells were treated with media only, whereas controls for isolated flavonoid treated cells were treated with media including 0.05 % (w/v) of the DMSO solvent. All media used during the treatments were serum-free DMEM supplemented with 0.2 % (w/v) BSA, filtered through a 0.2 µm filter. For the composition of treatment solutions, stock and final concentrations of compounds, see **Table 2.27**. For a typical analysis of the commercial berry extract used throughout the studies in this thesis see **Table 2.28**.

Table 2.27. Concentration and composition of Caco-2 cell treatments.

Treatment group	Stock concentration	Final concentration	Final treatment composition
Control	-	-	**DMEM** + 0.2 % (w/v) **BSA**
Berry extract	0.25 % (w/v)	0.125 % (w/v)	**DMEM** + 0.2 % (w/v) **BSA** + 0.125 % (w/v) **berry extract**
Control (with DMSO)	100 % (v/v)	0.05 % (v/v)	**DMEM** + 0.2 % (w/v) **BSA** + 0.05 % (v/v) **DMSO**
Quercetin	200 mM	100 µM	**DMEM** + 0.2 % (w/v) **BSA** + 0.05 % (v/v) **DMSO** + 100 µM **quercetin**
Phloretin	200 mM	100 µM	**DMEM** + 0.2 % (w/v) **BSA** + 0.05 % (v/v) **DMSO** + 100 µM **phloretin**
Phloridzin	200 mM	100 µM	**DMEM** + 0.2 % (w/v) **BSA** + 0.05 % (v/v) **DMSO** + 100 µM **phloridzin**

DMEM: Dulbecco's modified Eagle medium; BSA: Bovine serum albumin; DMSO: Dimethyl sulfoxide.

Table 2.28. Typical analysis of the berry extract.

Analysis/analyte	Quantity
ORAC	≥3700 µmol TE/g
Polyphenolic content	6.50 GAE-mg/g
Total anthocyanin contents	3.60 mg/g
Malvidin	0.32 mg/g
Cyanidin	1.60 mg/g
Delphinidin	0.94 mg/g
Petunidin	0.52 mg/g
pH (1 g/100 ml in water)	2.5-3.5

Recommended dose for human consumption is 30 mg taken twice a day. ORAC: Oxygen radical absorbance capacity; GAE: Gallic acid equivalence; TE: trolox equivalents.

2.2.3 Gene expression analysis

Gene expression was quantified through the use of qRT-PCR with transcript specific primers and SYBR green as a fluorescent cDNA binding dye. The following sections describe the process of gene expression analysis.

2.2.3.1 RNA isolation

Following treatment, total RNA was isolated using TRIzol® reagent according to the manufacturer's protocol which consisted of five steps:

1. **Homogenisation**: cells were washed once with ice-cold PBS and homogenised by adding TRIzol® directly to wells in a reagent to surface area ratio of 1 ml: 10 cm^2. Cells were scraped with a pipette tip and incubated at room temperature (RT) for 5 min
2. **Phase separation:** 0.2 ml of chloroform, per 1 ml of TRIzol®, was added and samples were transferred to tubes, vortexed for 15 s and incubated at RT for 2-3 min. Samples were then centrifuged for 15 min at 12,000 *g* at 4 °C. The colourless aqueous phase was retained for RNA isolation.
3. **RNA precipitation:** 0.5 ml of isopropanol, per 1 ml of TRIzol®, was added to the aqueous phase and incubated at RT for 10 min. Samples were then centrifuged for 10 min at 12,000 *g* at 4 °C. The RNA pellet formed at the bottom of the tube.
4. **RNA wash:** the supernatant was removed and the RNA pellet washed with 1 ml 75 % (v/v) ethanol in nuclease-free water, per 1 ml of TRIzol®. Samples were vortexed and centrifuged for 5 min at 7,500 *g* at 4 °C.
5. **Redissolving the RNA:** the supernatant was removed and tubes were then inverted in a fume hood allowing the pellet to dry for 15-20 min. Pellets were then redissolved in 50 µl nuclease-free water by repeated pipetting.

2.2.3.2 RNA integrity, purity and quantification

Immediately following RNA isolation, sample concentrations and purity were quantified using the NanoDrop spectrophotometer. For this, 1.2 µl of RNA sample was used to quantify RNA concentrations. A blank of nuclease-free water was used to optimise the instrument. Sample pedestals were first cleaned with nuclease-free water and ethanol prior to use. The purity of RNA was indicated by the 260/280 ratio. According to the manufacturer's protocol, a 260/280 ratio of ~ 2.0 was considered optimal.

RNA integrity was quantified using BioAnalyzer chips. An RNA integrity number (RIN) of isolated RNA was obtained. RIN of approximately ~10 was considered optimal. The chips were run according to the manufacturer's protocol.

2.2.3.3 Reverse transcription of complimentary DNA

Following RNA isolation and quantification, RNA was reverse transcribed into cDNA using a High Capacity Reverse Transcription Kit, producing cDNA suitable for use with qRT-PCR. Reverse transcription reactions were prepared as a mastermix and aliquoted for immediate use, then reverse transcription was carried out. The resulting cDNA was stored at -20 °C until use. See **Table 2.29** for reverse transcription reaction components and **Table 2.30** for thermal cycling conditions.

Table 2.29. Reverse transcription reagents and 2X reaction composition.

Reagent	Volume per 2X reaction mix (µl)*
10X RT buffer	2.0
25X dNTP mix (100 mM)	0.8
10X random primers	2.0
MultiScribe™ reverse transcriptase	1.0
RNase inhibitor	1.0
Nuclease-free water	3.2

*2 µg of total RNA is added to the reaction and diluted with nuclease free water to make a final reaction volume of 20 µl. RT: reverse transcription; dNTP: deoxyribonucleotide triphosphate.

Table 2.30. Reverse transcription thermal cycling programme.

Step	Primer Incubation	Reverse transcription	Enzyme inactivation	End of run
Setting	HOLD	HOLD	HOLD	HOLD
Temperature (°C)	25	37	85	4
Time (min)	10	120	5	∞

"∞" denotes short-term (up to 24 h) storage prior to transferring samples to -20 °C.
"HOLD" denotes a setting where temperature is constant.

2.2.3.4 Real-time quantitative polymerase chain reaction

Following cDNA synthesis samples were used with transcript-specific primers to amplify regions of mRNA for quantification of gene expression. A SYBR® Green Mastermix was used as the polymerase enzyme and DNA-binding dye in qRT-PCR experiments. On each qRT-PCR plate target genes and housekeeping genes were run together. The housekeeping genes used were 18S ribosomal RNA and glyceraldehyde 3-phosphate dehydrogenase (GAPDH). For detection of 18S, samples were diluted 10-fold due to the high abundance of the mRNA sequence. Standards were run for every gene amplified at five consecutive 10-fold dilutions from the sample concentration as 1 to the lowest concentration as 1/10,000 to quantify efficiency of amplification using the slope [Efficiency = $((10^{(-1/slope)})-1)100$]. Two non-template controls not containing any sample material and standards were run on every plate. See **Table 2.31** for qRT-PCR reaction components, **Table 2.32** for the thermal cycling programme, **Figure 2.4** for the programme interface and thermal cycler settings and **Table 2.33** for housekeeping gene primer sequences. All primers were either previously reported in literature or designed with the online primer design tool Primer3 (http://frodo.wi.mit.edu/; Rozen and Skaletsky, 2000). Target gene primer sequences are listed in each chapter. See **Section 9.1** for details of primer design and specificity.

Table 2.31. Quantitative RT-PCR reaction composition

Reagent	Volume per 20 µl reaction (µl)
SYBR green PCR Mastermix	10
Forward primer	0.8
Reverse primer	0.8
cDNA template*	0.8
Nuclease-free water	7.6

The quantity of the template cDNA strand was varied, depending on the desired amplicon. Between 25-250 ng cDNA was typically used per reaction.

Table 2.32. Quantitative RT-PCR thermal cycling procedure.

Step	Heating	Enzyme activation	Denaturation	Annealing/ extension*	Dissociation		
Setting	HOLD		CYCLE (40-55)		HOLD		
Temp. (°C)	50	95	95	60	95	60	95
Time (min)	2:00	10:00	0:15	1:00	0:15	0.:20	0:15

*data is collected during the annealing/extension phase of the qRT-PCR run.
"HOLD" denotes a setting where temperature is constant. "CYCLE" denotes a setting where temperature was cycled.

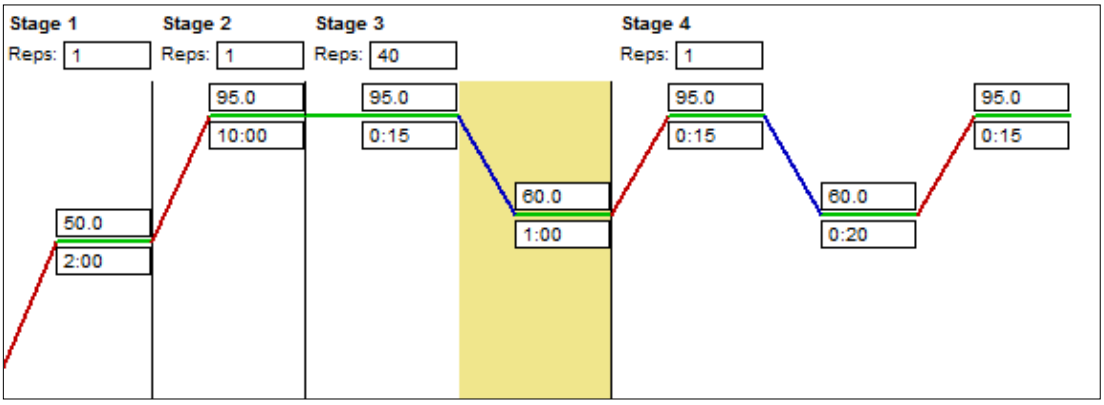

Figure 2.4. Sequence detection software thermal cycling protocol. Stage 1: heating. Stage 2: enzyme activation. Stage 3: denaturation and annealing/extension. Stage 4: Dissociation. "Reps" indicates the number of cycles the stages are repeated for. On the temperature indication line, the top box represents temperature in °C and lower box represents time in minutes. The Section highlighted in yellow is the data collection stage of the stage 3 cycle.

Table 2.33. Housekeeping gene primer sequences.

Gene symbol	Forward sequence (5'-3')	Reverse sequence (5'-3')
18S	AAC TTT CGA TGG TAG TCG CCG	CCT TGG ATG TGG TAG CCG TTT
GAPDH	CTG TTG CTG TAG CCA AAT TCG T	ACC CAC TCC TCC ACC TTT GA

18S: ribosomal RNA 18S; GAPDH: glyceraldehyde 3-phosphate dehydrogenase.

2.2.3.5 Quality control and gene expression data analysis

A standard curve for each gene was included to ensure the efficiency of PCR amplification was within 90-110 %, according to the manufacturers' protocol. See **Figure 2.5** for an example of standard curve demonstrating acceptable efficiency of amplification. A dissociation stage at the end of each qRT-PCR run was included to ensure primer specificity through melting curve analysis. **Figure 2.6** shows a typical melting curve indicating a single and specific product of amplification. Standard and melting curves from qRT-PCR analysis and their calculated efficiency of the reactions are in **Section 9.2**.

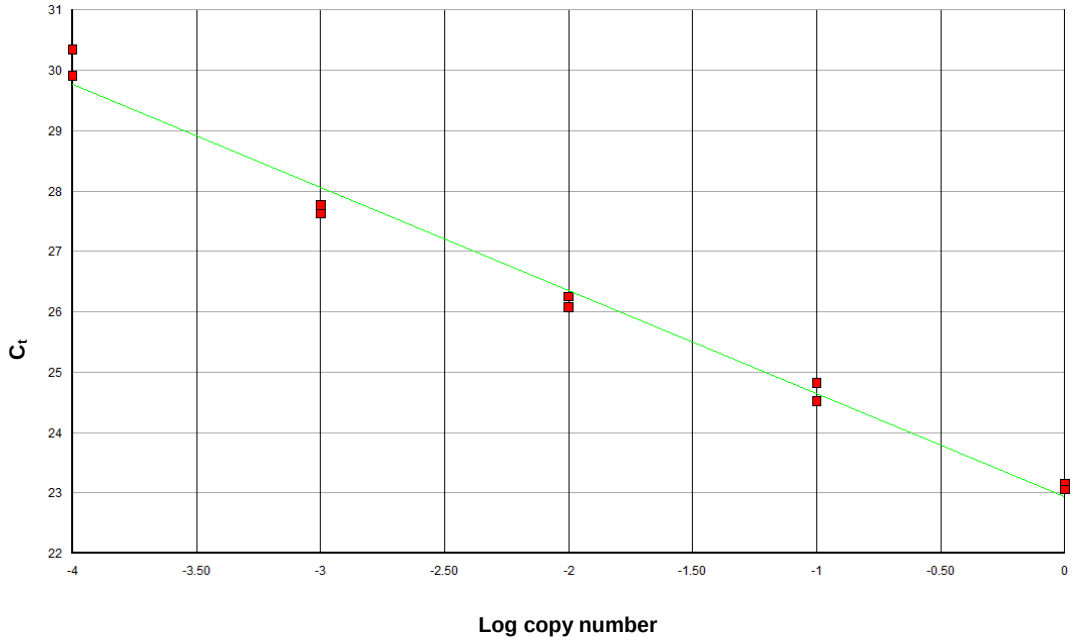

Figure 2.5. Example of sequence detection system generated standard curve.

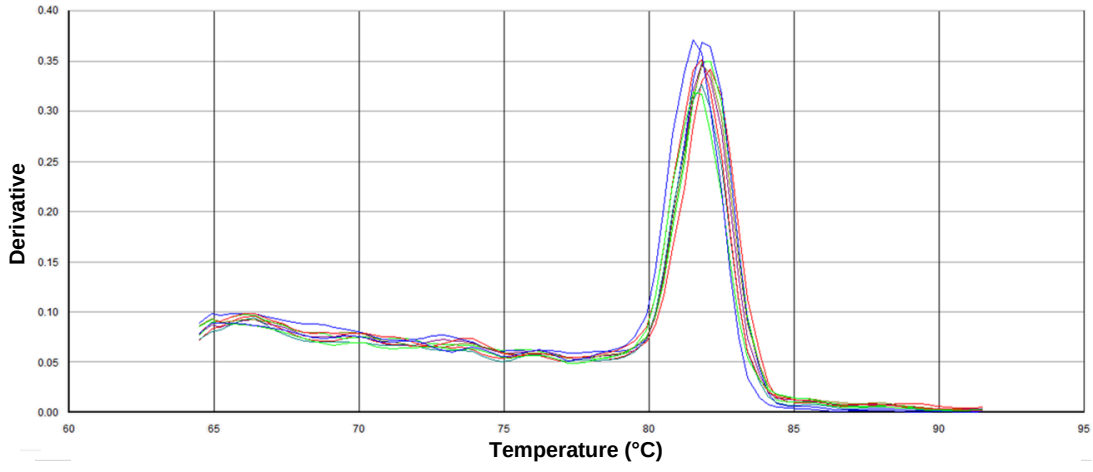

Figure 2.6. Example of sequence detection system generated results of dissociation stage for melting curve analysis.

After inspection of the quality controls mentioned above, expression data was derived by the $2^{(-\Delta\Delta Ct)}$ (*Livak*) method (Livak & Schmittgen, 2001; Schmittgen & Livak, 2008). The Livak method of gene expression analysis is in 3-steps, as follows:

1. **Normalisation of the gene of interest per sample**

   $$\Delta C_{T(sample)} = C_{T\ (sample\ GOI)} - C_{T\ (sample\ HKG)}$$

2. **Normalisation per treatment group**

   $$\Delta\Delta C_T = \Delta C_{T\ (treated\ sample)} - \Delta C_{T\ (control\ sample)}$$

3. **Calculating a normalised expression ratio**

   $$2^{(-\Delta\Delta Ct)}$$

Where, C_T: threshold cycle at which amplicon fluorescence passes above background. GOI: gene of interest. HKG: housekeeping gene.

The Livak method of gene expression analysis assumes efficiency of amplification is perfect or equal between all genes in the equation. The threshold cycle (C_T) value is derived from the linear exponential phase of PCR amplification (above low level background, and below the high level plateau). The equation is based on the fact that during the linear exponential phase of amplification, the levels of all amplicons are directly proportional to their starting amounts. As the increase in amplicon abundance during replication is exponential, the data are initially handled as logged values. Thus the C_T is normalised for each gene and expressed as a ratio for each sample, the efficiency of amplification is then raised to the power of the derived figure to be expressed as a ratio.

2.2.4 Protein abundance analysis

Protein abundance levels were quantified through the use of Western blotting and band-specific densitometry. The following sections describe the process of protein isolation and quantification. For buffer and gel compositions see **Section 2.1.4**.

2.2.4.1 Protein isolation and quantification

Total protein was isolated from Caco-2 cells, immediately following treatments, by adding a SDS lysis buffer directly into cell culture wells/flasks after washing with ice-cold PBS. Proteins were then prepared for Western blotting as follows. In 6-well plates 50-100 µl of lysis buffer (see **Section 2.1.4**, **Table 2.10** for composition) was used per well depending on the cell density. When using T-25 flasks, 150-300 µl of lysis buffer was added per flask depending on the cell density. If cell density was high, i.e. covering the entire growth surface in a thick layer, more lysis buffer was used. Caco-2 cell monolayers were then removed thoroughly using a cell scraper and the entire cell lysate was transferred to 2 ml tubes. Cells were lysed and homogenised over ice by repeatedly passing through a 1 ml syringe and needle. Cell lysates were then centrifuged at 600 rpm at 4 °C for 10 min until the supernatant was transparent. From the supernatant, 6µl was then taken for quantification using a Bradford spectrophotometric assay (Protein quantification kit-rapid, 51254-1KT, Sigma, Dorset, UK) based on a BSA standard curve ranging from 0 to 2000 µg/ml. Following quantification, samples were made into 40 µg aliquots and stored with sample loading buffer at -20 °C.

2.2.4.2 Western blotting

For the first step of Western blotting, gels were prepared for electrophoresis. Sodium dodecyl sulphate-polyacrylamide gels consisted of 10 % (w/v) acrylamide. After setting, gels were then placed into electrophoresis tanks which were then filled

with SDS running buffer. The electrophoresis tanks were operated at a constant voltage of 180 V and a variable current from 0-5 mA. Gels were run for approximately 40 min.

After electrophoresis, the proteins in the gel were then blotted onto a nitrocellulose membrane using a semi-dry transfer cell. The transfer was made by creating a layered stack in the following order, from top to bottom: Filter paper – gel – nitrocellulose membrane – filter paper. It was important to ensure that the filter paper, gel and membrane were of the same size. Stacked components were soaked in transfer buffer for at least 5 min, then placed on a moistened transfer cell surface, membrane-side down and gel-side up. Transfer was run at 35 mA per gel-membrane for 60-90 min. Following transfer, reversible Ponceau S staining (P7170, Sigma-Aldrich, Dorset, UK) was carried out to ensure efficiency of transfer. For an example of stained blot see **Figure 2.7.**

Figure 2.7. Ponceau S reversible protein staining. Ponceau S was used as a reversible stain for membranes following transfer to check for efficiency of protein transfer.

After destaining (by immersion in 0.1 M NaOH for 30 s and rinsing with distilled water) the membranes were placed in blocking solution for 30-60 min at room temperature with constant agitation at 60 rpm. After blocking, membranes were incubated with the primary antibody diluted into 3 ml of washing solution contained in a 50 ml falcon tube. Primary antibody incubation was carried out overnight at 4 °C on a roller-mixer to ensure even distribution of the antibody solution over the membrane. After the primary antibody incubation, membranes were washed at room temperature, 3 times for 10 min each, with washing solution. Membranes were then incubated with the appropriate secondary antibody, diluted into 3 ml of washing solution, for 60-90 min at room temperature. After the secondary antibody incubation, membranes were washed at room temperature, 3 times for 10 min each, with washing solution and were then ready for detection. All washes were done with constant agitation at 60 rpm, by placing membranes on a rocker. See **Table 2.34** for primary antibodies and concentrations used, secondary antibodies were used at the same dilution as the primary antibodies. Working antibody dilutions were determined by initially carrying out smaller scale Western blots with varying concentrations (1:2000, 1:1000, 1:500).

Table 2.34. Antibodies and working concentrations applied in Western blotting. Antibodies were diluted in PBST and 1 % (w/v) non-fat powdered milk.

Primary antibody	Working dilution	Supplier
Anti-SGLT1	1:500	Millipore, Consett, UK
Anti-GLUT2	1:500	Millipore, Consett, UK
Anti-DMT1	1:1000	Alpha Diagnostics, TX, USA
Anti-FPN	1:1000	Alpha Diagnostics, TX, USA
Anti-CTR1	1:1000	Novus Biologicals, Cambridge, UK
Anti-ATP7A	1:1000	Abcam, Cambridge, UK
Anti-β-Actin	1:2000	Sigma-Aldrich, Dorset, UK

2.2.4.3 Detection, densitometry and data analysis

After the incubations with primary and secondary antibodies were complete, membranes were briefly removed from the washing solution and placed on a clean, dry and flat surface ready for application of the detection reagents. The detection reagent components were mixed in a 1:1 ratio with a final volume of 1 ml per blotting membrane. Detection reagents (Novex® ECL chemiluminescent substrate reagent kit, WP20005, Invitrogen life technologies, Paisley, UK) were then gently and evenly pipetted onto the surface of the membranes before dripping off excess reagent. Membranes were then placed in a dark exposure cassette and covered with clear plastic. The photosensitive light-films were exposed to the membranes in a dark room for 5-15 min then developed and fixed with film processing solutions.See **Section 2.1.4** for materials and reagents.

The fixed films were manually digitised on a densitometer (BioRad Laboratories, Hertfordshire, UK) with film-specific settings. QuantityOne 1-D analysis software (BioRad Laboratories, Hertfordshire, UK) allowed autocorrection of the image, lane-specific background reduction and automated band-detection. Specific band density was quantified for each of the proteins to be detected. Normalisation was to the amount of protein loaded per well and to the housekeeping protein β-actin.

2.2.5 Functional uptake and transport experiments

Three experiments were carried out to quantify nutrient transport, one in each chapter, to investigate glucose, iron and copper absorption. Iron and glucose experiments were carried out with radiolabelled substrates, copper uptake experiments were carried out using inductively coupled plasma optical emission spectroscopy (ICP-OES). Each experiment was performed acutely (co-incubation of flavonoids and substrate for transport) or chronically (pre-treatment with flavonoids followed by separate functional experiment). The acute experiments were designed to investigate the effects when both compounds are present, i.e. structural, competitive, interactive effects. The chronic experiments were designed to investigate effects that may have arisen due to a transcriptional or translational effect only, i.e. could flavonoids induce an effect on gene or protein expression that has a functional consequence. The following section describes the protocols of the functional studies in each chapter.

2.2.5.1 Glucose uptake experiments

Glucose uptake experiments were carried out in the presence and absence of sodium, to identify differences between GLUT-mediated transport (active under both conditions) and SGLT-mediated transport (only active in the presence of sodium). Cells for this experiment were grown in 6 well plates.

Glucose free HBSS was used for the glucose uptake experiments; see **Section 2.1.5**, **Table 2.21** for composition of the uptake buffer. After loading buffers and treatments, cells were incubated at 37 °C for 15 min prior to initiating experiments. Radiolabelled glucose, D-[^{3}H]-glucose, was diluted into a stock solution of 20 mM glucose. This was then added into cell culture wells to initiate uptake. D-[^{3}H]-

glucose was diluted to give an activity of ~ 500,000 DPM/well, and the final glucose concentration was 1 mM.

Uptake was terminated after 2 minutes by aspirating uptake buffer and washing the cells 3 times with ice cold HBSS. After washing, 0.5 ml of 200 mM NaOH was added to each well; plates were then covered in cling film and cells were allowed to dissolve overnight at 4 °C. Cell lysate was then scraped and passed repeatedly through a 1 ml pipette, 20 µl of lysate was used for protein quantification and 200 µl was added to 5 ml of scintillation liquid (Ecoscint A, National Diagnostics, USA). Other control vials were also prepared, including the starting amount of glucose and a NaOH blank. All samples were subjected to scintillation counting.

2.2.5.2 Iron transport experiments

Iron transport experiments were carried out acutely and chronically, similar to the glucose uptake experiments above. For these experiments Caco-2 cells were grown on Transwell supports in 6-well plates. Two components of transport were measured for each experiment; the first being apical iron uptake and cellular retention, the second was the basolateral release of iron.

For all experiments, the apical compartment of the Transwell supports was loaded with 1.5 ml pH 6.5 MES buffer and the basolateral compartment was loaded with 2.5 ml pH 7.5 HBSS; see **Section 2.1.5**, **Tables 2.22** and **2.23** for composition of these buffers. After loading buffers, cells were incubated at 37 °C for 20 min prior to initiating experiments.

The source of iron was made by diluting the radioisotope $^{55}FeCl_3$ into a stock solution of $FeSO_4$ and ascorbate. Trace amounts of the radioisotopes were added to give ~ 500,000 DPM/well; the final concentrations of $FeSO_4$ and ascorbate in the

apical compartments were 1 and 10 µM, respectively. Uptake was allowed to progress for 20 min, whereas measurements of cellular retention and transport were allowed to progress for 120 min.

After 20 minutes or 120 minutes, the incubation was terminated by dipping each Transwell insert into ice cold HBSS 3 times; basolateral compartment media was not discarded. Transwell membranes were then drip dried briefly and cut away. Membranes were left overnight in 0.5 ml 200mM NaOH at 4 °C to dissolve cells. Membranes were then thoroughly scraped and the resulting cell lysate was passed through a 1 ml syringe. The following components were included for scintillation counting in 50 ml of scintillant: 150 µl cell lysate; 250 µl basolateral media; starting amount of the radiolabelled iron isotope and blanks for NaOH and basolateral media.

2.2.5.3 Copper uptake experiments

The experiments for copper uptake were carried out based on previous work in the laboratory of Dr. Paul Sharp, and were optimised in previous experiments by Dr. Katayoun Pourvali at Diabetes and Nutritional Sciences Division, King's College London. Copper uptake experiments were carried out with an acute treatment or following a chronic treatment on cells grown in T-25 flasks. Copper uptake was carried out in MES buffer pH 6.5 with and without the inclusion of 100 µM ascorbate as a reducing agent; see **Section 2.1.5**, **Tables 2.22** for the composition of the uptake buffer. To initiate uptake, $CuCl_2$ was added into the cell culture flasks that had been preequilibrated in with uptake buffer for 15 min, to give a final concentration of 10 µM.

Uptake was terminated after 120 min by washing cells with ice cold PBS. Cells were harvested (in 2 ml PBS; of which 20 µl was used for protein quantification) and dissolved (in 3 ml of 1 M nitric acid and 5 ml of 70 % (v/v) nitric acid). The 10 ml

solution of cell lysate was heated at 90 °C of 90 min, and then centrifuged at 5000 rpm for 10 min to remove any remaining cell debris.

Solubilised samples were analysed by ICP-OES (iCAP 6000 series; Thermo Scientific, UK). A multi element standard, with a copper content of 1006 ± 10 mg/L, was used for quantification. The specific wavelength for quantification of copper was 324.754 nm. Data were normalised to protein content and expressed as copper uptake per 120 min.

2.2.6 Statistical analysis

Statistical approaches and algorithms applied in microarray analysis are detailed in **Section 9.3. Bioinformatics analysis**. Each data set, for qRT-PCR, Western blotting and uptake and transport studies was normalised prior to statistical testing. Gene expression data were normalised to both 18S and GAPDH as housekeeping genes. In this regard, normalisation to multiple housekeeping genes is recommended by Vandesompele *et al* (2002) and Caradec *et al* (2010). Protein abundance data were normalised to both the amount of protein loaded and to the density of corresponding β-actin bands. Uptake and transport studies were normalised to total protein content. All data was tested using a non-paired Student's t-test, ANOVA with Dunnet's post-hoc test, ANOVA with post test for linear trend or Kruskal-Wallis with Dunn's post-hoc test. In all cases significance was indicated at $p \leq 0.05$. Other statistical tests are as indicated in the methods section of each chapter or in the legends of figures and tables.

CHAPTER THREE

Effects of berry extract on the transcriptome Caco-2 enterocytes

3 Effects of berry extract on the transcriptome of Caco-2 enterocytes

3.1 Introduction: The transcriptomic effects of flavonoids

Flavonoids are known to have wide ranging beneficial effects including antioxidant actions and reducing the risk of cancer, cardiovascular disease and diabetes (previously reviewed by Bravo, 1998 and Crozier *et al*, 2009). However, the precise mechanisms by which flavonoids influence health remain unknown. One powerful tool to investigate the therapeutic range and transcriptional mechanisms of such biologically active compounds is the application of genome wide arrays. Essentially, they identify the relative change in global mRNA expression and thus help to define novel testable hypotheses for future research. The transcriptomic effects of flavonoids have however only been investigated by a few groups which are briefly reviewed below.

Lefevre *et al* (2008) applied microarray technology as a "*hypothesis generating paradigm*". They found that anthocyanin supplementation of a proatherogenic diet down-regulated gene clusters associated with the *response to inflammation* and *oxidative stress* in murine liver. Their resulting gene-lists were highly enriched with pathways related to *cellular defense* and *energy metabolism* (Lefevre *et al*, 2008).

In another study, Tsuda *et al* (2006) investigated the effects of anthocyanin aglycones and glycosides on the expression of genes relating to adipocytokine expression in human adipocytes. Both aglycone and glycosides resulted in the alteration of 33 and 142 distinct genes, respectively. The unique gene expression profiles were attributed to differences in membrane permeability of the flavonoid treatments (Tsuda *et al*, 2006).

In contrast to the above study by Tsuda *et al* (2006), Natsume *et al* (2009) suggested that the effects of sugar moieties on quercetin-induced changes in gene expression were negligible. However, dosage was found to be a more significant determinant, as mice on a low flavonoid dose had a significantly different expression profile whereas there was no effect of the high dose (Natsume *et al*, 2009).

To our knowledge, few other groups have investigated the effects of flavonoids on transcriptome variation, particularly in cells of the intestinal epithelium with the use of diet derived flavonoids. We addressed this by examining the transcriptomic effects of berry flavonoids on enterocytes. A well characterised model of human intestinal epithelial cells was used, i.e. Caco-2 cells (Sun *et al*, 2008); and treated with a documented flavonoid-rich berry extract; i.e. Optiberry® (InterHealth Nutraceuticals, CA, USA) (Zafra-Stone *et al*, 2007). Gene expression microarray and bioinformatic analysis allowed the development of themes for further research.

3.2 Methods

Presented here is a brief description of the methods used in this chapter. For full details of reagents, buffer/media compositions and methods used see **Chapter 2.**

3.2.1 Experimental design

This study was designed to generate testable hypotheses with the application of transcriptome analysis. Human intestinal Caco-2 cells were treated with a flavonoid-rich berry extract. Following treatment, RNA was isolated and transcriptome variation measured using Affymetrix® microarray chips. Microarray data was analysed to identify areas of further investigation. We then validated microarray-detected gene expression values by qRT-PCR.

3.2.2 Cell line, culturing and treatments

Caco-2 cells between the passages of 44 and 47 were seeded into 6-well plates at a density of approximately 40,000 cells per well (4,000 cells per cm^2) and cultured for 19 days prior to treatment. Details of the maintenance of the cells and composition of cell culture medium have been previously described (see **Chapter 2** and Johnston *et al*, 2005). The treatment used was a flavonoid-rich berry extract (derived from blueberry, bilberry, cranberry, elderberry, raspberry seeds and strawberry; rich in the anthocyanins delphinidin, cyanidin, petunidin and malvidin, OptiBerry®, InterHealth Nutraceuticals, CA, USA) for 16 h at a final concentration of 0.125 % (w/v) prepared in DMEM. An identical medium, without berry extract, was used to treat control cells. There were 6 samples in each group.

Effects of berry extract treatment on cell viability and RNA content were tested. There were no effects on cell viability or RNA content (see **Results, Section 3.3.1**).

3.2.3 RNA sample preparation

Following treatment, RNA was isolated using TRIzol® reagent (Invitrogen™ life technologies, Paisley, UK) according to the manufacturer's protocol. RNA concentration was quantified with a NanoDrop spectrophotometer (Thermo Fisher Scientific, Leicestershire, UK) and RNA integrity was quantified with the 2100 BioAnalyzer (Agilent, Cheshire, UK) using the RNA 6000 Nano Kit (Agilent, Cheshire, UK) according to the manufacturer's protocols (Fleet *et al*, 2003; Brand *et al*, 2008). RNA was pooled from the 6 samples in each treatment group and applied to the microarray chips for global gene expression analysis. Reverse transcription was carried out according to the manufacturer's protocol using the High Capacity Reverse Transcription kit (Applied Biosystems™ Cheshire, UK).

3.2.4 Transcriptome analysis

Transcriptome analysis was carried out through the application of Affymetrix® GeneChip® Microarray systems. Two HGU-133A gene chips (Affymetrix Inc., CA, USA) were prepared, with a single chip for each treatment condition: i.e. berry extract and control. Following normalisation and filtering, resulting gene lists were subjected to ontological and pathway analysis. See **Section 9.3** for details of the informatics analyses applied to global gene expression data.

3.2.5 Gene ontology and pathway analysis

Genes that passed the normalisation and filtering were then subjected to gene ontological clustering and pathway analysis. Gene ontology (GO) clustering was performed on the Database for Annotation, Visualisation and Integrated Discovery (DAVID) bioinformatics resource (www.david.abcc.ncifcrf.gov) using the default analysis settings (Dennis *et al*, 2003; Huang da *et al*, 2009). Pathway analysis was performed on Ingenuity® Pathway Analysis (IPA) software (Ingenuity® Systems,

CA, USA; Maaser & Borlak, 2008). Multiple pathway analyses were performed with the following filters:

Analysis 1: *all molecules and/or relationships*

Analysis 2: *molecules and/or relationships where* ***species = human***

Analysis 3: *molecules and/or relationships were* ***cell lines = colon cancer***

Analysis 4: *molecules and/or relationships were* ***species = human*** *and* ***cell lines = colon cancer***

3.2.6 Real-time PCR

Genes were selected for validation using a candidate gene approach and on the basis of functional similarity. The DAVID functional classification tool was utilised to determine a similarity score (Kappa statistic) of genes relative to an initial candidate gene (also called "*bait*" gene). This was by a modified Fisher's exact test based on overlapping GO terms between the bait gene and other genes in the gene-list (Dennis *et al*, 2003). For the statistical approach of gene functional similarity clustering see **Section 9.3.3. Functional similarity clustering and the Kappa score**. Genes selected for validation by qRT-PCR were related to nutrient transport; namely, glucose or metal transport. The facilitative glucose transporter, GLUT2, was selected by a candidate gene approach. Metal transport genes were chosen by functional similarity to the divalent metal ion transporter DMT1.

Total RNA was isolated from cultured cells using TRIzol® (Invitrogen™ life technologies, Paisley, UK) according to the manufacturer's protocol. Following first strand cDNA synthesis (using the High Capacity Reverse Transcription kit; Applied Biosystems™ Cheshire, UK), gene expression levels were analysed by qRT-PCR using an ABI Prism 7700HT Sequence Detection System and a Power SYBR® Green PCR master mix kit (Applied Biosystems™ Cheshire, UK). Primers were

designed using the online design tool Primer3 (Rozen & Skaletsky, 2000) and sourced from MWG Eurofins (London, UK). Quantitative measurement of gene expression was derived from the $2^{(-\Delta\Delta Ct)}$ *method*, also known as the *Livak method* (Livak & Schmittgen, 2001; Schmittgen & Livak, 2008). Data were expressed as ratios to the control and normalised to the housekeeping genes 18S and GAPDH. The primer sequences used for each gene are in **Table 3.1**.

Table 3.1. Primer sequences for qRT-PCR gene expression analysis.

Gene symbol	Forward primer 5'-3'	Reverse primer 5'-3'
GLUT2	AGT TAG ATG AGG AAG TCA AAG CAA	TAG GCT GTC GGT AGC TGG
DMT1	AGT GGT TTA TGT CCG GGA CC	TTT AAC GTA GCC ACG GGT GG
HFE	CAC ACC ATC CAC TTT CAT GC	GCA TGG ACA TGG TCA GTC AC
ATP7B	CCA CAT GAA GCC CCT GAC	GAC CAC TTG TCC CCA TCA TC
ZIP2	GTG CAG AAC AGA TCA GCA AGT GA	CAA TGC CAG CGA CTC CAA A
ZNT10	ACT AAC TCC TTT CCA TTC CCC	TAT CCG CAG CTA TTG AGC C
MRS2	CAT ACC CAA CAC TGC TGA C	TTA CCC CAT CTT TTC CCT CC
CACNA1D	TGG TAG GAA CAG GTC CCA AG	GGG AGA AGC AGA CTC CAC AG
GLUT1	TCC ACG AGC ATC TTC GAG A	ATA CTG GAA GCA CAT GCC C
GMNN	TGT CCA AAA GGA AAC ATC GGA	ACT CCT GGG TGA CTC CTC CAA
CDKN1A	CTG CCC AAG CTC TAC CTT CC	CAG GTC CAC ATG GTC TTC CT
BUB1	AGG ATC TGC CCG CTT CCC	GTC GTC TGA TAG GTT ACT GG
18S	AAC TTT CGA TGG TAG TCG CCG	CCT TGG ATG TGG TAG CCG TTT
GAPDH	CTG TTG CTG TAG CCA AAT TCG T	ACC CAC TCC TCC ACC TTT GA

GLUT2: facilitative glucose transporter member 2; DMT1: divalent metal ion transporter 1; HFE: haemochromatosis protein; ATP7B: copper transporting ATPase β-polypeptide; ZIP2: zinc influx transporter member 2; ZNT10: zinc efflux transporter member 10; MRS2: magnesium homeostasis factor; CACNA1D: voltage-gated calcium channel; GLUT1: facilitative glucose transporter member 1: GMNN: geminin; CDKN1A: cyclin dependent kinase inhibitor 1A: BUB1: budding uninhibited by benzimidazoles; 18S: ribosomal RNA18S; GAPDH: glyceraldehyde 3-phosphate dehydrogenase.

3.2.7 Data and statistical analysis

Microarray data were normalised with the use of GeneChip® Operating Software (GCOS; Affymetrix Inc., CA, USA) by MAS 5.0 linear normalisation with standard default settings applied (Traka *et al*, 2005). Only genes with a fold-change of 1.9 or more and with a probe-set detection *p*-value of ≤ 0.05 were accepted as being differentially expressed; as dictated by GCOS default settings. Resulting gene lists (up-regulated and down-regulated) were then subjected to pathway analysis, GO clustering and functional similarity clustering. For details of informatics analysis see **Section 9.3. Bioinformatics analysis**. Note, in bioinformatics, the term "*enrichment*" refers to a statistically significant high proportion of genes, from a given category, occurring in the experimental gene-list. The category could mean a pathway or could mean a *"term"*; a term refers to a specific category of a larger database (e.g. *apical membrane* is a *term* from the GO category of *cellular components*) (Dennis *et al*, 2003).

Real time PCR data are expressed as means $\pm$ SEM of 6 observations per group. Statistical analysis was carried out using GraphPad Prism 5 (San Diego, CA, USA), A Student's unpaired t-test was used to compare means; significance was indicated when $p \leq 0.05$.

3.3 Results

3.3.1 Effects of berry extract on cell viability, RNA content and integrity

The effects of treatments on cell viability, RNA content and integrity were tested to ensure effects of berry extract were not due to pathological changes, but as normative responses. There was no effect of berry extract on cell viability (**Figure 3.1**), RNA content (**Figure 3.2**) nor RNA integrity for those samples used for either qRT-PCR or microarray analysis (**Figure 3.3**). For an example of representative traces of BioAnalyzer charts indicating RNA integrity see **Figure 3.4**.

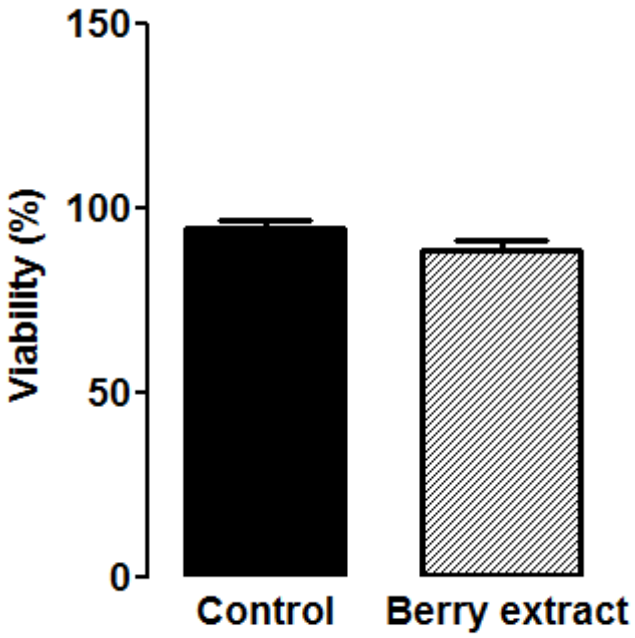

Figure 3.1. Caco-2 cell viability after berry extract treatment. Caco-2 cells were treated with berry extract at 0.125 % (w/v) for 16 h. Cell viability was quantified with the trypan blue dye-exclusion method. Data is presented as mean percentage viable cells ± SEM, *n* = 6, Student's t-test showed there was no significant difference between groups.

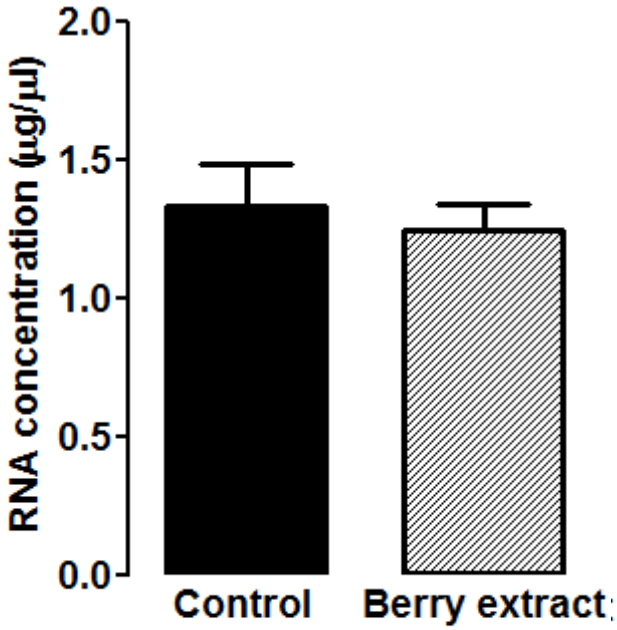

Figure 3.2. RNA concentration from Caco-2 cells after berry extract treatment. Caco-2 cells were treated with berry extract at 0.125 % (w/v) for 16 h. RNA concentration in the extracts of Caco-2 cells was quantified with the NanoDrop spectrophotometer. Data is presented as mean RNA concentration ± SEM, *n* = 6, Student's t-test showed there was no significant difference between groups.

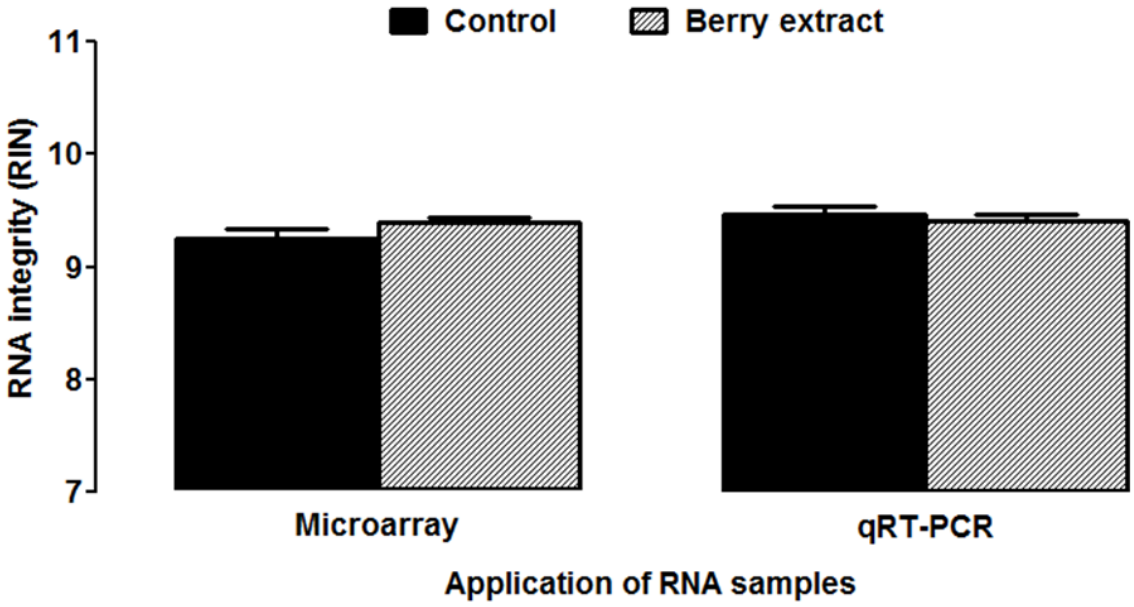

Figure 3.3. Integrity of Caco-2 cell RNA samples. Caco-2 cells were treated with berry extract at 0.125 % (w/v) for 16 h. RNA integrity was quantified with BioAnalyzer chips. Data is presented as mean RIN ± SEM, *n* = 6, ANOVA showed there was no significant difference between groups. RIN: RNA integrity number; qRT-PCR: quantitative real-time polymerase chain reaction.

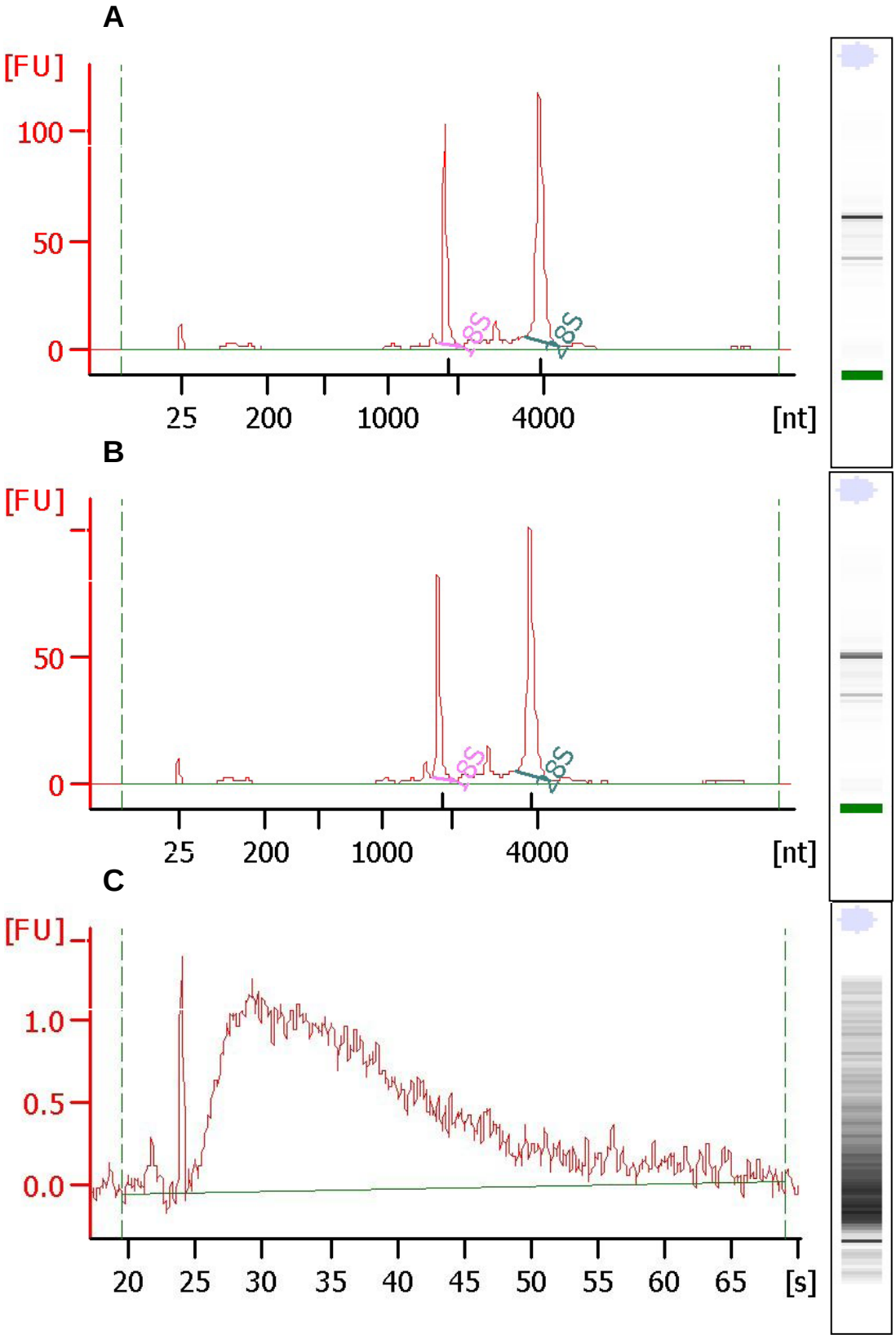

Figure 3.4. Example BioAnalyzer traces of Caco-2 cell RNA samples. Following RNA isolation, samples were tested with the BioAnalyzer to ensure high quality sample material with clearly defined peaks of 18S and 28S RNA (trace **A** for sample applied to microarray chips, and trace **B** for sample applied to qRT-PCR). Any degraded RNA samples (trace **C**) were not used in experiments. 18S/28S: ribosomal RNAs 18S and 28S. qRT-PCR: quantitative real-time polymerase chain reaction. [FU]: fluorescence units; [s]: time in seconds; [nt]: size in nucleotides.

3.3.2 Effects of berry extract on Caco-2 cell transcriptome

Affymetrix chip .CEL file images of the fluorescent probes for each chip are shown in **Figure 3.5**. Visual inspection of these chips indicated there was no uneven hybridisation, with a uniform balance of signals. A total of ~22'000 genes showed positive signals, i.e. expressed in either control or treated samples. Following normalisation and filtering, 2557 genes were accepted as altered by the berry extract, with a fold-change of 1.9 or more and a detection *p*-value of ≤ 0.05 (**Figure 3.6**). Of these, the expression of 761 genes was increased and 1796 decreased relative to the control samples. For a full set of the gene list, see **Section 9.4**.

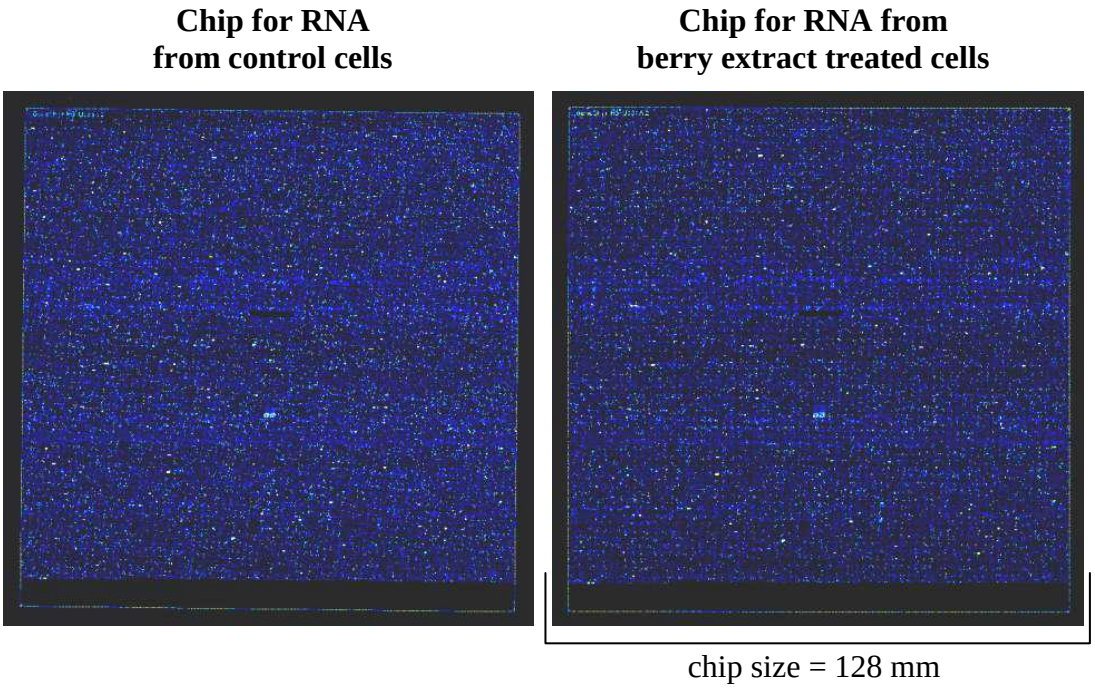

Figure 3.5. Graphic .CEL files generated from global gene expression analysis. Caco-2 cells were treated with berry extract at 0.125 % (w/v) for 16 h. RNA was isolated and applied to microarray chips. Each chip, one for control cells and the other for cells treated with berry extract, had 6 pooled RNA samples. Each spot on the graphic file represents a gene; each gene is represented by 11 probe-sets from along the gene's whole transcript. The microarray chips contain both positive controls as a set of 100 housekeeping genes, as well as pre-determined ranges of acceptable fluorescence. Negative controls are present for each probe-set in the form of mismatched probes to correct for cross- and random- fluorescence. Visual inspection shows a uniform balance of staining and signals across the chips.

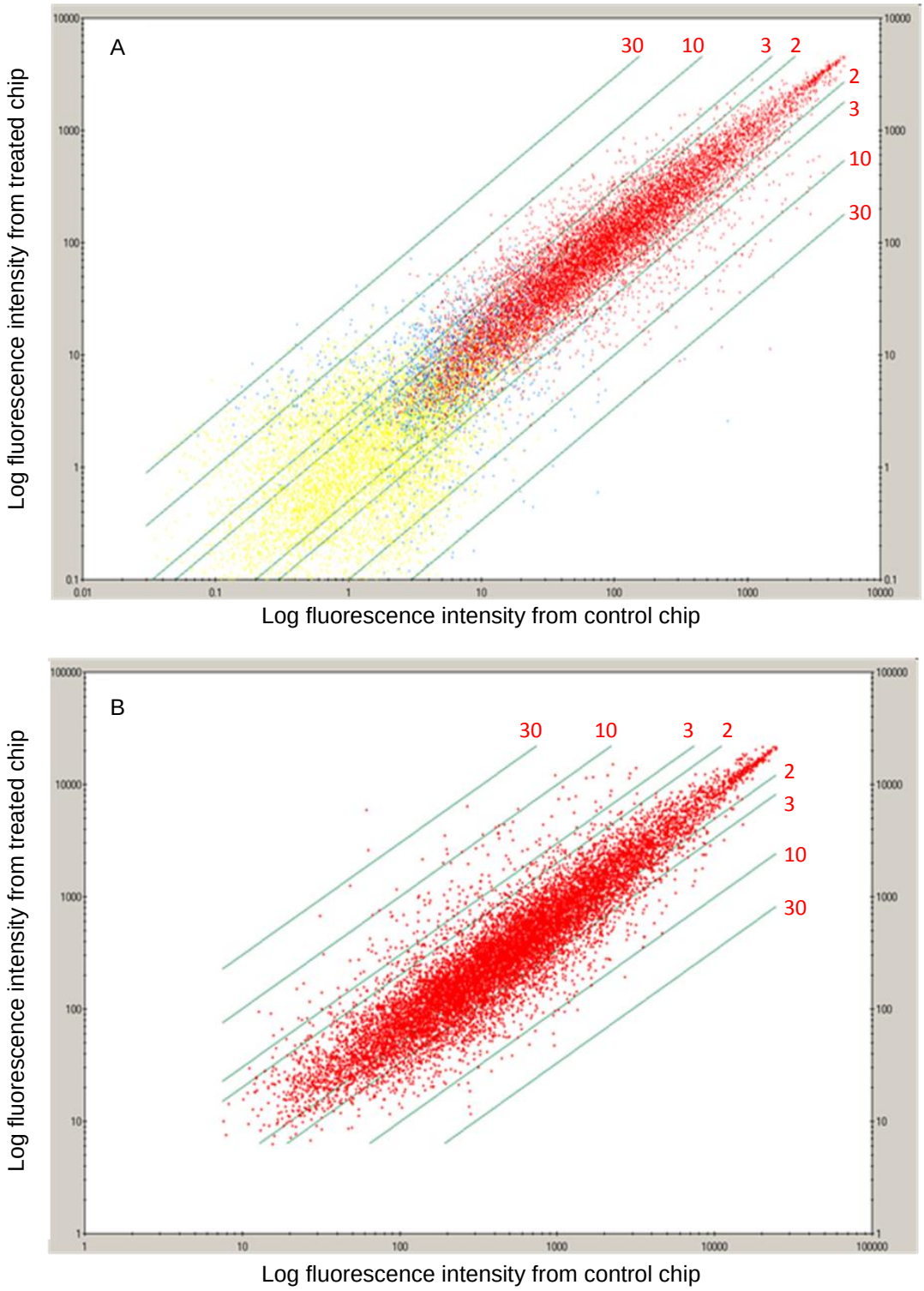

Figure 3.6. Gene expression fluorescence intensity between the control and berry extract treated cells. Caco-2 cells were treated with berry extract at 0.125 % (w/v) for 16 h. RNA was isolated and applied to global gene expression microarray chips, fluorescence intensity from the chip was quantified, data was then normalised and filtered. **A**) Microarray fluorescence intensity signals prior to normalisation and filtering; and **B**) after normalisation and filtering. Lines and red numbers indicate fold-changes of 2, 3, 10 and 30 respectively from centre. Red • - Present signal on both chips; Blue • - Present signal on one chip only; Yellow • - Absent signal on both chips.

3.3.3 Pathways affected by berry extract in Caco-2 cells

Pathway analysis indicated there were a large number of processes affected by the berry extract. Significance of enrichment of networks decreased considerably with increasing stringency of filtering. For a tabulated summary of the highest scoring pathways resulting from each filtering condition see **Table 3.2**. A number of associated functions of these pathways were common throughout the filtering process which included: *cell cycle*, *gastrointestinal disease*, *gene expression*, *molecular transport*, and *small molecule biochemistry*. For a description of the bioinformatics method for pathway analysis see **Appendix 9.3.1**.

3.3.4 Gene ontological and functional similarity clustering

GO term clustering analysis revealed a large number of enriched terms in our gene-list; a sample of these is presented in **Table 3.3**. GO terms enriched in our down-regulated gene-list include: *ion transport* and *carbohydrate metabolism*; see **Section 9.5.1 Down-regulated genes** for a complete list. GO terms enriched in our up-regulated gene-list were for *transport* and *protein localisation*; see **Section 9.5.2 Up-regulated genes** for a complete list. Gene functional similarity clustering, to DMT1, indentified 27 other genes related in nutrient and metal transport (**Figure 3.7**).

Table 3.2. Gene networks affected by berry extract in Caco-2 cells. Caco-2 cells were treated with berry extract at 0.125 % (w/v) for 16 h. RNA was isolated and applied to microarray chips. Microarray data was subjected to pathway analysis under 4 different filters with increasing analysis stringency. * Network score is $-\log_{10}$ of a Fisher's exact *p*-value.

Analysis number and filter/s	Number of networks identified	Associated functions of top 5 networks	Network score*
1: All molecules/ relationships	100	Cell Cycle, Cellular Assembly and Organisation, DNA Replication, Recombination, and Repair.	40
		Developmental Disorder, Genetic Disorder, Neurological Disease.	40
		Cellular Function and Maintenance, Skeletal and Muscular System Development and Function, Organ Development.	40
		Cell Cycle, Cancer, Gastrointestinal Disease.	37
		RNA Post-Transcriptional Modification, Endocrine System Development and Function, Small Molecule Biochemistry.	35
2: Molecules/ relationships were species = human	70	Cell Death, Inflammatory Disease, Hematological Disease.	30
		Cell Cycle, DNA Replication, Recombination, and Repair, Cellular Movement.	30
		Cell Death, Cellular Growth and Proliferation, Cell Cycle.	30
		Cancer, Cellular Movement, Reproductive System Disease.	13
		Carbohydrate Metabolism, Molecular Transport, Small Molecule Biochemistry.	12
3: Molecules/ relationships were cell lines = colon cancer cell lines	16	Cell Death, Cancer, Respiratory Disease	10
		Cancer, Gastrointestinal Disease, Reproductive System Disease	6
		Cancer, Cell Death, Reproductive System Disease	5
		Cell Death, Cancer, Cell Cycle	5
		Cancer, Cellular Growth and Proliferation, Gastrointestinal Disease	5
4: Molecules/ relationships were (species = human) & (cell lines = colon cancer cell lines)	19	Cell Death, Cancer, Cell Cycle	7
		Cancer, Cell Death, Connective Tissue Disorders	7
		Gene Expression, Cell Cycle, Cancer	4
		Cancer, Cell Death, Gastrointestinal Disease	3
		Cell Death, Cancer, Reproductive System Disease	2

Table 3.3. Highly enriched GO terms in berry extract treated Caco-2 cells. Caco-2 cells were treated with berry extract at 0.125 % (w/v) for 16 h. RNA was isolated and applied to microarray chips. Microarray data was subjected to GO clustering. GO: Gene ontology.

GO term category	GO terms	Up- or Down-regulated
Molecular function	Metal ion binding	↓
	Iron ion binding	↓
	Zinc ion binding	↓
	Transmembrane transporter activity	↑
	Substrate specific transmembrane transporter activity	↑
	Sugar: hydrogen ion transporter activity	↑
	Carbohydrate transmembrane transporter activity	↑
	ATPase activity coupled to transmembrane movement of substances	↑
	Glucose transmembrane transporter activity	↑
	Passive transmembrane transporter activity	↑
Biological Process	Carbohydrate metabolic processes	↓
	Metal ion homeostasis	↓
	Calcium ion homeostasis	↓
	Metal ion transport	↓
	Glucose metabolic process	↓
	Iron ion transport	↓
	Transport	↑
	Intracellular transport	↑
	Vesicle mediated transport	↑
	Regulation of intracellular transport	↑
	Metal ion transport	↑
Cellular component	Brush border	↓
	Integral to Golgi membrane	↓
	Apical plasma membrane	↓
	Basolateral plasma membrane	↑
	Membrane-bound vesicle	↑
	Late endosome	↑

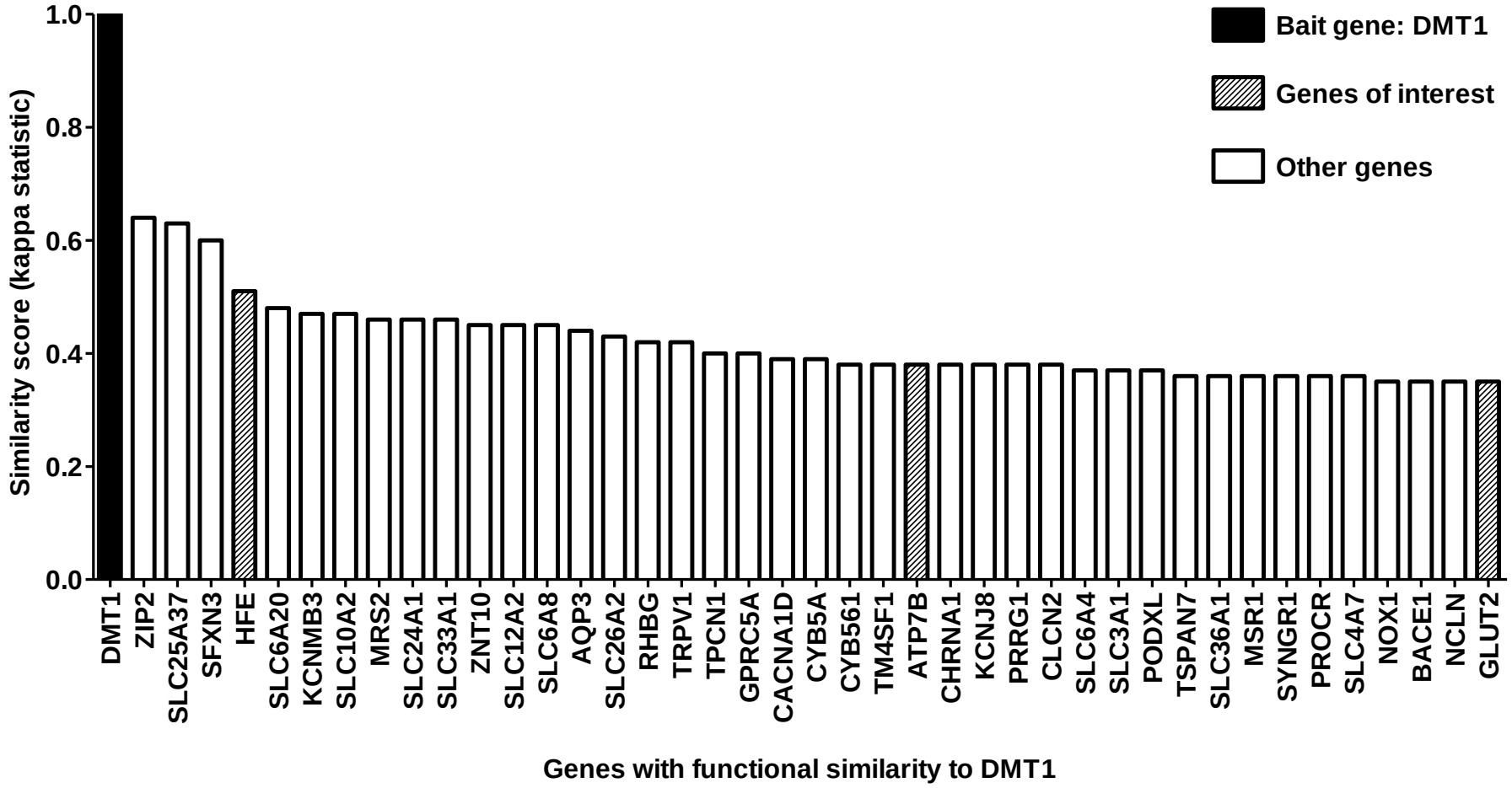

Figure 3.7. Differentially expressed genes with functional similarity to DMT1 in berry extract treated Caco-2 cells. Caco-2 cells were treated with berry extract at 0.125 % (w/v) for 16 h. RNA was isolated and applied to microarray chips. Microarray data was analysed by gene functional similarity to DMT1, the initial '*bait*' gene. Gene functional similarity (Kappa score) is determined by the overlap of gene ontology terms between all genes in the submitted gene list and the initial bait gene. From this list, some genes specifically relating to nutrient transport were chosen for further investigation. DMT1: Divalent metal ion transporter 1; HFE: Human haemochromatosis gene; ATP7B: Copper transporting ATPase β-polypeptide; GLUT2: facilitative glucose transporter 2.

3.3.5 Preliminary validation of microarray detected gene expression

Expression of DMT1, 7 functionally related genes and 4 randomly chosen genes were quantified by qRT-PCR as validation of microarray data. In terms of directionality, microarray-detected changes were similar to data obtained by qRT-PCR. There was a significant correlation between microarray-detected and qRT-PCR-detected changes in gene expression ($r^2 = 0.45$; $p \leq 0.05$) (**Figure 3.8**).

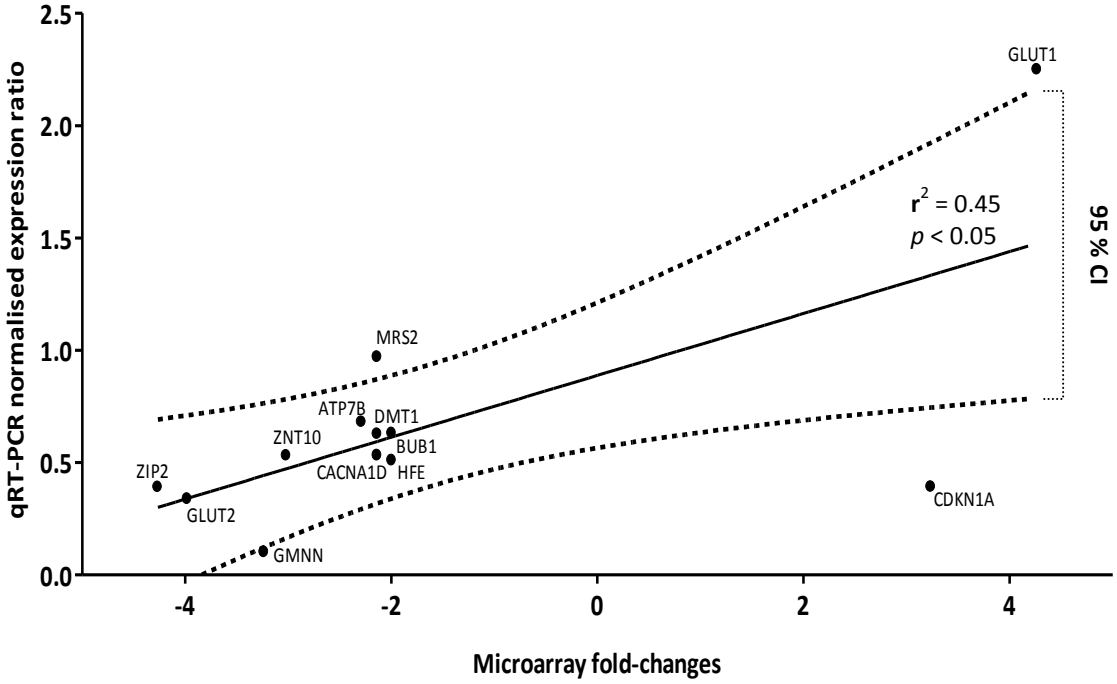

Figure 3.8. Quantitative PCR validation of microarray detected fold-changes from berry extract treated Caco-2 cells. Caco-2 cells were treated with berry extract at 0.125 % (w/v) for 16 h. RNA was isolated and applied to global gene expression microarray chips. A number of genes were chosen for validation of microarray data. Validation of gene expression changes was done using qRT-PCR. The microarray and qRT-PCR data are significantly correlated (solid line: $r^2 = 0.45$; $p \leq 0.05$; dashed lines are 95% confidence intervals). DMT1: divalent metal ion transporter 1. ATP7B: copper transporting ATPase β-polypeptide, HFE: haemochromatosis protein; GLUT2: facilitative glucose transporter 2. All others were arbitrarily chosen for purposes of validation; their biological roles are not pertinent to the subject of this thesis

3.4 Discussion

After consumption, flavonoids are known to be present at high concentrations in the intestinal lumen, up to 50 or 100 fold higher than those levels found in the circulation (Manach *et al*, 2005; Kwon *et al*, 2007). In this anatomical region the flavonoids have direct interaction with the absorptive enterocytes (Talavera *et al*, 2004; Matuschek *et al*, 2006). Although flavonoids are known to have a broad therapeutic spectrum, their precise transcriptional effects are unknown. We therefore tested the supposition that dietary flavonoids are capable of altering the human intestinal Caco-2 cell transcriptome. This was addressed by use of microarrays and bioinformatic analysis. Transcriptome analysis generated gene-lists that were later subjected to pathway analysis, GO analysis and functional similarity clustering. Finally, a number of genes were selected for validation, and to generate areas for further research.

Bioinformatic analysis revealed that flavonoids affected the expression of genes relating to gastrointestinal conditions, inflammation and nutrient transport. Functional similarity clustering, around our initial gene of interest DMT1, identified genes related to the transport of dietary metals (iron: HFE; copper: ATP7B) and glucose (GLUT2). Microarray data must be validated, to some degree, with the use of more sensitive and specific methods of gene expression analysis such as qRT-PCR. The expression of the above genes and other randomly chosen ones was validated as such, with qRT-PCR, thus lending support to the validity of our array. The following discussion focuses on our microarray analysis in the context of other published high-throughput data.

3.4.1 Effects of flavonoids on transcriptome variation

The term '*enrichment'* refers to the high proportions of co-functioning genes in a given gene-list. In other words, if an experimental gene-list is *enriched*, it will have a higher proportion of co-functioning genes than the background gene-list (e.g. human genome). Furthermore, *term* refers to detailed items in a given database; e.g. *oxygen binding* is a *term* from a database that encompasses *molecular functions* (Huang da *et al*, 2008). *Term*, is often used synonymously with the word *cluster*. However, comparison of results between microarray-based studies remains problematic due to inconsistent ways of reporting and due to different bioinformatic and statistical approaches.

In a study by Tsuda *et al* (2006), where adipocytes were treated with an anthocyanin extract, GO terms such as *carbohydrate metabolism, lipid metabolism, ion transport* and *cell cycle processes* were shown to be enriched. Our gene-list was also enriched with such terms. On a gene-by-gene basis Tsuda *et al* (2006) reported decreased expression of GLUT3 and ATP7A. These genes are isoforms of GLUT2 and ATP7B, respectively, both of which had decreased expression in our study. This indicates a common feature of flavonoid-induced ATPase and GLUT mRNA regulation between cell types. Lefevre *et al* (2008) found that grape-anthocyanins downregulated *mitochondrial function, energy metabolism* and *acute inflammatory response* GO clusters in hepatocytes. These were similarly enriched in our findings and are possibly attributed to the general antioxidant effects of flavonoids. In another study, conducted in humans (Boomgaarden *et al*, 2010), quercetin administration enriched GO clusters relating to *nucleic acid metabolism* and *apoptosis* in monocytes. This also agrees with our findings. However, the affected pathways (as opposed to ontological clusters) reported in the aforementioned study

were very different to the ones we identified. Therefore pathway activation may be more of a cell- or tissue-type specific phenomenon than GO term enrichment.

3.4.2 Transcriptomic evidence of flavonoids and nutrient interactions

Our array findings emphasise that flavonoids induce differential expression of genes that coordinate transport of metals and glucose. In this section there is a discussion of the evidence which supports the putative interactions between flavonoids and these nutrients.

3.4.2.1 Putative interactions of glucose and flavonoids

There have been reports of the putative anti-diabetic properties of flavonoids in other microarray-based studies (Suzuki *et al*, 2011; Viduranga *et al*, 2011). For example, the flavone baicalin has been found to reduce oxidative stress induced by hyperglycaemia. This was through the increased hepatic expression of antioxidant enzymes in Goto-Kakizaki rats fed baicalin (Viduranga *et al*, 2011). Furthermore, anthocyanidin treatments have been found to strongly inhibit adipocyte differentiation mediated via the insulin pathway (Suzuki *et al*, 2011).

In our study, berry extract treatment decreased the expression of GLUT2 mRNA, a major monosaccharide transporter. Furthermore, our gene-list, of berry extract treated cells, was enriched with the following ontology terms: *glucose transmembrane transporter activity*, *apical plasma membrane* and *basolateral plasma membrane*. These findings support the putative anti-diabetic properties of flavonoids, as GLUT2 is a major apical and basolateral channel for intestinal glucose transport. In-fact, permanent apical localisation of GLUT2 is a major characteristic of insulin resistant states and a popular animal model of diabetes (i.e. the *ob*/*ob* mouse) (Tobin *et al*, 2008; Ait-Omar *et al*, 2011). Therefore, differential expression

of GO terms related to glucose transporters and their cellular membrane localisations provide strong support for the beneficial anti-diabetic properties of flavonoids.

3.4.2.2 Putative interactions of dietary metals and flavonoids

Flavonoids are known to form complexes with metal ions; these interactions are known to influence the dietary metal transport processes (Kim *et al*, 2008; Lekka *et al*, 2009). In light of this, it is not surprising that the berry extract caused differential expression of a number of genes relating to dietary metal transport. Furthermore, enriched GO terms were related directly to dietary metal metabolism, these include: *metal ion binding*, *iron ion binding*, *zinc ion binding*, *metal ion transport*, *metal ion homeostasis* and *iron ion transport*. The differentially expressed genes in our array are specifically involved in the transport of dietary iron (HFE and DMT1), copper (ATP7B, and DMT1 is also known to transport copper), zinc (the zinc influx and efflux genes ZIP2 and ZNT10, respectively) and magnesium (the magnesium homeostasis factor MRS2).

Other array based studies have reported findings supporting flavonoid interactions with metal metabolism. Zhao *et al* (2011) reported that flavonoids induced differential expression of phase 2 enzymes and the ATP-binding cassette (ABC) transporter superfamily in rat livers. These groups of enzymes are involved in the metabolism, biotransformation and biliary excretion of quercetin. As well as the site of flavonoid metabolism and excretion, the liver is the main site of copper metabolism and excretion in the body. Thus, there are clear effects of flavonoids at the sites of copper absorption, metabolism and excretion; i.e. intestinal and hepatic tissues (Tsuda *et al*, 2006; Natsume *et al*, 2009; Zhao *et al*¸ 2011). Furthermore, specific genes involved in copper homeostasis are affected by flavonoids, (i.e. ATP7B and DMT1). In light of our findings and those from Tsuda *et al* (2006),

Natsume *et al* (2009) and Zhao *et al* (2011) there is transcriptomic evidence that flavonoids affect copper metabolism/excretion.

In the study by Natsume *et al* (2009) a 2 week administration of quercitin and its derivatives caused a decrease in expression of iron transport-related genes (e.g. FPN, MT, ferritin heavy chain) and several ATPases in mouse intestine. This is consistent with our *in-vitro* findings of the berry extract causing down-regulation of metal transport-related genes in enterocytes. Although different genes are reported by Natsume *et al* (2009), they are part of a single pathway, which is the intestinal transport of iron. The longer duration of treatment by Natsume *et al* (2009) may have activated pathways of crypt cell programming; in turn dictating the absorptive capacity of enterocytes (Parkkila *et al*, 1997; Bédrine-Ferran et al, 2004).

3.4.2.3 Flavonoids, metals, glucose and oxidative stress

It is well known that cellular glucose and metal homeostasis are tightly regulated, as an increase in either one will induce cellular oxidative stress (Núñez *et al*, 2001; Han & Park, 2011; Ogawa *et al*, 2011). Furthermore, nutrient transport is known to be sensitive to cellular oxidative states. In light of this, it is not surprising that flavonoid antioxidants may reverse the effects of such oxidative stress on transport processes (Han & Park, 2011; Jagetia & Reddy, 2011; Dhar *et al*, 2012).

Previous researchers have consistently reported GO terms relating directly to *oxidative stress*, *antioxidants* or *cellular oxidative state* following flavonoid treatments (Viduranga *et al*, 2011; Zhao *et al*, 2011). However, we did not find any GO terms relating directly to antioxidant potential, this may be due to the treatment durations, the sources of flavonoids, the cell line under investigation or the general study designs. Inasmuch as inclusion of a treatment condition to induce oxidative stress co-incubated with the flavonoids may result in enrichment of the

aforementioned GO terms; or given the volatile nature of redox reactions and responses, shorter durations may cause enrichment or oxidative stress related GO terms. However, the co-regulation of metal and glucose transport related genes, in our study, suggests there is an antioxidant role of flavonoids mediated through their nutrient interactions; i.e. preventing oxidative stress induced by high cellular metal or glucose concentrations.

3.5 Conclusions and implications for next chapters

In this study, microarray analysis was applied to derive biological themes arising from the effects of flavonoids on cells of the intestinal epithelium. Gene expression arrays are typically used as screening tools or to generate testable hypotheses.

Following Caco-2 cell treatment with berry flavonoids, informatic analysis identified a large number of pathways and ontological clusters of genes that were affected. Pathway analysis revealed networks with functions relating to cell cycle, gene expression, post-translational modification and molecular transport, among others. Numerous GO terms were enriched, including: *metal ion binding*, *glucose transmembrane transporter activity*, *transport*, *brush border* and *late endosome membrane*. The GO findings are consistent with previous findings from other groups. This indicates there are common mechanisms to regulate mRNA of these co-functioning genes.

We also applied functional similarity clustering around DMT1 as a bait gene. We found genes relating to metal transport, namely iron transport (HFE) and copper transport (ATP7B). Furthermore, the major glucose transporter, GLUT2, was also down-regulated. In the remainder of this thesis, we focused on these candidate genes. We investigated the effects of flavonoids on intestinal uptake of glucose, iron and copper.

CHAPTER FOUR

Effects of flavonoids on the expression and function of intestinal glucose transporters in Caco-2 enterocytes

4 Effects of flavonoids on the expression and function of intestinal glucose transporters in Caco-2 enterocytes

4.1 Introduction: Intestinal glucose uptake and dietary flavonoids

The primary step in glucose metabolism is intestinal glucose absorption; it is adaptable to luminal and systemic factors to maintain glucose homeostasis (Cui *et al*, 2003; Tobin *et al*, 2008). The classical mechanisms of intestinal glucose transport state that apical uptake is mediated via the sodium/glucose co-transporter member 1, SGLT1, and that basolateral release is mediated via the facilitative glucose transporter member 2, GLUT2. However, the apical uptake of glucose can occur through both a saturable component and a non-saturable diffusive component. The phloridzin-sensitive SGLT1 pathway accounts for saturable uptake. The diffusive component, however, is suggested to be mediated via GLUT2 at an apical localisation (Debnam & Levin, 1975; Kellet & Helliwell, 2000).

Current models suggest that under conditions of high luminal glucose, GLUT2 translocates to the apical membrane, which increases glucose uptake by up to 3-fold more than SGLT1 alone (Gouyon *et al*, 2003). Under healthy conditions, GLUT2 is then retracted from the apical membrane in response to insulin signaling after plasma glucose levels increase (Tobin *et al*, 2008). However, in insulin-resistant states, GLUT2 is permanently localised at the apical membrane. It does not respond to insulin signaling, thereby chronically increasing glucose influx (Corpe *et al*, 1996; Tobin *et al*, 2008). This high transport capacity of GLUT2, its translocation properties and its permanent apical presence during insulin resistance, makes it a major candidate for the control of glucose absorption. Although pharmacological regimes are currently used to maintain plasma glucose, they have numerous side-

effects (for example, hypoglycaemia, weight gain, diarrhea). Furthermore, pharmacological intervention remains supplementary to rigorous dietary and lifestyle management. In light of this, there has been an emergence of interest in the putative therapeutic properties of polyphenolics in order to optimise dietary management of this disease (Cheng & Fantus, 2005; Martinuea *et al*, 2006).

It is currently well known that intestinal glucose uptake is sensitive to polyphenols, exemplified by the inhibitory effects of apple polyphenol phloridzin and apple tree leaf polyphenol phloretin, on SGLT1 and GLUT2 mediated uptake, respectively (Alvarado, 1967). Other flavonoids have been confirmed to inhibit glucose uptake, such as quercetin, cyanidin and catechins (Park, 1999). The most potent inhibitors of glucose uptake are flavones or flavonols with hydroxylation of the C5 and/or C7 positions (Park, 1999). Furthermore, past research has established selective interaction of glycosylated compounds such as neohesperidin and phloridzin with SGLT1 (Gee *et al*, 1998; Walgren *et al*, 1998; Walgren *et al*, 2000; Wolfram *et al*, 2002; Walle & Walle, 2003). In contrast, aglycone flavonoids, like phloretin, target GLUT2 (Johnston *et al*, 2005; Kwon *et al*, 2007). In light of this, quercetin, its derivatives and structurally similar flavonoids, may be effective regulators for both absorptive components of intestinal glucose uptake.

Previous studies of the modulatory effects of flavonoids on glucose uptake were conducted with acute treatments of 1 h or less (for example Gee *et al*, 1998; Wolfram *et al*, 2002; Johnston *et al*, 2005). Such short durations would not have allowed transcriptional or translational events to have fully taken place; therefore the measurement of such a response would not have been possible. Furthermore, studies used isolated synthetic flavonoids, i.e. not from a food matrix, thus disregarding the potential synergistic effects of a heterogeneous mixture of polyphenolics.

The aim of this study was to address the issues raised above and in particular the hypothesis that dietary polyphenolics modulate glucose uptake and the expression of intestinal glucose transporters. Berries are a rich source of flavonoids, and quercetin is the most abundant polyphenol in the diet. Therefore in this study we have used a flavonoid-rich berry extract, (i.e. Optiberry®), quercetin and the well documented phloretin and phloridzin in the established Caco-2 cell model of human enterocytes.

4.2 Methods

Presented here is a brief description of the methods used in this chapter. For full details of reagents, buffer/media compositions and methods used see **Chapter 2**.

4.2.1 Cell culture

Caco-2 TC7 cells between the passages of 44 and 47 were seeded into 6-well plates at a density of approximately 40,000 cells per well (4,000 cells per cm^2) and cultured for 19 days prior to treatment. Details of the maintenance of the cells and composition of cell culture medium have been previously described (see **Chapter 2** and Johnston *et al*, 2005).

The treatment used was a flavonoid-rich berry extract (derived from blueberry, bilberry, cranberry, elderberry, raspberry seeds and strawberry; rich in the anthocyanins delphinidin, cyanidin, petunidin and malvidin, OptiBerry®, InterHealth Nutraceuticals, CA, USA) at a final concentration of 0.125 % (w/v). Isolated flavonoids used were quercetin, phloretin and phloridzin at a final concentration of 100 µM. Isolated flavonoids were dissolved in DMSO, which was then diluted into the treatment media or buffer to give a final DMSO concentration of 0.05 % (v/v). All treatments were prepared in DMEM for gene expression, protein abundance studies and chronic-exposure glucose-uptake experiments. Treatments for acute-exposure glucose-uptake experiments were prepared in HBSS. Controls for the berry extract cells were treated with identical medium without the berry extract. Controls for isolated flavonoid-treated cells were treated with identical medium, containing 0.05 % (v/v) DMSO, without the flavonoids. All treatments were added followed by gentle mixing.

The effect of flavonoid and solvent treatments on cell viability, RNA and protein content of the cells were tested. There were no effects of any treatments on cell viability, RNA or protein content (see **Results, Section 4.3.1**).

4.2.2 Real-time qPCR

Total RNA was isolated from cultured cells using TRIzol® (Invitrogen™ life technologies, Paisley, UK) according to the manufacturer's protocol. Following first strand cDNA synthesis (using a high-capacity cDNA reverse transcription kit, Applied Biosystems™ Cheshire, UK), expression levels of GLUT2 and SGLT1 mRNA and of 18S and GAPDH mRNA (used as housekeeping genes) were analysed by real-time PCR using an ABI Prism 7700HT Sequence Detection System and a Power SYBR® Green PCR master mix kit (Applied Biosystems™ Cheshire, UK). Primers were designed using the online design tool Primer3 (Rozen & Skaletsky, 2000) and sourced from MWG Eurofins (London, UK). Quantitative measurement of gene expression was derived from the $2^{(-\Delta\Delta Ct)}$ *method*, also known as the *Livak method* (Livak & Schmittgen, 2001; Schmittgen & Livak, 2008). Data were expressed as ratios to the control and normalised to the housekeeping genes 18S and GAPDH. The primer sequences used for each gene are in **Table 4.1**.

Table 4.1. Primer sequences for qRT-PCR gene expression analysis.

Gene symbol	Forward primer 5'-3'	Reverse primer 5'-3'
GLUT2	AGT TAG ATG AGG AAG TCA AAG CAA	TAG GCT GTC GGT AGC TGG
SGLT1	TCT TCG ATT ACA TCC AGT CCA	TCT CCT CTT CCT CAG TCA TC
18S	AAC TTT CGA TGG TAG TCG CCG	CCT TGG ATG TGG TAG CCG TTT
GAPDH	CTG TTG CTG TAG CCA AAT TCG T	ACC CAC TCC TCC ACC TTT GA

GLUT2: facilitative glucose transporter member 2; SGLT1: sodium-glucose cotransporter member 1; 18S: ribosomal RNA18S; GAPDH: glyceraldehyde 3-phosphate dehydrogenase.

4.2.3 Western blotting

Total protein from Caco-2 cells was prepared as described previously (Chaston *et al*., 2008). Total proteins (40 μg) were solubilised in loading buffer and subjected to SDS-PAGE. Following transfer to nitrocellulose, membranes were exposed to GLU2 or SGLT1 antibodies; β-actin levels were used to normalise. Proteins were visualised using a horseradish peroxidase-linked secondary antibody and Novex® ECL chemiluminescent substrate reagent kit (Invitrogen™ Life Technologies, Paisley UK). Band densities were quantified on a densitometer (GS-800™) and Quantity One software (Bio-Rad Laboratories, Hertfordshire, UK). For antibody concentrations and reagents see **Section 2.2.4. Protein abundance analysis**.

4.2.4 Glucose uptake assays

For full description of glucose uptake assays see **Section 2.2.5.1. Glucose uptake experiments**, for buffer composition, radionuclides and suppliers see **Section 2.1.5. Materials used in nutrient uptake and transport studies**; this section only briefly describes the protocol applied. Glucose uptake assays were performed with D-[^{3}H]-glucose and designed to identify interactive and transcriptional/translational effects of flavonoids on glucose uptake. Caco-2 cells were exposed to flavonoid treatments acutely (15 min) or chronically (16 h). For acute incubations, D-[^{3}H]-glucose was added into the treatment solution. In chronic incubation studies, treatment solutions were replaced with uptake buffer containing only D-[^{3}H]-glucose. Uptake carried out in the presence and absence of sodium allowed differentiation between effects on sodium-dependant (mediated by GLUT2 and SGLT1) and sodium-independent (mediated by GLUT2) pathways. The difference between the two, when sodium-dependent was greater than sodium-independent uptake, the difference indicated SGLT1-mediated uptake.

4.2.5 Data and statistical analysis

Data are expressed as means ± SEM of 4, 6 or 12 observations per group depending on the experiment. Statistical analysis was carried out using GraphPad Prism 5 (San Diego, CA, USA). In studies containing 2 experimental groups Student's unpaired t-test was used to compare means. Differences between multiple groups were calculated using a 1-way ANOVA with Dunnett's post-hoc test. For data that was not normally distributed a Kruskal-Wallis test was used with Dunn's post-hoc test. In all instances significance was indicated when $p \leq 0.05$.

4.3 Results

4.3.1 Effects of flavonoids on cell viability, RNA and protein content

The effects of treatments on cell viability, RNA content and protein content were examined to ensure effects were not due to pathological changes, but as normative responses. There was no effect of flavonoids or solvent on cell viability (**Figure 4.1**), RNA content (**Figure 4.2**), or protein content (**Figure 4.3**).

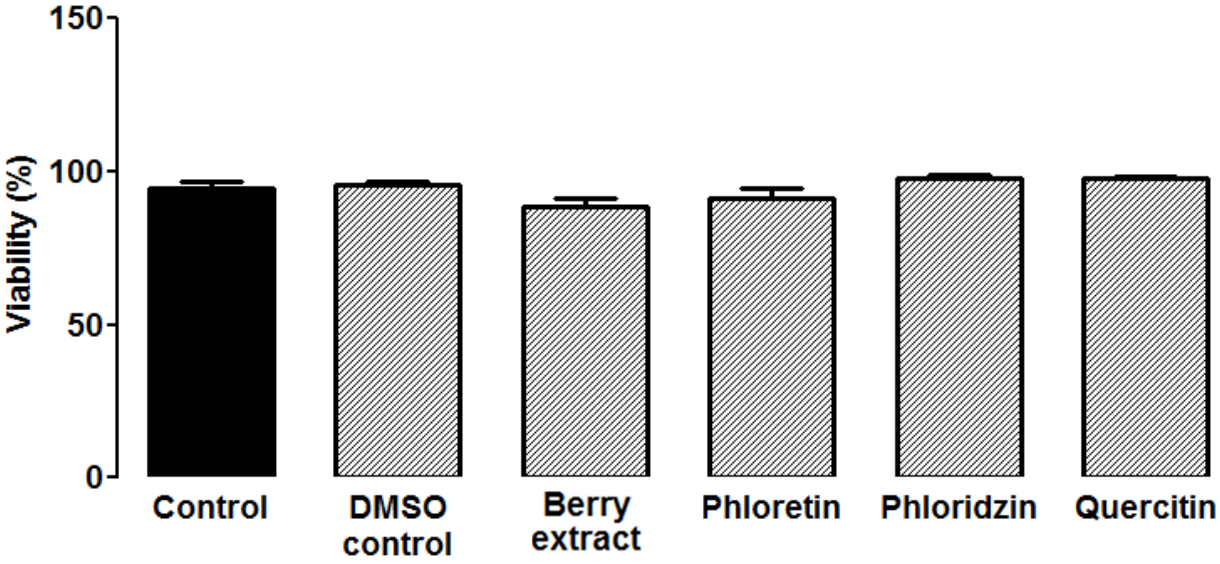

Figure 4.1. Caco-2 cell viability after flavonoid treatments. Caco-2 cells were treated with berry extract at a concentration of 0.125 % (w/v), phloretin, phloridzin or quercetin at 100 µM, or DMSO at a concentration of 0.05 % (w/v) for 16 h. Cell viability was quantified by the trypan blue dye-exclusion method. Data is presented as mean percentage viable cells ± SEM, n = 4. ANOVA and Dunnet's post-hoc test showed there was no significant difference between groups. DMSO: dimethyl sulfoxide.

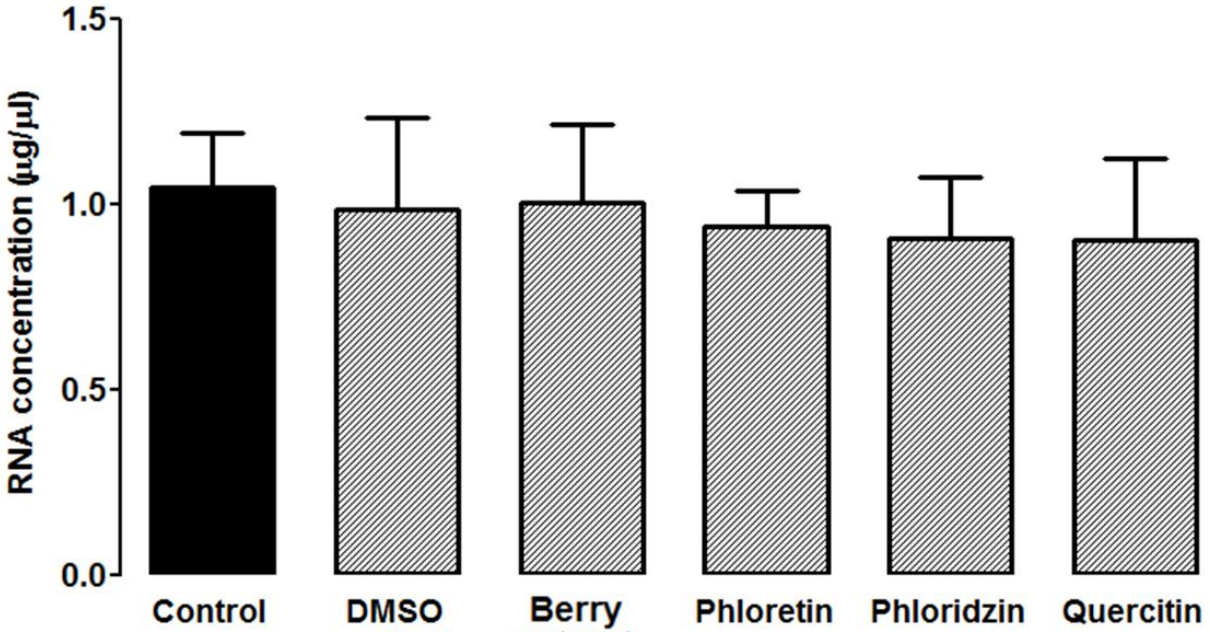

Figure 4.2. RNA concentration from Caco-2 cells after flavonoid treatment. Caco-2 cells were treated with berry extract at a concentration of 0.125 % (w/v), phloretin, phloridzin or quercetin at 100 µM, or DMSO at a concentration of 0.05 % (w/v) for 16 h. RNA concentration in the extracts of Caco-2 cells was quantified with the NanoDrop spectrophotometer. Data is presented as mean RNA concentration ± SEM, *n* = 6. ANOVA and Dunnet's post-hoc test showed there was no significant difference between groups. DMSO: dimethyl sulfoxide.

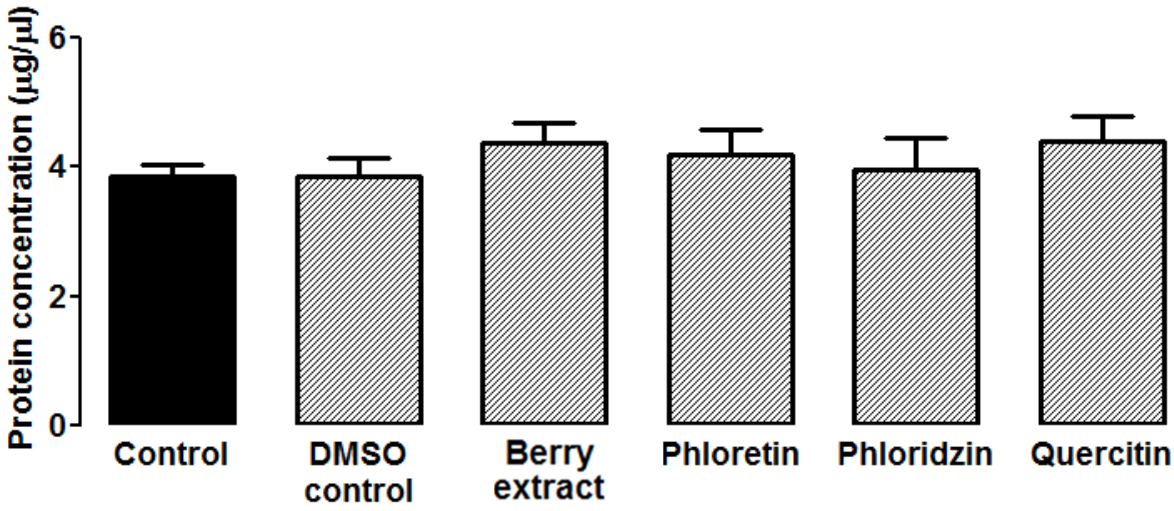

Figure 4.3. Protein concentration from Caco-2 cells after flavonoid treatment. Caco-2 cells were treated with berry extract at a concentration of 0.125 % (w/v), phloretin, phloridzin or quercetin at 100 µM, or DMSO at a concentration of 0.05 % (w/v) for 16 h. Protein concentration was quantified by the Bradford spectrophotometric assay. Data is presented as mean protein concentration ± SEM, *n* = 6. ANOVA and Dunnet's post-hoc test showed there was no significant difference between groups. DMSO: dimethyl sulfoxide.

4.3.2 Effects of flavonoids on glucose transporter gene expression

Expression of GLUT2 and SGLT1, the main glucose transport genes, was quantified across a number of concentrations of the berry extract and across different treatment durations. Significant inhibitory effects were observed on GLUT2 gene expression at 0.0125 % (w/v) ($p < 0.001$) and at 0.25 % (w/v) ($p < 0.05$; **Figure 4.4**, **panel A**). The expression of GLUT2 at the 0.016 % (w/v) dose (0.79 ± 0.1) was only slightly higher than that at 0.25 % (w/v) dose (0.72 ± 0.2); this slight difference in expression level caused the expression at 0.016 % (w/v) to be just out of the significance threshold, whereas the 0.25 % (w/v) dose expression level was borderline significant ($p \leq 0.05$). As for SGLT1, there was significant inhibition of gene expression at 0.25 % (w/v) ($p < 0.05$; **Figure 4.5**, **panel B**). As for the effects of treatment duration (all with 0.125 % (w/v)), significant effects on GLUT2 gene expression were between 12 h ($p < 0.01$) and 16 h ($p < 0.001$) of treatment (**Figure 4.5**, **panel A**). There was a slight linear trend of the effects of treatment duration on GLUT2 expression, indicating decreased expression with increasing duration of treatment (slope= -0.1; $r^2 = 0.1$; $p < 0.05$; **Figure 4.5**).

Flavonoid treatments were tested on GLUT2 and SGLT1 expression at 0.125 % (w/v) berry extract or at 100 µM of quercetin, phloretin or phloridzin; all treatments were for 16 h. GLUT2 mRNA decreased significantly with the berry extract ($p < 0.001$), quercetin ($p < 0.001$), phloretin ($p < 0.01$) and phloridzin ($p < 0.001$; **Figure 4.6**, **panel A**). SGLT1 mRNA also decreased significantly with the berry extract ($p < 0.01$), quercetin ($p < 0.001$) and phloridzin ($p < 0.05$; **Figure 4.6**, **panel B**).

Note that multiple comparison tests account for overall data variability, and not just variability between 2 groups. This explains disparity between ANOVA findings (time and dose-dependent) and findings from bivariate tests of specific treatments.

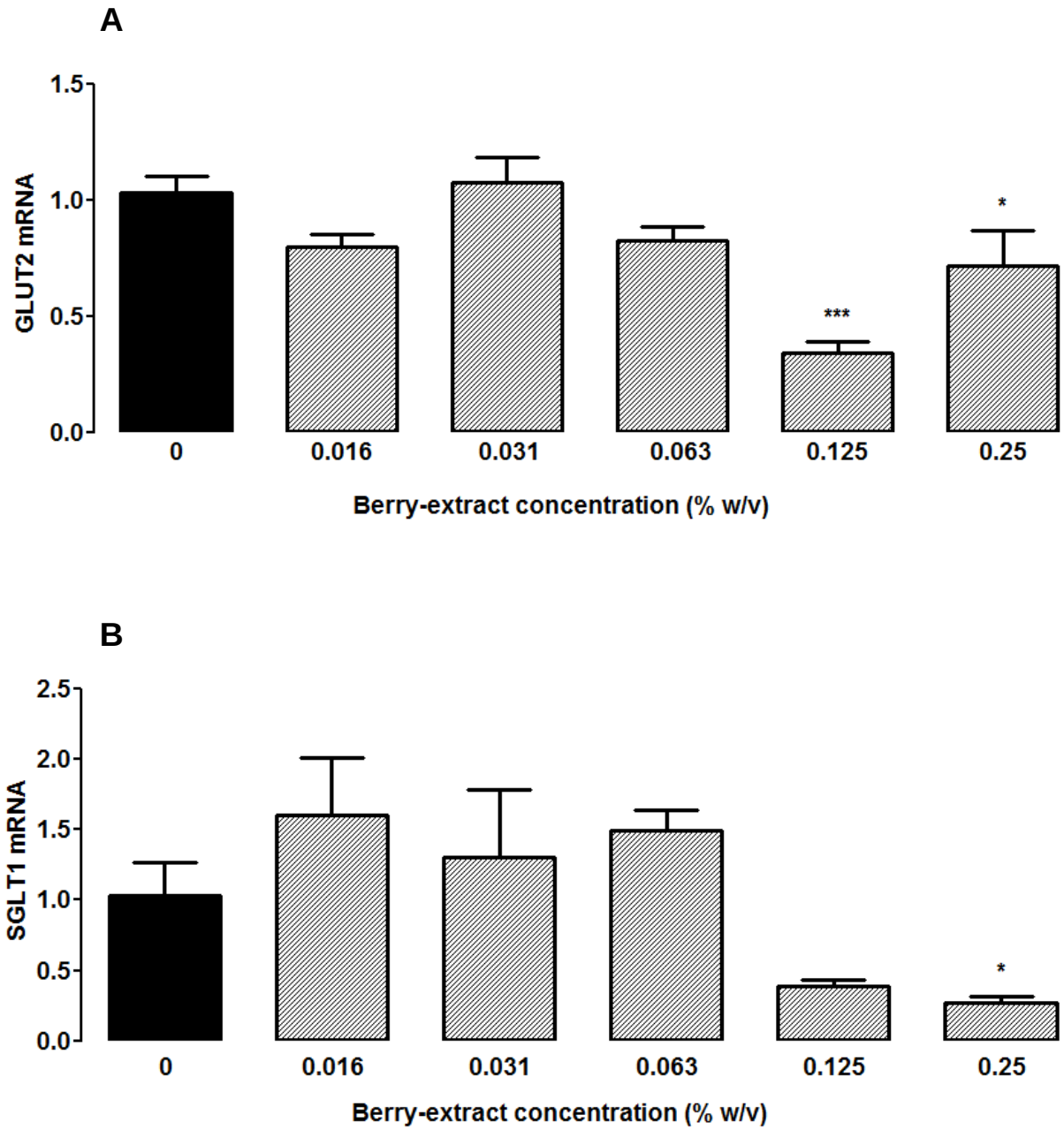

Figure 4.4. Dose-dependent effects of berry extract on GLUT2 and SGLT1 mRNA expression. Caco-2 cells were treated for 16 h with a berry extract at different doses from 0.25 % (w/v) in 2-fold dilutions until 0.016 % (w/v). Levels of GLUT2 (A) and SGLT1 (B) mRNA were quantified by qRT-PCR and normalised against 18S and GAPDH as housekeeping genes. Data are presented as mean normalised expression ratio ± SEM, $n = 6$, statistical significance was determined by an ANOVA and Dunnet's post-hoc test against the 0 % (w/v) concentration. (*) $p \leq 0.05$, (***) $p \leq 0.001$. GLUT2: facilitative glucose transporter 2. SGLT1: sodium/glucose cotransporter 1. 18S: ribosomal RNA 18S. GAPDH: glyceraldehyde 3-phosphate dehydrogenase. qRT-PCR: quantitative real-time polymerase chain reaction.

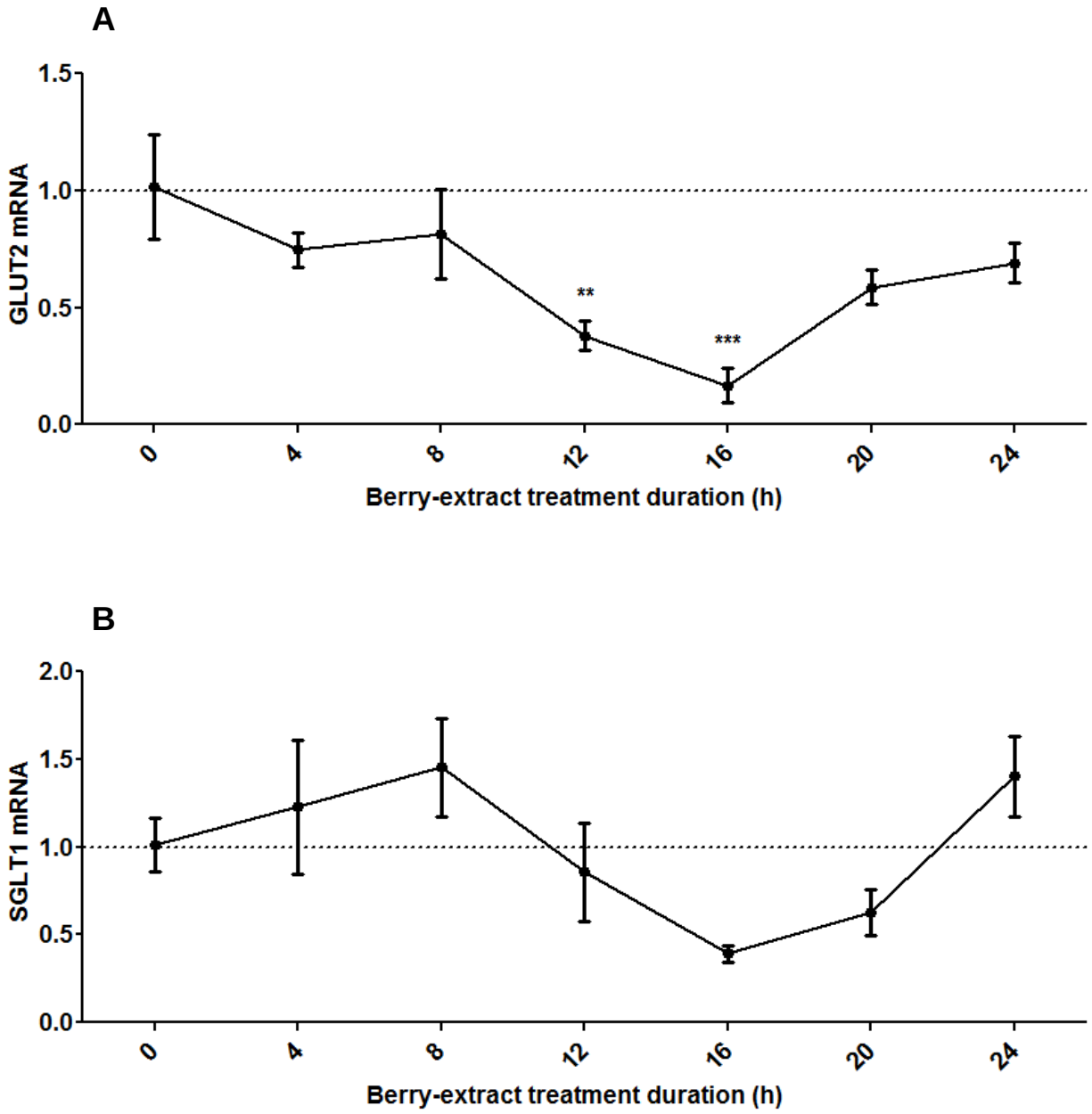

Figure 4.5. Time-dependent effects of berry extract on GLUT2 and SGLT1 mRNA expression. Caco-2 cells were treated with berry extract at 0.125 % (w/v) from 4 h to 24 h. Levels of GLUT2 (A) and SGLT1 (B) mRNA were quantified by qRT-PCR and normalised against 18S and GAPDH as housekeeping genes. Values are mean normalised expression ratio ± SEM, n = 6, statistical significance was determined by an ANOVA and Dunnet's post-hoc test against the 0 h time-point. (**) $p \leq 0.01$, (***) $p \leq 0.001$. ANOVA indicated SGLT1 gene expression as significantly different across the treatment durations ($p \leq 0.05$). There was a significant linear trend for GLUT2 expression (slope= -0.1; $r^2 = 0.1$; $p \leq 0.05$). GLUT2: facilitative glucose transporter 2; SGLT1: sodium/glucose cotransporter 1. 18S: ribosomal RNA 18S. GAPDH: glyceraldehyde 3-phosphate dehydrogenase. qRT-PCR: quantitative real-time polymerase chain reaction.

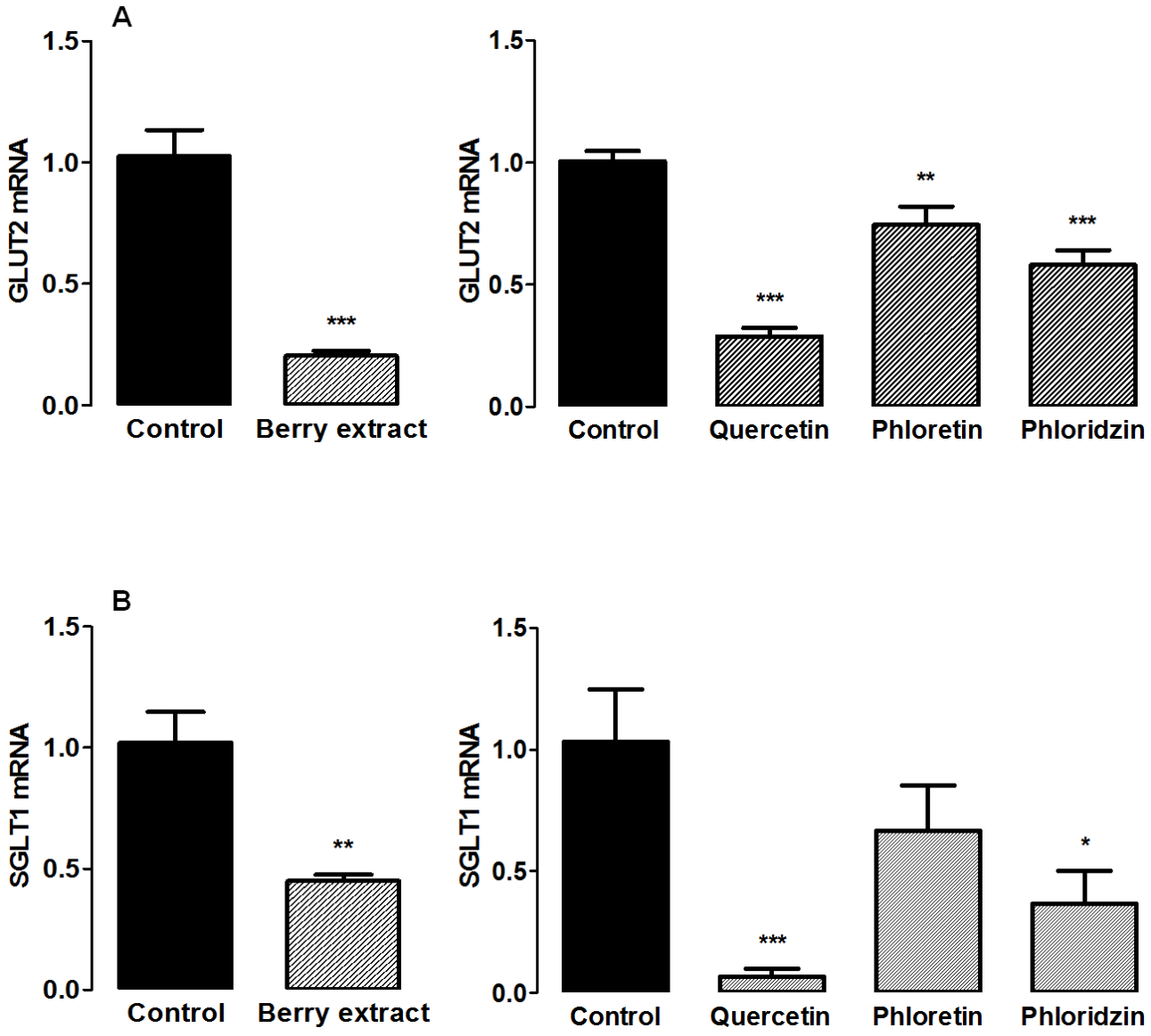

Figure 4.6. Effects of flavonoids on GLUT2 and SGLT1 mRNA expression. Caco-2 cells were treated with berry extract at a concentration of 0.125 % (w/v), phloretin, phloridzin or quercetin at 100 µM, or DMSO at a concentration of 0.05 % (w/v) for 16 h. Expression of GLUT2 (A) and SGLT1 (B) was quantified by qRT-PCR and normalised to 18S and GAPDH as housekeeping genes. Data is presented as mean normalised expression ratio relative to the control ± SEM; n = 6. Statistical significance was determined by an unpaired t-test or ANOVA with Dunnet's post-hoc test against the relevant control. (*) $p \leq 0.05$, (**) $p \leq 0.01$, (***) $p \leq 0.001$. GLUT2: facilitative glucose transporter 2. SGLT1: sodium/glucose cotransporter 1. 18S: ribosomal RNA 18S. GAPDH: glyceraldehyde 3-phosphate dehydrogenase. DMSO: dimethyl sulfoxide. qRT-PCR: quantitative real-time polymerase chain reaction.

4.3.3 Effects of the flavonoids on glucose transporter protein expression

Expression of GLUT2 transporter protein decreased significantly in response to the berry extract treatment ($p < 0.05$; **Figure 4.7**, **panel A**). There was no effect on the expression of SGLT1 transporter protein (**Figure 4.7**, **panel B**)

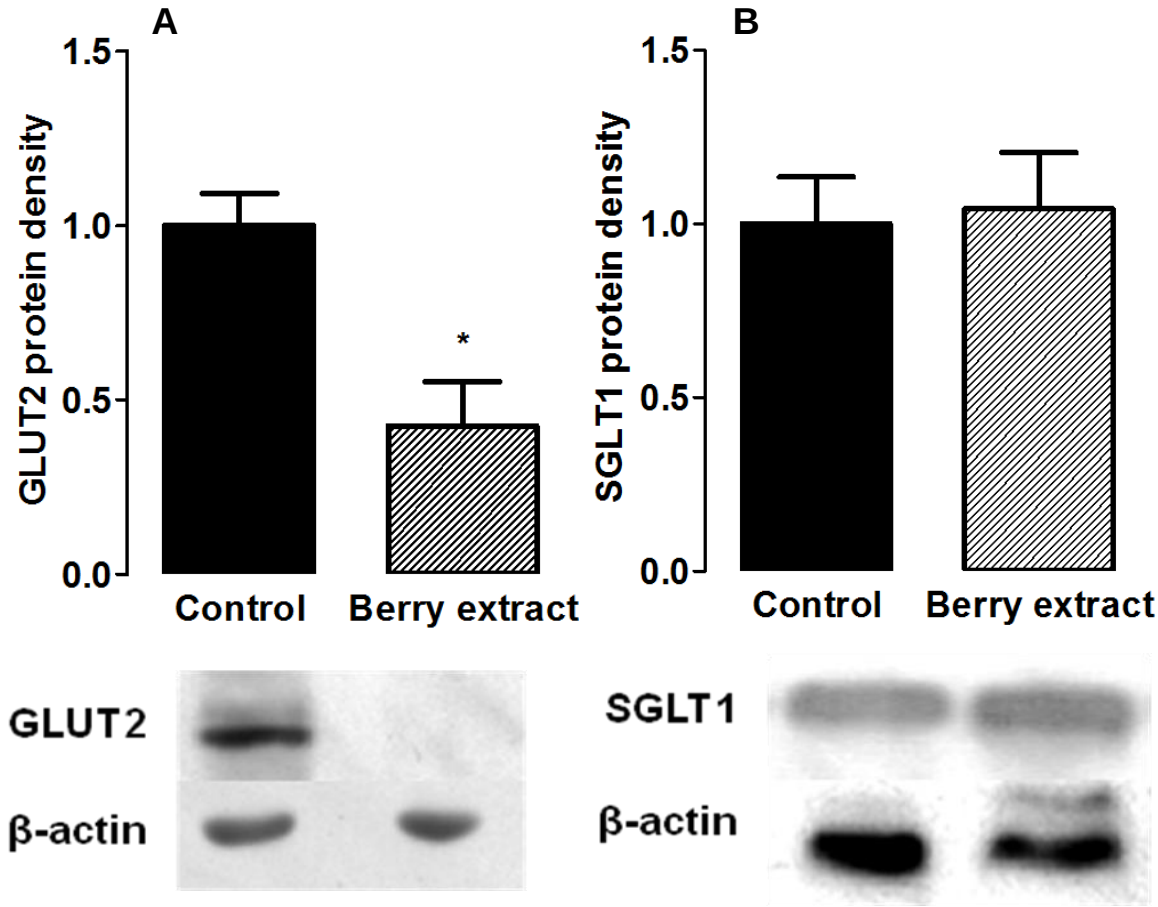

Figure 4.7. Effects of flavonoids on GLUT2 and SGLT1 protein expression. Caco-2 cells were treated with berry extract at a concentration of 0.125 % (w/v) for 16 h. Levels of GLUT2 (A) and SGLT1 (B) protein were quantified by Western blotting and normalised to β-actin as a housekeeping protein. Data is presented as mean normalised protein density expressed relative to the control ± SEM, $n = 4$. Statistical significance was determined by an unpaired t-test. (*) $p \leq 0.05$. GLUT2: facilitative glucose transporter 2. SGLT1: sodium/glucose cotransporter 1.

4.3.4 Effects of flavonoids on glucose uptake

In this section, our interest was in 1) the *acute* inhibitory effects of flavonoids on glucose uptake and 2) the *chronic* inhibitory effects of flavonoids on glucose uptake. Differences between transport systems, i.e. total uptake, GLUT-mediated uptake or SGLT-mediated uptake, were not investigated. We investigated the inhibitory potential of flavonoids on these components of uptake.

Acutely, total glucose uptake, GLUT-mediated and SGLT-mediated glucose uptake were significantly decreased by the berry extract ($p < 0.01$; **Figure 4.8**, **panel A**). Quercetin and phloretin decreased total, GLUT-mediated and SGLT-mediated glucose uptake ($p < 0.05$; **Figure 4.8**, **panel B**). Phloridzin significantly decreased SGLT-mediated glucose uptake only ($p < 0.05$; **Figure 4.8**, **panel B**).

Following chronic treatment with berry extract there was no significant effects on total glucose uptake, GLUT-mediated uptake or SGLT-mediated uptake (**Figure 4.9**, **panel A**). Chronic treatment with quercetin, phloretin or phloridzin also had no significant effect (**Figure 4.9**, **panel B**).

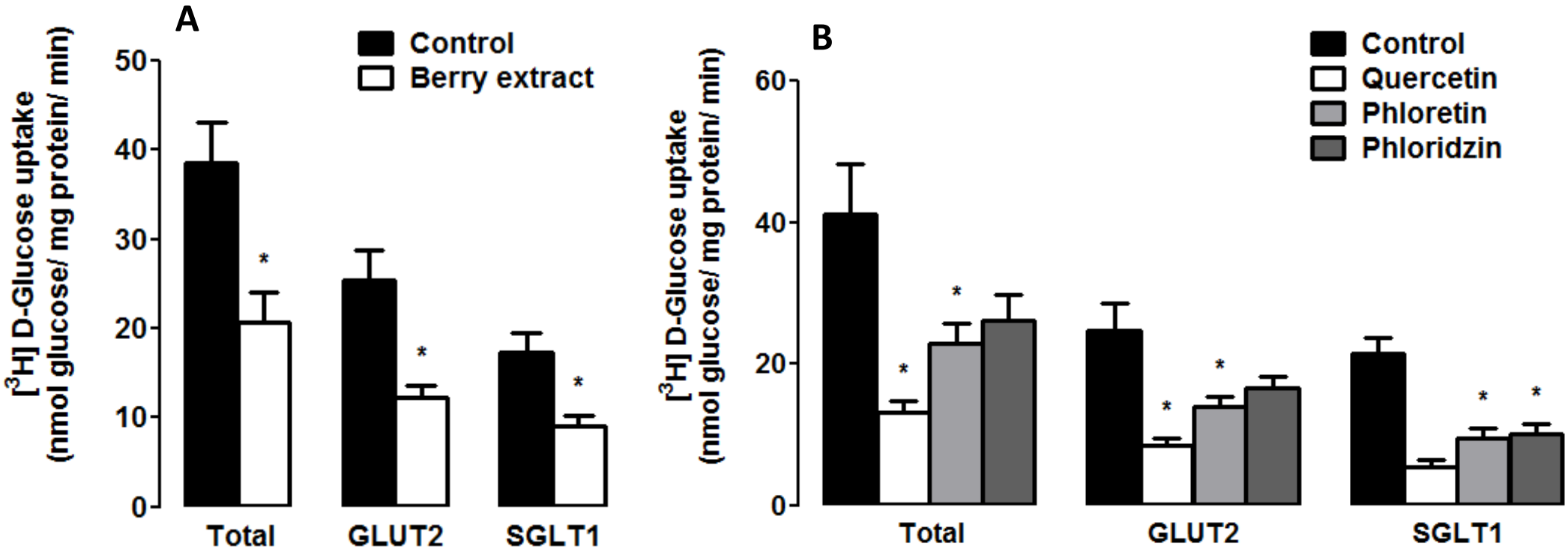

Figure 4.8. Acute effects of flavonoids on total, GLUT2-mediated and SGLT1-mediated glucose uptake. Total glucose uptake, GLUT2-mediated glucose uptake and SGLT1 mediated glucose uptake were measured in Caco-2 cells treated acutely, 15 min, with (A) 0.125 % (w/v) berry extract (white bars) or with (B) 100 µM isolated flavonoids quercetin (white bars), phloretin (light grey bars) or phloridzin (dark grey bars); control bars are black. Data are presented as the mean ± SEM, $n = 12$. (*) $p \leq 0.05$. To determine significance, an unpaired t-test was used for the berry extract and control group, and a Kruskal-Wallis test was used for quercetin, phloretin and phloridzin compared with the control group.

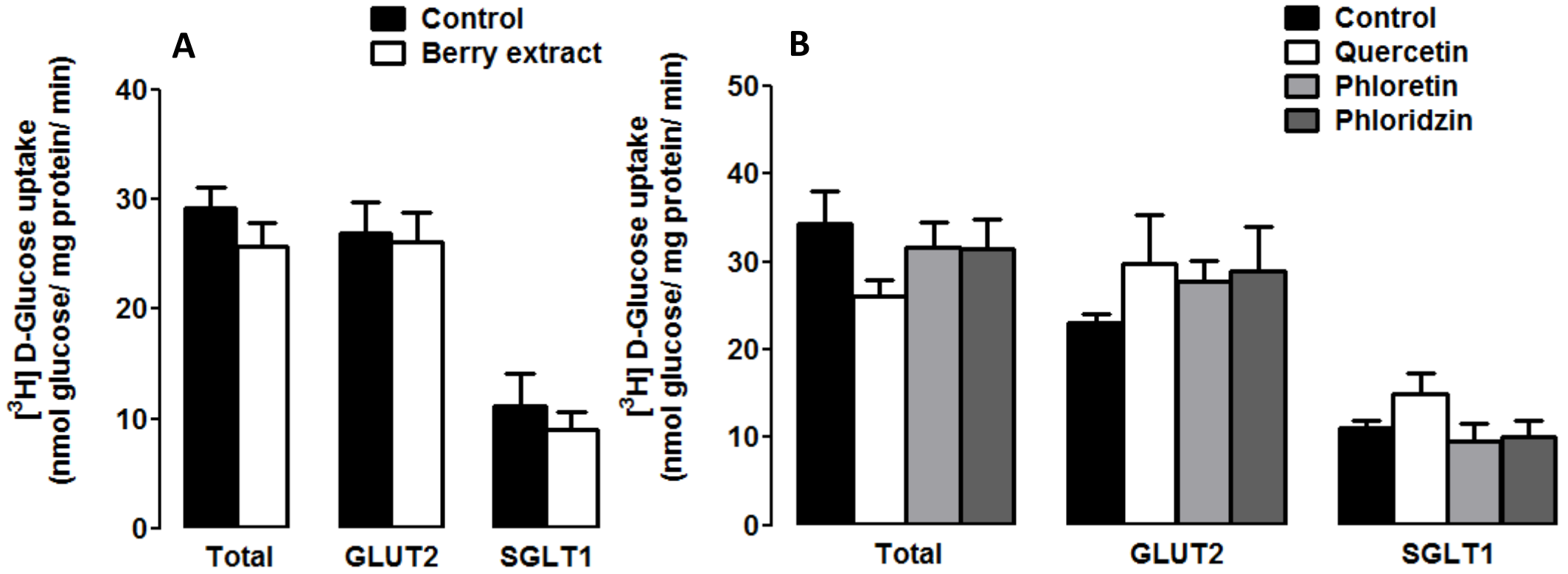

Figure 4.9.Chronic effects of flavonoids on total, GLUT2-mediated and SGLT1-mediated glucose uptake. Total glucose uptake, GLUT2-mediated glucose uptake and SGLT1 mediated glucose uptake were measured in Caco-2 cells treated acutely, 15 min, with (A) 0.125 % (w/v) berry extract (white bars) or with (B) 100 µM isolated flavonoids quercetin (white bars), phloretin (light grey bars) or phloridzin (dark grey bars); control bars are black. Data are presented as the mean ± SEM, $n = 12$. (*****) $p \leq 0.05$. To determine significance, an unpaired t-test was used for the berry extract and control group, and a Kruskal-Wallis test was used for quercetin, phloretin and phloridzin compared with the control group.

4.4 Discussion

There are 366 million people worldwide affected with diabetes, 90 % of these cases are type II diabetes (Diabetes UK, 2009). This disease is managed through rigorous lifestyle modification and/or pharmaceutical interventions to maintain optimal glucose homeostasis and thus prevent complications, such as cardiovascular disease. A failure to maintain glucose balance leads to the development of type II diabetes. Given that current pharmaceutical options cause undesirable side-effects (e.g. hypoglycaemia, weight gain, nausea), there has been an emergence of interest in the use of naturally occurring glucose modulatory substances, such as flavonoids. The acute effects of flavonoids on glucose uptake have been reported by numerous studies (e.g. Park, 1999; Johnston *et al*, 2005). However, there has been little research into the chronic effects of these compounds.

We addressed the hypothesis that dietary flavonoids chronically and acutely modulate glucose uptake processes in enterocytes. This was done by treating Caco-2 cells with a flavonoid-rich berry extract, quercetin, phloretin and phloridzin, then quantifying transporter expression and function.

We demonstrated that chronic treatment with flavonoids decreased glucose transporter gene expression, with concomitant decreases in GLUT2 protein abundance. However, radiolabelled studies showed there was no affect on glucose uptake. In contrast, acute flavonoid treatments markedly inhibited both GLUT2 and SGLT1 mediated glucose uptake.

4.4.1 Flavonoids and glucose transporter gene expression

GLUT2 gene expression decreased in a dose- and time-dependent manner when treated with the berry extract. The strongest effects on GLUT2 gene expression were

at 16 h with 0.125 % (w/v); the remainder of our experiments was based on this finding. GLUT2 mRNA also decreased when Caco-2 cells were treated with quercetin, phloretin or phloridzin. The common effect of flavonoid treatments on GLUT2 mRNA expression indicates a similar underlying mechanism.

Typically, GLUT2 mRNA is regulated by the presence of substrates and by hormonal cues, such as insulin (Cui *et al*, 2003, Goestemeyer *et al*, 2007; Tobin *et al*, 2008). GLUT2 mRNA expression correlates directly to glucose availability. Thus a decreased intracellular or extracellular availability of glucose, decreases GLUT2 gene expression (Inagaki *et al*, 1992; Mahraoui *et al*, 1994; Cui *et al*, 2003). Although GLUT2 is regulated by glucose, it is not known to contain a glucose or carbohydrate responsive element in its mRNA transcript (Rencurel *et al*, 1996). Therefore GLUT2 may be responding to other cues. However, the inhibitory effects of flavonoids on glucose uptake are the likely cause of low intracellular glucose and in-turn decreased GLUT2 mRNA expression.

As for SGLT1 mRNA levels, significant inhibitory effects were observed at 16 h of treatment with 0.125 % (w/v) of the berry extract, with quercetin or with phloridzin. Previous research has similarly reported decreased SGLT1 mRNA in the intestine in response to polyphenolic extracts (Oliveira *et al*, 2008). Furthermore, phloridzin is a classical inhibitor of SGLT1-mediated glucose uptake and is known to reverse the over-expression of SGLT1 mRNA that occurs in diabetes (Alvarado & Crane, 1962; Masumoto *et al*, 2009; Walle & Walle, 2003). Quercetin and its derivatives are also known inhibitors of SGLT1-mediated uptake (Kwon *et al*, 2007).

SGLT1 mRNA regulation is known to be independent of glucose. However, there is a degree of correlation with GLUT2 mRNA expression throughout cellular differentiation (Mahraoui *et al*, 1994). SGLT1 mRNA increases under conditions of

oxidative stress or when treated with metal compounds (Miyamoto *et al*, 1993; Blumenthal *et al*, 1998). Its expression decreases during hypertension, sodium loading or in response to polyphenol-rich plant extracts (Mate *et al*, 2006; Oliveira *et al*, 2008). It is consistently reported that mRNA fluctuation is not always in line with protein abundance nor does it affect transport function (Smith *et al*, 1992; Lescale-Matys *et al*, 1993; Mate *et al*, 2006). As flavonoids are known antioxidants, and SGLT1 mRNA is known to be sensitive to oxidative states (Aherne & O'Brien, 1999; Myhrstad *et al*, 2002; Han *et al*, 2005), the decreased SGLT1 mRNA is possibly a response to changes in cellular oxidative balance with the increase in antioxidant capacity with the flavonoid treatments (Li *et al*, 2004).

4.4.2 Flavonoids and glucose transporter protein expression

The GLUT2 protein is primarily localised at the basolateral membrane and rapidly translocates to the apical membrane when monosaccharide demand is high. GLUT2 is endocytosed and degraded in response to insulin signaling following a rise in plasma glucose (Corpe *et al*, 1996; Tobin *et al*, 2008).

We found there was decreased abundance of GLUT2 protein in response to treatment with the berry extract. This is a result of either increased protein degradation and/or decreased translation. Decreased translation would arise following the decreased expression of GLUT2 mRNA as discussed above. However, noting that there is no significant effect on GLUT2-mediated glucose uptake, it is likely that degradation may be site-specific. In other words, GLUT2 that is not localised for apical uptake is subjected to degradation. Rather, the basolaterally or intracellularly localised GLUT2 would have been targeted. Alternatively, another glucose uptake route may have been made available, or that the apical presence of GLUT2 is not the rate-limiting factor for glucose uptake. Further experiments to characterise the migration

and degradation patterns of GLUT2 will enable a better understanding of our current observations to be obtained.

4.4.3 Acute effects of flavonoids on glucose uptake

Other studies have demonstrated the acute inhibitory effects of flavonoids on glucose uptake (Park, 1999; Song *et al*, 2002; Kwon *et al*, 2007; Johnston *et al*, 2005). We carried out an acute treatment, in line with this previous research, to ensure the inhibitory potential of our treatment compounds was similar to those previously reported. Furthermore, acute treatments indicate mechanisms that require simultaneous presence of both the substrate and inhibitor compounds.

Phloretin, and its glucoside phloridzin, were included as known inhibitors of GLUT2- and SGLT1-mediated glucose uptake, respectively (Alvarado, 1967). Our experiments with phloretin and phloridzin confirmed the presence and activity of both transporters.

Flavanols are known as the most potent flavonoid inhibitors of glucose uptake, thus quercetin was included as a marker flavonol (Park, 1999). In our experiments, quercetin significantly inhibited GLUT2- and SGLT1-mediated glucose uptake. Other studies have shown similar results (Song *et al*, 2002; Kwon *et al*, 2007).

The berry extract used in this work for the thesis is rich in delphinidin, malvidin, cyanidin and petunidin (InterHealth Nutraceuticals). These anthocyanins are all hydroxylated at the C-5 and C-7 positions. Hydroxylation at these positions has been previously identified as a structural feature that increases inhibitory potential of flavonoids towards glucose uptake (Park, 1999). The berry extract also, as expected, acutely inhibited both GLUT2- and SGLT1-mediated uptake.

There are currently a number of hypotheses regarding the flavonoid inhibition of glucose uptake. The study by Park (1999) is of particular importance as he investigated 10 different flavonoid species, the structural classes of which spanned flavones, flavonols, flavanones, isoflavones, anthocyanidins and catechins. As well as a number of structural classes, he investigated different hydroxylation patterns, presence of double bonds on the 6-member rings, orientation of the B-ring, presence of a ketone group and moiety effects on the inhibitory properties of these compounds. Park (1999) found that hydroxylation at certain positions was important for inhibition (namely: C-5 and C-7 are necessary, but hydroxylation at C-3 and C-3' had no effect). Orientation of the B-ring is important; i.e. flavonoids have a higher inhibitory capacity than isoflavonoids that have the B-ring conjugated at C-3 rather than C-2; presence of a double bond between C-2 and C-3 also increased inhibitory capacity. Finally, no single component of the flavonoid backbone structure induced an inhibition of glucose uptake, e.g. chromone, coumarin and catechol all failed to inhibit glucose uptake; furthermore the backbone structure without C-5 and C-7 hydroxylation did not have inhibitory potential. Other studies have implied that glucose moieties will bind to the same transporter binding site as hexoses, thus competitively impeding monosaccharide transport, possible by steric hindrance preventing transport of the glucose alone (Johnston *et al*, 2005; Kwon *et al*, 2007). Alternatively, both aglycone and glycoside flavonoids may bind to a separate binding site or to membranes, affecting both membrane integrity and transporter function (Nakayama *et al*, 2000; Johnston *et al*, 2005). However, despite the possibility of non-specific polyphenol interactions with *any* glucose binding site, or with *any* membrane (potentially affecting other nutrient transporters); this inhibition has been observed in many cell lines, in transfected cells and in *Xenopus* oocytes, the effect appears to be glucose transporter specific (Kwon *et al*, 2007).

The study by Martineau *et al* (2006) is one of only a few groups to have investigated the mechanisms whereby polyphenolic plant extracts may aid in the maintenance of circulating glucose. They investigated effects of blueberry plant extracts on 3T3-L1 adipocytes and C2C12 muscle cells, expressing GLUT1 and GLUT4 facilitative transporters (Martineau *et al*, 2006). These have similar properties to GLUT2 in enterocytes and hepatocytes (Klip & Paquet, 1990). The treatment compounds in the aforementioned study consisted of lyophilised ethanolic extracts from blueberry plant and fruits. In their study, the root, stem and leaf extracts contained numerous phenolic compounds, whereas anthocyanins were only found in the fruit. All the extracts increased glucose uptake in myocytes and adipocytes, except for the anthocyanin containing fruit extract. The blueberry fruit extract inhibited both basal and insulin-stimulated glucose uptake in myocytes (GLUT4) and adipocytes (GLUT1) (Martineau *et al*, 2006). Thus, in line with our findings, there is a specific and potent inhibition of GLUT-type transporters by anthocyanin flavonoids.

4.4.4 Chronic effects of flavonoids on glucose uptake

Quantifying the relative amount of protein provides information on the potential functional capacity. On the other hand quantifying mRNA allows one to ascribe mechanisms to the changes observed in function. Thus, a glucose uptake assay following chronic flavonoid treatment is the only reliable way to evaluate the chronic effects on glucose uptake function. Furthermore, chronic treatments allow time for any compensatory mechanisms to develop.

In our studies, chronic treatments had no significant effect on glucose uptake, despite decreased GLUT2 protein abundance. This suggests that the apical availability of GLUT2 was probably not affected by the decreased abundance of the protein. However, this must be confirmed by localisation experiments, or by studies of total

transepithelial transport of glucose. Alternatively, a different transport route may have been recruited for glucose uptake.

Regarding SGLT1, there was no effect of chronic flavonoid treatment on the protein or on SGLT1-mediated glucose uptake.

4.5 Conclusions

We have reported, for the first time, the effects of berry flavonoids on glucose transporter expression and function in a model of human enterocytes. A flavonoid-rich berry extract induced a decrease in the mRNA expression of two key glucose transporters; quercetin, phloretin and phloridzin induce a similar response. There is a concomitant decrease in expression of the GLUT2 protein. These changes in expression do not affect cellular glucose uptake. However, when applied acutely, flavonoids inhibited glucose uptake. These acute inhibitory effects did not affect longer term function (i.e. presence of flavonoid compounds is necessary to exert inhibition) although they are likely to have caused the observed changes in transporter expression.

Overall, these findings indicate dietary flavonoids are effective acute inhibitors of intestinal glucose uptake. Given this property, other health benefits and the high safety profile of flavonoids, they are likely candidates for the non-pharmacological management of type II diabetic conditions. Further research is required to characterise protein trafficking, the response patterns of GLUT2 and to characterise the transepithelial flux of glucose.

4.6 Future work

Our results, together with previous research, leave a number of questions to be answered. These are mainly related to the chronic effects we have observed. The resulting effects and questions are summarised schematically in **Figure 4.10**. Most important are the translational effects on GLUT2 and the transcriptional effects on SGLT1. Following the chronic treatments, GLUT2 protein abundance decreased, without a functional consequence (i.e. no significant change in glucose uptake). Our studies could not distinguish between apical, basolateral and intracellular GLUT2 pools and it is possible that the actions of berry flavonoids are specific to one of these sites. Alternatively, presence of the protein *per se* is not the rate limiting step with regards to its function. In support of this possibility, studies by Helliwell *et al* (2000) show that both transporter protein abundance and the intrinsic activity of sugar transporters are important determinants of overall rates of transport.

Furthermore, flavonoids have been reported to possess insulin-like properties (Anderson *et al*,2004; Martineau *et al*, 2006; Su *et al*, 2006); insulin is known to affect the apical presence of GLUT2 and thus its glucose importing functions (Tobin *et al*, 2008).

SGLT1 is also know to traffic between intracellular pools and the apical membrane (Khoursandi *et al*, 2004) and it is possible that berry polyphenols influence cellular distribution of transporter protein without altering overall SGLT1 protein levels. However, polyphenols have been reported to previously alter SGLT1 mRNA expression; albeit through unknown the mechanisms (Oliviera *et al*, 2008). Finally, the roles of other flavonoid importers, and their effects on basolateral glucose release, or the roles of basolateral GLUT2 in flavonoid efflux, require investigation. These and other areas of future work are discussed in the following sections.

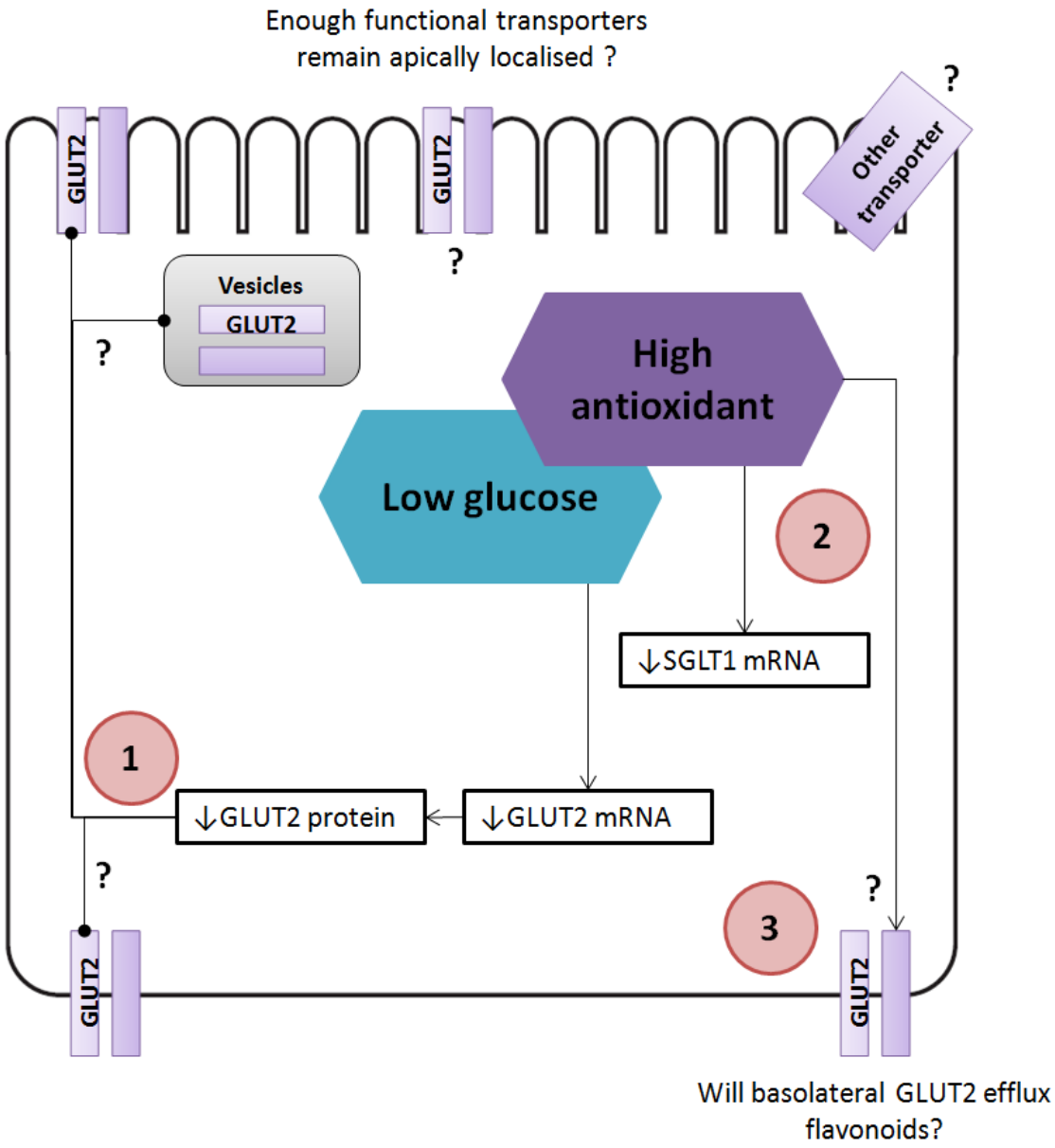

Figure 4.10. Future work into the chronic effects of flavonoids on glucose transport. Following chronic flavonoid treatment of Caco-2 cell monolayers a number of observations were made that require further investigation. **1)** There was a decrease in GLUT2 mRNA and protein, with no effect on GLUT-mediated glucose uptake. This may be due to site targeted degradation of the GLUT2 protein, to a site that is not related to its apical uptake role, there may be other unknown compensatory routes of glucose uptake, or merely that apical presence of the transporter is not the rate limiting step of its function, i.e. a non-saturable capacity. **2)** Cellular distribution, but not total, SGLT1 protein may also change following exposure to flavonoids. The down-regulation of GLUT2 and SGLT1 mRNA are likely to be a flavonoid effect, or a downstream effect of high cellular flavonoids as previous research has found polyphenolic compounds to decrease SGLT1 mRNA as well; it is also likely that the electrochemical or oxidative balance within the cell will have the modulatory effect on SGLT1 mRNA. **3)** Whether basolateral GLUT2 will provide an efflux route for flavonoids that have accumulated, this is also assuming that flavonoids will not have induced the degradation or basolateral GLUT2. Furthermore, it is not known if the function of GLUT2 transporting glucose also be inhibited at the basolateral membrane

4.6.1 Elucidating the mechanisms of inhibition

Previous researchers have attempted to establish modes of flavonoid inhibition. This has resulted in divergent findings due to the diversity of flavonoid structures, the various metabolic fates of these compounds and the various tissues and cell lines they have been tested in (Park, 1999; Cermak *et al*, 2004; Johnston *et al*, 2005; Kwon *et al*, 2007). It has however been a general assumption that aglycones preferentially inhibit GLUT2 and glycosides preferentially inhibit SGLT1 (**Figure 4.11**); however the modes of inhibition have been inconsistently reported.

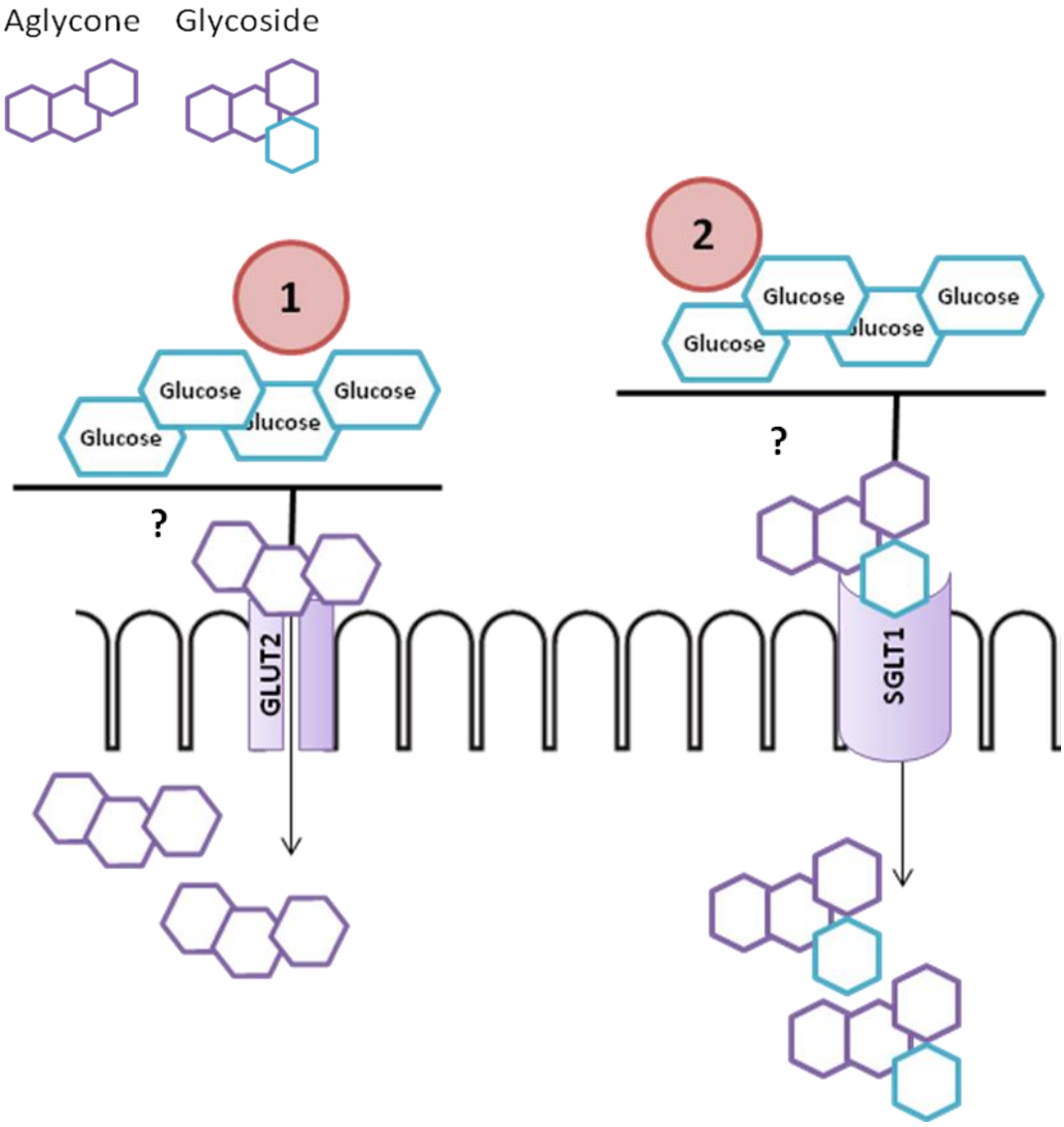

Figure 4.11. Flavonoid inhibition of glucose transporters. Inhibition of glucose transporters will cause intracellular accumulation of mixed flavonoid species and a decrease in cellular glucose. The nature of inhibition (competitive, non-competitive) has not been fully elucidated. **1)** Aglycone flavonoids are expected to inhibit GLUT2; **2)** Glycosides are expected to inhibit SGLT1. GLUT2: facilitative glucose transporter member 2; sodium-glucose cotransporter 1.

To determine the modes of inhibition of the compounds we used, firstly the active components of the berry extract need to be identified. A subsequent series of kinetic analysis studies must be carried out in Caco-2 cells. When the enzyme reaction constants are determined, if the maximum rate of transport (V_{max}) does not change then inhibition is competitive, whereas decreasing V_{max} means the inhibition is non-competitive. Determining effects on the Michaelis and dissociation constants (K_m & K_d) will also aid in determining the mode of inhibition. Parallel alterations in these constants will dictate that inhibition is competitive. When K_m, K_d and V_{max} are altered, this indicates mixed type inhibition (Park, 1999; Ader *et al*, 2000; Manzano & Williamson, 2010). Previous reports state that inhibition of apical uptake is of mixed type, with GLUT2 beifng inhibited non-competitively and SGLT1 being inhibited competitively; whereas basolateral release of glucose is inhibited in a non-competitive manner, indicating an effect on GLUT2 only (Manzano & Williamson, 2010). From a mechanistic perspective it is important to determine these parameters, both with the acute treatment conditions and following the chronic exposure, particularly with regards to our findings of decreased GLUT2 protein abundance, with no apparent effect on function. In addition, selective interaction of individual polyphenols with SGLT1 and / or GLUT2 could be assessed by expressing each transporter in *Xenopus* oocytes and determining the effect on glucose uptake (e.g. Kwon et al 2007).

4.6.2 Localisation and contribution of glucose transporters:

It is of particular importance to determine the cellular localisation of the transporters we have investigated and to determine whether other hexose transporters are affected or recruited to compensate loss of GLUT2 or SGLT1 activity. As GLUT2 translocates in response to its substrates (Kellet & Helliwell, 2000; Chaudhry *et al*,

2011), it is important to determine its localisation at the appropriate area to be inhibited, and to determine the location of its degraded units (after 16 h). Although, the function and orientation for inhibition of GLUT2 is partially resolved as we have shown glucose uptake in the absence of sodium, and other researchers have shown GLUT2 to appear at the correct membrane (Kwon *et al*, 2007). Furthermore, despite the decrease in GLUT2 protein following chronic treatment, there is no effect on transport capacity, this may be due to targeted degradation of GLUT2 protein either basolaterally or from the subapical vesicles, which can also be resolved by localisation of the transporters with confocal microscopy.

It is also worth determining the contribution of GLUT1 and GLUT5 to the hexose and/or flavonoid uptake, although GLUT5 is a fructose transporter and therefore may not directly affect glucose metabolism. Nonetheless, the contribution of *other* transporters (not GLUT2 or SGLT1) can be quantified either by inclusion of flooding doses of phloretin, phloridzin, cytochalasin B and disruption of the electrochemical gradient, expressing transporters in *Xenopus* oocytes or targeted deletion of GLUT2 and SGLT1 with siRNA.

4.6.3 Determining effects on basolateral glucose flux:

An important mechanistic and physiological question remains as to whether flavonoids inhibit both components of absorption; i.e. apical uptake from the lumen and basolateral release into circulation. This component is physiologically important when determining if effects seen are truly acute, as flavonoid metabolism will involve, the apical reflux of flavonoids as well as the biliary excretion back into intestinal lumen (Walle, 2004; Lotito *et al*, 2011; Planas *et al*, 2012). Therefore if flavonoids are present or are reabsorbed prior to the introduction of dietary glucose into the intestinal lumen, there may be a persistent intracellular inhibitor of glucose

transport. This can be determined initially by applying confocal microscopy or membrane separation Western blotting to ensure GLUT2 is remains localised at the basolateral membrane following longer treatment with flavonoids and that it is at the expected position for intracellular inhibition by flavonoids. Furthermore, we can determine if other routes are available for basolateral glucose or flavonoid release by pre-treatment with phloretin or with cytochalasin B.

CHAPTER FIVE

Effects of berry extract on the expression and function of intestinal iron transport pathway in Caco-2 enterocytes

5 Effects of berry extract on the expression and function of intestinal iron transport pathway in Caco-2 enterocytes

5.1 Introduction: Intestinal iron transport and dietary flavonoids

Iron is an essential element with diverse biological roles, e.g. as a prosthetic group in redox reactions and as an essential part of haem, serving to transport and store oxygen (Noyes *et al*, 1964; Lopes *et al*, 2010). As a consequence of its essentiality, even small changes in its metabolic homeostasis can cause a number of diseases, such as anaemia in states of low iron and haemochromatosis in high iron states (Kaplan *et al*, 2011).

Humans lack regulated mechanisms for the disposal of excess iron. The only way that iron can be excreted is through the unregulated exfoliation of epithelial cells and through bleeding. Therefore, body iron levels must be maintained at the site of absorption, at the intestinal epithelium.

Intestinal epithelial cells express a number of specialised proteins to absorb and handle iron from the diet. Intestinal iron absorption is regulated systemically in response to the hepatically expressed peptide hepcidin. It is also regulated locally by dietary factors and the iron responsive element / iron regulatory protein (IRE/IRP) system (Anderson *et al*, 2002b; Sharp & Srai, 2007; Hentze *et al*, 2011). Furthermore, the bioavailability of dietary iron is also dependent on the presence of other dietary constituents, such as flavonoids, that can either impede or enhance its absorption (Kim *et al*, 2008; Thumser *et al*, 2010).

Non-haem iron is the most abundant form of iron in the diet. It is ingested in its ferric form, which must be reduced to its ferrous form in the intestine before absorption (Han *et al*, 1995). This reduction is mediated by the apical membrane

reductase activity of duodenal cytochrome B reductase (DCYTB) or by luminal dietary reducing agents (McKie *et al*, 2001). Following reduction, ferrous iron becomes a substrate for the apical divalent metal ion transporter (DMT1) which mediates influx of iron into the enterocyte (Han *et al*, 1995; Gunshin *et al*, 1997). Iron then joins the intracellular iron pool by binding to ferritin, or is effluxed from the basolateral membrane via ferroportin (FPN) (McKie *et al*, 2000). After efflux, ferrous iron is oxidised by the basolateral ferroxidase hephaestin (HEPH) (Vulpe *et al*, 1999). Ferric iron can then be bound by plasma transferrin for distribution throughout the body (Núñez & Tapia, 1999). The haemochromatosis protein, HFE, is also expressed in duodenal enterocytes. HFE is assumed to act as an intracellular inhibitor of DMT1-mediated iron uptake or as a regulatory protein for the interaction of transferrin (Tf) and its receptors (TfR1/ TfR2) (Arredondo *et al*, 2006).

The absorption of iron is greatly influenced by the presence of dietary compounds such as vitamin C and flavonoids (Teucher *et al*, 2004; Thumser *et al*, 2010; Ma *et al*, 2011). Vitamin C is known as a chelator or as a reducing agent which enhances the uptake of iron (Thumser *et al*, 2010). Flavonoids are also known for their reducing capacity and their ability to chelate dietary metals. Both these properties are affect the transport and bioavailability of iron (Ren *et al*, 2008; Vlachodimitropoulo *et al*, 2010a; Vlachodimitropoulo *et al*, 2010b). However, little is known about the concordant regulation of related mRNA levels and iron absorption *per se* in response to flavonoids. To address this we investigated the effects of a flavonoid-rich berry extract on iron transport and DCYTB, DMT1, HFE, TfR1, FPN and HEPH expression in Caco-2 cells.

5.2 Methods

Presented here is a brief description of the methods used in this chapter. For full details of reagents, buffer/media compositions and methods used see **Chapter 2.**

5.2.1 Cell culture

Caco-2 TC7 cells between the passages of 44 and 47 were seeded into 6-well plates at a density of approximately 40,000 cells per well (4,000 cells per cm^2) and cultured for 19 days prior to treatment. For iron transport experiments, cells were seeded on Transwell® inserts in 6-well plates. Details of the maintenance of the cells and composition of cell culture medium have been previously described (see **Chapter 2** and Johnston *et al*, 2005).

The treatment used was a flavonoid-rich berry extract (derived from blueberry, bilberry, cranberry, elderberry, raspberry seeds and strawberry; rich in the anthocyanins delphinidin, cyanidin, petunidin and malvidin, OptiBerry®, InterHealth Nutraceuticals, CA, USA) at a final concentration of 0.125 % (w/v). Treatment was prepared in DMEM for gene and protein expression and chronic-exposure iron transport studies. Treatments for acute-exposure iron transport experiments were prepared in HBSS. An identical medium or buffer, without the berry extract, was used for the control cells.

The effects of berry extract treatments on cell viability, RNA content and protein content of the cells were tested. There were no effects of any treatments on cell viability, RNA or protein content (see **Results, Section 5.3.1**).

5.2.2 Real-time qPCR

Total RNA was isolated from the cultured cells using TRIzol® (Invitrogen™ Life Technologies, Paisley, UK) according to the manufacturer's instructions. Following first strand cDNA synthesis (using a high-capacity cDNA reverse transcription kit, Applied Biosystems™ Cheshire, UK), expression levels of iron transport-related gene mRNA, 18S mRNA and GAPDH mRNA were analysed by qRT-PCR using an ABI Prism 7700HT Sequence Detection System and a Power SYBR® Green PCR master mix kit (Applied Biosystems™ Cheshire, UK). Primers were designed using the online design tool Primer3 (Rozen & Skaletsky, 2000) and sourced from MWG Eurofins (London, UK). Quantitative measurement of gene expression was derived from the $2^{(-\Delta\Delta Ct)}$ *method*, also known as the *Livak method* (Livak & Schmittgen, 2001; Schmittgen & Livak, 2008). Data were expressed as ratios to the control and normalised to the housekeeping genes 18S and GAPDH. The primer sequences used for each gene are in **Table 5.1**.

Table 5.1. Primer sequences for qRT-PCR gene expression analysis.

Gene symbol	Forward primer 5'-3'	Reverse primer 5'-3'
DCYTB	TCA TCC AGG GCA TCG CCA TC	CGG AGC CCA TGG AAG CAG AA
DMT1	AGT GGT TTA TGT CCG GGA CC	TTT AAC GTA GCC ACG GGT GG
HFE	CAC ACC ATC CAC TTT CAT GC	GCA TGG ACA TGG TCA GTC AC
TfR1	TGA GAA AAC AAT GCA AAA TGT GA	CCC AGT TGC TGT CCT GAT ATA GA
FPN	GGG GTC GCG TAG TGT CAT	CAG GTA GTC GGC CAA GGA T
HEPH	CAC ACC ATC CAC TTT CAT GC	GCA TGG ACA TGG TAC GTC AC
18S	AAC TTT CGA TGG TAG TCG CCG	CCT TGG ATG TGG TAG CCG TTT
GAPDH	CTG TTG CTG TAG CCA AAT TCG T	ACC CAC TCC TCC ACC TTT GA

DCYTB: duodenal cytochrome B reductase; DMT1: divalent metal ion transporter 1; HFE: haemochromatosis protein; TfR1: transferrin receptor 1; FPN: ferroportin; HEPH: hephaestin; 18S: ribosomal RNA18S; GAPDH: glyceraldehyde 3-phosphate dehydrogenase.

5.2.3 Protein abundance analysis

Total protein from Caco-2 cells was prepared as described previously (Chaston *et al.*, 2008). Total proteins (40 μg) were solubilised in sample loading buffer and subjected to SDS-PAGE. Following immobilisation on nitrocellulose, the proteins were exposed to anti-DMT1 or anti-FPN antibodies (1:1000 dilution, Source Bioscience, Nottingham, UK). Blotted membranes were visualised using a horseradish peroxidase-linked secondary antibody and Novex® ECL chemiluminescent substrate reagent kit (Invitrogen™ Life Technologies, Paisley UK). Band densities were quantified using a densitometer (GS-800™) and Quantity One software (Bio-Rad Laboratories, Hertfordshire, UK). Protein levels of β-actin were also measured (anti-actin antibody, 1:2000 dilution, Sigma-Aldrich). Protein density data were normalised to β-actin as the housekeeping protein. For antibody concentrations and reagents see **Section 2.2.4. Protein abundance analysis**.

5.2.4 Iron uptake and transport assays

This section contains a brief description (for further details see **Section 2.2.5 Functional uptake and transport experiments**) of the iron uptake and transport assays, similar to those previously described (Johnston *et al*, 2005; Kim *et al*, 2008). Iron uptake and transepithelial transport were carried out using [^{55}Fe]-ferric chloride (Perkin-Elmer, Bucks, UK). Cells for these experiments were grown on Transwell® inserts to allow loading into the apical compartments and transport to the basolateral compartments. See **Figure 5.1** for an illustration of how Transwell® inserts work to identify the separate components of iron transport (i.e. apical uptake and basolateral release).

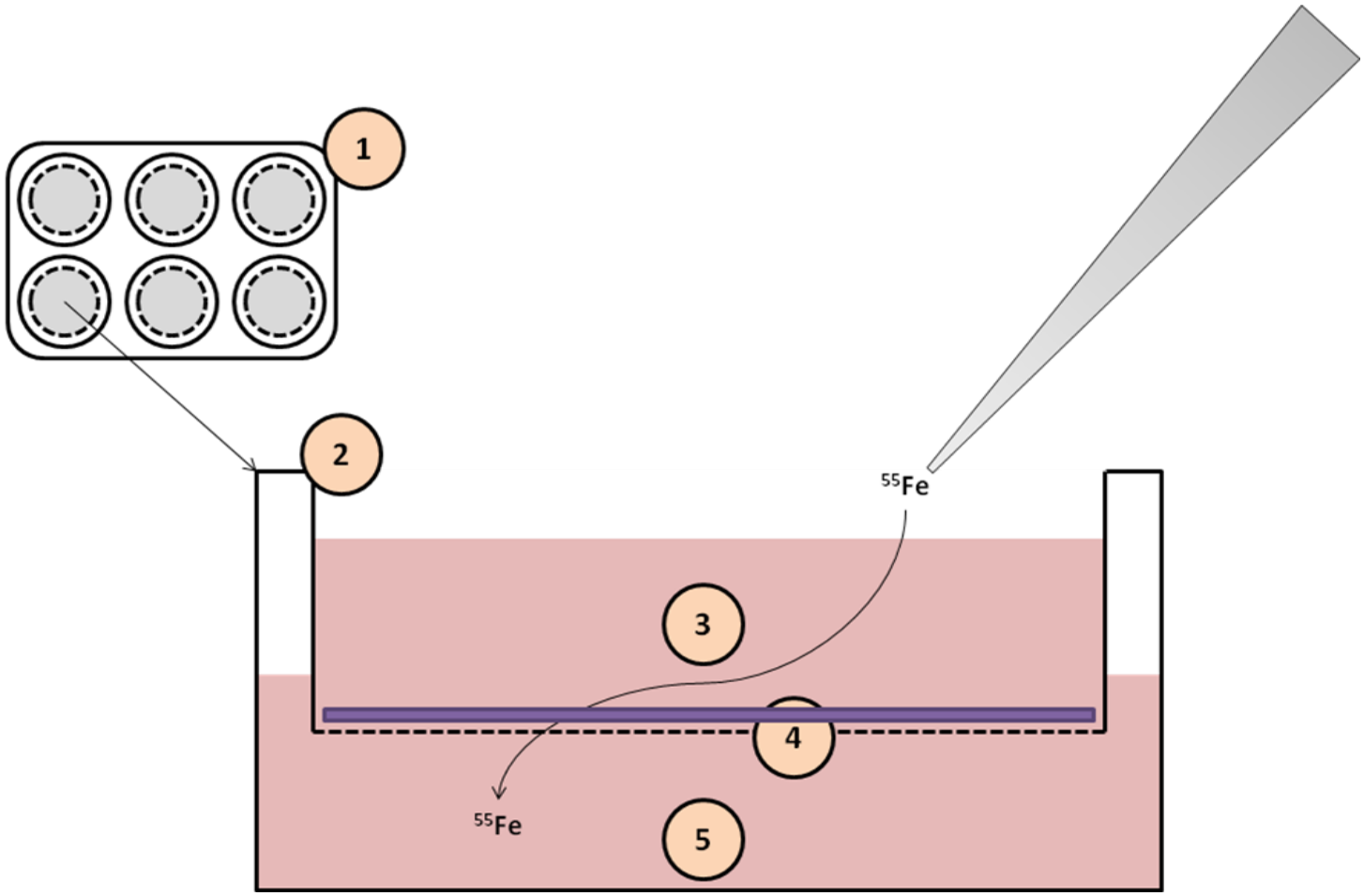

Figure 5.1.Transwell® insert system applied in ^{55}Fe uptake experiments. The Transwell® insert system allows the compartmentalisation of two components of nutrient transport; both apical uptake and basolateral release. **1)** The inserts fit into standard 6-well cell culture plates **2)** Inserts allow cells to become confluent and polarise on a semipermeable membrane, where both apical and basolateral sides of the cells are exposed to media **3)** Apical chamber media or buffer is in contact with the apical surface of the Caco-2 cells and represents conditions within the intestinal lumen **4)** The semipermeable membrane allows a physical barrier for cells to grow on, as well as separating the apical media or buffer from the basolateral media or buffer, thus allowing the quantification of apical to basolateral transport, as opposed to cellular uptake alone **5)** The basolateral chamber carries media or buffer in contact with the basolateral side of the Caco-2 cells and represents conditions in circulation, analytical substrates (e.g. ^{55}Fe) detected in this area represents substrates that have completely passed through the cell monolayer.

Uptake and transport assays were designed to identify the acute interactive effects of berry extract treatment or the chronic transcriptional or translational effect of a 16 h berry extract treatment. During acute effects ^{55}Fe was added to the apical buffer compartment with the flavonoid treatments, whereas for the chronic effects the treatment media was replaced with buffer containing ^{55}Fe and no flavonoids.

To quantify iron uptake, after 20 min of exposure to the radioisotope, the buffer was removed, and inserts were washed 3 times in ice-cold PBS and drip dried briefly before dissolving cells in 500 µL of 200 mM NaOH overnight at 4 °C. An aliquot of this cell lysate was subjected to scintillation counting. To quantify ^{55}Fe transepithelial transport, the cells were exposed to the radioisotope for 2 h at 37 °C. Transport was then terminated by washing and dissolving as above. Two hours were allowed for the measurement of transepithelial transport as the time frame for cellular accumulation and basolateral release is longer than that required simply to measure apical uptake (20 min).

An aliquot of the cell lysate and basolateral media were then subjected to scintillation counting. Background of scintillant only and starting amount of ^{55}Fe were also subjected to scintillation counting. Aliquots of cell lysate from each experiment were also taken to quantify protein concentration for normalisation purposes.

Data from functional studies was expressed as follows: (1) iron uptake into Caco-2 cell monolayer within 20 min of exposure to iron; (2) iron retention in Caco-2 cell monolayer following 120 min of exposure to iron; (3) iron released into basolateral compartment following 120 min of exposure to iron; (4) percentage of effluxed iron relative to total iron uptake (i.e. iron retention + iron release) in the Caco-2 cell monolayer following 120 min of exposure to iron.

5.2.5 Data and statistical analysis

Data are expressed as means ± SEM of 4 or 6 observations per group depending on the experiment. Statistical analysis was carried out using GraphPad Prism 5 (San Diego, CA, USA). In studies containing 2 experimental groups Student's unpaired t-test or a Mann-Whitney test was used to compare means. Differences between multiple groups were calculated using a 1-way ANOVA with Dunnett's post-hoc test. In both instances, significance was indicated when $p \leq 0.05$.

5.3 Results

5.3.1 Effects of berry extract on cell viability, RNA and protein content

Indices of cell viability, RNA and protein content were tested to ensure effects of berry extract were not due to pathological changes, but as normative responses. There was no effect of berry extract on cell viability (**Figure 5.2**), RNA content (**Figure 5.3**), or protein content (**Figure 5.4**).

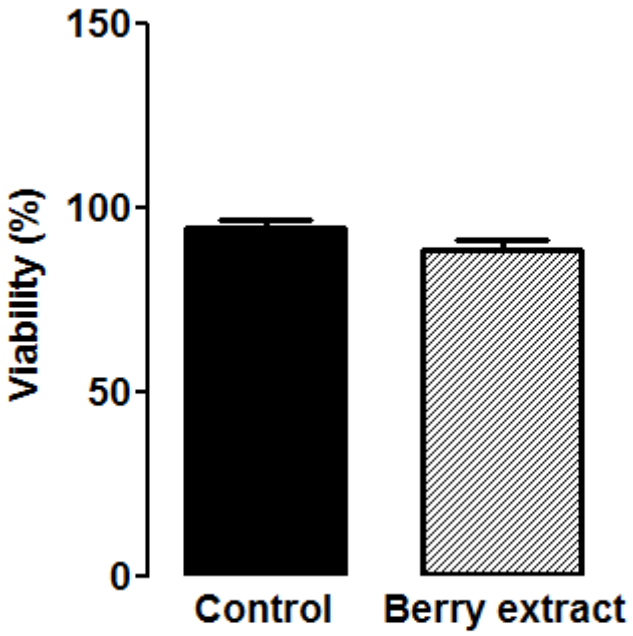

Figure 5.2 Caco-2 cell viability after berry extract treatment. Caco-2 cells were treated with berry extract at 0.125 % (w/v) for 16 h. Cell viability was quantified with the trypan blue dye-exclusion method. Data is presented as mean percentage viable cells ± SEM, *n* = 6. Student's t-test showed there was no significant difference between groups.

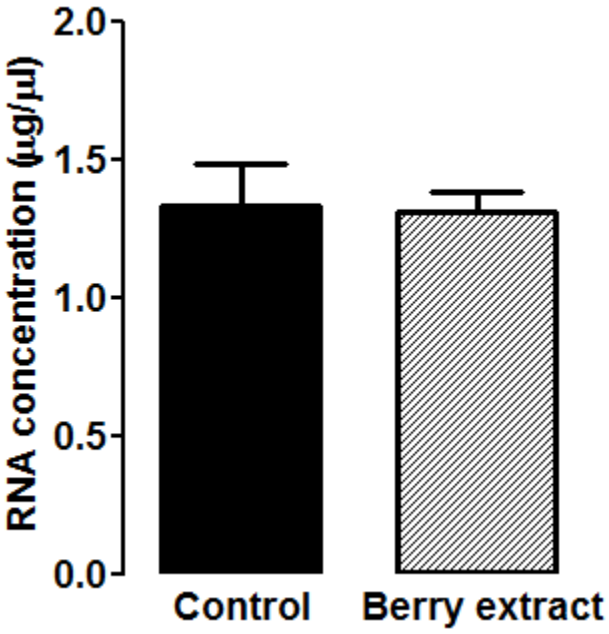

Figure 5.3. RNA concentration from Caco-2 cells after berry extract treatment. Caco-2 cells were treated with berry extract at 0.125 % (w/v) for 16 h. RNA concentration in the extracts of Caco-2 cells was quantified with the NanoDrop spectrophotometer. Data is presented as mean RNA concentration ± SEM, *n* = 6. Student's t-test showed there was no significant difference between groups.

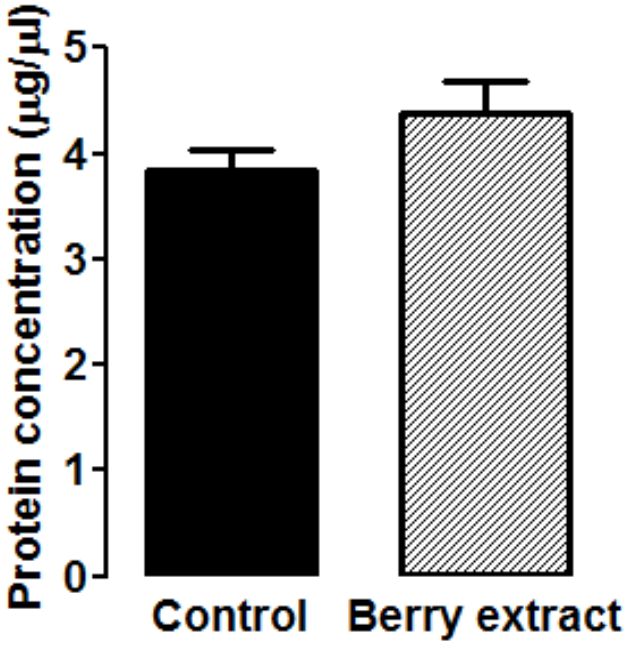

Figure 5.4. Protein concentration from Caco-2 cells after berry extract treatment. Caco-2 cells were treated with berry extract at 0.125 % (w/v) for 16 h. Protein concentration was quantified by the Bradford spectrophotometric assay. Data is presented as mean protein concentration ± SEM; *n* = 6. Student's t-test showed there was no significant difference between groups.

5.3.2 Effects of berry extract on iron transport-related gene expression

Varying concentrations of berry extract were tested on DMT1 and FPN gene expression, from 0.25 % (w/v) in 4 consecutive two-fold dilutions until 0.016 % (w/v). Inhibitory effects on DMT1 expression were observed at 0.125 % (w/v) ($p < 0.05$; **Figure 5.5**, **panel A**). FPN first increased in expression at 0.031 % (w/v), then there was a decrease at 0.25 % (w/v) ($p < 0.05$; **Figure 5.5**, **panel B**). The effects on gene expression of different incubation times with the berry extract were also tested on DMT1 and FPN expression. Inhibitory effects on DMT1 gene expression were observed at 4 h and persisted until 24 h, there was a significant linear trend with increased treatment duration ($r^2 = 0.03$; $p < 0.01$; **Figure 5.6**, **panel A**).

The effects of the berry extract 16 h treatment at 0.125 % (w/v) were tested on the genes that coordinate the enterocytic iron transport pathway. DMT1 and DCYTB mRNA were decreased in response to the berry extract ($p < 0.05$; **Figure 5.7**, **panel A** for DMT1; **panel B** for DCYTB). Expression of HFE was decreased, whereas TfR1 was increased ($p < 0.01$, **Figure 5.7**, **panel C** for HFE; **panel D** for TfR1).

The levels of significance at the same treatment conditions vary. For example: DMT1 expression at 0.125 % (w/v) dose in **Figure 5.4**, 16 h time point in **Figure 5.5** and in **Figure 5.6**, all have the same treatment time, dose and condition. However, biological variation and, more importantly, the different statistical approaches, result in varying levels of significance. A multivariate test, for the dose-response or time course, will give a lower level of significance than the bivariate test applied in the 2-condition analysis. This is because a multivariate test takes into account overall variability over a number of conditions, whereas the bivariate will only account for variability within the two conditions being tested.

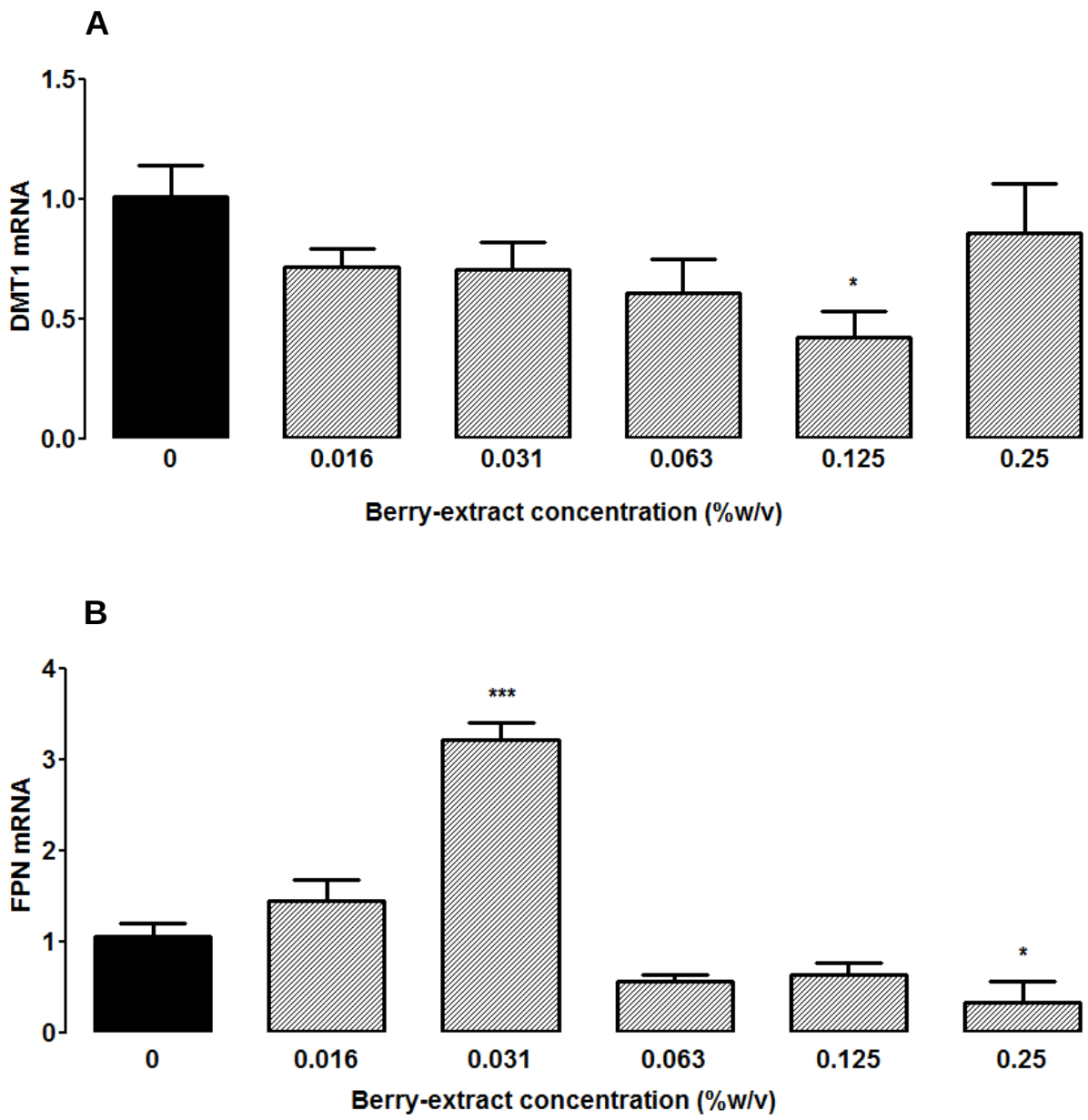

Figure 5.5. Dose-dependent effects of berry extract on DMT1 and FPN mRNA expression. Caco-2 cells were treated with a berry extract for 16 h at different doses from 0.25 % (w/v) in 2-fold dilutions until 0.016 % (w/v). DMT1 (A) and FPN (B) mRNA were quantified by qRT-PCR and normalised against 18S and GAPDH as housekeeping genes. Data are presented as mean normalised expression ratio ± SEM, n = 6, statistical significance was determined by an ANOVA and Dunnet's post-hoc test against the 0% (w/v) concentration. (*) $p \leq 0.05$, (***) $p \leq 0.001$. DMT1: divalent metal ion transporter 1. FPN: ferroportin. 18S: ribosomal RNA 18S. GAPDH: glyceraldehyde 3-phosphate dehydrogenase. qRT-PCR: quantitative real-time polymerase chain reaction.

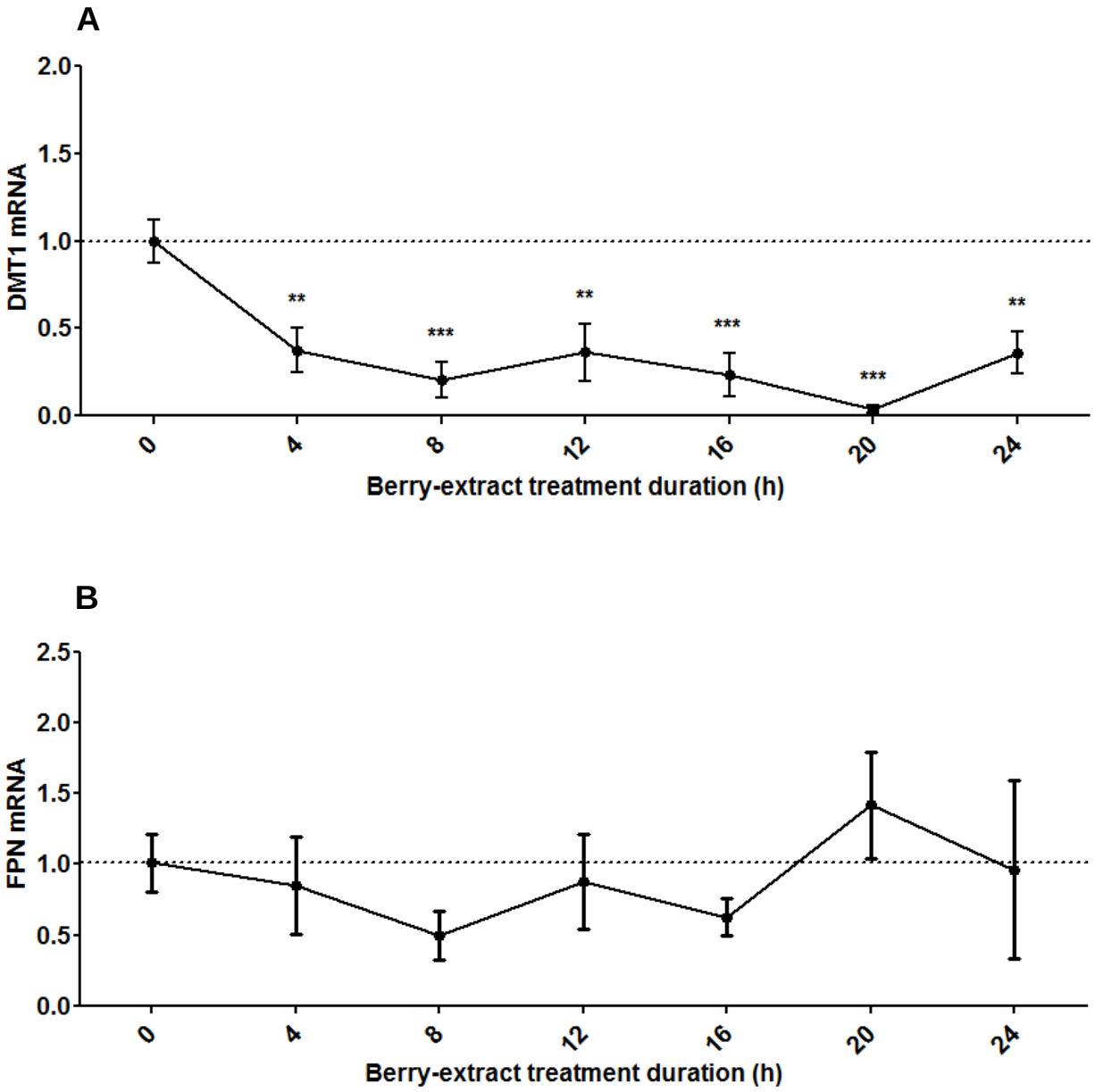

Figure 5.6. Time-dependent effects of berry extract on DMT1 and FPN mRNA expression. Caco-2 cells were treated with berry extract at 0.125 % (w/v) from 4 h to 24 h. Levels of DMT1 (A) and FPN (B) mRNA were quantified by qRT-PCR and normalised against 18S and GAPDH as housekeeping genes. Values are mean normalised expression ratio ± SEM, $n = 6$, statistical significance was determined by an ANOVA and Dunnet's post-hoc test against the 0 h time-point. (**) $p \leq 0.01$, (***) $p \leq 0.001$. DMT1 expression had a significant linear trend (***) $p \leq 0.001$. DMT1: divalent metal ion transporter 1. FPN: ferroportin. 18S: ribosomal RNA 18S. GAPDH: glyceraldehyde 3-phosphate dehydrogenase. qRT-PCR: quantitative real-time polymerase chain reaction.

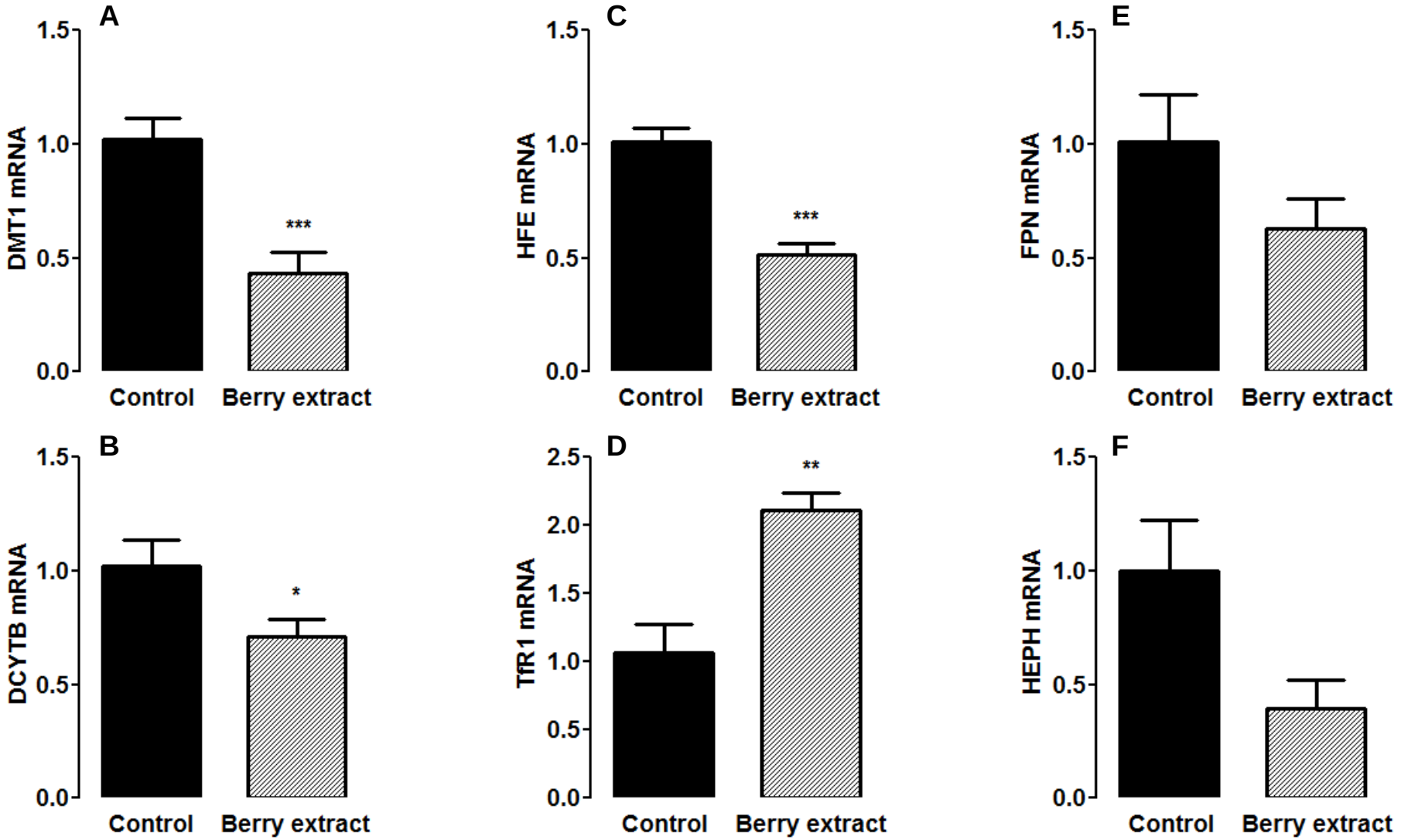

Figure 5.7. Effect of berry extract on mRNA expression of iron transport-related genes. Caco-2 cells were treated with 0.125 % (w/v) of berry extract for 16 h. Levels of DMT1 (A), DCYTB (B), HFE (C), TfR1 (D), FPN (E) and HEPH (F) were quantified and normalised to 18S and GAPDH as housekeeping genes. mRNA data are presented as the mean (relative to the control) ± SEM, $n = 6$. (*) $p \leq 0.05$, (**) $p \leq 0.01$, (***) $p \leq 0.001$. Student's t-test was used to determine statistical significance. DMT1: divalent metal iron transporter 1. DCYTB: duodenal cytochrome B reductase. HFE: haemochromatosis protein. TfR1: transferrin receptor 1. FPN: ferroportin. HEPH: hephaestin. 18S: ribosomal RNA 18S. GAPDH: glyceraldehyde 3-phosphate dehydrogenase. qRT-PCR: quantitative real-time polymerase chain reaction.

5.3.3 Effects of berry extract on DMT1 and FPN protein expression

Following a 16 h treatment with the berry extract at 0.125 % (w/v) protein abundance of DMT1 and FPN was quantified by Western blot. There was no effect on the total abundance of either protein (**Figure 5.8**).

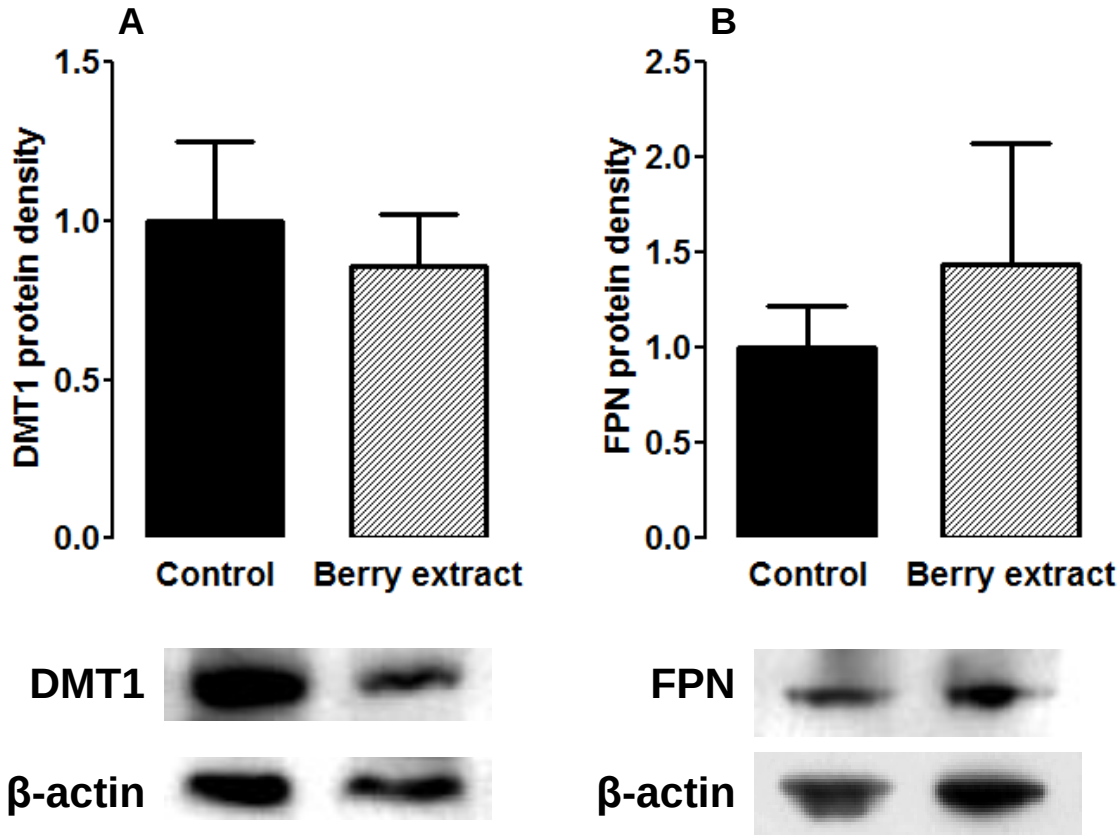

Figure 5.8. Effect of berry extract on DMT1 and FPN protein expression. Total protein was prepared from Caco-2 cells treated with 0.125 % (w/v) berry extract for 16 h. Levels of DMT1 or FPN protein were normalised to β-actin as a housekeeping protein. Representative blots for DMT1 (A) and β-actin are shown in the lower left panel, with semiquantitative densitometry data in the upper left panel. Representative blots for FPN (B) and β-actin are shown in the lower right panel, with semiquantitative densitometry data in the upper right panel. Expression levels of the housekeeper protein β-actin were not altered by berry extract treatment. Densitometry data are presented as the mean (relative to the control) ± SEM, $n = 4$. Student's t-test showed there was no significant difference between groups.

5.3.4 Effects of berry extract on iron transport

In this section our interest was in the *acute* and *chronic* effects of flavonoids on the transepithelial transport of iron. We investigated: 1) the apical uptake of iron, within 20 min of iron loading; 2) the cellular retention *and* the basolateral release of iron, within 120 min of iron loading; and 3) the rate of effluxed iron relative to total uptake (expressed as a percentage) within 120 min of iron loading.

Under acute treatment conditions, the berry extract treatment increased apical iron uptake ($p < 0.05$; **Figure 5.9**, **panel A**). At 120 min, there was a significant decrease of cellular retention and basolateral release of iron ($p < 0.05$; **Figure 5.9**, **panel A and panel B, respectively**).

Following chronic berry extract treatment, apical iron uptake was decreased ($p < 0.05$; **Figure 5.10**, **panel A**). After 120 min there were no significant effects on cellular retention or basolateral release of iron (**Figure 5.10**, **panels B and C**).

As for the transepithelial flux of iron, the percentage of effluxed iron decreased after both acute ($p < 0.05$; **Figure 5.11**, **panel A**) and chronic ($p < 0.05$; **Figure 5.11**, **panel B**) treatments.

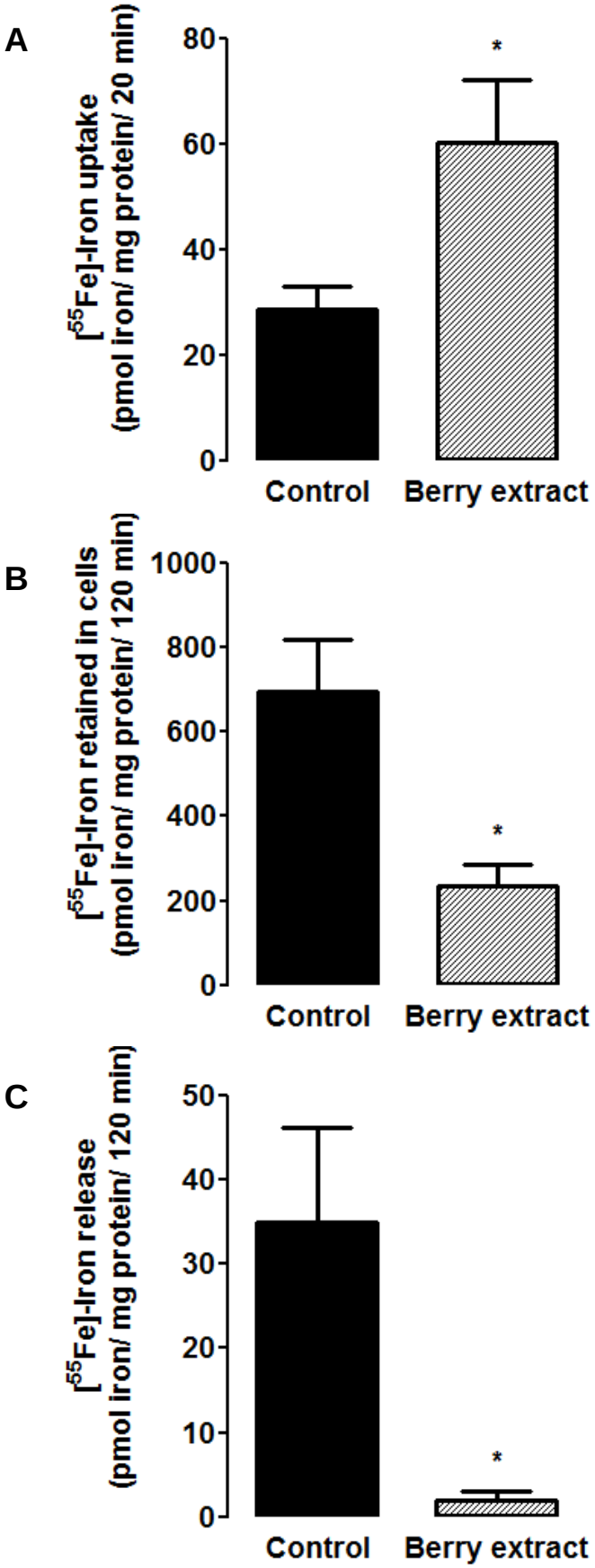

Figure 5.9. Acute effects of berry extract on iron uptake and release. Caco-2 cells cultured on membrane supports were treated acutely (20 min) with 0.125 % (w/v) berry extract and iron uptake was initiated. Apical uptake of iron was measured following 20 min (A), the cellular retention of iron was measured following 120 min (B); and the basolateral release of iron was measured after 120 min (C). Data are presented as the mean ± SEM, n = 6, Mann-Whitney or Student's t-test was used to determine statistical significance; (*) $p \leq 0.05$.

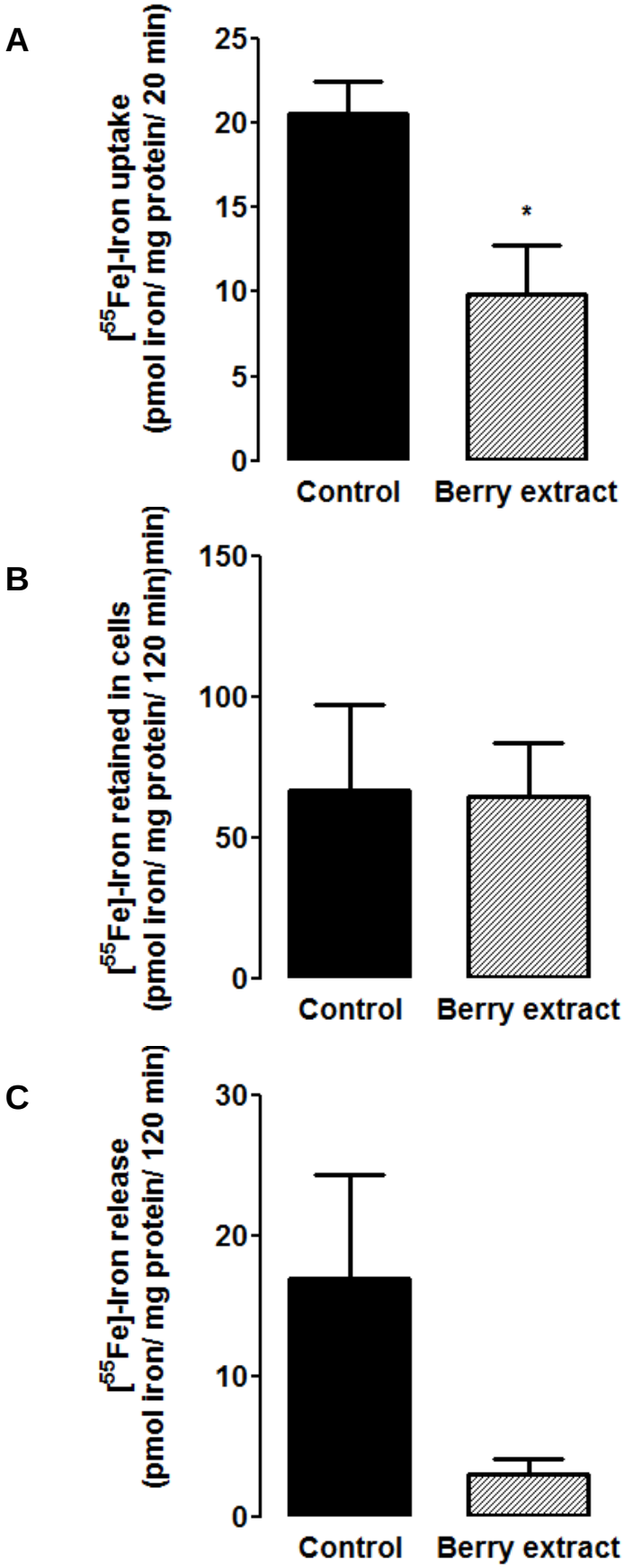

Figure 5.10. Chronic effects of berry extract on iron uptake and release. Caco-2 cells cultured on membrane supports were treated chronically (16 h) with 0.125 % (w/v) berry extract then iron uptake was initiated. Apical uptake of iron was measured following 20 min (A), the cellular retention of iron was measured following 120 min (B); and the basolateral release of iron was measured after 120 min (C). Data are presented as the mean ± SEM, n = 6, Mann-Whitney or Student's t-test was used to determine statistical significance; (*) $p \leq 0.05$.

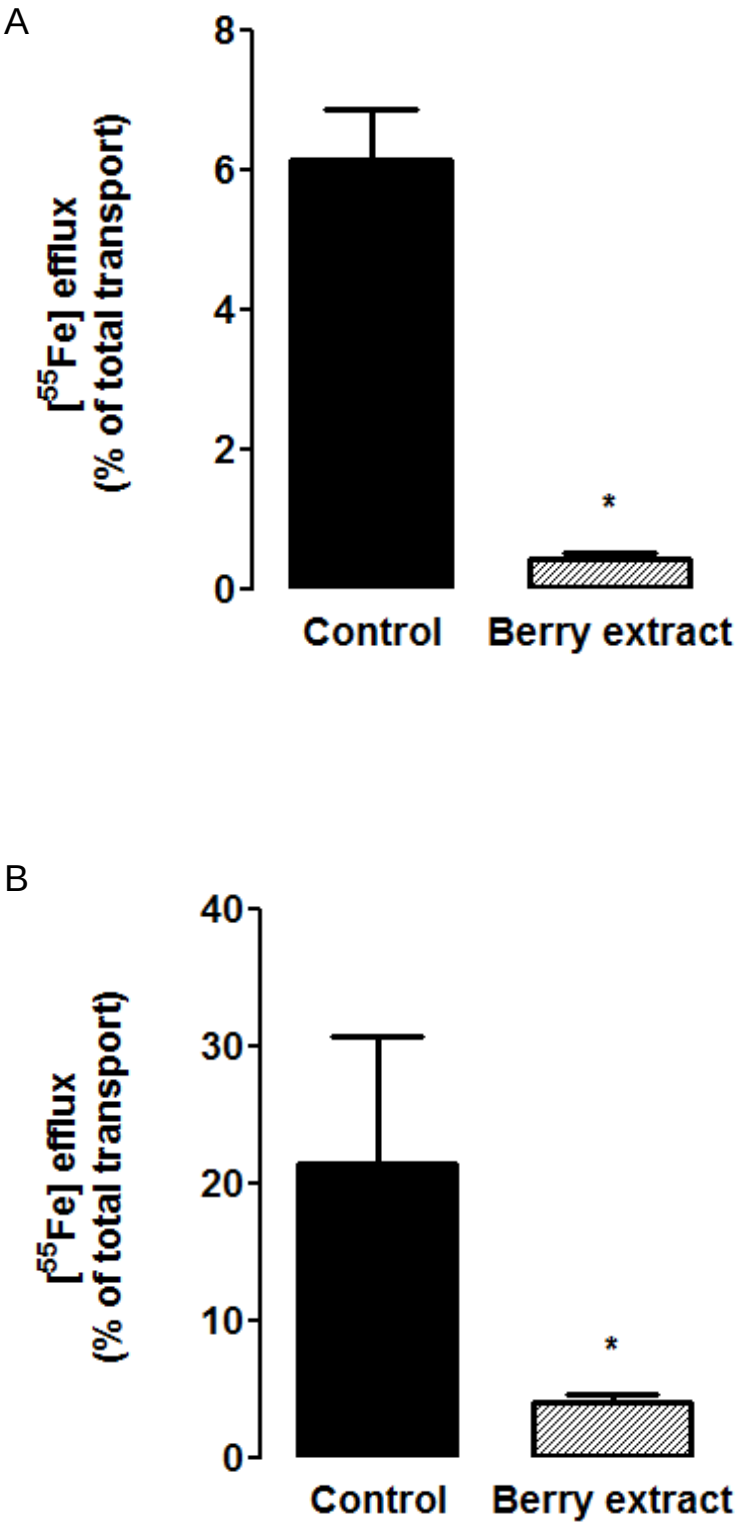

Figure 5.11. Effects of berry extract on transepithelial flux of iron. Caco-2 cells cultured on membrane supports were treated acutely for 20 min (A) or chronically for 16 h (B) with 0.125 % (w/v) berry extract then iron transport was initiated. ^{55}Fe effluxed into the basolateral compartment was expressed as a percentage of all the ^{55}Fe that was effluxed and that was remaining in cell lysate. Data are presented as the mean ± SEM, n = 6, Mann-Whitney test was used to determine statistical significance; (*) $p \leq 0.05$.

5.4 Discussion

In order to prevent the development of iron overload or anemia, total body iron must be tightly regulated at the stage of intestinal absorption, i.e. enterocytes. This is essential as humans are not equipped with a regulated excretory mechanism for excess iron. The transepithelial transport process of iron is coordinated by a number of genes that respond to systemic, local and luminal stimuli. The luminal stimuli are largely under our dietary control and depend on the presence of substances, such as ascorbate and flavonoids, which influence iron availability. Effects of dietary, luminal contents on the iron transport process are, in turn, likely to influence the function and expression of the transport pathway. However, the chronic effect of dietary flavonoids on iron transport and transporter expression hitherto remains to be elucidated.

We addressed the hypothesis that a flavonoid-rich berry extract will alter the expression of the genes and proteins that regulate intestinal iron transport and will in turn influence iron transport in Caco-2 cells. Caco-2 cells are an established model of human intestinal epithelial cells expressing the necessary proteins for the transport of dietary iron (Sharp *et al*, 2002). We demonstrated that berry extract treatment decreases expression of those genes responsible for the apical uptake of iron, DCYTB and DMT1. The expression of HFE and TfR1 decreased and increased, respectively. HFE, transfected into Caco-2 cells, is known to inhibit apical uptake of iron; TfR1 and HFE in crypt cells, form a complex to cycle iron from circulation back into the cell; thus HFE and TfR1 work cooperatively, putatively, to lower systemic iron levels (Feder *et al*, 1998; Arredondo *et al*, 2001; Trinder *et al*, 2002; Arredondo *et al*, 2006). In terms of function, iron uptake was increased with acute berry extract treatment. Following chronic treatment, iron uptake was decreased. The

transepithelial flux of iron was decreased with berry extract, following both acute and chronic treatments.

Our results thus indicate berry extract flavonoids can elicit a transcriptional response from iron-transport related genes. Furthermore, chronic treatment with the berry extract decreases the transepithelial flux of iron. Under acute settings, the flavonoids in our experiment replicate other findings from other studies. These indicate structural interactions with flavonoids or transporters that enhance apical uptake and diminish basolateral release (i.e. Kim *et al*, 2008).

5.4.1 Effects of berry extract on gene and protein expression

5.4.1.1 DCYTB expression

In our experiments the expression of DCYTB mRNA was decreased following berry extract treatment. *In-vivo* DCYTB expression is dependent on iron requirement, increasing in conditions favouring iron influx and decreasing in states of high cellular iron status (Frazer *et al*, 2002; Frazer *et al*, 2003; Zoller *et al*, 2003). In our study, the decreased expression of DCYTB, following berry extract treatment, indicates Caco-2 cells are replete with iron.

It must be noted that Caco-2 cells are not known to highly express the DCYTB protein. To resolve this, other studies use transfected Caco-2 cells (Latunde-Dada *et al*, 2008). Alternatively, other metalloreductase activity is in place to compensate for a lack of DCYTB protein. This notion is supported by studies in DCYTB-null mice which do not develop iron-deficiency (Gunshin *et al*, 2005). However we resolved this by adding ascorbate, a well known dietary reductant, to the iron prior to administration in our transport studies.

5.4.1.2 DMT1 expression

DMT1 gene expression decreased in response to treatment with the berry extract. DMT1 is typically expressed in at least two transcript variants, one with an IRE region in its transcript (DMT1+IRE) and one without (DMT1-IRE) (Lee *et al*, 1998). In enterocytes the DMT1+IRE isoform is predominant and responds strongly to iron. Its expression increases in response to low iron and decreases in response to high iron (Canonne-Hergaux, 1999; Gunshin *et al*¸ 2001). Regarding our findings, DMT1 mRNA expression may have decreased as a response to iron accumulation in the enterocyte. Accumulation of iron is strongly reflected by the time-course of DMT1 mRNA expression in this study, in which there was an immediate and persistent inhibition of gene expression.

5.4.1.3 HFE expression

The precise role of HFE in the intestine remains unclear. One proposed role of HFE is its function as an intracellular inhibitor of DMT1-mediated iron uptake. This is supported by experiments showing decreased apical iron uptake when HFE, β2m and TfR1 co-localise with DMT1 at the apical membrane; (Griffiths *et al*, 2000; Arredondo *et* al, 2001; Arredondo *et al*, 2006). Furthermore, defects in the HFE gene cause iron overload haemochromatosis and mice lacking this gene have increased DMT1-mediated iron uptake (Fleming *et al*, 1999).

The regulators of HFE are unknown. There is evidence to support reciprocal regulation to DMT1 or as a negative regulator of DMT1 (Han *et al*, 1999). *In-vitro* HFE expression has been found to be dependent on the presence of serum, and not iron (Tallkvist *et al*, 2000). This negates a correlation of HFE expression to a major transcript variant of DMT1. Others suggest HFE expression is regulated by alternative splicing, and acts as a signaling peptide (Martins *et al*, 2011).

5.4.1.4 TfR1 expression

Systemically, TfR1 is known to bind to Tf to facilitate cellular iron absorption; whereas in enterocytes TfR1 and HFE interact to regulate iron transport. TfR1's transcript contains an IRE region thus its expression is strongly induced by iron (Brookes *et al*, 2006; Lee *et al*, 1998; Tallkvist *et al*, 2000). It is reciprocally regulated to HFE, and is expressed only in the presence of serum. (Tallkvist *et al*, 2000). The expression profile we have observed following treatment with the berry extract supports the reciprocal regulation to HFE and the intracellular accumulation of iron.

TfR1 is known to form a complex with HFE and β_2m. This complex is suggested to be an inhibitory component for apical DMT1-mediated uptake. Furthermore, HFE binding decreases TfR1 cycling time. This results in blocked Tf binding sites and therefore decreased efflux capacity thus impeding basolateral iron release (Griffiths *et al*, 2000; Ikuta *et al*, 2000; Tallkvist *et al*, 2000).

5.4.2 Effects of berry extract on functional iron transport

5.4.2.1 Acute effects of berry extract on iron transport

Functional studies were carried out acutely to characterise the effects of co-incubating iron with flavonoids. Initially, the uptake of iron was increased in the presence of the berry extract flavonoids. This is consistent with previous findings (Kim *et al*, 2008).

Proposed mechanisms for the initial increase in uptake include more available ferrous iron as a result of flavonoid reducing capacity. However, excess ascorbate was added as a reductant to ensure availability of ferrous iron. Alternatively, metal-polyphenol complexes are formed and transported across the apical membrane via a

different transporter to DMT1 (Kim *et al*, 2008; Ren *et al*, 2008; Vlachodimitropoulo *et al*, 2010b).

Following 120 minutes, the berry extract treatment caused the rate of iron efflux to decrease relative to the control. The cellular retention and basolateral release of iron were both decreased. The decreased cellular retention of iron is likely to be the result of cellular feedback mechanisms to limit the initial increase in iron uptake. This could be mediated by rapid redistribution of DMT1 away from absorptive membranes (Sharp *et al*, 2002). Alternatively, there may be an efflux of iron from the apical route via an unknown transporter. An adaptive mechanism, such as this, is necessary for cell survival, as basolateral release of iron was diminished. Previous research suggests that the metal-polyphenol complex transported into the cell is too large to be effluxed by FPN (Kim *et al*, 2008).

5.4.2.2 Chronic effects of berry extract on iron transport

Chronic incubations were carried out to characterise the functional relevance of the effects of the berry extract on mRNA or protein expression. Chronic berry extract treatment initially decreased the apical uptake of iron. This is consistent with the decrease in expression of the genes that coordinate apical iron uptake, i.e. DCYTB and DMT1. Following 120 minutes of exposure to iron, the cellular retention and basolateral release of iron returned to the control levels. However, the percentage of effluxed iron was significantly decreased in the cells treated with the berry extract.

The dietary reductant ascorbate is known to increase iron uptake and has been reported to negate the inhibitory effects of flavonoids on iron absorption (Ma *et al*, 2011). In our studies, the inclusion of ascorbate does not appear to have affected the inhibitory effect of flavonoids on iron absorption. The mechanisms for these divergent findings remain to be elucidated.

5.5 Conclusions

Our findings indicate that flavonoids acutely stimulate the uptake and impede the basolateral release of iron, thus causing intracellular iron accumulation. Over a prolonged period (as with our chronic studies) the cellular responses would be that of iron overload; i.e. a cellular adaptation to limit influx and maintain efflux of iron. This is reflected in the expression profiles of those genes that coordinate iron uptake and in our functional studies following chronic treatment. There are no previous studies, to our knowledge, that have investigated the chronic effects of flavonoid treatments on intestinal iron transport. Our research has thus contributed to the understanding of nutrient interactions and the effects that these have on the function of the intestinal epithelium with respect to transport. Further studies are required to understand the mechanisms behind the observed effects and their application to improving the dietary management of dysregulated iron balance.

5.6 Future work

5.6.1 Acute interactions of flavonoids and iron

Our findings regarding the effects of flavonoids on iron absorption leave a number of questions that remain to be answered. **Figure 5.12** gives an outline of the acute effects of flavonoids on cellular iron metabolism with resulting points of future investigation. Briefly, given previous work in the area, several mechanisms might contribute to increased iron uptake following acute exposure to berry flavonoids; including: increased iron reducing capacity in the presence of flavonoids (Kim *et al*, 2008) or through flavonoids acting as substrates for DCYTB (Vlachodimitropoulou *et al*, 2010a). Polyphenol-iron complexes formed at the apical pole of enterocytes could be imported via GLUT transporters (as transporters of flavonoids) or via other unknown routes (Vlachodimitropoulou *et al*, 2010b). Polyphenols, might also form chelates of iron intracellularly, and these are too large to exit via FPN, the only known basolateral release route for iron (McKie *et al*, 2000). Furthermore, intracellular flavonoids may have a direct inhibitory action on FPN-mediated efflux by interacting directly with the basolateral transporters or membranes. The fate of the iron-polyphenol complex remains unknown, it may undergo further metabolism, or may be recycled back into the apical medium. The latter supposition is credible since following 120 min, despite an initial increase in iron uptake, cellular retention as well as the transepithelial flux of iron decrease below control levels.

Efflux of polyphenol-iron complexes into the basolateral medium could be addressed by adding phloretin or cytochalasin-B, which will inhibit GLUT-mediated transport to the basolateral medium. The metabolic fates of these complexes could also potentially be monitored with confocal fluorescence microscopy, as flavonoids do emit at specific wavelengths. Determining the exchange of iron distribution between

ferritin pools, labile iron pools and flavonoids will also aid in determining the cooperation between these compounds and the modulation of cellular iron stores. If metals affect the fluorescence of the flavonoid compounds, tritiated flavonoids as well as iron-55 can be applied to determine redistribution between cellular pools and the subcellular activity of flavonoids; i.e. mitochondrial or nuclear accumulation etc. (Mukai *et al*, 2009).

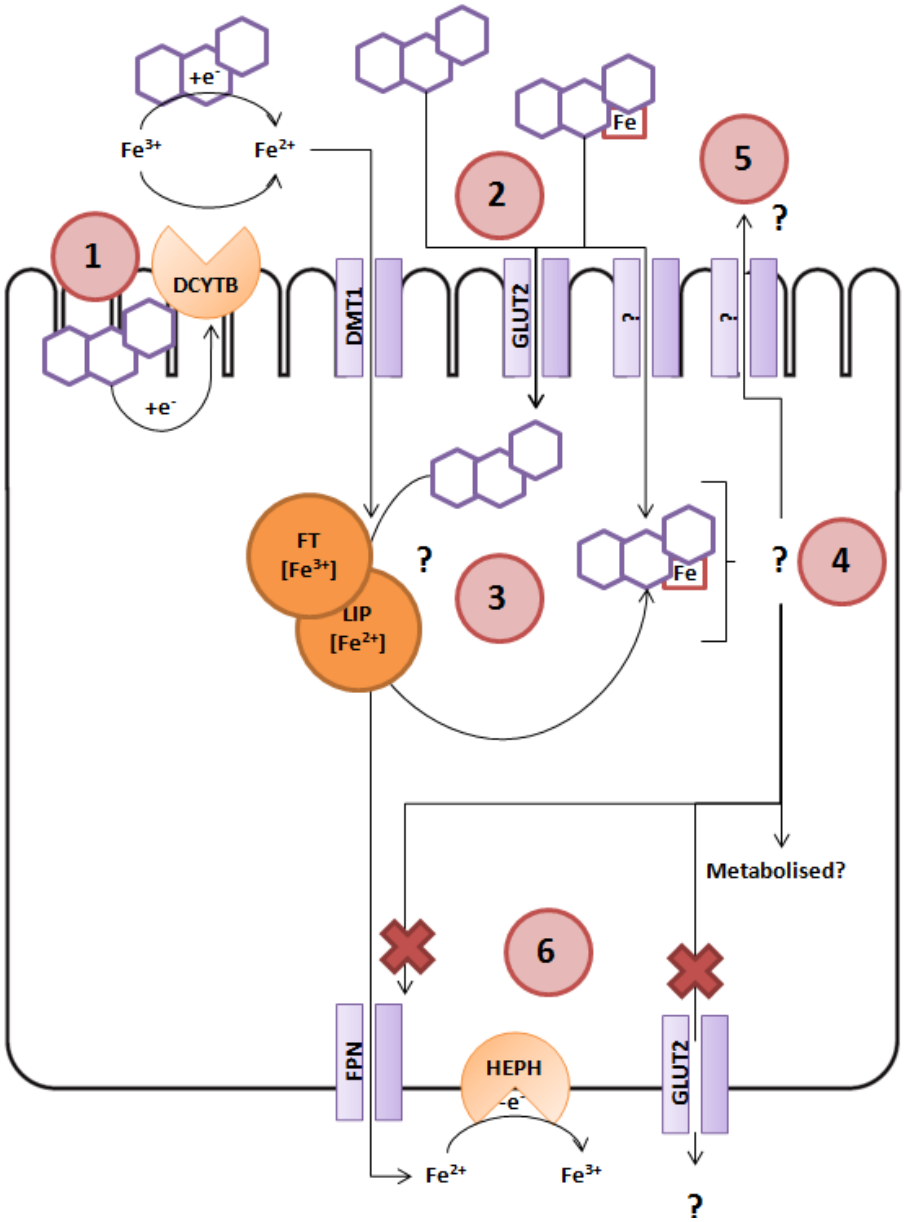

Figure 5.12. Model of the acute effects on flavonoid treatment. Acute flavonoid treatment increases the uptake of iron and decreases the cellular retention and basolateral release of iron; this results in an overall decrease in iron transport through enterocytes. **1)** Several mechanisms contribute to higher iron uptake, including the direct extracellular reduction of Fe^{3+} by flavonoids; alternatively cellular flavonoids can be substrates for DCYTB, catalysing the apical reductase step. **2)** Flavonoids will form chelates with iron, either intracellularly or extracellularly, extracellular chelates enter the cell via GLUT2 or other unknown routes. **3)** Cellular flavonoids may also interact with the LIP or FT to bind iron. **4)** Cellular destination or metabolism of iron-flavonoid chelates is unknown. **5)** There may be an apical efflux route for chelates, as GLUT-type transporters have been shown to carry out this function. **6)** There is no known efflux route for such complexes, causing the decreased trans-epithelial flux of iron. DCYTB: duodenal cytochrome B reductase; DMT1: divalent metal ion transporter 1; GLUT2: facilitative glucose transporter 2; FT: ferritin; LIP: labile iron pool; FPN: ferroportin; HEPH: hephaestin.

5.6.2 Chronic effects of flavonoids on iron metabolism

From the chronic studies with flavonoids, we have seen that chronic exposure to flavonoids causes a decrease in the transepithelial flux of iron. Unlike the acute studies, in which the flavonoids are present at the same time as the iron substrate, the rate-limiting step of transport can be determined here. Following chronic treatment, clearly apical uptake is the rate-limiting step. The results of the Western blotting of uptake proteins did not present an overt explanation as to why this may be the case, as levels of the apical uptake protein, DMT1, appeared slightly lower but did not change significantly. Uptake via DMT1 can be endogenously modified by re-distribution of transporter proteins away from the cell surface to endosomal/lysosomal compartments within the cell (Johnson *et al*, 2005). Exposure to berry flavonoids could affect cellular distribution of DMT1 without modifying total transporter protein levels. This hypothesis should be addressed, as with the gene expression array results in **Chapter 3**, several gene ontology terms relate to late endosomal/lysosomal compartments (**Section 9.5**). We can test this supposition by confocal microscopy investigating transporter distribution as well as subcellular fractionation following exposure to berry flavonoids to determine whether transporter protein levels change within specific cellular compartments.

We can also hypothesise that there may be a significant contribution of flavonoid-iron chelates to total iron uptake, and that this uptake could be mediated via GLUT2. As the decrease in uptake, coincides with a decrease in GLUT2 protein abundance (**Chapter 5**). Again, inhibition of GLUT2 transport with phloretin and inhibition of DMT1 by disrupting the pH gradient will determine the relative contribution of these transporters.

The above points are reflected in **Figure 5.13**.

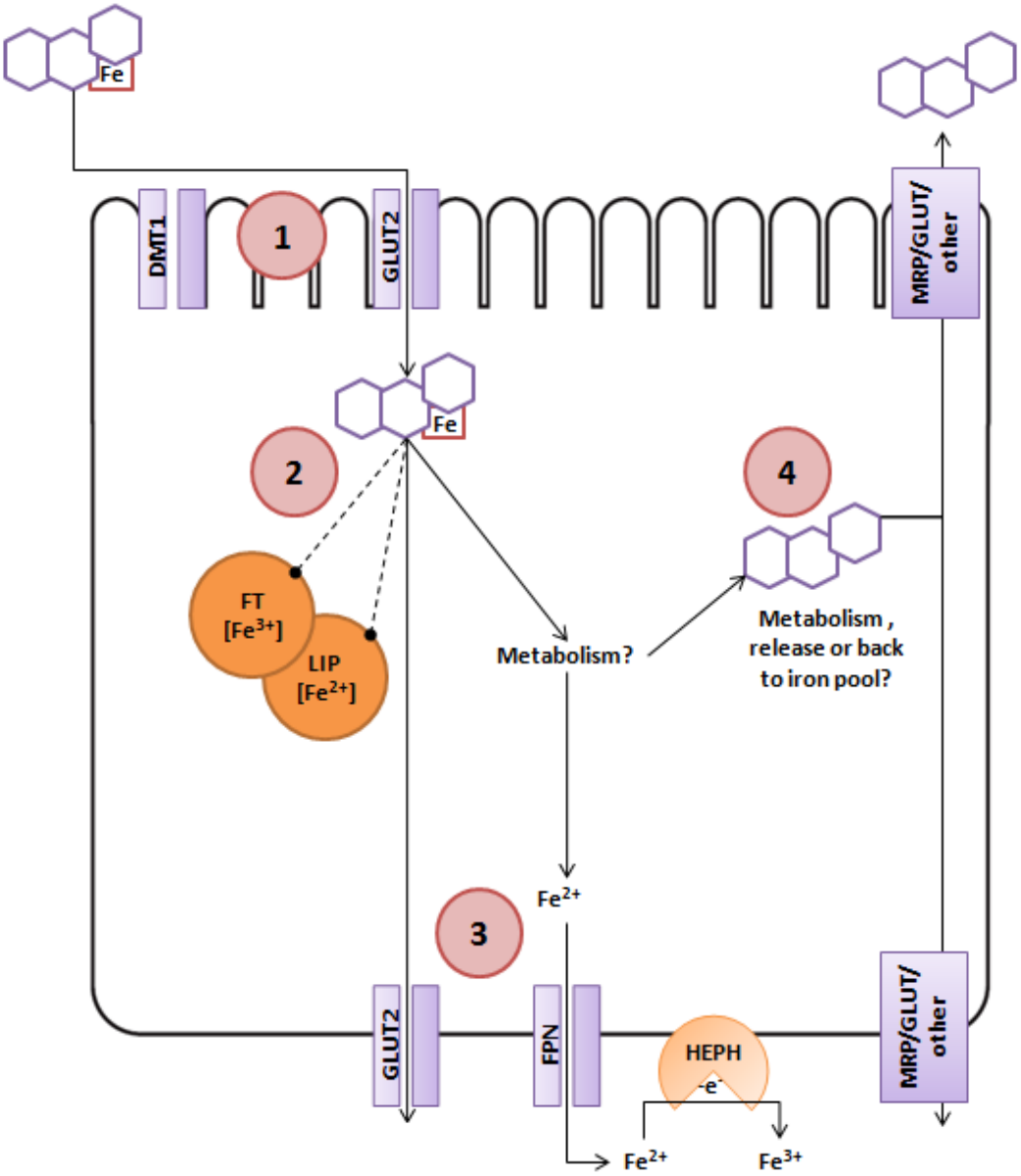

Figure 5.13. Effects of flavonoids on iron absorption. 1) flavonoid-iron complexes may be transported into the cell via a separate route, GLUT2, other flavonoid transporters or unknown routes. **2)** Intracellularly, it is not known if the chelate will interact with the cellular iron pools or will undergo separate metabolism. **3)** It is not known if a basolateral efflux route exists for these chelates, or if downstream metabolism will liberate any iron for transport via ferroportin. **4)** Finally, the role of flavonoids, if metabolised or bound to iron is known, will this complex undergo efflux via unknown routes at the apical or basolateral membranes.

5.6.3 Effects of flavonoids on iron-transport related genes

The molecular effects we observed of flavonoids on gene expression are perhaps the most worthy of further investigation. As the expression profile we have seen does not completely adhere to what is expected as a response to a single substrate. There are other possibilities, such as the influence of flavonoids on oxidative state, and the downstream events that arise from this. Future work to investigate the effects of flavonoids on gene expression is discussed in the following section.

5.6.3.1 The iron effect

When investigating any area of iron metabolism, the *local* regulatory potential must be taken into account. This is mediated by the IRE/IRP system. Of the genes we have tested, DMT1 and TfR1 contain IRE regions in their 3'UTR, whereas FPN contains an IRE region in the 5'UTR end of its transcript. IRP levels and / or activity increase when there is a lack of iron; if IRP binds to the 3'UTR, they stabilise and protect mRNA species, whereas binding to the 5'UTR end prevents translation of the gene product (reviewed by Sharp & Srai, 2007). Therefore with regards to our findings, the decrease in DMT1 mRNA following prolonged treatment with flavonoids would be consistent with cellular iron loading, decreased activity of IRP and as a result a decreased DMT1 mRNA stability. However, the response of TfR1 mRNA is not consistent with this mechanism. We must confirm the presence or absence of an *iron* effect on these genes. Quantifying the presence of IRP proteins with Western blotting will confirm their contribution to the observed effects. Quantifying the effects that flavonoids have on cellular iron pools is also important, for both acute and chronic investigations, as well as intermediate exposure times. Measuring ferritin as a surrogate marker for iron levels and Phen-Green fluorescence to indicate the abundance of the labile iron pool would help to address this.

5.6.3.2 The effect of hypoxia-inducible factors

Hypoxia-inducible factor 2α (HIF-2α) is known to be expressed under hypoxic conditions and to induce the expression of components of the iron uptake pathway (Mastrogiannaki *et al*, 2009; Hu *et al*, 2010). HIF-2α interacts directly with the DMT1 and FPN promoter regions to induce their expression (Mastrogiannaki *et al*, 2009; Taylor *et al*, 2011). Knockout of HIF-2α has been shown to decrease expression of DMT1, DCYTB and FPN; these findings are very similar to the gene expression profile we have found following a chronic treatment with flavonoid compounds.

Flavonoids have been shown to induce accumulation of HIFs through chelating iron, thus making iron unavailable as a cofactor for HIF prolyl hydroxylases; enzymes which label HIF subunits for rapid proteasomal degradation (Park *et al*, 2008). However, HIF-2α contains an IRE in its 5'UTR sequence which means under iron deficient conditions, translation would be decreased. The effect of berry flavonoids on HIF-2α mRNA and protein levels should therefore be measured to determine whether it plays a role in iron transporter regulation.

5.6.3.3 The crypt-villus axis and co-culture models

One of the most controversial elements of iron metabolism surrounds the function and expression of HFE. The leading assumptions with HFE are that this gene is primarily expressed basolaterally in crypt enterocytes. Its assumed functions are: 1) HFE binds to TfR1 and aid in the internalisation of Tf-bound iron from the circulation back into intestinal epithelial layers; and 2) in transfected Caco-2 cells, HFE inhibits apical DMT1-mediated iron uptake (Fleming *et al*, 1999; Arredondo *et al*, 2001; Arredondo *et al*, 2006; Martins *et al*, 2011). The most reasonable approach for determining the effects of flavonoids on this gene, and elucidating the functional

consequences would be to investigate the effects of feeding flavonoids on the expression and distribution of HFE along the crypt-villus axis in animal models and in Caco-2 cells. These studies could be carried out at various stages of cell differentiation; Caco-2 cells have previously been applied in differentiation studies and as models of the crypt-villus maturation process (Tremblay *et al*, 2006; Bedrine-Ferran *et al*, 2009). In light of this, it would be preferable to investigate the differentiation and maturation through an *in-vivo* model. Knockdown of HFE in Caco-2 cells using siRNA and the use of HFE-knockout mice would be useful models to further study the role of this gene in flavonoid-mediated regulation of intestinal iron transport.

The other important peptide in iron metabolism, which we have not investigated in this system, is hepcidin. To investigate the effects of this decrease in iron flux on hepcidin expression we can apply a co-culture model of enterocytes and hepatocytes (Chaston *et al*, 2008). As well as allowing the response and feedback of hepcidin to be measured (giving a more physiological context to our results), the co-culture system will allow us to determine transport efficiencies and effects of hepatic phase 2 metabolism on flavonoids, or the effects of *systemic* polyphenolics on iron metabolism in hepatocytes. Hepcidin knockout mice will be useful to further test the interactions between hepcidin and flavonoids in the regulation of intestinal iron transport.

CHAPTER SIX

Effects of berry extract on the expression and function of intestinal copper transport pathway in Caco-2 enterocytes

6 Effects of berry extract on the expression and function of intestinal copper transport pathway in Caco-2 enterocytes

6.1 Introduction: Intestinal copper transport and dietary flavonoids

The trace element copper is essential for life, as an integral part of several redox enzymes; e.g. hephaestin and ceruloplasmin (Vulpe *et al*, 1999; Eisenstein, 2000; de Romaña *et al*, 2011). However, in excess copper generates free radicals through the Fenton reaction (Speisky *et al*, 2009). In light of this, the maintenance of copper homeostasis must be tightly regulated. The intestine is important in maintaining copper balance, via absorption from dietary sources or reabsorption from bile, pancreatic juices, gastric juices and saliva (Owen, 1964; Turnlund *et al*, 1999). Several factors influence intestinal copper absorption including age, gender, dietary copper content and the presence of other nutrients (Johnson, 1989). Imbalances in copper homeostasis are rare, though they occur in two major diseases: Menke's disease and Wilson's disease. These diseases result from genetic mutations in the two copper transporting ATPases, ATP7A and ATP7B, respectively (Cox & Moore, 2002; Lutsenko, 2008).

The primary step in copper metabolism is the transport of ingested copper across the intestinal epithelium. Following this, copper is transported and distributed via the portal venous system (Puig & Thiele, 2002). The first step in intestinal copper absorption is the reduction of cupric copper. This occurs through dietary reductants such as ascorbate and candidate reductases such as DCYTB and the Steap proteins (Kuo *et al*, 2004; Ohgami *et al*, 2006; Wyman *et al*, 2008). Once reduced, cuprous copper can be transported into the enterocyte via the apical importer CTR1 (Lee *et al*, 2000). Once in the enterocyte, copper can be bound by any one of a number of chaperone proteins, such as the HAH1 or CCS. Each chaperone has its specific

destination for intracellular copper delivery (Harrison *et al*, 2000). Copper that is bound to HAH1 is delivered to ATP7A or ATP7B (Hamza *et al*, 2003). ATP7A is necessary for the efflux of copper from the basolateral membrane of enterocytes (Yamaguchi *et al*, 1996; La Fontaine *et al*, 1998). The role of intestinal ATP7B (highly expressed in hepatocytes as a copper efflux protein) remains unclear. Both ATPases are implicated in the cupration of metalloenzymes at the trans-Golgi network (Nyasae *et al*, 2007; Weiss *et al*, 2008).

Copper is known to interact with other nutrients. For example, adequate copper status is necessary for the metabolism of iron (Tennant *et al*, 2002). Additionally, copper and iron are both substrates for DMT1, thus presenting competition for each other (Arredondo *et al*, 2003). Both of these metals are influenced by the presence of ascorbate and by polyphenolic compounds (Kuo *et al*, 2004; Ren *et al*, 2008; Lekka *et al*, 2009; Thumser *et al*, 2010). However, the effects of flavonoids on copper absorption and on the genes and proteins that coordinate copper absorption remain unknown. To address this we investigated the effects of a flavonoid-rich berry extract on copper uptake and on the expression of copper transport-related genes and proteins in Caco-2 cells.

6.2 Methods

Presented here is a brief description of the methods used in this chapter. For full details of reagents, buffer/media compositions and methods used see **Chapter 2.**

6.2.1 Cell culture

Caco-2 TC7 cells between the passages of 44 and 47 were seeded into 6-well plates at a density of 40,000 cells per well (4,000 cells per cm^2) and cultured for 19 days prior to treatment. For copper uptake studies, cells were grown on T-25 flasks at a density of 100,000 cells per flask. Details of the maintenance of the cells and composition of cell culture medium have been previously described (see **Chapter 2** and Johnston *et al*, 2005).

The treatment used was a flavonoid-rich berry extract (derived from blueberry, bilberry, cranberry, elderberry, raspberry seeds and strawberry; rich in the anthocyanins delphinidin, cyanidin, petunidin and malvidin, OptiBerry®, InterHealth Nutraceuticals, CA, USA) at a final concentration of 0.125 % (w/v). Treatment was prepared in Dulbecco's modified Eagle's medium for gene and protein expression and chronic-exposure copper-uptake studies. Treatments for acute-exposure copper-uptake experiments were prepared in 2-(*N*-morpholino) ethanesulfonic acid buffered salt solution (MBSS). An identical medium, without the berry extract, was used for the control cells.

The effect of berry extract treatments on cell viability, RNA and protein content of the cells were tested. There were no effects of any treatments on cell viability, RNA or protein content (see **Results, Section 6.3.1**).

6.2.2 Real-time qPCR

Total RNA was isolated from the cultured cells using TRIzol® (Invitrogen™ Life Technologies, Paisley, UK) according to the manufacturer's instructions. Following first strand cDNA synthesis (using a high-capacity cDNA reverse transcription kit, Applied Biosystems™ Cheshire, UK), expression levels of copper transport-related gene mRNA and 18S and GAPDH mRNA (used as housekeeping genes) were analysed by real-time PCR using an ABI Prism 7700HT Sequence Detection System and a Power SYBR® Green PCR master mix kit (Applied Biosystems™ Cheshire, UK). Primers were designed using the online design tool Primer3 (Rozen & Skaletsky, 2000) and sourced from MWG Eurofins (London, UK). Quantitative measurement of gene expression was derived from the $2^{(-\Delta\Delta Ct)}$ *method*, also known as the *Livak method* (Livak & Schmittgen, 2001; Schmittgen & Livak, 2008). Data were expressed as ratios to the control and normalised to the housekeeping genes 18S and GAPDH. The primer sequences used for each gene are in **Table 6.1**.

Table 6.1. Primer sequences for qRT-PCR gene expression analysis.

Gene symbol	Forward primer 5'-3'	Reverse primer 5'-3'
CTR1	GCC ACC CAT GAG ATG TCT TT	CCA TCA ATC CTG GCT GAA GT
HAH1	CAC AGC ATG GAC ACT CTG CT	AAG TCC CAG GTC TGT CTG GA
ATP7A	TCC TTC TTC CCG CCT TAA AT	GAA ATG CCG CTT CTG ACT TC
ATP7B	CCA CAT GAA GCC CCT GAC	GAC CAC TTG TCC CCA TCA TC
18S	AAC TTT CGA TGG TAG TCG CCG	CCT TGG ATG TGG TAG CCG TTT
GAPDH	CTG TTG CTG TAG CCA AAT TCG T	ACC CAC TCC TCC ACC TTT GA

CTR1: copper transporter 1; HAH1: human antioxidant protein homologue 1; ATP7A: copper transporting ATPase α polypeptide; ATP7B: copper transporting ATPase β-polypeptide; 18S: ribosomal RNA18S; GAPDH: glyceraldehyde 3-phosphate dehydrogenase.

6.2.3 Western blotting

Total protein from Caco-2 cells was prepared as described previously (Chaston et al., 2008). Total proteins (40 μg) were solubilised in sample loading buffer and subjected to SDS-PAGE. Following immobilisation on nitrocellulose, the proteins were exposed to anti-CTR1 or anti-ATP7A antibodies (1:1000 dilution, Source Bioscience, Nottingham, UK). Blotted membranes were visualised using a horseradish peroxidase-linked secondary antibody and Novex® ECL chemiluminescent substrate reagent kit (Invitrogen™ Life Technologies, Paisley UK). Band densities were quantified using a densitometer (GS-800™) and Quantity One software (Bio-Rad Laboratories, Hertfordshire, UK). Actin protein levels were also measured (anti-actin antibody, 1:2000 dilution, Sigma-Aldrich). Protein density data were expressed normalised to actin as the housekeeping protein. For antibody concentrations and reagents see **Section 2.2.4. Protein abundance analysis**.

6.2.4 Copper uptake assays

This section contains a brief description (for further details see **Section 2.2.5 Functional uptake and transport experiments**) Uptake was carried out in MBSS, both in the presence and absence of 100 μM ascorbate as a reducing agent. Caco-2 cells, grown in T-25 flasks to allow for a higher cell density, were treated with berry extract acutely or chronically. For the acute studies, Caco-2 cells were pre-equilibrated with berry extract for 15 min and 10 μM copper chloride was added to initiate uptake. In the chronic studies, cells were exposed to berry extract for 16 h. At the end of this incubation period the treatment solutions were removed and the cells were washed in uptake buffer. Fresh berry extract-free MBSS uptake buffer containing 10 μM copper chloride was added to initiate uptake.

Copper uptake was terminated after 120 min by washing cells in ice cold PBS. Cells were harvested in 2 ml PBS, dissolved in 3 ml 1M nitric acid and 5 ml 68-70% nitric acid. Cell lysate was further digested at 90°C for 90 min and the remaining cell debris was removed by centrifugation at 5000 rpm for 10 min. These samples were run through inductively coupled plasma optical emission spectroscopy (ICP-OES; iCAP 6000 series; Thermo Scientific, UK) for mineral analysis. A multi element standard (Merck, Germany, Cat No. 11335), containing 1006±10 mg/L copper, was used to construct a calibration curve. The optimum specific wavelength for measurement of copper concentrations was 324.754 nm. Data were normalised to amounts of total protein, quantified using the protein quantification kit-rapid (Fluka, from Sigma-Aldrich). Data were expressed as total copper uptake per 120 minutes.

6.2.5 Data and statistical analysis

Data are expressed as means $\pm$ SEM. Statistical analysis was carried out using GraphPad Prism 5 (San Diego, CA, USA). In studies containing 2 experimental groups Student's unpaired t-test was used to compare means. Differences between multiple groups were calculated using a 1-way ANOVA with Dunnett's post-hoc test. In all instances significance was indicated when $p \leq 0.05$.

6.3 Results

6.3.1 Effects of berry extract on cell viability, RNA and protein content

The effects of treatments on cell viability, RNA content and protein content were tested to ensure effects of berry extract were not due to pathological changes, but as normative responses. There was no effect of berry extract on cell viability (**Figure 6.1**), RNA content (**Figure 6.2**), or protein content (**Figure 6.3**).

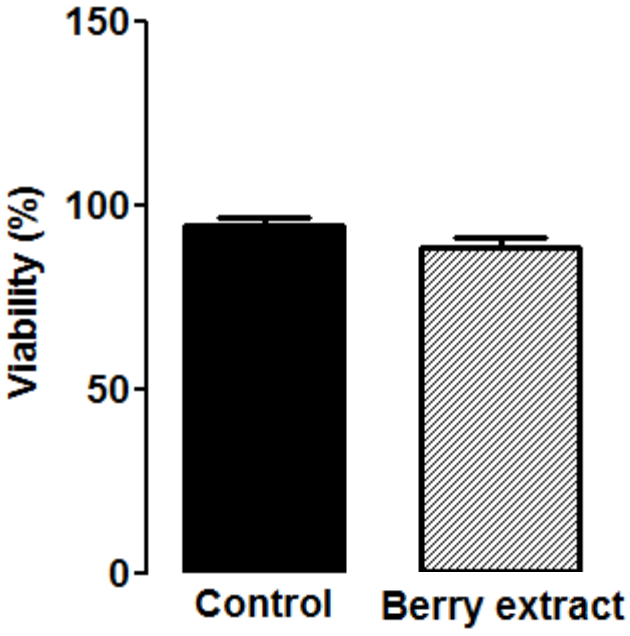

Figure 6.1. Caco-2 cell viability after berry extract treatment. Caco-2 cells were treated with berry extract at 0.125 % (w/v) for 16 h. Cell viability was quantified with the trypan blue dye-exclusion method. Data is presented as mean percentage viable cells ± SEM, *n* = 6. Student's t-test showed there was no significant difference between groups.

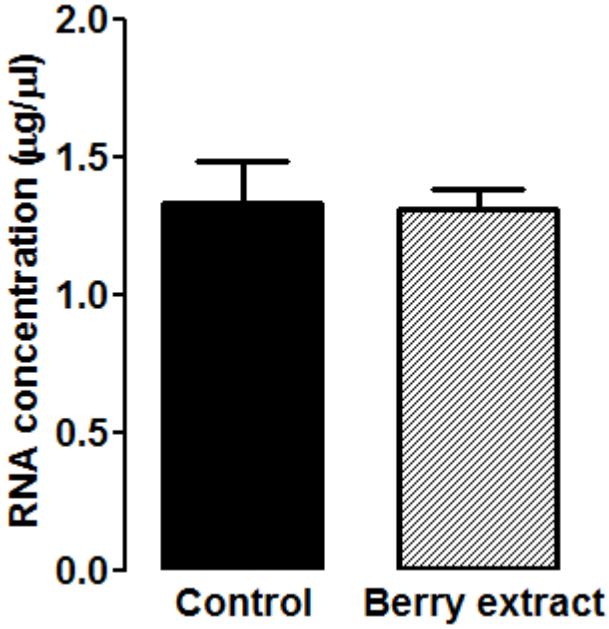

Figure 6.2. RNA concentration from Caco-2 cells after berry extract treatment. Caco-2 cells were treated with berry extract at 0.125 % (w/v) for 16 h. RNA concentration in the extracts of Caco-2 cells was quantified with the NanoDrop spectrophotometer. Data is presented as mean RNA concentration ± SEM, *n* = 6. Student's t-test showed there was no significant difference between groups.

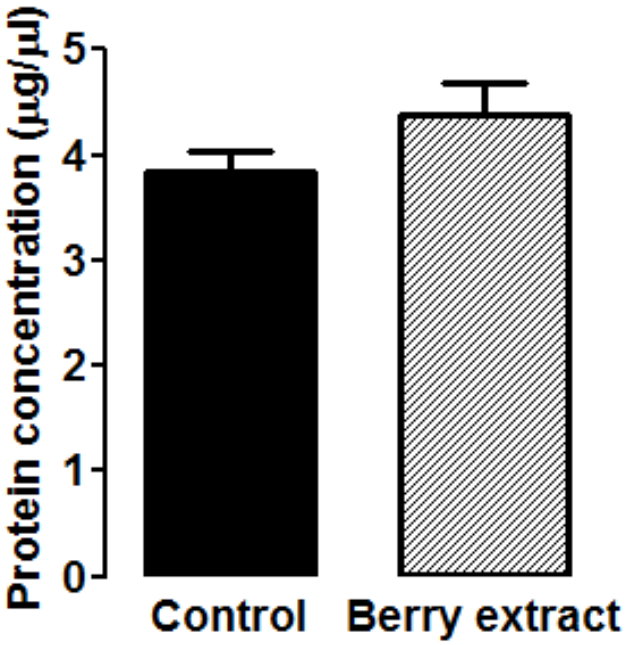

Figure 6.3. Protein concentration from Caco-2 cells after berry extract treatment. Caco-2 cells were treated with berry extract at a concentration of 0.125 % (w/v) for 16 h. Protein concentration was quantified by a Bradford spectrophotometric assay. Data is presented as mean protein concentration ± SEM; *n* = 6. Student's t-test showed there was no significant difference between groups.

6.3.2 Effects of berry extract on copper-transport related gene expression

Expression of CTR1 and ATP7A, the main genes involved in apical influx and basolateral efflux of copper, respectively, was quantified across a number of concentrations of the berry extract and across different treatment durations. CTR1 expression decreased with increasing concentration; a significant decrease in expression started at 0.031 % (w/v) ($p < 0.05$) and continued to decrease until the highest concentration 0.25 % (w/v) ($p < 0.001$; **Figure 6.4**, **panel A**). ATP7A expression decreased at 0.125% (w/v) and continued to decrease at a higher concentration ($p < 0.01$; **Figure 6.4**, **panel B**).

As for the time-dependent effects, CTR1 had an initial increase in expression at 4 h ($p < 0.001$) and decrease in expression at 16 h ($p < 0.05$; **Figure 6.5**, **panel A**). ATP7A, decreased at the 16 h time point ($p < 0.05$; **Figure 6.5**, **panel B**).

When treated with the berry extract for 16 h at a concentration of 0.125% (w/v) the expression of all the genes tested was significantly decreased (**Figure 6.6**). These were CTR1 ($p < 0.01$; **panel A**), HAH1 ($p < 0.05$; **panel B**), ATP7A ($p < 0.05$; **panel C**) and ATP7B ($p < 0.01$; **panel D**).

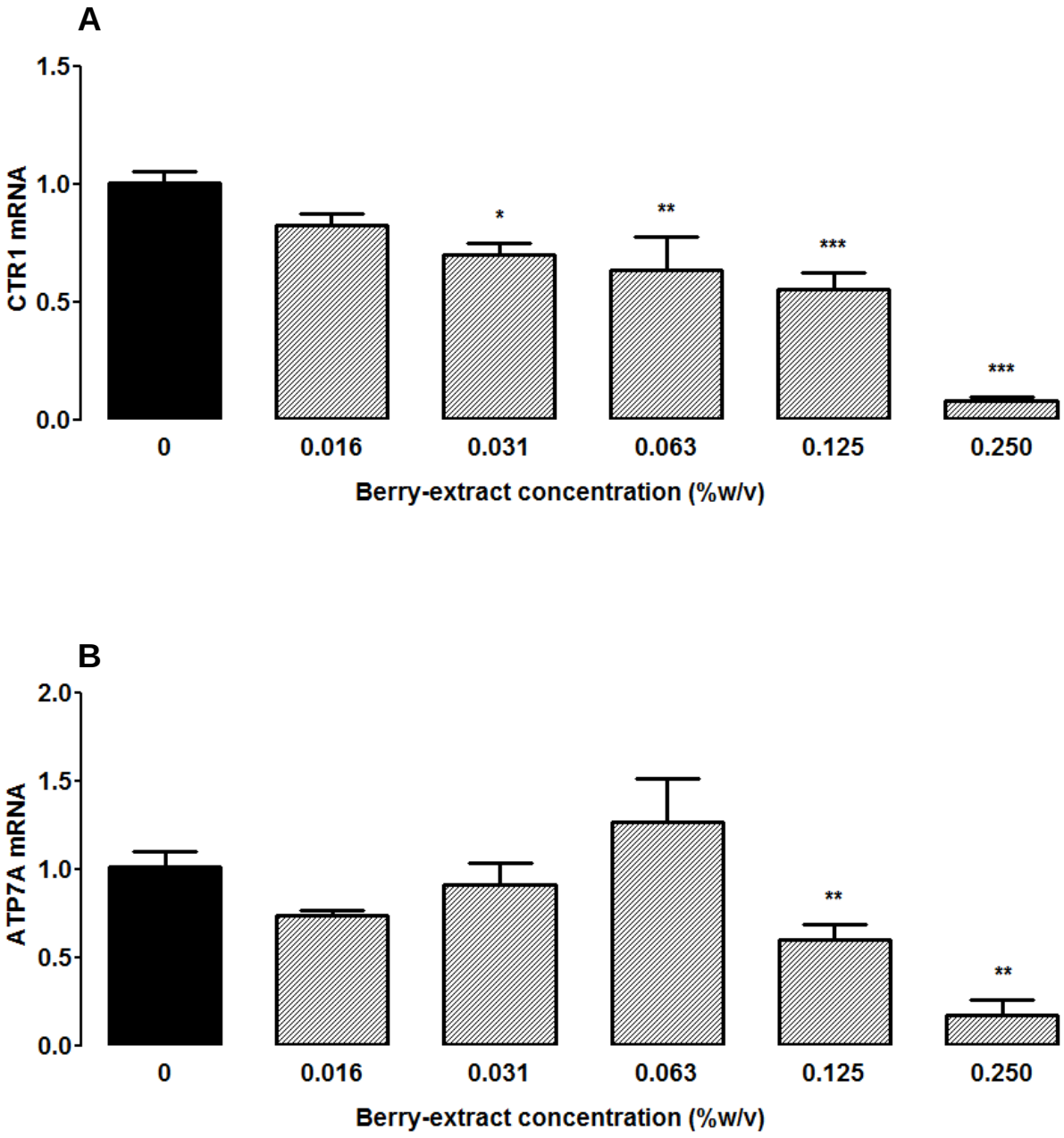

Figure 6.4. Dose-dependent effects of berry extract on CTR1 and ATP7A mRNA expression. Caco-2 cells were treated with a berry extract at different doses from 0.25 % (w/v) in 2-fold dilutions until 0.016 % (w/v). CTR11 (A) and ATP7A (B) mRNA were quantified by qRT-PCR and normalised against 18S and GAPDH as housekeeping genes. Data are presented as mean normalised expression ratio ± SEM, n = 6, statistical significance was determined by an ANOVA and Dunnet's post-hoc test against the 0 % (w/v) concentration. (*) $p \leq 0.05$, (**) $p \leq 0.01$, (***) $p \leq 0.001$. CTR1: copper transporter 1. ATP7A: copper transporting ATPase α-polypeptide. 18S: ribosomal RNA 18S. GAPDH: glyceraldehyde 3-phosphate dehydrogenase. qRT-PCR: quantitative real-time polymerase chain reaction.

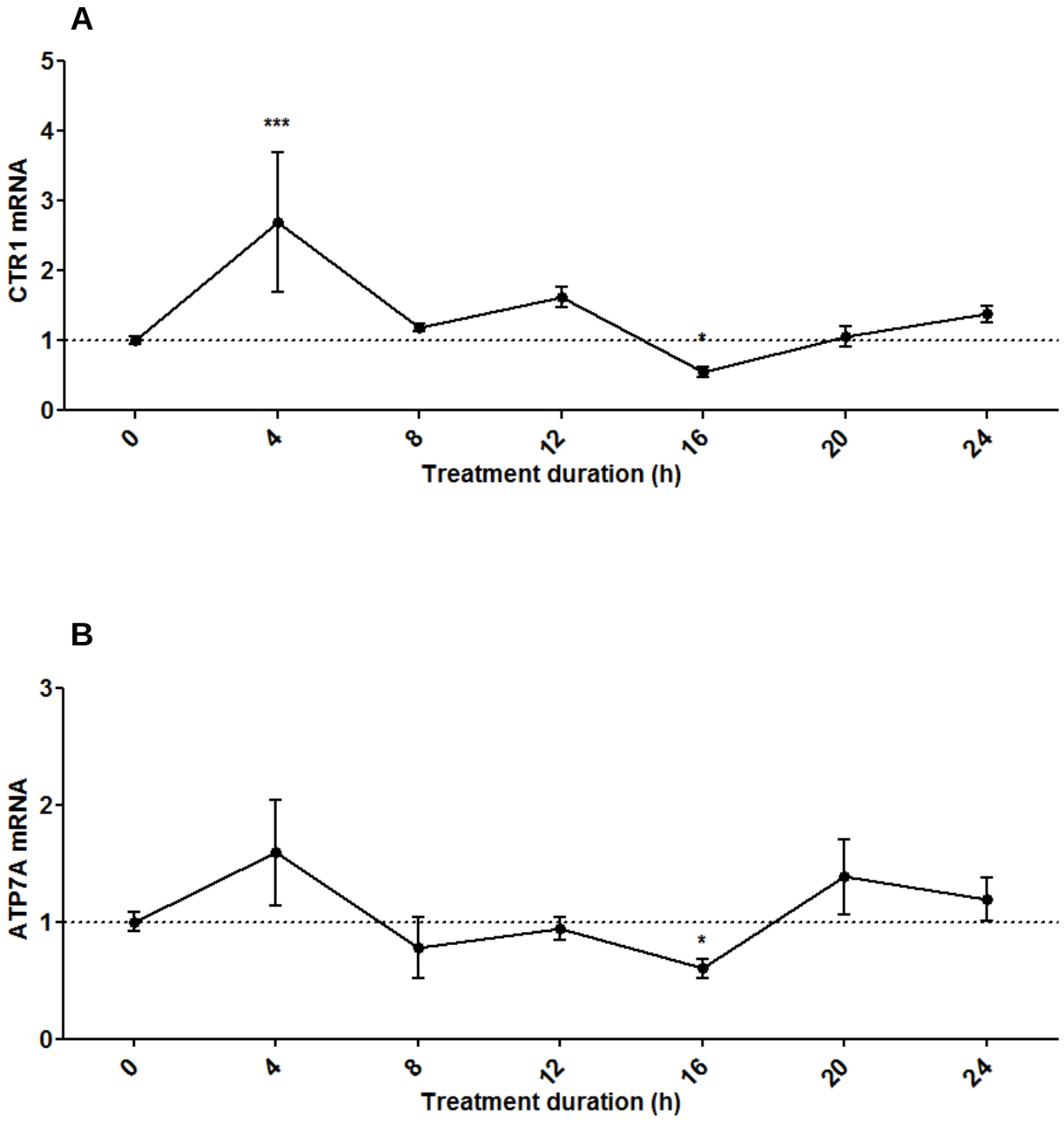

Figure 6.5. Time-dependent effects of berry extract on CTR1 and ATP7A mRNA expression. Caco-2 cells were treated with berry extract at 0.125 % (w/v) from 4 h to 24 h. Levels of CTR1 (A) and ATP7A (B) mRNA were quantified by qRT-PCR and normalised against 18S and GAPDH as housekeeping genes. Values are mean normalised expression ratio ± SEM, n = 6. Statistical significance was determined by an ANOVA and Dunnet's post-hoc test against the 0 h time-point. (*) $p \leq 0.05$. CTR1 expression had a significant linear trend (*) $p \leq 0.05$. CTR1: copper transporter 1. ATP7A: copper transporting ATPase α-polypeptide. 18S: ribosomal RNA 18S. GAPDH: glyceraldehyde 3-phosphate dehydrogenase. qRT-PCR: quantitative real-time polymerase chain reaction.

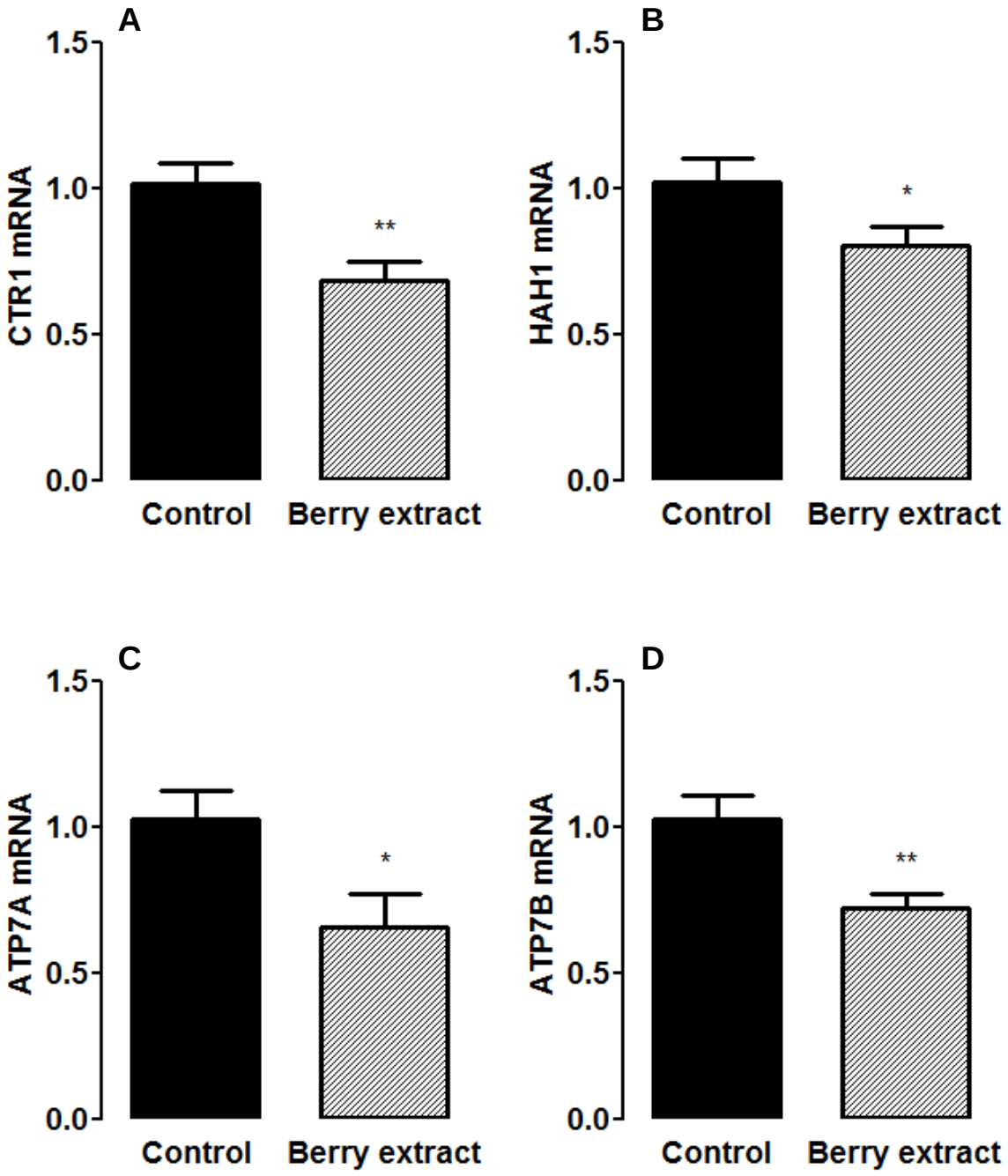

Figure 6.6. Effect of berry extract on mRNA expression of copper transport-related genes Caco-2 cells were treated with 0.125 % (w/v) of berry extract for 16 h. Levels of CTR1 (A), HAH1 (B), ATP7A (C) and ATP7B (D) were quantified and normalised to 18S and GAPDH as housekeeping genes. mRNA data are presented as the mean (relative to the control) ± SEM, n = 6, (*) $p \leq 0.05$, (**) $p \leq 0.01$. To determine significance an unpaired t-test was used against the control group. CTR1: Copper transporter 1. HAH1: human antioxidant homolog 1. ATP7A: copper transporting ATPase α-polypeptide. ATP7B: copper transporting ATPase β-polypeptide. 18S: ribosomal RNA 18S. GAPDH: glyceraldehyde 3-phosphate dehydrogenase. qRT-PCR: quantitative real-time polymerase chain reaction.

6.3.3 Effects of berry extract on CTR1 and ATP7A protein expression

The effects of the berry extract on those proteins that are important for apical uptake (CTR1) and basolateral release (ATP7A) of copper was quantified. There was no significant effect on the abundance of either protein following 16 h treatment with the berry extract (**Figure 6.7**).

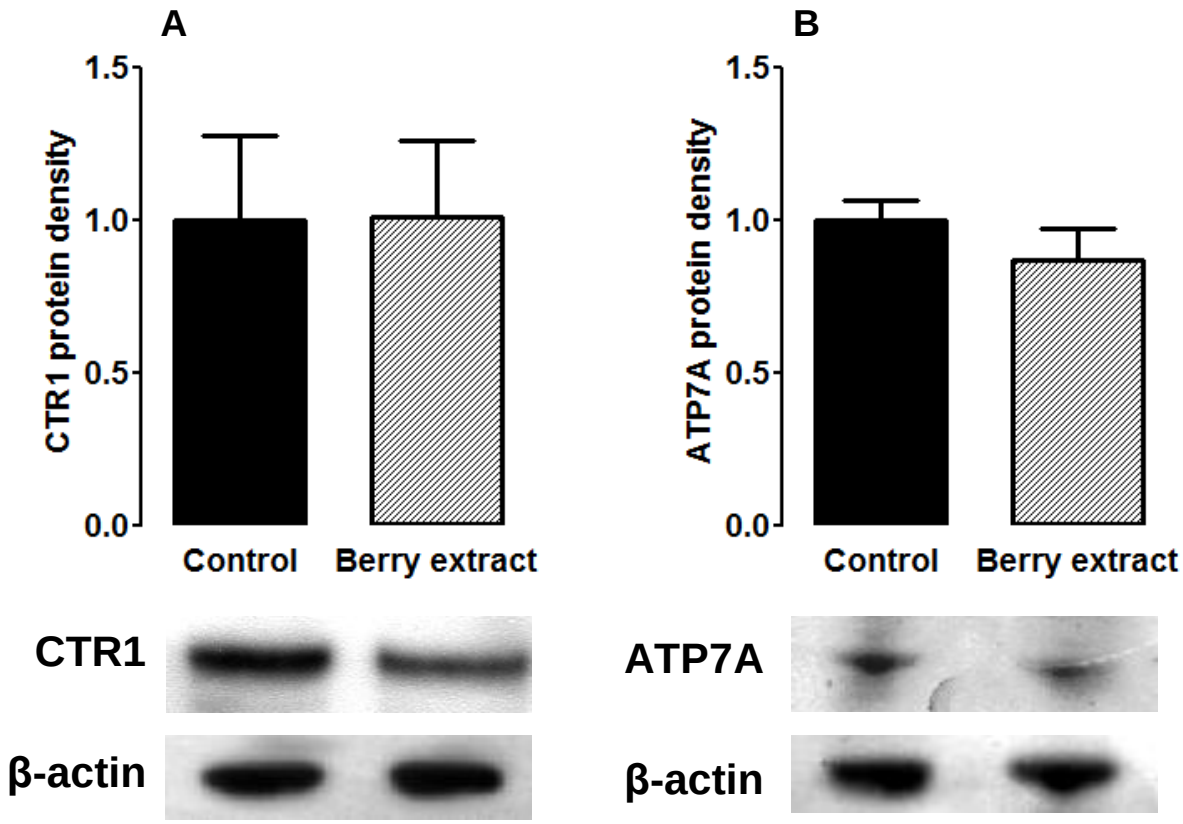

Figure 6.7. Effect of berry extract on CTR1 and ATP7A protein expression. Total protein was prepared from Caco-2 cells treated with 0.125 % (w/v) berry extract for 16 h. Levels of CTR1 or ATP7A protein were normalised to β-actin as a housekeeping protein. Representative blots for CTR1 (A) and β-actin are shown in the lower left panel, with semiquantitative densitometry data in the upper left panel. Representative blots for ATP7A (B) and β-actin are shown in the lower right panel, with semiquantitative densitometry data in the upper right panel. Expression levels of the housekeeper protein β-actin were not altered by berry extract treatment. Densitometry data are presented as the mean (relative to the control) ± SEM, $n = 4$ (*) $p \leq 0.05$. Student's t-test showed there was no significant difference between groups. CTR1: copper transporter 1. ATP7A: copper transporting ATPase α-polypeptide.

6.3.4 Effects of berry extract on copper uptake

The functional effects of berry extract on intestinal copper uptake were measured both in the presence and absence of ascorbate. We therefore investigated whether berry extract, at a final concentration of 0.125 % (w/v), can acutely (following 15 min exposure) or chronically (following a 16 h exposure) influence copper uptake.

Only in the presence of ascorbate (higher reducing capacity, i.e. transport of cuprous copper) was the increase rate of copper uptake significant under both acute treatments ($p < 0.01$; **Figure 6.8**, **panel A**) and chronic treatments ($p < 0.001$; **Figure 6.9**, **panel A**) with the berry extract.

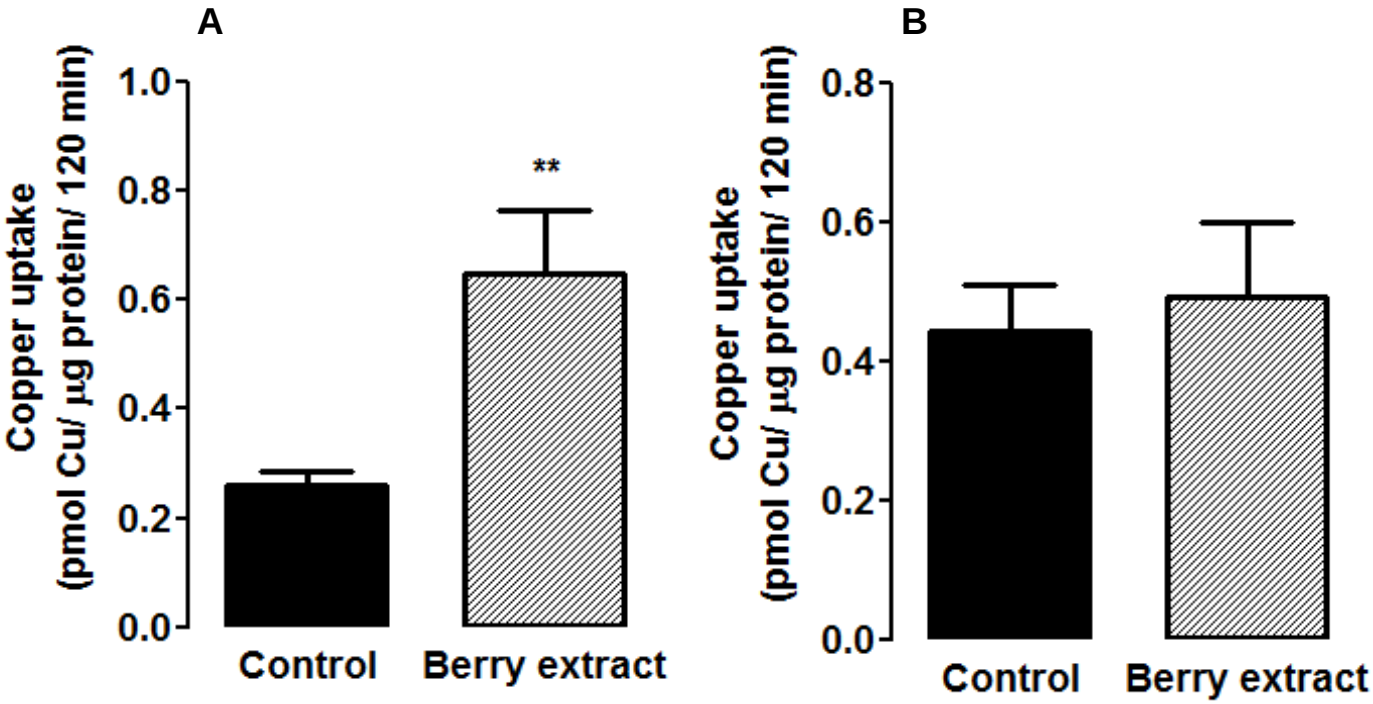

Figure 6.8. Acute effects of berry extract and ascorbate on copper uptake. Caco-2 cells were treated acutely, for 15 min, with 0.125 % (w/v) berry extract and subjected to copper uptake in the presence (A) or absence (B) of ascorbate as a reducing agent. Data are presented as the mean ± SEM, $n = 6$. Unpaired t-test was used to determine significance against the control (**) $p \leq 0.01$.

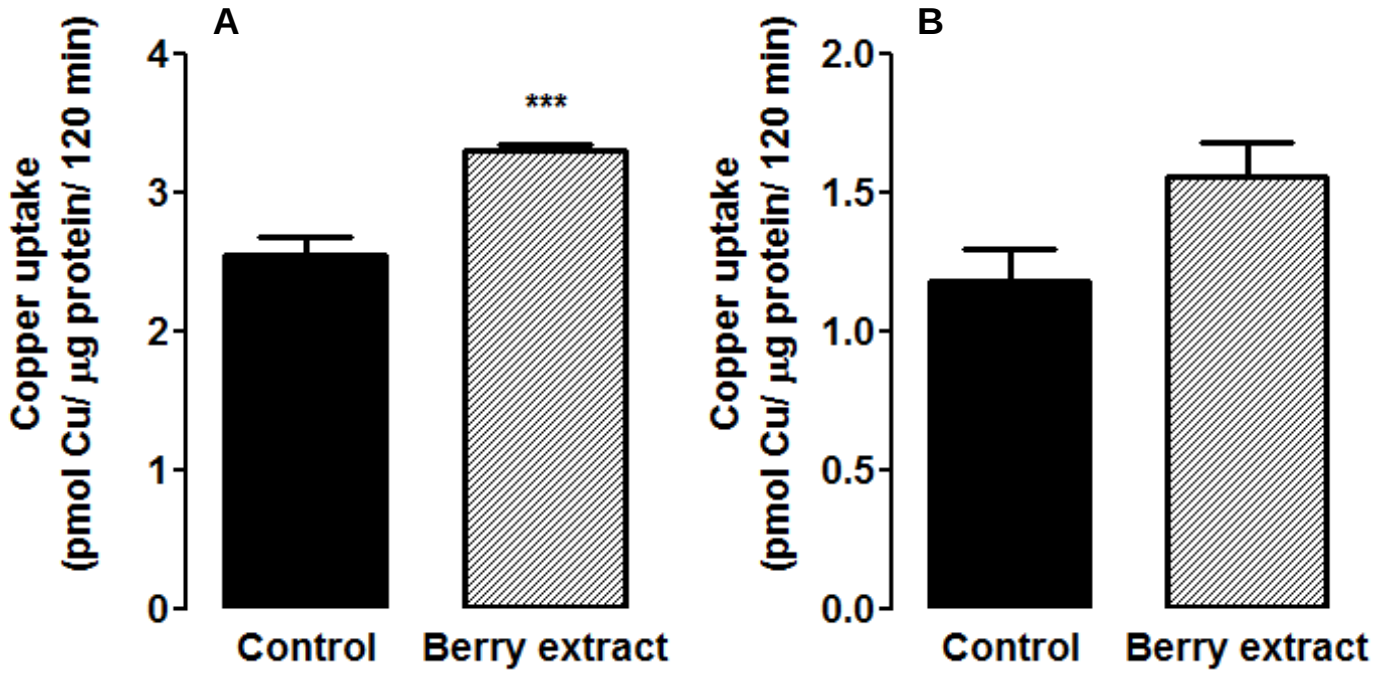

Figure 6.9. Chronic effects of berry extract and ascorbate on copper uptake. Caco-2 cells were treated chronically, for 16 h, with 0.125 % (w/v) berry extract and subjected to copper uptake in the presence (A) or absence (B) of ascorbate as a reducing agent. Data are presented as the mean ± SEM, $n = 6$. Unpaired t-test was used to determine significance against the control (***) $p \leq 0.001$.

6.4 Discussion

The intestinal absorption of dietary copper is coordinated by a number of genes and proteins mediating apical uptake (i.e. CTR1), intracellular binding (i.e. HAH1) and the distribution and basolateral efflux of copper (i.e. ATP7A and ATP7B). The intestine is the main site responsible for maintaining copper balance, and the absorption of copper is greatly influenced by the presence of other dietary constituents. In this regard, dietary flavonoids and ascorbate have been demonstrated to influence the absorption of copper as well as other dietary metals (Kim *et al*, 2008; Lekka *et al*, 2009). Although the structural interactions between flavonoids and copper have been characterised, the functional, transcriptional and translational implications remain unknown.

To address this we investigated the effects of a flavonoid-rich berry extract on the expression of genes and proteins related to copper uptake in Caco-2 cells. Further to this we investigated the chronic and acute effects of berry extract on copper absorption. We found decreased abundance of CTR1, HAH1, ATP7A and ATP7B mRNA following chronic berry extract treatment. There was no concomitant effect on the abundance of either CTR1 or ATP7A proteins. In functional experiments, the berry extract enhanced the uptake of copper with both chronic and acute treatments, albeit only in the presence of ascorbate.

6.4.1 Regulating copper transport-related gene and protein expression

The intestinal absorption of copper is tightly regulated. It has been demonstrated that prolonged exposure to high copper causes accumulation in enterocytes, whilst maintaining plasma copper status (Arredondo *et al*, 2000; Bauerly *et al*, 2004). Furthermore, the responses of enterocytes to low and high copper are presumed to be different, i.e. different genes, proteins or mechanisms (Arredondo *et al*, 2000).

Expression of the genes that mediate enterocytic copper metabolism is regulated by iron or other factors, but not by the presence of their substrate, copper. Instead, post-translational mechanisms are in place to respond to local copper balance. Degradation and trafficking of copper transport-related proteins between intracellular and membrane compartments is the main response to copper load (Bauerly *et al*, 2004; Nyasae *et al*, 2007; Weiss *et al*, 2008). In light of this, the effects of our flavonoid treatment on gene expression cannot be attributed to copper content *per se* (as is the case with other dietary metals such as iron). Rather, flavonoids may interact with other mechanisms or regulatory pathways that indirectly influence the expression of these genes.

6.4.2 Effects of berry extract on gene and protein expression

6.4.2.1 Berry extract and CTR1 expression

Following berry extract treatment, we found a decrease in CTR1 mRNA expression, but no effect on CTR1 protein. CTR1 is the primary importer of copper into enterocytes. Although mammalian CTR1 mRNA responds to copper status during early development, this responsiveness is lost in adulthood and thus CTR1 mRNA expression becomes independent of its substrate (Lee *et al*, 2000; Lee *et al*, 2001; Sharp, 2003; Bauerly *et al*, 2005). In Caco-2 cells there is a copper-dependent relocalisation and degradation of the CTR1 protein, but no effect on mRNA, following copper loading (Bauerly *et al*, 2004; Nose *et al*, 2010).

Miyayama *et al* (2011) reported that CTR1 mRNA expression decreases in response to silencing or knockout of copper chaperones. Despite previous reports, this effect on CTR1 gene expression was attributed to excess copper. Presumably any copper-related effects on CTR1 mRNA expression would, in that case, be related to *unbound* copper, chaperone abundance or chaperone properties (Miyayama *et al*,

2011). Furthermore, in drosophila, the induction of CTR1 by copper starvation is a normal transcriptional response. However, a recent study has found that in HAH-knockouts, CTR1 expression is not induced (Hua *et al*, 2011). In light of the aforementioned studies, the decrease in CTR1 mRNA we observed may be induced by the concomitant decrease in HAH1 expression. Alternatively, it may be a response to high intracellular copper, chelated to flavonoids, rather than to the typical chaperone molecules.

6.4.2.2 Berry extract and HAH1 expression

HAH1 delivers copper to ATP7A and ATP7B and maintains copper cellular distribution in enterocytes and hepatocytes (Larin *et al*, 1999; Strausak *et al*, 2003; McRae *et al*, 2010). In our study, there was a decrease in mRNA expression of HAH1 following treatment with the berry extract.

Little is known regarding the regulation of mammalian HAH1 mRNA. *In-vivo* expression profiles of HAH1 are highest in tissues with high metal content. This indicates the importance of metal binding and maintaining functionality of metalloenzymes (Naeve *et al*, 1999). In light of this, copper chaperone expression is likely to be in accordance with the need for copper binding or distribution. Expression of copper chaperones is also known to increase when another copper chaperone has been silenced or knocked down (Miyayama *et al*, 2011).

With regards to our findings, the decreased expression of HAH1 indicates either: 1) decreased requirement for copper binding as it may be bound to flavonoids; or 2) the regulation of HAH1 mRNA may be concordant with the expression of the target proteins for copper delivery, i.e. ATP7A and ATP7B.

6.4.2.3 Berry extract and ATP7B expression

The role of intestinally expressed ATP7B has not been fully characterised, though it is assumed to be involved in copper efflux, enzyme metallation and copper sequestration (Terada *et al*, 1999; Weiss *et al*, 2008). The copper-dependent regulation of ATP7B is through post-translational mechanisms, e.g. high copper induces ATP7B translocation to dispersed vesicles (Weiss *et al*, 2008).

The transcriptional regulation of ATP7B is independent of copper status. However, transcriptome variation studies have shown that ATP7B mRNA expression decreases with iron loading (Bédrine-Ferran *et al*, 2004). Therefore, from the expression profile seen in our study, we can speculate that there may be an increase in intracellular iron in response to berry extract. Indeed, this is supported by our findings in **Chapter 5**.

6.4.2.4 Berry extract and ATP7A expression

ATP7A is involved in the efflux of copper and in enzyme metallation (Petris & Mercer, 1999). This protein is also known to be post-translationally regulated by copper (Petris *et al*¸ 1996). In Caco-2 cells, copper loading decreases ATP7A activity, without affecting mRNA or total protein levels (Bauerly *et al*, 2004). This decrease in enterocytic efflux is a protective mechanism, as copper accumulation at the epithelium prevents high plasma levels and accumulation in other organs.

Intestinal ATP7A expression responds to systemic signals, e.g. mice with cardiac specific CTR1-knockout have increased intestinal ATP7A activity, leading to elevated serum copper levels and decreased hepatic copper stores (Kim *et al*, 2010). Furthermore, the silencing or knockout of copper chaperones induces the expression of ATP7A, promoting copper efflux to maintain cellular homeostasis (Miyayama *et al*, 2011). In light of this, ATP7A expression may coincide with copper chaperone

properties; this is similar to CTR1. ATP7A is expressed in at least three splice variants that are strongly induced in rat enterocytes in response to iron deprivation (Collins *et al*, 2009). This supposes that high iron will reduce ATP7A expression. Indeed this was observed, i.e. increased iron (in **Chapter 5**) and reduced ATP7A (this section).

6.4.3 Effects of berry extract on functional copper uptake

Chronic and acute berry extract treatment both increased copper uptake, albeit only in the presence of ascorbate. Ascorbate, as a reducing agent, allows more cuprous copper to be available. Cuprous copper is transported exclusively by CTR1. This indicates that the enhancing effects of berry flavonoids on copper uptake are mediated via CTR1 alone. Alternatively, a separate transport route may be recruited.

Furthermore, flavonoids are effective metal chelators (Ren *et al*, 2008; Lekka *et al*, 2009). Chelators, such as triethylenetetramine, are often applied in research to deprive cells of copper (Zerounian *et al*, 2003). Following treatment with chelators copper uptake is typically increased. Therefore, the higher rate of copper uptake in the chronic berry extract study may have simply been a consequence of prior copper deprivation. Following the chronic treatments, there is also a markedly higher rate of copper uptake relative to the acutely treated cells, which would not have had chelators present beforehand (i.e. 1.5-3.0 pmol Cu/ µg protein/ 120 min following chronic treatment and ~0.5 pmol Cu/ µg protein/ 120 min following acute treatment).

In light of the above, the increase in copper uptake during acute and chronic treatments may be mediated via separate mechanisms. The mechanism from chronic studies may have been due to chelation-mediated copper depletion. In contrast, the increased uptake from acute studies is more likely due to redox or structural interactions which increase availability of transportable copper.

6.5 Conclusions

We have investigated the effects of dietary berry flavonoids on the expression and function of the copper uptake pathway in enterocytes. We found that a flavonoid-rich berry extract decreases expression of the genes that modulate copper transport, with a concomitant increase in copper uptake in the presence of ascorbate. This indicates increased CTR1 activity. Our findings contribute to the knowledgebase regarding nutrient interactions and will aid in optimising dietary management in conditions of copper or iron imbalance. The metabolism of iron is dependent on maintaining adequate copper levels. If copper status varies, iron status will vary and *vice versa* in a two-way process.

6.6 Future work

Flavonoids, in the presence of additional reducing capacity in the form of ascorbate, significantly increase copper uptake. Given that the transcriptional regulation of copper transport-related genes has not been fully elucidated, our findings raised numerous points for future investigation, mainly related to the functional implications of flavonoid treatments. These are discussed in the following section, for a summary of the flavonoid effects and the areas for future work see **Figure 6.10**.

6.6.1 Enhancement of copper uptake

During both acute and chronic treatments there was an increased uptake of copper into Caco-2 monolayers; the mechanism for this increased uptake is unknown. The leading hypotheses regarding these changes are an enhanced reducing capacity or the formation of polyphenol complexes that will be transported by other means.

Flavonoids and ascorbate are known to be powerful reductants; as well as providing substrates for apical reductase activity (Vlachodimitropoulo *et al*, 2010a). Furthermore, the complexation of copper to flavonoids has previously been demonstrated (Lekka *et al*, 2009). Polyphenol-metal complexes that contain iron are thought to flux via GLUT-type transporters, or possibly through other flavonoid influx routes (Vlachodimitropoulo *et al*, 2010b). The formation of polyphenol-metal chelates has been shown to increase iron uptake as well as ascorbate being a well known enhancer of iron uptake. Thus the increase in copper uptake may be attributed to a similar synergy between increased reducing capacity and the availability of more transportable substrates, in the form of chelates.

To address the above hypotheses regarding copper absorption a series of studies can be carried out to elucidate the contributing transporter proteins. The current candidate transporters that will contribute to the copper influx by CTR1 are DMT1

or GLUT2. Targeted deletion of DMT1 by siRNA and inhibition of GLUT2 by phloretin will allow us to determine if CTR1 is the only contributing protein to the increased influx of copper. Furthermore, localising each of these proteins to the apical membrane will confirm their correct location for influx.

6.6.2 Effects on copper efflux

In these experiments we could not assess the effects of flavonoids on the second component of absorption, that being basolateral efflux. This can be easily quantified by applying a Transwell® system, as in **Chapter 5**, using radiolabelled copper-64. This will allow us to quantify effects on basolateral transfer of copper, and therefore also the function of ATP7A. Specific deletion of ATP7A by siRNA will allow us to elucidate if another efflux route for copper is recruited in this process.

6.6.3 Effects of flavonoids on chaperones and gene expression

Given that copper may be bound by flavonoids, either extracellularly and imported, or may be bound intracellularly after apical influx, the question remains whether these forms of chelated copper are metabolically accessible to classical copper chaperones or if they have a separate metabolic route. This can be elucidated by Western blot protein analysis of specific forms of the copper chaperone proteins; i.e. the apo-proteins versus the holo-proteins.

Previous research has found that flavonoids will inhibit the degradation of HIFs by binding to iron, preventing the correct function of prolyl hydroxylase. In which case, HIFs will accumulate intracellularly. ATP7A and CTR1 have been shown to be induced by HIF-2α, and knockout or silencing of HIF-2α results in decreased expression of these genes (Xie & Collins, 2011; Pourvali *et al*, 2012).

In light of the above, the expression effects of flavonoids may be largely due to their effects on the hypoxia response pathway. Quantifying expression of HIFs and the metabolic availability of copper bound to flavonoids will give a better understanding to the downstream events that coordinate copper transport.

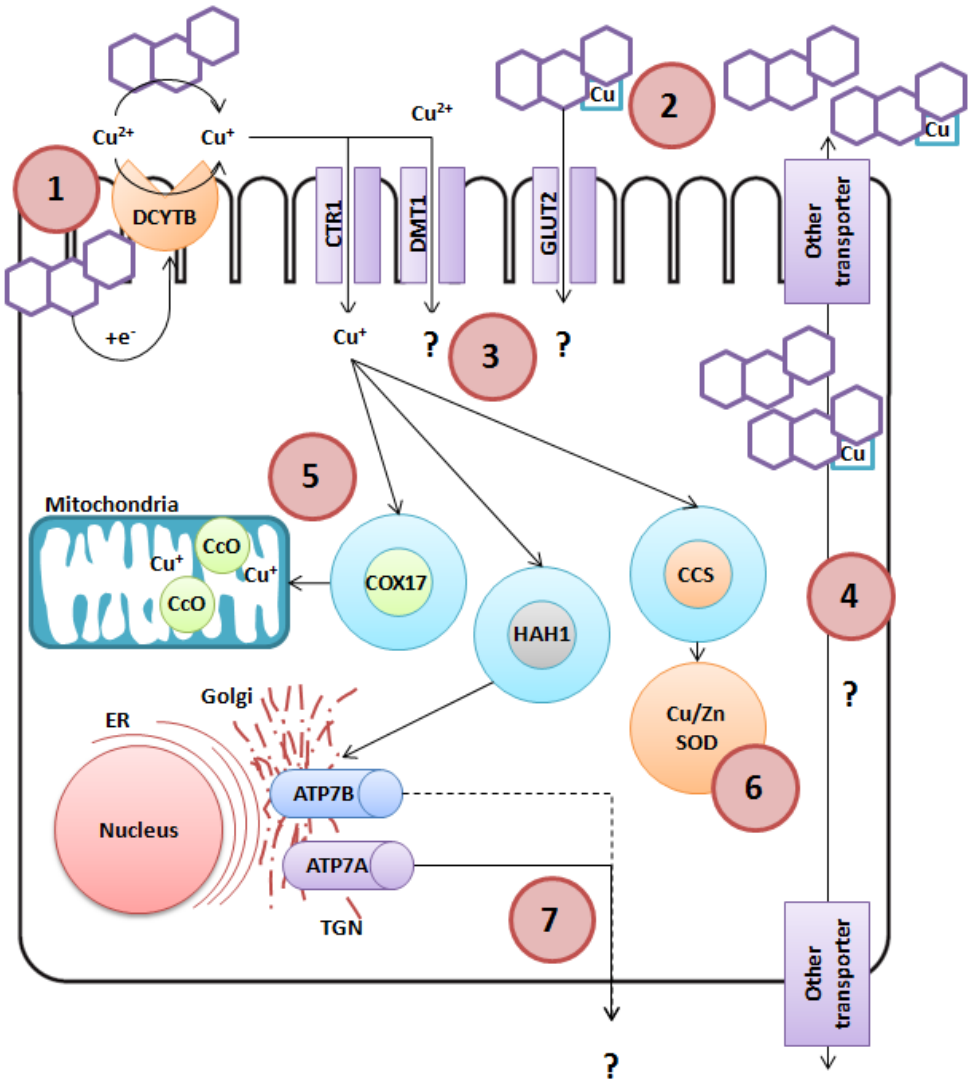

Figure 6.10.Model of effects of flavonoids on copper uptake. 1) Higher copper uptake may have been due to increased reducing capacity by flavonoids, reducing copper extracellularly or providing more substrate for apical reductase activity. **2)** An alternative source of copper influx may be the uptake of copper-flavonoid complexes via GLUT-type transporter or other routes. **3)** The destination of copper imported via DMT1, GLUT or other transporters (aside from CTR1) is unknown; this source of copper may not be metabolically accessible. Copper that is imported via CTR1 will bind to a chaperone molecule (COX17, HAH1 or CCS), each with a specific destination **4)** Flavonoids may also act as extracellular copper chelators, "leaching" copper from cellular compartments or providing an intra- to extracellular copper shuttle. **5)** The effects of flavonoids on COX17 and on CcO expression are unknown. **6)** The effects of flavonoids on CCS and on Cu/Zn-SOD expression are unknown. **7)** Although we have quantified the expression of ATP7A and ATP7B, the effects that flavonoids will have on their function remains to be elucidated.

CHAPTER SEVEN

Summary of the thesis

7 Summary of the thesis and general discussion

We investigated the effects of dietary berry flavonoids on the human intestinal Caco-2 cells. Initially we carried out a microarray study where several pathways related to nutrient transport were identified to have been altered. These pathways pertained to the transport of glucose, iron and copper. From the aforementioned study, work was focused to identify the processes whereby berry flavonoids modulate nutrient transport. For brevity, only the most significant findings are discussed in this section.

7.1 Transcriptomic effects of berry extract on Caco-2 enterocytes

The initial investigation of the Caco-2 cell transcriptome following berry extract treatment revealed differential expression of 2557 genes. Of these, 761 genes had increased expression whereas 1796 decreased. Pathway analysis identified a large number of pathways that were significantly affected. These included pathways related to the *cell cycle*, *gene expression*, *molecular transport* and *small molecule biochemistry*. GO analysis revealed clusters relating to *metal ion transport* and *carbohydrate metabolism*, as well as several others such as *ATPase activity* and *brush border cellular components*.

Following traditionally applied pathway analysis and GO clustering, we carried out functional similarity clustering with DMT1 as the bait gene, a *bait* gene forms the basis around which other genes are clustered for similar function (for details of informatics approaches with the gene expression array see **Section 9.3 Bioinformatics analysis**). There were 27 other genes functionally related to DMT1, including those pertaining to glucose (GLUT2), iron (HFE) and copper (ATP7B) transport. We then investigated the expression and function of each pathway involved in the transport of the aforementioned nutrients.

7.2 Effects of flavonoids on intestinal glucose uptake

In **Chapter 4** we addressed the hypothesis that dietary flavonoids influence glucose uptake processes in human intestine epithelial cells. This was investigated by treating Caco-2 cells with a flavonoid-rich berry extract, or with the synthetic flavonoids quercetin, phloretin or phloridzin.

Treatment of Caco-2 cells with either the berry extract or with quercetin decreased mRNA expression of both GLUT2 and SGLT1, the main enterocyte glucose transporters. With concomitant decrease in abundance of the GLUT2 following berry extract treatment. Further to this, we investigated the functional effects of flavonoid treatments, both chronically and acutely, using radiolabelled glucose. Chronic treatments were used to characterise the transcriptional and translational effects on function of GLUT2 and SGLT1. Acute treatments were used to characterise the interactive or competitive effects of flavonoids, i.e. co-incubation of flavonoids and glucose. Chronic treatment did not induce an inhibitory effect on glucose uptake. However, acute treatment with the berry extract and quercetin decreased glucose uptake mediated by GLUT2 and by SGLT1. The acute inhibitory effects of phloretin and phloridzin confirmed the presence and function of both glucose transporters in this cell line. As phloretin and phloridzin are specific inhibitors of GLUT2 and SGLT1 mediated uptake, respectively.

Our findings indicated that, in line with previous research, there is an acute inhibitory effect of flavonoids on glucose uptake and that flavonols (i.e. quercetin) are particularly potent inhibitors (Park, 1999; Kwon *et al*, 2007). Furthermore, although chronic flavonoid treatment inhibited the expression of glucose transporters, their function was not affected. Put simply, this suggests that the

molecular events that occurred from chronic flavonoid treatments are not rate-limiting factors for glucose uptake.

It seems that flavonoids must be present to cause an inhibitory effect on glucose uptake, as we have noted in our acute experiments. Therefore, the effects we observed on gene and protein expression are more likely to be a consequence of the acute inhibition of glucose uptake. Further research is required to characterise the effects of flavonoids on protein trafficking or downstream events such as activation of carbohydrate response elements.

7.3 Effects of berry extract on intestinal iron transport

In **Chapter 5** we addressed the hypothesis that dietary berry flavonoids influence intestinal iron transport processes in Caco-2 cells. Following treatment with the berry extract there was decreased expression of DMT1, DCYTB and HFE, and a concomitant increase in TfR1 expression. These genes coordinate and regulate the apical uptake of iron. The gene expression profile indicated high intracellular iron content.

We then investigated the acute and chronic effects of berry extract on iron transport. Acute treatment resulted in increased iron uptake, with decreased cellular retention and basolateral release of iron. In contrast, chronic treatment decreased iron uptake with but did not affect the cellular retention or basolateral release. However, both acute and chronic treatments with berry extract resulted in decreased transepithelial flux of iron and thus cellular iron accumulation.

In light of the above, the gene expression profile we have observed may have arisen due to a high cellular iron content resulting from initial acute interactions with flavonoids. High levels of cellular iron retention following flavonoid treatments have

been previously ascribed to increased apical uptake and impeded basolateral release (Kim *et al*, 2008). Several mechanisms have been suggested for this, including: 1) flavonoid reducing capacity provides more Fe^{2+} as a substrate for DMT1 (Mira *et al*, 2002); 2) formation of metal-polyphenol complexes that are transportable into cells through other routes such as SVCT1 or GLUT2 (Song *et al*, 2002; Vlachodimitropoulou *et al*, 2010b); 3) complexed iron accumulates because it cannot be effluxed via the FPN route (Kim *et al*, 2008).

These findings highlight the role of flavonoids in the management of iron anaemia or overload. With the administration of flavonoids, there is an accumulation of iron at the intestinal epithelium. Potentially, this may decrease plasma peaks in iron, and reduce systemic accumulation in tissues. This is important in light of the fact that current treatment regimens for dysregulated iron status have side effects such as gastrointestinal distress and infection risks. Further research is required to characterise the full potential of flavonoids in correcting iron imbalances.

7.4 Effects of berry extract on intestinal copper uptake

In **Chapter 6** we addressed the hypothesis that dietary berry flavonoids influence intestinal copper uptake processes in Caco-2 cells. Components of the copper uptake pathway that were investigated were the apical copper importer, CTR1 and the intracellular chaperone, HAH1. The targets of the HAH1 protein, ATP7A and ATP7B, were also investigated. Berry extract treatment decreased expression of all these genes. Unlike iron or glucose metabolism, the genes involved in copper uptake are not regulated by their substrate. Instead they are regulated by iron, and the expression profile seen following berry extract treatment reflects high intracellular iron, i.e. decreased expression of ATP7A and ATP7B.

Copper uptake was investigated in the presence or absence of ascorbate, as a dietary reductant, following acute and chronic berry extract treatment. With ascorbate cuprous copper is available, and is only transportable via CTR1. In these functional studies there was an increase in copper transport under both acute and chronic treatment conditions, only in the presence of ascorbate. This suggests that increased copper influx is mediated via the CTR1 transporter. Alternatively, separate transport routes may be recruited. Furthermore, following chronic treatments, copper deprivation due to chelation reactions may have caused an increase in influx when copper uptake was initiated. Our findings indicate that berry flavonoids, acutely and chronically, enhance CTR1-mediated intestinal copper uptake. The transcriptional and translational events that occur following treatment are indicative of high intracellular iron. With these findings we can confirm that flavonoids are a dietary means of enhancing copper uptake. Enhancing copper uptake should ensure efficient iron absorption, given that the complete transepithelial flux of iron is dependent on the cuproenzymes HEPH. However our findings from the preceding chapter indicate iron transport is decreased. Further research is required to characterise the interactions between metal ions, their pathways and the influence of flavonoids.

CHAPTER EIGHT

Reference list

8 Reference list

Ader P, Wessmann A & Wolffram S (2000) Bioavailability and metabolism of the flavonol quercetin in the pig. *Free Radic Biol Med* **28**, 1056-1067.

Aherne SA & O'Brien NM (1999) Protection by the flavonoids myricetin, quercetin, and rutin against hydrogen peroxide-induced DNA damage in Caco-2 and Hep G2 cells. *Nutr Cancer* **34**, 160-166.

Aherne SA & O'Brien NM (2002) Dietary flavonols: chemistry, food content, and metabolism. *Nutrition* **18**, 75-81.

Ait-Omar A, Monteiro-Sepulveda M, Poitou C, Le Gall M, Cotillard A, Gilet J, Garbin K, Houllier A, Chateau D, Lacombe A, Veyrie N, Hugol D, Tordjman J, Magnan C, Serradas P, Clement K, Leturque A & Brot-Laroche E (2011) GLUT2 accumulation in enterocyte apical and intracellular membranes: a study in morbidly obese human subjects and ob/ob and high fat-fed mice. *Diabetes* **60**, 2598-2607.

Alvarado F & Crane RK (1962) Phlorizin as a competitive inhibitor of the active transport of sugars by hamster small intestine, in vitro. *Biochim Biophys Acta* **56**, 170-172.

Alvarado F (1967) Hypothesis for the interaction of phlorizin and phloretin with membrane carriers for sugars. *Biochim Biophys Acta* **135**, 483-495.

Anderson GJ, Powell LW & Halliday JW (1990) Transferrin receptor distribution and regulation in the rat small intestine. Effect of iron stores and erythropoiesis. *Gastroenterology* **98**, 576-585.

Anderson GJ, Frazer DM, McKie AT & Vulpe CD (2002a) The ceruloplasmin homolog hephaestin and the control of intestinal iron absorption. *Blood Cells Mol Dis* **29**, 367-375.

Anderson RA, Broadhurst CL, Polansky MM, Schmidt WF, Khan A, Flanagan VP, Schoene NW & Graves DJ (2004) Isolation and characterization of polyphenol type-A polymers from cinnamon with insulin-like biological activity. *J Agric Food Chem* **52**, 65-70.

Anderson GJ, Frazer DM, Wilkins SJ, Becker EM, Millard KN, Murphy TL, McKie AT & Vulpe CD (2002b) Relationship between intestinal iron-transporter expression, hepatic hepcidin levels and the control of iron absorption. *Biochem Soc Trans* **30**, 724-726.

Arredondo M, Uauy R & Gonzalez M (2000) Regulation of copper uptake and transport in intestinal cell monolayers by acute and chronic copper exposure. *Biochim Biophys Acta* **1474**, 169-176.

Arredondo M, Munoz P, Mura CV & Núñez MT (2001) HFE inhibits apical iron uptake by intestinal epithelial (Caco-2) cells. *FASEB J* **15**, 1276-1278.

Arredondo M, Munoz P, Mura CV & Núñez MT (2003) DMT1, a physiologically relevant apical Cu1+ transporter of intestinal cells. *Am J Physiol Cell Physiol* **284**, C1525-1530.

Arredondo M, Tapia V, Rojas A, Aguirre P, Reyes F, Marzolo MP & Núñez MT (2006) Apical distribution of HFE-beta2-microglobulin is associated with inhibition of apical iron uptake in intestinal epithelia cells. *Biometals* **19**, 379-388.

Arts IC, Sesink AL & Hollman PC (2002) Quercetin-3-glucoside is transported by the glucose carrier SGLT1 across the brush border membrane of rat small intestine. *J Nutr* **132**, 2823; author reply 2824.

Aziz AA, Edwards CA, Lean ME & Crozier A (1998) Absorption and excretion of conjugated flavonols, including quercetin-4'-O-beta-glucoside and isorhamnetin-4'-O-beta-glucoside by human volunteers after the consumption of onions. *Free Radic Res* **29**, 257-269.

Bauche IB, El Mkadem SA, Pottier AM, Senou M, Many MC, Rezsohazy R, Penicaud L, Maeda N, Funahashi T & Brichard SM (2007) Overexpression of adiponectin targeted to adipose tissue in transgenic mice: impaired adipocyte differentiation. *Endocrinology* **148**, 1539-1549.

Bauerly KA, Kelleher SL & Lönnerdal B (2004) Functional and molecular responses of suckling rat pups and human intestinal Caco-2 cells to copper treatment. *J Nutr Biochem* **15**, 155-162.

Bauerly KA, Kelleher SL & Lönnerdal B (2005) Effects of copper supplementation on copper absorption, tissue distribution, and copper transporter expression in an infant rat model. *Am J Physiol Gastrointest Liver Physiol* **288**, G1007-1014.

Bédrine-Ferran H, Le Meur N, Gicquel I, Le Cunff M, Soriano N, Guisle I, Mottier S, Monnier A, Teusan R, Fergelot P, Le Gall JY, Leger J & Mosser J (2004) Transcriptome variations in human CaCo-2 cells: a model for enterocyte differentiation and its link to iron absorption. *Genomics* **83**, 772-789.

Beking K & Vieira A (2011) An assessment of dietary flavonoid intake in the UK and Ireland. *Int J Food Sci Nutr* **62**, 17-19.

Bertinato J & L'Abbe MR (2004) Maintaining copper homeostasis: regulation of copper-trafficking proteins in response to copper deficiency or overload. *J Nutr Biochem* **15**, 316-322.

Blumenthal SS, Ren L, Lewand DL, Krezoski SK & Petering DH (1998) Cadmium decreases SGLT1 messenger RNA in mouse kidney cells. *Toxicol Appl Pharmacol* **149**, 49-54.

Bokkenheuser VD, Shackleton CH & Winter J (1987) Hydrolysis of dietary flavonoid glycosides by strains of intestinal Bacteroides from humans. *Biochem J* **248**, 953-956.

Boomgaarden I, Egert S, Rimbach G, Wolffram S, Muller MJ & Doring F (2010) Quercetin supplementation and its effect on human monocyte gene expression profiles in vivo. *Br J Nutr* **104**, 336-345.

Bosetti C, Pelucchi C & La Vecchia C (2009) Diet and cancer in Mediterranean countries: carbohydrates and fats. *Public Health Nutr* **12**, 1595-1600.

Brand W, van der Wel PA, Rein MJ, Barron D, Williamson G, van Bladeren PJ & Rietjens IM (2008) Metabolism and transport of the citrus flavonoid hesperetin in Caco-2 cell monolayers. *Drug Metab Dispos* **36**, 1794-1802.

Bravo L (1998) Polyphenols: chemistry, dietary sources, metabolism, and nutritional significance. *Nutr Rev* **56**, 317-333.

Brissot P, Troadec MB & Loreal O (2004) Intestinal absorption of iron in HFE-1 hemochromatosis: local or systemic process? *J Hepatol* **40**, 702-709.

Brookes MJ, Hughes S, Turner FE, Reynolds G, Sharma N, Ismail T, Berx G, McKie AT, Hotchin N, Anderson GJ, Iqbal T & Tselepis C (2006) Modulation of iron transport proteins in human colorectal carcinogenesis. *Gut* **55**, 1449-1460.

Brouwer IA, Lemmens AG & Beynen AC (1993) Dietary fructose v. glucose lowers ferrous-iron absorption in rats. *Br J Nutr* **70**, 171-178.

Canonne-Hergaux F, Gruenheid S, Ponka P & Gros P (1999) Cellular and subcellular localisation of the Nramp2 iron transporter in the intestinal brush border and regulation by dietary iron. *Blood* **93**, 4406-4417.

Caradec J, Sirab N, Keumeugni C, Moutereau S, Chimingqi M, Matar C, Revaud D, Bah M, Manivet P, Conti M & Loric S (2010) 'Desperate house genes': the dramatic example of hypoxia. *Br J Cancer* **102**, 1037-1043.

Cermak R, Landgraf S & Wolffram S (2004) Quercetin glucosides inhibit glucose uptake into brush-border-membrane vesicles of porcine jejunum. *Br J Nutr* **91**, 849-855.

Chambers BK & Camire ME (2003) Can cranberry supplementation benefit adults with type 2 diabetes? *Diabetes Care* **26**, 2695-2696.

Chaston T, Chung B, Mascarenhas M, Marks J, Patel B, Srai SK & Sharp P (2008) Evidence for differential effects of hepcidin in macrophages and intestinal epithelial cells. *Gut* **57**, 374-382.

Chaudhry RM, Scow JS, Madhavan S, Duenes JA & Sarr MG (2012) Acute enterocyte adaptation to luminal glucose: a posttranslational mechanism for rapid apical recruitment of the transporter GLUT2. *J Gastrointest Surg* **16**, 312-319; discussion 319.

Cheeseman CI (1993) GLUT2 is the transporter for fructose across the rat intestinal basolateral membrane. *Gastroenterology* **105**, 1050-1056.

Chen ZY, Chan PT, Ho KY, Fung KP & Wang J (1996) Antioxidant activity of natural flavonoids is governed by number and location of their aromatic hydroxyl groups. *Chem Phys Lipids* **79**, 157-163.

Chen H, Attieh ZK, Dang T, Huang G, van der Hee RM & Vulpe C (2009) Decreased hephaestin expression and activity leads to decreased iron efflux from differentiated Caco2 cells. *J Cell Biochem* **107**, 803-808.

Cheng AY & Fantus IG (2005) Oral antihyperglycemic therapy for type 2 diabetes mellitus. *CMAJ* **172**, 213-226.

Cheng M, Gao HQ, Xu L, Li BY, Zhang H & Li XH (2007) Cardioprotective effects of grape seed proanthocyanidins extracts in streptozocin induced diabetic rats. *J Cardiovasc Pharmacol* **50**, 503-509.

Chira K, Schmauch G, Saucier C, Fabre S & Teissedre PL (2009) Grape variety effect on proanthocyanidin composition and sensory perception of skin and seed tannin extracts from bordeaux wine grapes (Cabernet Sauvignon and Merlot) for two consecutive vintages (2006 and 2007). *J Agric Food Chem* **57**, 545-553.

Chun OK, Chung SJ & Song WO (2007) Estimated dietary flavonoid intake and major food sources of U.S. adults. *J Nutr* **137**, 1244-1252.

Collins JF (2006) Gene chip analyses reveal differential genetic responses to iron deficiency in rat duodenum and jejunum. *Biol Res* **39**, 25-37.

Collins JF, Hua P, Lu Y & Ranganathan PN (2009) Alternative splicing of the Menkes copper Atpase (Atp7a) transcript in the rat intestinal epithelium. *Am J Physiol Gastrointest Liver Physiol* **297**, G695-707.

Cooper S (2003) Reappraisal of serum starvation, the restriction point, G0, and G1 phase arrest points. *FASEB J* **17**, 333-340.

Corpe CP, Basaleh MM, Affleck J, Gould G, Jess TJ & Kellett GL (1996) The regulation of GLUT5 and GLUT2 activity in the adaptation of intestinal brush-border fructose transport in diabetes. *Pflugers Arch* **432**, 192-201.

Cox DW & Moore SD (2002) Copper transporting P-type ATPases and human disease. *J Bioenerg Biomembr* **34**, 333-338.

Crozier A, Jaganath IB & Clifford MN (2009) Dietary phenolics: chemistry, bioavailability and effects on health. *Nat Prod Rep* **26**, 1001-1043.

Cui XL, Jiang L & Ferraris RP (2003) Regulation of rat intestinal GLUT2 mRNA abundance by luminal and systemic factors. *Biochim Biophys Acta* **1612**, 178-185.

Cui Y, Morgenstern H, Greenland S, Tashkin DP, Mao JT, Cai L, Cozen W, Mack TM, Lu QY & Zhang ZF (2008) Dietary flavonoid intake and lung cancer--a population-based case-control study. *Cancer* **112**, 2241-2248.

Das NP & Sothy SP (1971) Studies on flavonoid metabolism. Biliary and urinary excretion of metabolites of (+)-(U- 14 C)catechin. *Biochem J* **125**, 417-423.

Day AJ, DuPont MS, Ridley S, Rhodes M, Rhodes MJ, Morgan MR & Williamson G (1998) Deglycosylation of flavonoid and isoflavonoid glycosides by human small intestine and liver beta-glucosidase activity. *FEBS Lett* **436**, 71-75.

Day AJ, Canada FJ, Diaz JC, Kroon PA, McLauchlan R, Faulds CB, Plumb GW, Morgan MR & Williamson G (2000) Dietary flavonoid and isoflavone glycosides are hydrolysed by the lactase site of lactase phlorizin hydrolase. *FEBS Lett* **468**, 166-170.

De Domenico I, Ward DM, di Patti MC, Jeong SY, David S, Musci G & Kaplan J (2007a) Ferroxidase activity is required for the stability of cell surface ferroportin in cells expressing GPI-ceruloplasmin. *EMBO J* **26**, 2823-2831.

De Domenico I, Ward DM, Langelier C, Vaughn MB, Nemeth E, Sundquist WI, Ganz T, Musci G & Kaplan J (2007b) The molecular mechanism of hepcidin-mediated ferroportin down-regulation. *Mol Biol Cell* **18**, 2569-2578.

de Romaña DL, Olivares M, Uauy R & Araya M (2011) Risks and benefits of copper in light of new insights of copper homeostasis. *J Trace Elem Med Biol* **25**, 3-13.

Debnam ES & Levin RJ (1975) Effects of fasting and semistarvation on the kinetics of active and passive sugar absorption across the small intestine in vivo. *J Physiol* **252**, 681-700.

Dennis G, Jr., Sherman BT, Hosack DA, Yang J, Gao W, Lane HC & Lempicki RA (2003) DAVID: Database for Annotation, Visualisation, and Integrated Discovery. *Genome Biol* **4**, P3.

Dhar P, Tayade AB, Bajpai PK, Sharma VK, Das SK, Chaurasia OP, Srivastava RB & Singh SB (2012) Antioxidant Capacities and Total Polyphenol Contents of Hydro-ethanolic Extract of Phytococktail from Trans-Himalaya. *J Food Sci* **77**, C156-161.

Di Giacomo C, Acquaviva R, Sorrenti V, Vanella A, Grasso S, Barcellona ML, Galvano F, Vanella L & Renis M (2009) Oxidative and antioxidant status in plasma of runners: effect of oral supplementation with natural antioxidants. *J Med Food* **12**, 145-150.

Diabetes UK (2009) What is Type 2 Diabetes? *Diabetes UK* http://www.diabetes.org.uk/Guide-to-diabetes/Introduction-to-diabetes/What_is_diabetes/What-is-Type-2-diabetes/

Díez-Sampedro A, Loo DD, Wright EM, Zampighi GA & Hirayama BA (2004) Coupled sodium/glucose cotransport by SGLT1 requires a negative charge at position 454. *Biochemistry* **43**, 13175-13184.

Eisenstein RS (2000) Discovery of the ceruloplasmin homologue hephaestin: new insight into the copper/iron connection. *Nutr Rev* **58**, 22-26.

Feder JN, Penny DM, Irrinki A, Lee VK, Lebron JA, Watson N, Tsuchihashi Z, Sigal E, Bjorkman PJ & Schatzman RC (1998) The hemochromatosis gene product complexes with the transferrin receptor and lowers its affinity for ligand binding. *Proc Natl Acad Sci U S A* **95**, 1472-1477.

Fleet JC, Wang L, Vitek O, Craig BA & Edenberg HJ (2003) Gene expression profiling of Caco-2 BBe cells suggests a role for specific signalling pathways during intestinal differentiation. *Physiol Genomics* **13**, 57-68.

Fleming RE, Migas MC, Zhou X, Jiang J, Britton RS, Brunt EM, Tomatsu S, Waheed A, Bacon BR & Sly WS (1999) Mechanism of increased iron absorption in murine model of hereditary hemochromatosis: increased duodenal expression of the iron transporter DMT1. *Proc Natl Acad Sci U S A* **96**, 3143-3148.

Frazer DM, Wilkins SJ, Becker EM, Vulpe CD, McKie AT, Trinder D & Anderson GJ (2002) Hepcidin expression inversely correlates with the expression of duodenal iron transporters and iron absorption in rats. *Gastroenterology* **123**, 835-844.

Frazer DM, Wilkins SJ, Becker EM, Murphy TL, Vulpe CD, McKie AT & Anderson GJ (2003) A rapid decrease in the expression of DMT1 and Dcytb but not Ireg1 or hephaestin explains the mucosal block phenomenon of iron absorption. *Gut* **52**, 340-346.

Gee JM, DuPont MS, Rhodes MJ & Johnson IT (1998) Quercetin glucosides interact with the intestinal glucose transport pathway. *Free Radic Biol Med* **25**, 19-25.

Geissler C & Powers HJ (2005) *Human Nutrition*. United Kingdom: Elsevier/Churchill Livingstone.

Goestemeyer AK, Marks J, Srai SK, Debnam ES & Unwin RJ (2007) GLUT2 protein at the rat proximal tubule brush border membrane correlates with

protein kinase C (PKC)-betal and plasma glucose concentration. *Diabetologia* **50**, 2209-2217.

Gould GW & Holman GD (1993) The glucose transporter family: structure, function and tissue-specific expression. *Biochem J* **295 (Pt 2)**, 329-341.

Gouyon F, Caillaud L, Carriere V, Klein C, Dalet V, Citadelle D, Kellett GL, Thorens B, Leturque A & Brot-Laroche E (2003) Simple-sugar meals target GLUT2 at enterocyte apical membranes to improve sugar absorption: a study in GLUT2-null mice. *J Physiol* **552**, 823-832.

Griffiths WJ, Kelly AL, Smith SJ & Cox TM (2000) Localisation of iron transport and regulatory proteins in human cells. *QJM* **93**, 575-587.

Guillam MT, Hummler E, Schaerer E, Yeh JI, Birnbaum MJ, Beermann F, Schmidt A, Deriaz N & Thorens B (1997) Early diabetes and abnormal postnatal pancreatic islet development in mice lacking Glut-2. *Nat Genet* **17**, 327-330.

Gunshin H, Allerson CR, Polycarpou-Schwarz M, Rofts A, Rogers JT, Kishi F, Hentze MW, Rouault TA, Andrews NC & Hediger MA (2001) Iron-dependent regulation of the divalent metal ion transporter. *FEBS Lett* **509**, 309-316.

Gunshin H, Starr CN, DiRenzo C, Fleming MD, Jin J, Greer, EL, Sellers VM, Galica SM & Andrews NC (2005) Cybrd1 (duodenal cytochrome b) is not necessary for dietary iron absorption in mice. *Blood* **106**, 2879-2883.

Hamza I, Faisst A, Prohaska J, Chen J, Gruss P & Gitlin JD (2001) The metallochaperone Atox1 plays a critical role in perinatal copper homeostasis. *Proc Natl Acad Sci U S A* **98**, 6848-6852.

Hamza I, Prohaska J & Gitlin JD (2003) Essential role for Atox1 in the copper-mediated intracellular trafficking of the Menkes ATPase. *Proc Natl Acad Sci U S A* **100**, 1215-1220.

Han O, Failla ML, Hill AD, Morris ER & Smith JC, Jr. (1995) Reduction of Fe(III) is required for uptake of nonheme iron by Caco-2 cells. *J Nutr* **125**, 1291-1299.

Han O, Fleet JC & Wood RJ (1999) Reciprocal regulation of HFE and NNamp2 gene expression by iron in human intestinal cells. *J Nutr* **129**, 98-104.

Han DW, Kim HH, Lee MH, Baek HS, Lee KY, Hyon SH & Park JC (2005) Protection of osteoblastic cells from freeze/thaw cycle-induced oxidative stress by green tea polyphenol. *Biotechnol Lett* **27**, 655-660.

Han HJ & Park SH (2011) High glucose stimulates glutamate uptakes in pancreatic beta-cells. *Lab Anim Res* **27**, 327-331.

Harrison MD, Jones CE, Solioz M & Dameron CT (2000) Intracellular copper routing: the role of copper chaperones. *Trends Biochem Sci* **25**, 29-32.

Hattori H, Okuda K, Murase T, Shigetsura Y, Narise K, Semenza GL & Nagasawa H (2011) Isolation, identification, and biological evaluation of HIF-1-modulating compounds from Brazilian green propolis. *Bioorg Med Chem* **19**, 5392-5401.

Helliwell PA, Richardson M, Affleck J & Kellett GL (2000) Stimulation of fructose transport across the intestinal brush-border membrane by PMA is mediated by GLUT2 and dynamically regulated by protein kinase C. *Biochem J* **350 Pt 1**, 149-154.

Hentze MW, Muckenthaler MU, Galy B & Camaschella C (2011) Two to tango: regulation of Mammalian iron metabolism. *Cell* **142**, 24-38.

Herraez A (2006) Biomolecules in the computer: Jmol to the rescue. *Biochem Mol Biol Educ* **34**, 255-261.

Hertog MG, Hollman PC, Katan MB & Kromhout D (1993) Intake of potentially anticarcinogenic flavonoids and their determinants in adults in The Netherlands. *Nutr Cancer* **20**, 21-29.

Hertog MG, Kromhout D, Aravanis C, Blackburn H, Buzina R, Fidanza F, Giampaoli S, Jansen A, Menotti A & Nedeljkovic S (1995) Flavonoid intake and long-term risk of coronary heart disease and cancer in the seven countries study. *Arch Intern Med* **155**, 381-386.

Hollman PC, de Vries JH, van Leeuwen SD, Mengelers MJ & Katan MB (1995) Absorption of dietary quercetin glycosides and quercetin in healthy ileostomy volunteers. *Am J Clin Nutr* **62**, 1276-1282.

Hollman PC, Bijsman MN, van Gameren Y, Cnossen EP, de Vries JH & Katan MB (1999) The sugar moiety is a major determinant of the absorption of dietary flavonoid glycosides in man. *Free Radic Res* **31**, 569-573.

Holt EM, Steffen LM, Moran A, Basu S, Steinberger J, Ross JA, Hong CP & Sinaiko AR (2009) Fruit and vegetable consumption and its relation to markers of inflammation and oxidative stress in adolescents. *J Am Diet Assoc* **109**, 414-421.

Hsu CL, Wu CH, Huang SL & Yen GC (2009) Phenolic compounds rutin and o-coumaric acid ameliorate obesity induced by high-fat diet in rats. *J Agric Food Chem* **57**, 425-431.

Hu HT, Ma QY, Zhang D, Shen SG, Han L, Ma YD, Li RF & Xie KP (2010) HIF-1alpha links beta-adrenoceptor agonists and pancreatic cancer cells under normoxic condition. *Acta Pharmacol Sin* **31**, 102-110.

Hua H, Gunther V, Georgiev O & Schaffner W (2011) Distorted copper homeostasis with decreased sensitivity to cisplatin upon chaperone Atox1 deletion in Drosophila. *Biometals* **24**, 445-453.

Huang da W, Sherman BT, Stephens R, Baseler MW, Lane HC & Lempicki RA (2008) DAVID gene ID conversion tool. *Bioinformation* **2**, 428-430.

Huang da W, Sherman BT & Lempicki RA (2009) Systematic and integrative analysis of large gene lists using DAVID bioinformatics resources. *Nat Protoc* **4**, 44-57.

Ikuta K, Fujimoto Y, Suzuki Y, Tanaka K, Saito H, Ohhira M, Sasaki K & Kohgo Y (2000) Overexpression of hemochromatosis protein, HFE, alters transferrin recycling process in human hepatoma cells. *Biochim Biophys Acta* **1496**, 221-231.

Inagaki N, Yasuda K, Inoue G, Okamoto Y, Yano H, Someya Y, Ohmoto Y, Deguchi K, Imagawa K & Imura H (1992) Glucose as regulator of glucose transport activity and glucose-transporter mRNA in hamster beta-cell line. *Diabetes* **41**, 592-597.

Jagetia GC & Reddy TK (2011) Alleviation of iron induced oxidative stress by the grape fruit flavanone naringin in vitro. *Chem Biol Interact* **190**, 121-128.

Johannot L & Somerset SM (2006) Age-related variations in flavonoid intake and sources in the Australian population. *Public Health Nutr* **9**, 1045-1054.

Johnson PE (1989) Factors affecting copper absorption in humans and animals. *Adv Exp Med Biol* **258**, 71-79.

Johnson DM, Yamaji S, Tennant J, Srai SK & Sharp PA (2005) Regulation of divalent metal transporter expression in human intestinal epithelial cells following exposure to non-haem iron. *FEBS Lett* **579**, 1923-1929.

Johnston K, Sharp P, Clifford M & Morgan L (2005) Dietary polyphenols decrease glucose uptake by human intestinal Caco-2 cells. *FEBS Lett* **579**, 1653-1657.

Kanakis CD, Tarantilis PA, Polissiou MG, Diamantoglou S & Tajmir-Riahi HA (2007) An overview of DNA and RNA bindings to antioxidant flavonoids. *Cell Biochem Biophys* **49**, 29-36.

Kaplan J, Ward DM & De Domenico I (2011) The molecular basis of iron overload disorders and iron-linked anemias. *Int J Hematol* **93**, 14-20.

Kelleher SL & Lönnerdal B (2006) Mammary gland copper transport is stimulated by prolactin through alterations in Ctr1 and Atp7A localisation. *Am J Physiol Regul Integr Comp Physiol* **291**, R1181-1191.

Kellett GL & Helliwell PA (2000) The diffusive component of intestinal glucose absorption is mediated by the glucose-induced recruitment of GLUT2 to the brush-border membrane. *Biochem J* **350 Pt 1**, 155-162.

Kellett GL, Brot-Laroche E, Mace OJ & Leturque A (2008) Sugar absorption in the intestine: the role of GLUT2. *Annu Rev Nutr* **28**, 35-54.

Kim EY, Ham SK, Shigenaga MK & Han O (2008) Bioactive dietary polyphenolic compounds reduce nonheme iron transport across human intestinal cell monolayers. *J Nutr* **138**, 1647-1651.

Khoursandi S, Scharlau D, Herter P, Kuhnen C, Martin D, Kinne RK & Kipp H (2004) Different modes of sodium-D-glucose cotransporter-mediated D-glucose uptake regulation in Caco-2 cells. *Am J Physiol Cell Physiol* **287**, C1041-1047.

Kim BE, Turski ML, Nose Y, Casad M, Rockman HA & Thiele DJ (2010) Cardiac copper deficiency activates a systemic signalling mechanism that communicates with the copper acquisition and storage organs. *Cell Metab* **11**, 353-363.

Klip A & Paquet MR (1990) Glucose transport and glucose transporters in muscle and their metabolic regulation. *Diabetes Care* **13**, 228-243.

Knaggs AR (2003) The biosynthesis of shikimate metabolites. *Nat Prod Rep* **20**, 119-136.

Kroon PA, Clifford MN, Crozier A, Day AJ, Donovan JL, Manach C & Williamson G (2004) How should we assess the effects of exposure to dietary polyphenols in vitro? *Am J Clin Nutr* **80**, 15-21.

Kuo SM, Tan D & Boyer JC (2004) Cellular vitamin C accumulation in the presence of copper. *Biol Trace Elem Res* **100**, 125-136.

Kwon O, Eck P, Chen S, Corpe CP, Lee JH, Kruhlak M & Levine M (2007) Inhibition of the intestinal glucose transporter GLUT2 by flavonoids. *FASEB J* **21**, 366-377.

La Fontaine S, Firth SD, Lockhart PJ, Brooks H, Parton RG, Camakaris J & Mercer JF (1998) Functional analysis and intracellular localisation of the human menkes protein (MNK) stably expressed from a cDNA construct in Chinese hamster ovary cells (CHO-K1). *Hum Mol Genet* **7**, 1293-1300.

Lako J, Wattanapenpaiboon N, Wahlqvist M & Trenerry C (2006) Phytochemical intakes of the Fijian population. *Asia Pac J Clin Nutr* **15**, 275-285.

Larin D, Mekios C, Das K, Ross B, Yang AS & Gilliam TC (1999) Characterisation of the interaction between the Wilson and Menkes disease proteins and the cytoplasmic copper chaperone, HAH1p. *J Biol Chem* **274**, 28497-28504.

Latunde-Dada GO, Simpson RJ & McKie AT (2008) Duodenal cytochrome B expression stimulates iron uptake by human intestinal epithelial cells. *J Nutr* **138**, 991-995.

Lebron JA, Bennett MJ, Vaughn DE, Chirino AJ, Snow PM, Mintier GA, Feder JN & Bjorkman PJ (1998) Crystal structure of the hemochromatosis protein HFE and characterisation of its interaction with transferrin receptor. *Cell* **93**, 111-123.

Lee PL, Gelbart T, West C, Halloran C & Beutler E (1998) The human Nramp2 gene: characterisation of the gene structure, alternative splicing, promoter region and polymorphisms. *Blood Cells Mol Dis* **24**, 199-215.

Lee J, Prohaska JR, Dagenais SL, Glover TW & Thiele DJ (2000) Isolation of a murine copper transporter gene, tissue specific expression and functional complementation of a yeast copper transport mutant. *Gene* **254**, 87-96.

Lee J, Prohaska JR & Thiele DJ (2001) Essential role for mammalian copper transporter Ctr1 in copper homeostasis and embryonic development. *Proc Natl Acad Sci U S A* **98**, 6842-6847.

Lee J, Pena MM, Nose Y & Thiele DJ (2002) Biochemical characterisation of the human copper transporter Ctr1. *J Biol Chem* **277**, 4380-4387.

Lee PL & Beutler E (2009) Regulation of hepcidin and iron-overload disease. *Annu Rev Pathol* **4**, 489-515.

Lefevre M, Wiles JE, Zhang X, Howard LR, Gupta S, Smith AA, Ju ZY & DeLany JP (2008) Gene expression microarray analysis of the effects of grape anthocyanins in mice: a test of a hypothesis-generating paradigm. *Metabolism* **57**, S52-57.

Lekka Ch E, Ren J, Meng S & Kaxiras E (2009) Structural, electronic, and optical properties of representative Cu-flavonoid complexes. *J Phys Chem B* **113**, 6478-6483.

Lescale-Matys L, Dyer J, Scott D, Freeman TC, Wright EM & Shirazi-Beechey SP (1993) Regulation of the ovine intestinal Na+/glucose co-transporter (SGLT1) is dissociated from mRNA abundance. *Biochem J* **291 (Pt 2)**, 435-440.

Leturque A, Brot-Laroche E & Le Gall M (2009) GLUT2 mutations, translocation, and receptor function in diet sugar managing. *Am J Physiol Endocrinol Metab* **296**, E985-992.

Li H, Gu Y, Zhang Y, Lucas MJ & Wang Y (2004) High glucose levels down-regulate glucose transporter expression that correlates with increased oxidative stress in placental trophoblast cells in vitro. *J Soc Gynecol Investig* **11**, 75-81.

Livak KJ & Schmittgen TD (2001) Analysis of relative gene expression data using real-time quantitative PCR and the 2(-Delta Delta C(T)) Method. *Methods* **25**, 402-408.

Lönnerdal B (2008) Intestinal regulation of copper homeostasis: a developmental perspective. *Am J Clin Nutr* **88**, 846S-850S.

Lopes TJ, Luganskaja T, Vujic Spasic M, Hentze MW, Muckenthaler MU, Schumann K & Reich JG (2010) Systems analysis of iron metabolism: the network of iron pools and fluxes. *BMC Syst Biol* **4**, 112.

Lörinczi E, Tsivkovskii R, Haase W, Bamberg E, Lutsenko S & Friedrich T (2008) Delivery of the Cu-transporting ATPase ATP7B to the plasma membrane in Xenopus oocytes. *Biochim Biophys Acta* **1778**, 896-906.

Losso JN & Bawadi HA (2005) Hypoxia inducible factor pathways as targets for functional foods. *J Agric Food Chem* **53**, 3751-3768.

Lotito SB, Zhang WJ, Yang CS, Crozier A & Frei B (2011) Metabolic conversion of dietary flavonoids alters their anti-inflammatory and antioxidant properties. *Free Radic Biol Med* **51**, 454-463.

Lutsenko S (2008) Atp7b-/- mice as a model for studies of Wilson's disease. *Biochem Soc Trans* **36**, 1233-1238.

Lutsenko S, LeShane ES & Shinde U (2007) Biochemical basis of regulation of human copper-transporting ATPases. *Arch Biochem Biophys* **463**, 134-148.

Ma Q, Kim EY & Han O (2010) Bioactive dietary polyphenols decrease heme iron absorption by decreasing basolateral iron release in human intestinal Caco-2 cells. *J Nutr* **140**, 1117-1121.

Maaser K & Borlak J (2008) A genome-wide expression analysis identifies a network of EpCAM-induced cell cycle regulators. *Br J Cancer* **99**, 1635-1643.

Mace OJ, Morgan EL, Affleck JA, Lister N & Kellett GL (2007) Calcium absorption by Cav1.3 induces terminal web myosin II phosphorylation and apical GLUT2 insertion in rat intestine. *J Physiol* **580**, 605-616.

Mace OJ, Lister N, Morgan E, Shepherd E, Affleck J, Helliwell P, Bronk JR, Kellett GL, Meredith D, Boyd R, Pieri M, Bailey PD, Pettcrew R & Foley D (2009) An energy supply network of nutrient absorption coordinated by calcium and T1R taste receptors in rat small intestine. *J Physiol* **587**, 195-210.

Mahraoui L, Rodolosse A, Barbat A, Dussaulx E, Zweibaum A, Rousset M & Brot-Laroche E (1994) Presence and differential expression of SGLT1, GLUT1, GLUT2, GLUT3 and GLUT5 hexose-transporter mRNAs in Caco-2 cell clones in relation to cell growth and glucose consumption. *Biochem J* **298 Pt 3**, 629-633.

Manach C, Morand C, Crespy V, Demigne C, Texier O, Regerat F & Remesy C (1998) Quercetin is recovered in human plasma as conjugated derivatives which retain antioxidant properties. *FEBS Lett* **426**, 331-336.

Manach C, Williamson G, Morand C, Scalbert A & Remesy (2005) Bioavailability and bioefficacy of polyphenols in humans. I. Review of 97 bioavailability studies. *Am J Clin Nutr* **81**, 230S-242S.

Manzano S & Williamson G (2010) Polyphenols and phenolic acids from strawberry and apple decrease glucose uptake and transport by human intestinal Caco-2 cells. *Mol Nutr Food Res* **54**, 1773-1780.

Martineau LC, Couture A, Spoor D, Benhaddou-Andaloussi A, Harris C, Meddah B, Leduc C, Burt A, Vuong T, Mai Le P, Prentki M, Bennett SA, Arnason JT & Haddad PS (2006) Anti-diabetic properties of the Canadian lowbush blueberry Vaccinium angustifolium Ait. *Phytomedicine* **13**, 612-623.

Martins R, Silva B, Proenca D & Faustino P (2011) Differential HFE gene expression is regulated by alternative splicing in human tissues. *PLoS One* **6**, e17542.

Mastrogiannaki M, Matak P, Keith B, Simon MC, Vaulont S & Peyssonnaux C (2009) HIF-2alpha, but not HIF-1alpha, promotes iron absorption in mice. *J Clin Invest* **119**, 1159-1166.

Masumoto S, Akimoto Y, Oike H & Kobori M (2009) Dietary phloridzin reduces blood glucose levels and reverses Sglt1 expression in the small intestine in streptozotocin-induced diabetic mice. *J Agric Food Chem* **57**, 4651-4656.

Mate A, Barfull A, Hermosa AM, Gomez-Amores L, Vazquez CM & Planas JM (2006) Regulation of sodium-glucose cotransporter SGLT1 in the intestine of hypertensive rats. *Am J Physiol Regul Integr Comp Physiol* **291**, R760-767.

Matuschek MC, Hendriks WH, McGhie TK & Reynolds GW (2006) The jejunum is the main site of absorption for anthocyanins in mice. *J Nutr Biochem* **17**, 31-36.

McGinnis S & Madden TL (2004) BLAST: at the core of a powerful and diverse set of sequence analysis tools. *Nucleic Acids Res* **32**, W20-5.

McKie AT, Marciani P, Rolfs A, Brennan K, Wehr K, Barrow D, Miret S, Bomford A, Peters TJ, Farzaneh F, Hediger MA, Hentze MW & Simpson RJ (2000) A novel duodenal iron-regulated transporter, IREG1, implicated in the basolateral transfer of iron to the circulation. *Mol Cell* **5**, 299-309.

McKie AT, Barrow D, Latunde-Dada GO, Rolfs A, Sager G, Mudaly E, Mudaly M, Richardson C, Barlow D, Bomford A, Peters TJ, Raja KB, Shirali S, Hediger MA, Farzaneh F & Simpson RJ (2001) An iron-regulated ferric reductase associated with the absorption of dietary iron. *Science* **291**, 1755-1759.

McRae R, Lai B & Fahrni CJ (2010) Copper redistribution in Atox1-deficient mouse fibroblast cells. *J Biol Inorg Chem* **15**, 99-105.

Mira L, Fernandez MT, Santos M, Rocha R, Florencio MH & Jennings KR (2002) Interactions of flavonoids with iron and copper ions: a mechanism for their antioxidant activity. *Free Radic Res* **36**, 1199-1208.

Miyamoto K, Hase K, Takagi T, Fujii T, Taketani Y, Minami H, Oka T & Nakabou Y (1993) Differential responses of intestinal glucose transporter mRNA transcripts to levels of dietary sugars. *Biochem J* **295 (Pt 1)**, 211-215.

Miyayama T, Ishizuka Y, Iijima T, Hiraoka D & Ogra Y (2011) Roles of copper chaperone for superoxide dismutase 1 and metallothionein in copper homeostasis. *Metallomics* **3**, 693-701.

Morgan EL, Mace OJ, Affleck J & Kellett GL (2007) Apical GLUT2 and Cav1.3: regulation of rat intestinal glucose and calcium absorption. *J Physiol* **580**, 593-604.

Mukai R, Shirai Y, Saito N, Yoshida K & Ashida H (2009) Subcellular localization of flavonol aglycone in hepatocytes visualized by confocal laser scanning fluorescence microscope. *Cytotechnology* **59**, 177-182.

Mullie P, Clarys P, Deriemaeker P & Hebbelinck M (2008) Estimation of daily human intake of food flavonoids. *Int J Food Sci Nutr* **59**, 291-298.

Mursu J, Nurmi T, Tuomainen TP, Salonen JT, Pukkala E & Voutilainen S (2008) Intake of flavonoids and risk of cancer in Finnish men: The Kuopio Ischaemic Heart Disease Risk Factor Study. *Int J Cancer* **123**, 660-663.

Myhrstad MC, Carlsen H, Nordstrom O, Blomhoff R & Moskaug JO (2002) Flavonoids increase the intracellular glutathione level by transactivation of the gamma-glutamylcysteine synthetase catalytical subunit promoter. *Free Radic Biol Med* **32**, 386-393.

Naeve GS, Vana AM, Eggold JR, Kelner GS, Maki R, Desouza EB & Foster AC (1999) Expression profile of the copper homeostasis gene, rAtox1, in the rat brain. *Neuroscience* **93**, 1179-1187.

Nakayama T, Hashimoto T, Kajiya K & Kumazawa S (2000) Affinity of polyphenols for lipid bilayers. *Biofactors* **13**, 147-151.

Nakayama M, Aihara M, Chen YN, Araie M, Tomita-Yokotani K & Iwashina T (2011) Neuroprotective effects of flavonoids on hypoxia-, glutamate-, and oxidative stress-induced retinal ganglion cell death. *Mol Vis* **17**, 1784-1793.

Natsume Y, Kadota K, Satsu H & Shimizu M (2009) Effect of quercetin on the gene expression profile of the mouse intestine. *Biosci Biotechnol Biochem* **73**, 722-725.

Nemeth E, Tuttle MS, Powelson J, Vaughn MB, Donovan A, Ward DM, Ganz T & Kaplan J (2004) Hepcidin regulates cellular iron efflux by binding to ferroportin and inducing its internalisation. *Science* **306**, 2090-2093.

Nijveldt RJ, van Nood E, van Hoorn DE, Boelens PG, van Norren K & van Leeuwen PA (2001) Flavonoids: a review of probable mechanisms of action and potential applications. *Am J Clin Nutr* **74**, 418-425.

Noordeen NA, Khera TK, Sun G, Longbottom ER, Pullen TJ, da Silva Xavier G, Rutter GA & Leclerc I (2010) Carbohydrate-responsive element-binding protein (ChREBP) is a negative regulator of ARNT/HIF-1beta gene expression in pancreatic islet beta-cells. *Diabetes* **59**, 153-160.

Nose Y, Kim BE & Thiele DJ (2006) Ctr1 drives intestinal copper absorption and is essential for growth, iron metabolism, and neonatal cardiac function. *Cell Metab* **4**, 235-244.

Nose Y, Wood LK, Kim BE, Prohaska JR, Fry RS, Spears JW & Thiele DJ (2010) Ctr1 is an apical copper transporter in mammalian intestinal epithelial cells in vivo that is controlled at the level of protein stability. *J Biol Chem* **285**, 32385-32392.

Noyes WD, Hosain F & Finch CA (1964) Incorporation of Radioiron into Marrow Heme. *J Lab Clin Med* **64**, 574-580.

Núñez MT & Tapia V (1999) Transferrin stimulates iron absorption, exocytosis, and secretion in cultured intestinal cells. *Am J Physiol* **276**, C1085-1090.

Núñez MT, Tapia V, Toyokuni S & Okada S (2001) Iron-induced oxidative damage in colon carcinoma (Caco-2) cells. *Free Radic Res* **34**, 57-68.

Nyasae L, Bustos R, Braiterman L, Eipper B & Hubbard A (2007) Dynamics of endogenous ATP7A (Menkes protein) in intestinal epithelial cells: copper-dependent redistribution between two intracellular sites. *Am J Physiol Gastrointest Liver Physiol* **292**, G1181-1194.

Nyman NA & Kumpulainen JT (2001) Determination of anthocyanidins in berries and red wine by high-performance liquid chromatography. *J Agric Food Chem* **49**, 4183-4187.

Ogawa D, Asanuma M, Miyazaki I, Tachibana H, Wada J, Sogawa N, Sugaya T, Kitamura S, Maeshima Y, Shikata K & Makino H High glucose increases metallothionein expression in renal proximal tubular epithelial cells. *Exp Diabetes Res* **2011**, 534872.

Ohgami RS, Campagna DR, McDonald A & Fleming MD (2006) The Steap proteins are metalloreductases. *Blood* **108**, 1388-1394.

Oliveira DM, Freitas HS, Souza MF, Arcari DP, Ribeiro ML, Carvalho PO & Bastos DH (2008) Yerba Mate (Ilex paraguariensis) aqueous extract decreases intestinal SGLT1 gene expression but does not affect other biochemical parameters in alloxan-diabetic Wistar rats. *J Agric Food Chem* **56**, 10527-10532.

Owen CA, Jr. (1964) Absorption and Excretion of Cu64-Labeled Copper by the Rat. *Am J Physiol* **207**, 1203-1206.

Pardee AB (1974) A restriction point for control of normal animal cell proliferation. *Proc Natl Acad Sci U S A* **71**, 1286-1290.

Pardee AB (1989) G1 events and regulation of cell proliferation. *Science* **246**, 603-608.

Park JB (1999) Flavonoids are potential inhibitors of glucose uptake in U937 cells. *Biochem Biophys Res Commun* **260**, 568-574.

Park SS, Bae I & Lee YJ (2008) Flavonoids-induced accumulation of hypoxia-inducible factor (HIF)-1alpha/2alpha is mediated through chelation of iron. *J Cell Biochem* **6**, 1989-98.

Parkkila S, Waheed A, Britton RS, Feder JN, Tsuchihashi Z, Schatzman RC, Bacon BR & Sly WS (1997) Immunohistochemistry of HLA-H, the protein defective in patients with hereditary hemochromatosis, reveals unique pattern of expression in gastrointestinal tract. *Proc Natl Acad Sci U S A* **94**, 2534-2539.

Passamonti S, Vrhovsek U & Mattivi F (2002) The interaction of anthocyanins with bilitranslocase. *Biochem Biophys Res Commun* **296**, 631-636.

Pearson WR & Lipman DJ (1988) Improved tools for biological sequence comparison. *Proc Natl Acad Sci U S A* **85**, 2444-2448.

Petris MJ, Mercer JF, Culvenor JG, Lockhart P, Gleeson PA & Camakaris J (1996) Ligand-regulated transport of the Menkes copper P-type ATPase efflux pump from the Golgi apparatus to the plasma membrane: a novel mechanism of regulated trafficking. *EMBO J* **15**, 6084-6095.

Petris MJ & Mercer JF (1999) The Menkes protein (ATP7A; MNK) cycles via the plasma membrane both in basal and elevated extracellular copper using a C-terminal di-leucine endocytic signal. *Hum Mol Genet* **8**, 2107-2115.

Petris MJ, Strausak D & Mercer JF (2000) The Menkes copper transporter is required for the activation of tyrosinase. *Hum Mol Genet* **9**, 2845-2851.

Planas JM, Alfaras I, Colom H & Juan ME (2012) The bioavailability and distribution of trans-reservatrol are constrained by ABC transporters. *Arch Biochem Biophys***.** *In-press.*

Pourvali K, Matak, P, Latunde-Dada GO, Solomou S, Mastrogiannaki M, Peyssonnaux C & Sharp PA (2012) Basal expression of copper transporter 1 in intestinal epithelial cells is regulated by hypoxia-inducible factor 2α. *FEBS Lett* **16**, 2423-7.

Prior RL & Wu X (2006) Anthocyanins: structural characteristics that result in unique metabolic patterns and biological activities. *Free Radic Res* **40**, 1014-1028.

Prior RL, Wu X & Gu L (2006) Identification and urinary excretion of metabolites of 5-(hydroxymethyl)-2-furfural in human subjects following consumption of dried plums or dried plum juice. *J Agric Food Chem* **54**, 3744-3749.

Prior RL, Wu X, Gu L, Hager TJ, Hager A & Howard LR (2008) Whole berries versus berry anthocyanins: interactions with dietary fat levels in the C57BL/6J mouse model of obesity. *J Agric Food Chem* **56**, 647-653.

Prohaska JR (2011) Impact of copper limitation on expression and function of multicopper oxidases (ferroxidases). *Adv Nutr* **2**, 89-95.

Puig S & Thiele DJ (2002) Molecular mechanisms of copper uptake and distribution. *Curr Opin Chem Biol* **6**, 171-180.

Pruitt KD, Tatusova T, Brown GR & Maglott DR (2012) NCBI Reference Sequences (RefSeq): current status, new features and genome annotation policy. *Nucleic Acids Res* **40**, D130-135.

Qin Z, Itoh S, Jeney V, Ushio-Fukai M & Fukai T (2006) Essential role for the Menkes ATPase in activation of extracellular superoxide dismutase: implication for vascular oxidative stress. *FASEB J* **20**, 334-336.

Reeves PG, Demars LC, Johnson WT & Lukaski HC (2005) Dietary copper deficiency reduces iron absorption and duodenal enterocyte hephaestin protein in male and female rats. *J Nutr* **135**, 92-98.

Ren J, Meng S, Lekka Ch E & Kaxiras E (2008) Complexation of flavonoids with iron: structure and optical signatures. *J Phys Chem B* **112**, 1845-1850.

Rencurel F, Waeber G, Antoine B, Rocchiccioli F, Maulard P, Girard J & Leturque A (1996) Requirement of glucose metabolism for regulation of glucose transporter type 2 (GLUT2) gene expression in liver. *Biochem J* **314 (Pt 3)**, 903-909.

Renis M, Calandra L, Scifo C, Tomasello B, Cardile V, Vanella L, Bei R, La Fauci L & Galvano F (2008) Response of cell cycle/stress-related protein expression and DNA damage upon treatment of CaCo2 cells with anthocyanins. *Br J Nutr* **100**, 27-35.

Rozen S & Skaletsky H (2000) Primer3 on the WWW for general users and for biologist programmers. *Methods Mol Biol* **132**, 365-386.

Sadilova E, Carle R & Stintzing FC (2007) Thermal degradation of anthocyanins and its impact on color and in vitro antioxidant capacity. *Mol Nutr Food Res* **51**, 1461-1471.

Santer R, Schneppenheim R, Dombrowski A, Gotze H, Steinmann B & Schaub J (1997) Mutations in GLUT2, the gene for the liver-type glucose transporter, in patients with Fanconi-Bickel syndrome. *Nat Genet* **17**, 324-326.

Scheiber MD, Liu JH, Subbiah MT, Rebar RW & Setchell KD (2001) Dietary inclusion of whole soy foods results in significant reductions in clinical risk factors for osteoporosis and cardiovascular disease in normal postmenopausal women. *Menopause* **8**, 384-392.

Schlief ML, Craig AM & Gitlin JD (2005) NMDA receptor activation mediates copper homeostasis in hippocampal neurons. *J Neurosci* **25**, 239-246.

Schmittgen TD & Livak KJ (2008) Analyzing real-time PCR data by the comparative C(T) method. *Nat Protoc* **3**, 1101-1108.

Sharp P & Srai SK (2007) Molecular mechanisms involved in intestinal iron absorption. *World J Gastroenterol* **13**, 4716-4724.

Sharp P, Tandy S, Yamaji S, Tennant J, Williams M & Singh Srai SK (2002) Rapid regulation of divalent metal transporter (DMT1) protein but not mRNA expression by non-haem iron in human intestinal Caco-2 cells. *FEBS Lett* **510**, 71-76.

Sharp PA (2003) Ctr1 and its role in body copper homeostasis. *Int J Biochem Cell Biol* **35**, 288-291.

Sivakumar PM, Priya S & Doble M (2009) Synthesis, biological evaluation, mechanism of action and quantitative structure-activity relationship studies of chalcones as antibacterial agents. *Chem Biol Drug Des* **73**, 403-415.

Smith MW, Turvey A & Freeman TC (1992) Appearance of phloridzin-sensitive glucose transport is not controlled at mRNA level in rabbit jejunal enterocytes. *Exp Physiol* **77**, 525-528.

Song J, Kwon O, Chen S, Daruwala R, Eck P, Park JB & Levine M (2002) Flavonoid inhibition of sodium-dependent vitamin C transporter 1 (SVCT1) and glucose transporter isoform 2 (GLUT2), intestinal transporters for vitamin C and Glucose. *J Biol Chem* **277**, 15252-15260.

Song WO & Chun OK (2008) Tea is the major source of flavan-3-ol and flavonol in the U.S. diet. *J Nutr* **138**, 1543S-1547S.

Speisky H, Gomez M, Burgos-Bravo F, Lopez-Alarcon C, Jullian C, Olea-Azar C & Aliaga ME (2009) Generation of superoxide radicals by copper-glutathione complexes: redox-consequences associated with their interaction with reduced glutathione. *Bioorg Med Chem* **17**, 1803-1810.

Spencer JP, Chowrimootoo G, Choudhury R, Debnam ES, Srai SK & Rice-Evans C (1999) The small intestine can both absorb and glucuronidate luminal flavonoids. *FEBS Lett* **458**, 224-230.

Spencer JP (2003) Metabolism of tea flavonoids in the gastrointestinal tract. *J Nutr* **133**, 3255S-3261S.

Strausak D, Howie MK, Firth SD, Schlicksupp A, Pipkorn R, Multhaup G & Mercer JF (2003) Kinetic analysis of the interaction of the copper chaperone Atox1 with the metal binding sites of the Menkes protein. *J Biol Chem* **278**, 20821-20827.

Su HC, Hung LM & Chen JK (2006) Resveratrol, a red wine antioxidant, possesses an insulin-like effect in streptozotocin-induced diabetic rats. *Am J Physiol Endocrinol Metab* **290**, E1339-1346.

Sun H, Chow EC, Liu S, Du Y & Pang KS (2008) The Caco-2 cell monolayer: usefulness and limitations. *Expert Opin Drug Metab Toxicol* **4**, 395-411.

Suzuki R, Masami T, Takanashi M, Hussain A, Yuan B, Toyoda H & Kuroda M (2011) Anthocyanidins-enriched bilberry extracts inhibit 3T3-L1 adipocyte differentiation via the insulin pathway. *Nutrition & Metabolism* **8**, 1-9.

Talavera S, Felgines C, Texier O, Besson C, Manach C, Lamaison JL & Remesy C (2004) Anthocyanins are efficiently absorbed from the small intestine in rats. *J Nutr* **134**, 2275-2279.

Tallkvist J, Bowlus CL & Lönnerdal B (2000) Functional and molecular responses of human intestinal Caco-2 cells to iron treatment. *Am J Clin Nutr* **72**, 770-775.

Tandy S, Williams M, Leggett A, Lopez-Jimenez M, Dedes M, Ramesh B, Srai SK & Sharp P (2000) Nramp2 expression is associated with pH-dependent iron uptake across the apical membrane of human intestinal Caco-2 cells. *J Biol Chem* **275**, 1023-1029.

Tao TY, Liu F, Klomp L, Wijmenga C & Gitlin JD (2003) The copper toxicosis gene product Murr1 directly interacts with the Wilson disease protein. *J Biol Chem* **278**, 41593-41596.

Tavani A, Spertini L, Bosetti C, Parpinel M, Gnagnarella P, Bravi F, Peterson J, Dwyer J, Lagiou P, Negri E & La Vecchia C (2006) Intake of specific flavonoids and risk of acute myocardial infarction in Italy. *Public Health Nutr* **9**, 369-374.

Taylor M, Qu A, Anderson ER, Matsubara T, Martin A, Gonzalez FJ & Shah YM (2011) Hypoxia-inducible factor-2alpha mediates the adaptive increase of intestinal ferroportin during iron deficiency in mice. *Gastroenterology* **140**, 2044-2055.

Tchaparian EH, Uriu-Adams JY, Keen CL, Mitchell AE & Rucker RB (2000) Lysyl oxidase and P-ATPase-7A expression during embryonic development in the rat. *Arch Biochem Biophys* **379**, 71-77.

Tennant J, Stansfield M, Yamaji S, Srai SK & Sharp P (2002) Effects of copper on the expression of metal transporters in human intestinal Caco-2 cells. *FEBS Lett* **527**, 239-244.

Terada K, Aiba N, Yang XL, Iida M, Nakai M, Miura N & Sugiyama T (1999) Biliary excretion of copper in LEC rat after introduction of copper transporting P-type ATPase, ATP7B. *FEBS Lett* **448**, 53-56.

Terada K, Nakako T, Yang XL, Iida M, Aiba N, Minamiya Y, Nakai M, Sakaki T, Miura N & Sugiyama T (1998) Restoration of holoceruloplasmin synthesis in LEC rat after infusion of recombinant adenovirus bearing WND cDNA. *J Biol Chem* **273**, 1815-1820.

Teucher B, Olivares M & Cori H (2004) Enhancers of iron absorption: ascorbic acid and other organic acids. *Int J Vitam Nutr Res* **74**, 403-419.

Thanou MM, Kotze AF, Scharringhausen T, Luessen HL, de Boer AG, Verhoef JC & Junginger HE (2000) Effect of degree of quaternisation of N-trimethyl chitosan chloride for enhanced transport of hydrophilic compounds across intestinal caco-2 cell monolayers. *J Control Release* **64**, 15-25.

Thumser AE, Abd Rashed A, Sharp PA & Lodge JK (2010) Ascorbate enhances iron uptake into intestinal cells through formation of a $FeCl_3$–ascorbate complex *Food Chem* **123**, 281-285.

Tobin V, Le Gall M, Fioramonti X, Stolarczyk E, Blazquez AG, Klein C, Prigent M, Serradas P, Cuif MH, Magnan C, Leturque A & Brot-Laroche E (2008) Insulin internalises GLUT2 in the enterocytes of healthy but not insulin-resistant mice. *Diabetes* **57**, 555-562.

Traka M, Gasper AV, Smith JA, Hawkey CJ, Bao Y & Mithen RF (2005) Transcriptome analysis of human colon Caco-2 cells exposed to sulforaphane. *J Nutr* **135**, 1865-1872.

Tremblay E, Auclair J, Delvin E, Levy E, Menard D, Pshezhetsky AV, Rivard N, Seidman EG, Sinnett D, Vachon PH & Beaulieu JF (2006) Gene expression profiles of normal proliferating and differentiating human intestinal epithelial cells: a comparison with the Caco-2 cell model. *J Cell Biochem* **99**, 1175-1186.

Trinder D, Fox C, Vautier G & Olynyk JK (2002) Molecular pathogenesis of iron overload. *Gut* **51**, 290-295.

Tsuda T, Ueno Y, Yoshikawa T, Kojo H & Osawa T (2006) Microarray profiling of gene expression in human adipocytes in response to anthocyanins. *Biochem Pharmacol* **71**, 1184-1197.

Turnlund JR, Keyes WR, Peiffer GL & Scott KC (1998) Copper absorption, excretion, and retention by young men consuming low dietary copper determined by using the stable isotope 65Cu. *Am J Clin Nutr* **67**, 1219-1225.

Uyeda K & Repa JJ (2006) Carbohydrate response element binding protein, ChREBP, a transcription factor coupling hepatic glucose utilisation and lipid synthesis. *Cell Metab* **4**, 107-110.

Vandesompele J, De Preter K, Pattyn F, Poppe B, Van Roy N, De Paepe A & Speleman F (2002) Accurate normalisation of real-time quantitative RT-PCR data by geometric averaging of multiple internal control genes. *Genome Biol* **3**, RESEARCH0034.

Veldhuis NA, Valova VA, Gaeth AP, Palstra N, Hannan KM, Michell BJ, Kelly LE, Jennings I, Kemp BE, Pearson RB, Robinson PJ & Camakaris J (2009) Phosphorylation regulates copper-responsive trafficking of the Menkes copper transporting P-type ATPase. *Int J Biochem Cell Biol*.

Viduranga Y, Waisundara VY, Siu SY, Hsu A, Huang D & Tan BK (2011) Baicalin upregulates the genetic expression of antioxidant enzymes in Type-2 diabetic Goto-Kakizaki rats. *Life Sci* **88**, 1016-1025.

Vlachodimitropoulou E, Naftalin RJ & Sharp PA (2010a) Quercetin is a substrate for the transmembrane oxidoreductase Dcytb. *Free Radic Biol Med* **48**, 1366-1369.

Vlachodimitropoulou E, Sharp PA & Naftalin RJ (2010b) Quercetin-iron chelates are transported via glucose transporters. *Free Radic Biol Med* **50**, 934-944.

Vulpe CD, Kuo YM, Murphy TL, Cowley L, Askwith C, Libina N, Gitschier J & Anderson GJ (1999) Hephaestin, a ceruloplasmin homologue implicated in intestinal iron transport, is defective in the sla mouse. *Nat Genet* **21**, 195-199.

Vuorela S, Kreander K, Karonen M, Nieminen R, Hamalainen M, Galkin A, Laitinen L, Salminen JP, Moilanen E, Pihlaja K, Vuorela H, Vuorela P & Heinonen M (2005) Preclinical evaluation of rapeseed, raspberry, and pine bark phenolics for health related effects. *J Agric Food Chem* **53**, 5922-5931.

Walgren RA, Walle UK & Walle T (1998) Transport of quercetin and its glucosides across human intestinal epithelial Caco-2 cells. *Biochem Pharmacol* **55**, 1721-1727.

Walgren RA, Lin JT, Kinne RK & Walle T (2000) Cellular uptake of dietary flavonoid quercetin 4'-beta-glucoside by sodium-dependent glucose transporter SGLT1. *J Pharmacol Exp Ther* **294**, 837-843.

Walker JM, Tsivkovskii R & Lutsenko S (2002) Metallochaperone Atox1 transfers copper to the NH2-terminal domain of the Wilson's disease protein and regulates its catalytic activity. *J Biol Chem* **277**, 27953-27959.

Walle T, Otake Y, Walle UK & Wilson FA (2000) Quercetin glucosides are completely hydrolyzed in ileostomy patients before absorption. *J Nutr* **130**, 2658-2661.

Walle T & Walle UK (2003) The beta-D-glucoside and sodium-dependent glucose transporter 1 (SGLT1)-inhibitor phloridzin is transported by both SGLT1 and multidrug resistance-associated proteins 1/2. *Drug Metab Dispos* **31**, 1288-1291.

Walle T (2004) Absorption and metabolism of flavonoids. *Free Radic Biol Med* **36**, 829-837.

Wang J & Pantopoulos K (2011) Regulation of cellular iron metabolism. *Biochem J* **434**, 365-381.

Weiss KH, Lozoya JC, Tuma S, Gotthardt D, Reichert J, Ehehalt R, Stremmel W & Fullekrug J (2008) Copper-induced translocation of the Wilson disease protein ATP7B independent of Murr1/COMMD1 and Rab7. *Am J Pathol* **173**, 1783-1794.

White C, Kambe T, Fulcher YG, Sachdev SW, Bush AI, Fritsche K, Lee J, Quinn TP & Petris MJ (2009) Copper transport into the secretory pathway is regulated by oxygen in macrophages. *J Cell Sci* **122**, 1315-1321.

Wolffram S, Block M & Ader P (2002) Quercetin-3-glucoside is transported by the glucose carrier SGLT1 across the brush border membrane of rat small intestine. *J Nutr* **132**, 630-635.

Wyman S, Simpson RJ, McKie AT & Sharp PA (2008) Dcytb (Cybrd1) functions as both a ferric and a cupric reductase in vitro. *FEBS Lett* **582**, 1901-1906.

Xiao J, Kai G, Ni X, Yang F & Chen X (2011) Interaction of natural polyphenols with alpha-amylase in vitro: molecular property-affinity relationship aspect. *Mol Biosyst* **7**, 1883-1890.

Xie L & Collins JF (2011) Transcriptional regulation of the Menkes copper ATPase (Atp7a) gene by hypoxia-inducible factor (HIF2α) in intestinal epithelial cells. *Am J Physiol Cell Physiol* **300**, C1298-1305.

Yamaguchi Y, Heiny ME, Suzuki M & Gitlin JD (1996) Biochemical characterisation and intracellular localisation of the Menkes disease protein. *Proc Natl Acad Sci U S A* **93**, 14030-14035.

Yamaji S, Sharp P, Ramesh B & Srai SK (2004) Inhibition of iron transport across human intestinal epithelial cells by hepcidin. *Blood* **104**, 2178-2180.

Yamaji S, Tennant J, Tandy S, Williams M, Singh Srai SK & Sharp P (2001) Zinc regulates the function and expression of the iron transporters DMT1 and IREG1 in human intestinal Caco-2 cells. *FEBS Lett* **507**, 137-141.

Yamashita H, Takenoshita M, Sakurai M, Bruick RK, Henzel WJ, Shillinglaw W, Arnot D & Uyeda K (2001) A glucose-responsive transcription factor that regulates carbohydrate metabolism in the liver. *Proc Natl Acad Sci U S A* **98**, 9116-9121.

Yochum L, Kushi LH, Meyer K & Folsom AR (1999) Dietary flavonoid intake and risk of cardiovascular disease in postmenopausal women. *Am J Epidemiol* **149**, 943-949.

Zafra-Stone S, Yasmin T, Bagchi M, Chatterjee A, Vinson JA & Bagchi D (2007) Berry anthocyanins as novel antioxidants in human health and disease prevention. *Mol Nutr Food Res* **51**, 675-683.

Zamora-Ros R, Andres-Lacueva C, Lamuela-Raventos RM, Berenguer T, Jakszyn P, Barricarte A, Ardanaz E, Amiano P, Dorronsoro M, Larranaga N, Martinez C, Sanchez MJ, Navarro C, Chirlaque MD, Tormo MJ, Quiros JR & Gonzalez CA (2010) Estimation of dietary sources and flavonoid intake in a Spanish adult population (EPIC-Spain). *J Am Diet Assoc* **110**, 390-398.

Zerounian NR, Redekosky C, Malpe R & Linder MC (2003) Regulation of copper absorption by copper availability in the Caco-2 cell intestinal model. *Am J Physiol Gastrointest Liver Physiol* **284**, G739-747.

Zhao L, Wu J, Yang J, Wei J, Gao W & Guo C (2011) Dietary quercetin supplementation increases serum antioxidant capacity and alters hepatic gene expression profile in rats. *Exp Biol Med (Maywood)* **236**, 701-706.

Zoller H, Theurl I, Koch RO, McKie AT, Vogel W & Weiss G (2003) Duodenal cytochrome b and hephaestin expression in patients with iron deficiency and hemochromatosis. *Gastroenterology* **125**, 746-754.

CHAPTER NINE

Appendices

9 Appendices

9.1 Primer design and specificity

All primer sequences were designed by Primer3 (Rozen & Skaletsky, 2000) and sequences were subjected to Basic Local Alignment Search Tool (BLAST) analysis to ensure specificity of the amplicon (McGinnis & Madden, 2004).

The first step of designing primers for qRT-PCR was to find the transcript of the gene of interest for investigation. The gene was first located in the The Reference Sequence (Refseq) database, provided by the National Centre of Biotechnology Information (NCBI) (Pruitt *et al*, 2012). The mRNA sequence was selected based on accession number (e.g. NM_001859) and the transcript was used in its FASTA format (a standardised bioinformatics format containing sequence information; Pearson & Lipman, 1988).

FASTA sequence was applied to the Primer3 web interface; primers were picked directly from this sequence. Selection criteria for primer and amplicon designed were as follows:

- Amplicon length between 75-200 bases
- Avoid repeats in amplicon of more than 4 of the same base
- Amplicon and primer GC content between 50 and 60 % each
- Primer melting temperature between 50 and 65 °C
- Avoid secondary structures of primers and of amplicons

Once selected, amplicons were subjected to BLAST and melting curve analysis to ensure transcript specificity and selectivity.

9.2 Efficiency of gene expression analysis

Gene expression analysis was carried out using quantitative real-time polymerase chain reaction (qRT-PCR). With every experiment a number of quality controls were in place. These were: **1)** inclusion of genes of interest and housekeeping genes in the same plate for every experiment, to decrease variation between plates and runs; **2)** inclusion of a standard curve for every set of samples run on every plate, this was to ensure the efficiency of PCR amplification; **3)** inclusion of a dissociation step and melting curve analysis to ensure the amplification of a single product and to ensure there was no primer-dimer formation during amplification. Examples of the standard curves and dissociation curves that resulted from qRT-PCR analysis of every gene tested are shown in this section. They are listed in the following order (housekeeping genes, followed by order of appearance in experimental chapters) 18S, GAPDH, GLUT2, SGLT1, DMT1, DCYTB, HFE, TfR1, FPN, HEPH, CTR1, HAH1, ATP7A and ATP7B.

9.2.1 Ribosomal RNA 18S

Standard and melting curves were drawn for 18S to ensure efficiency and specificity of amplification. See figures below.

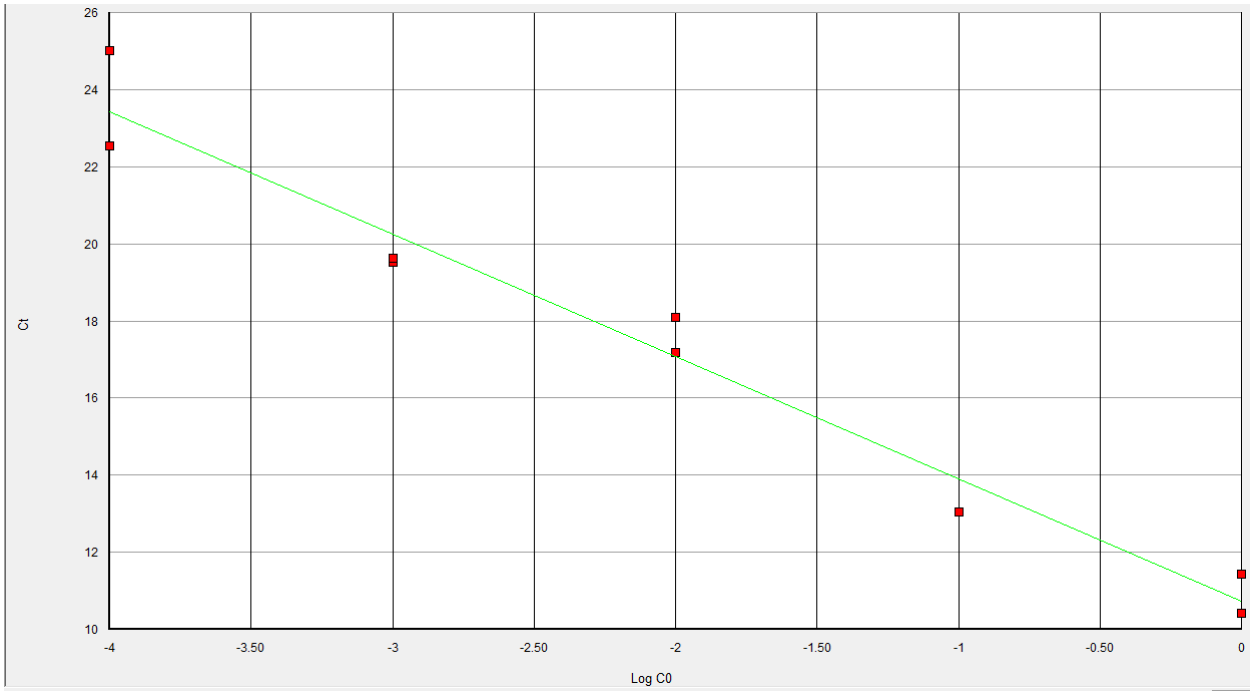

Efficiency: 105 %; slope: -3.2; R^2: 0.97

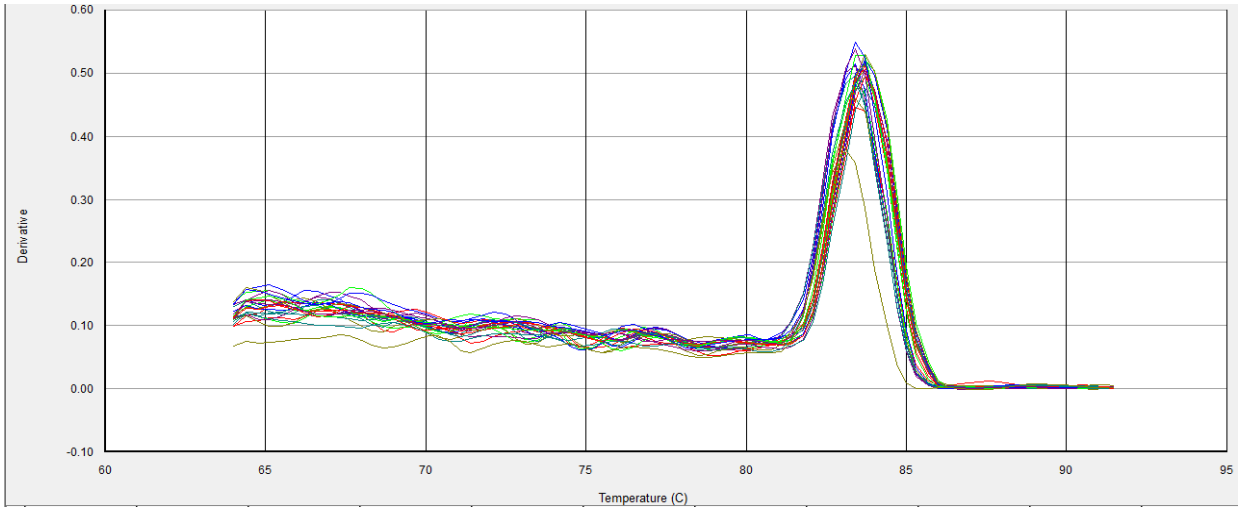

9.2.2 Glyceraldehyde-3-monophosphate dehydrogenase (GAPDH)

Standard and melting curves were drawn for GAPDH to ensure efficiency and specificity of amplification. See figures below.

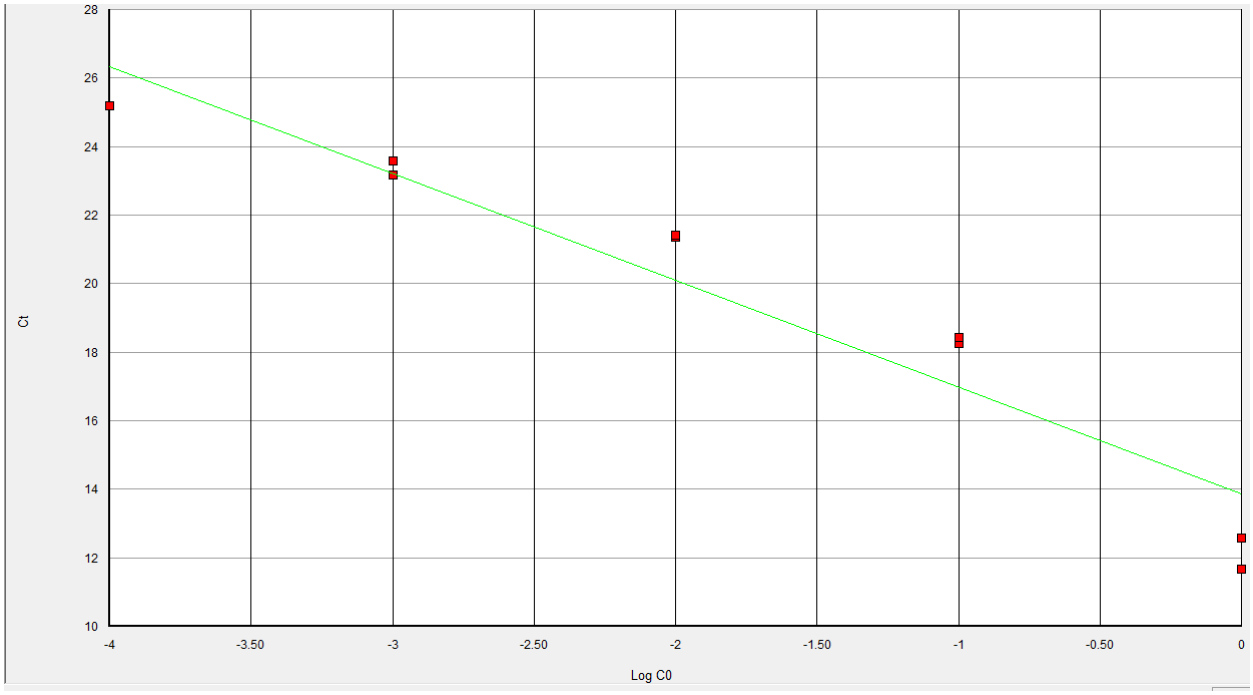

Efficiency: 110 %; slope: -3.1; R^2: 0.92

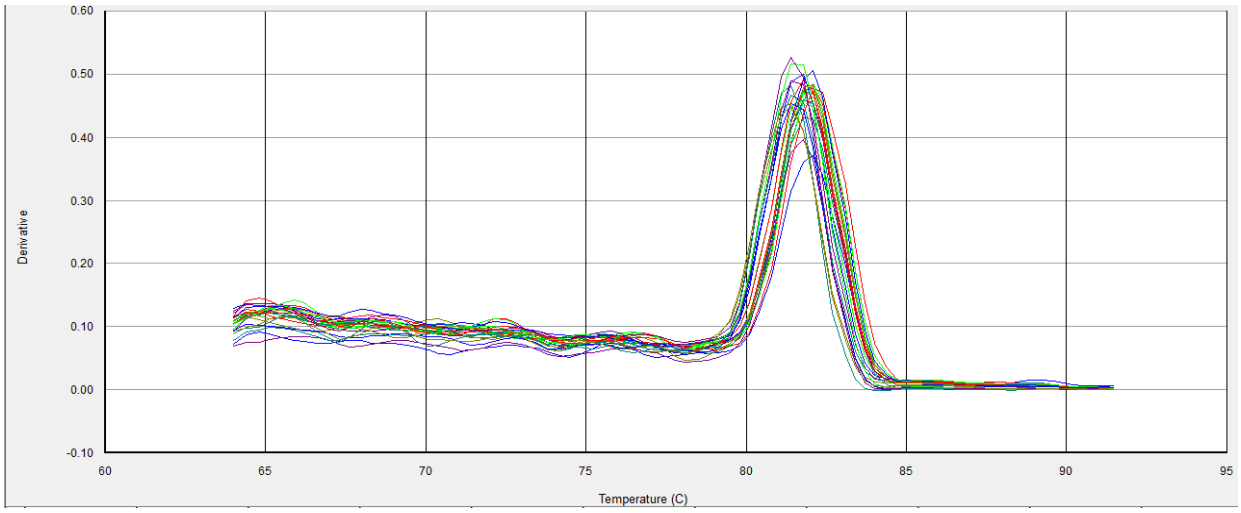

9.2.3 Facilitative glucose transporter 2 (GLUT2)

Standard and melting curves were drawn for GLUT2 to ensure efficiency and specificity of amplification. See figures below.

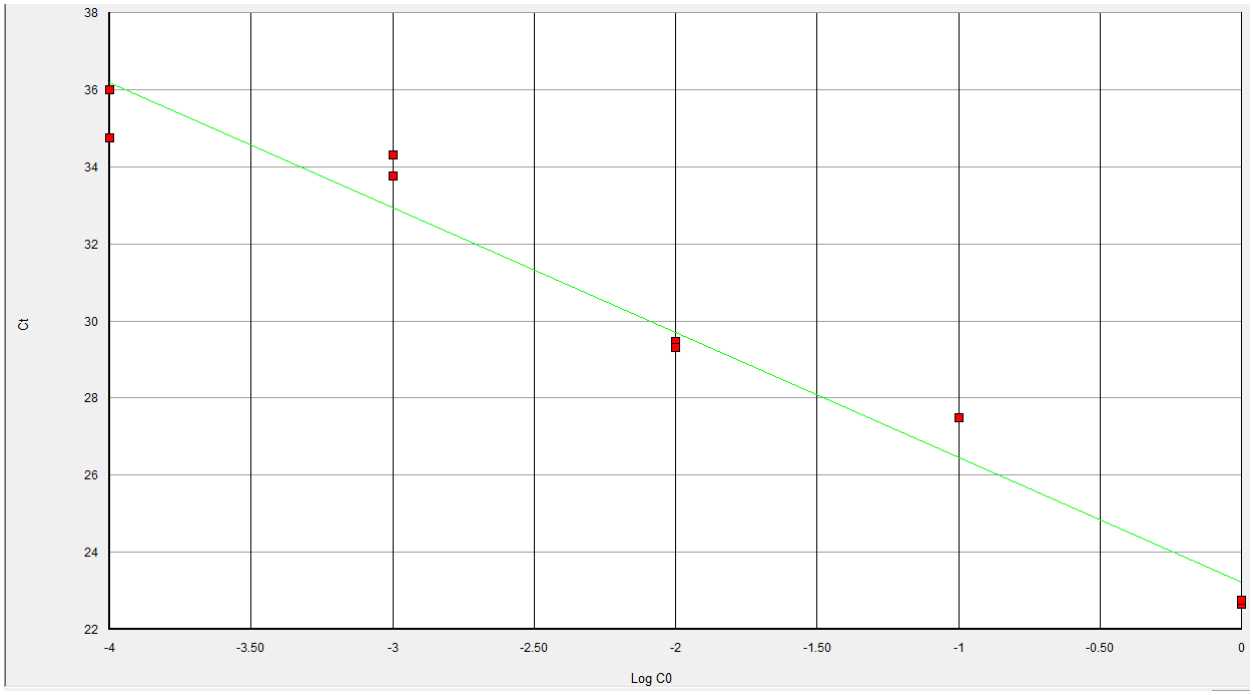

Efficiency: 105 %; slope: -3.2; R^2: 0.97

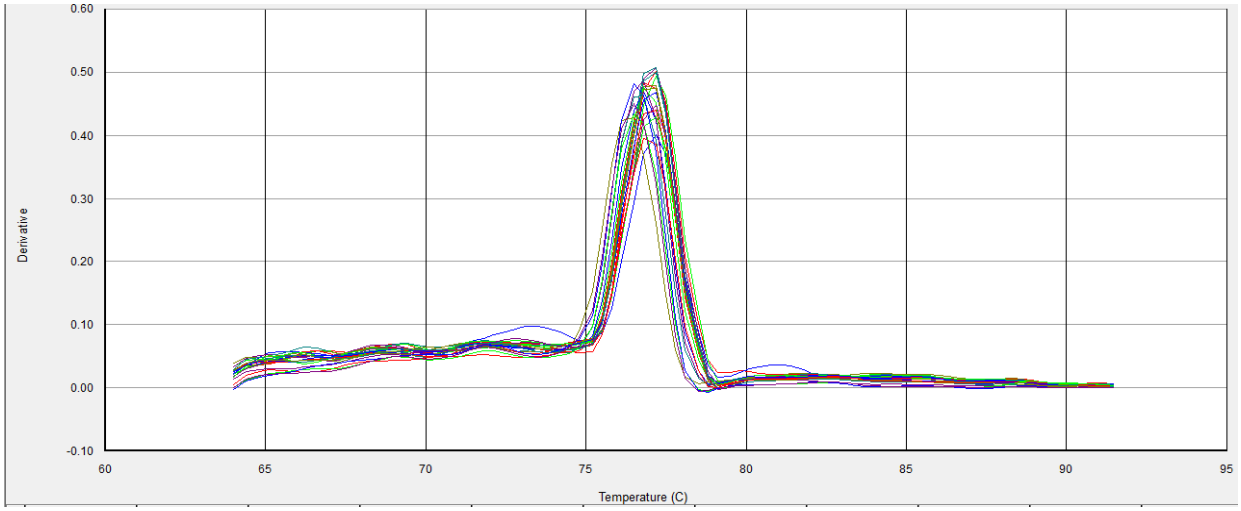

9.2.4 Sodium/glucose cotransporter 1 (SGLT1)

Standard and melting curves were drawn for GLUT2 to ensure efficiency and specificity of amplification. See figures below.

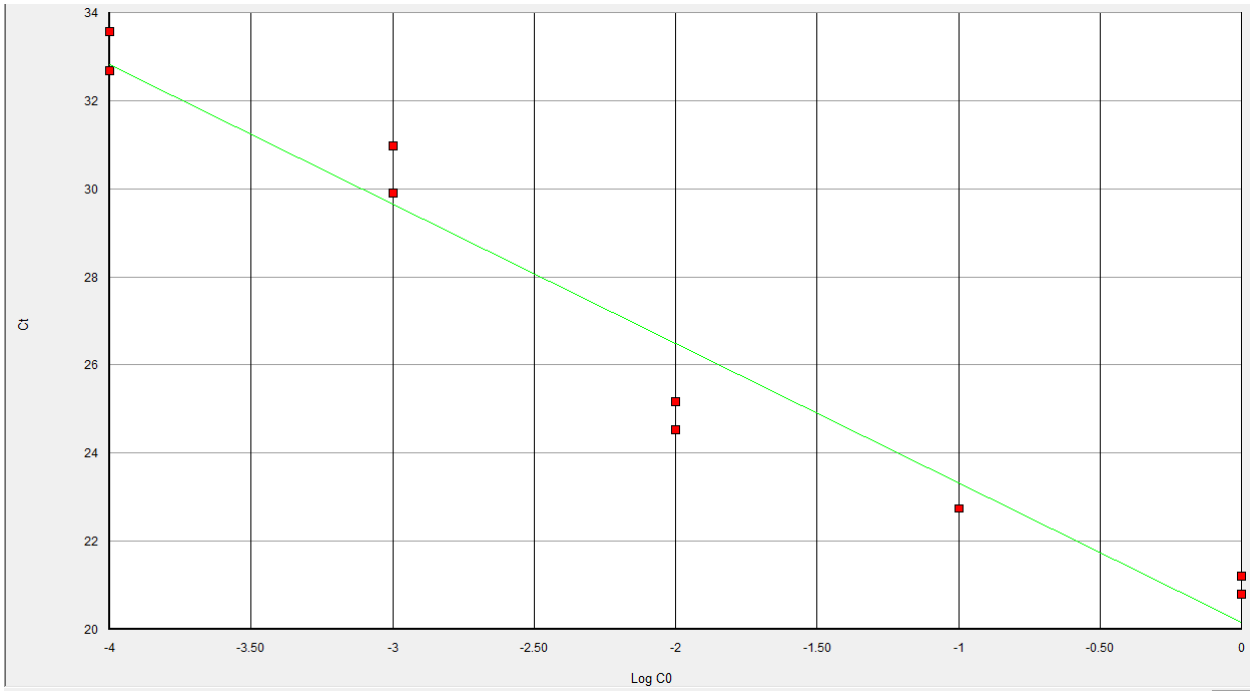

Efficiency: 105 %; slope: -3.2; R^2: 0.95

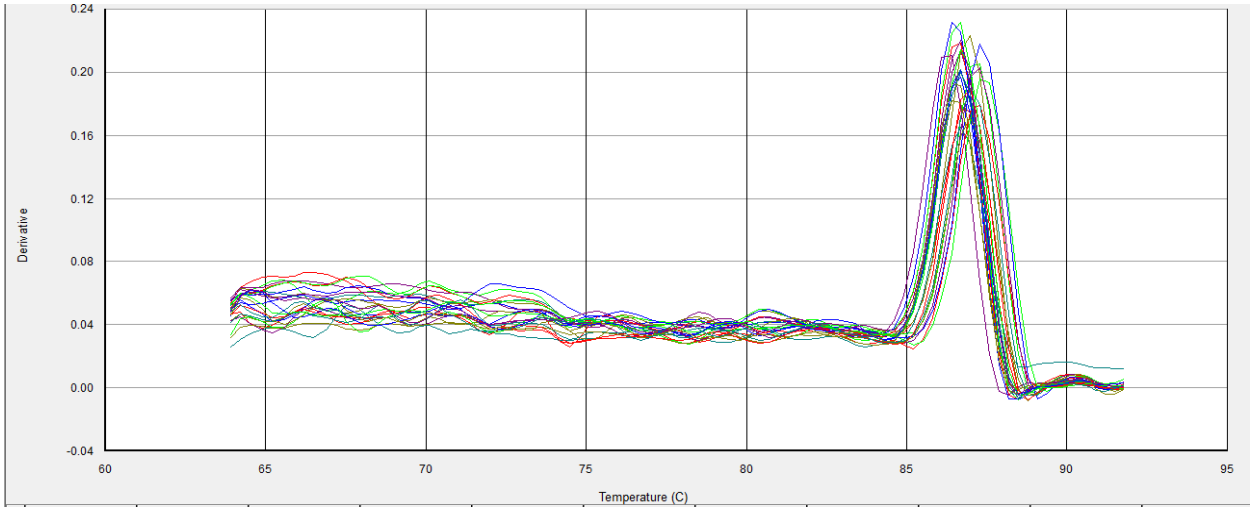

9.2.5 Divalent metal ion transporter 1 (DMT1)

Standard and melting curves were drawn for DMT1 to ensure efficiency and specificity of amplification. See figures below.

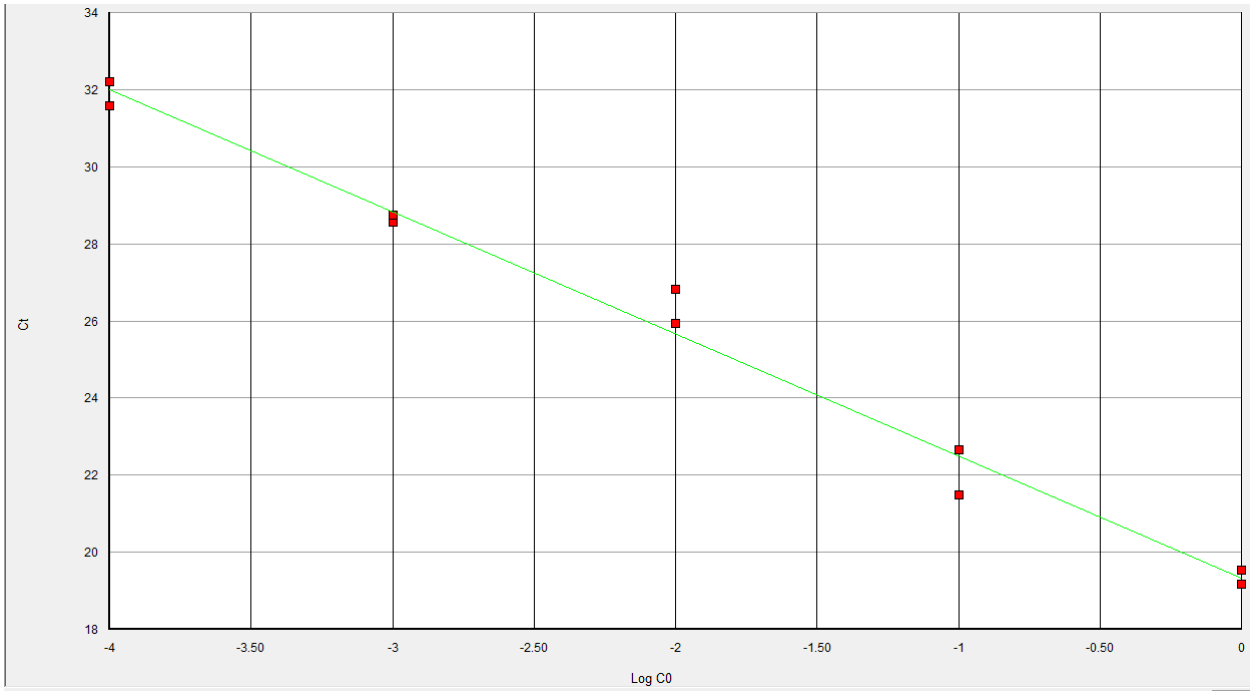

Efficiency: 105 %; slope: -3.2; R^2: 0.99

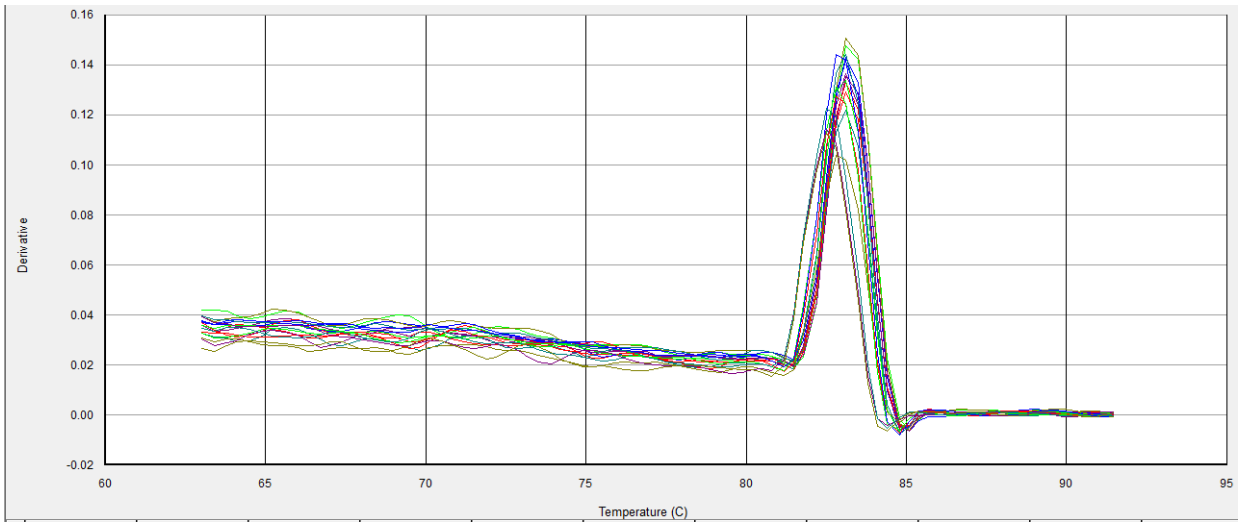

9.2.6 Duodenal Cytochrome B reductase (DCYTB)

Standard and melting curves were drawn for DCYTB to ensure efficiency and specificity of amplification. See figures below.

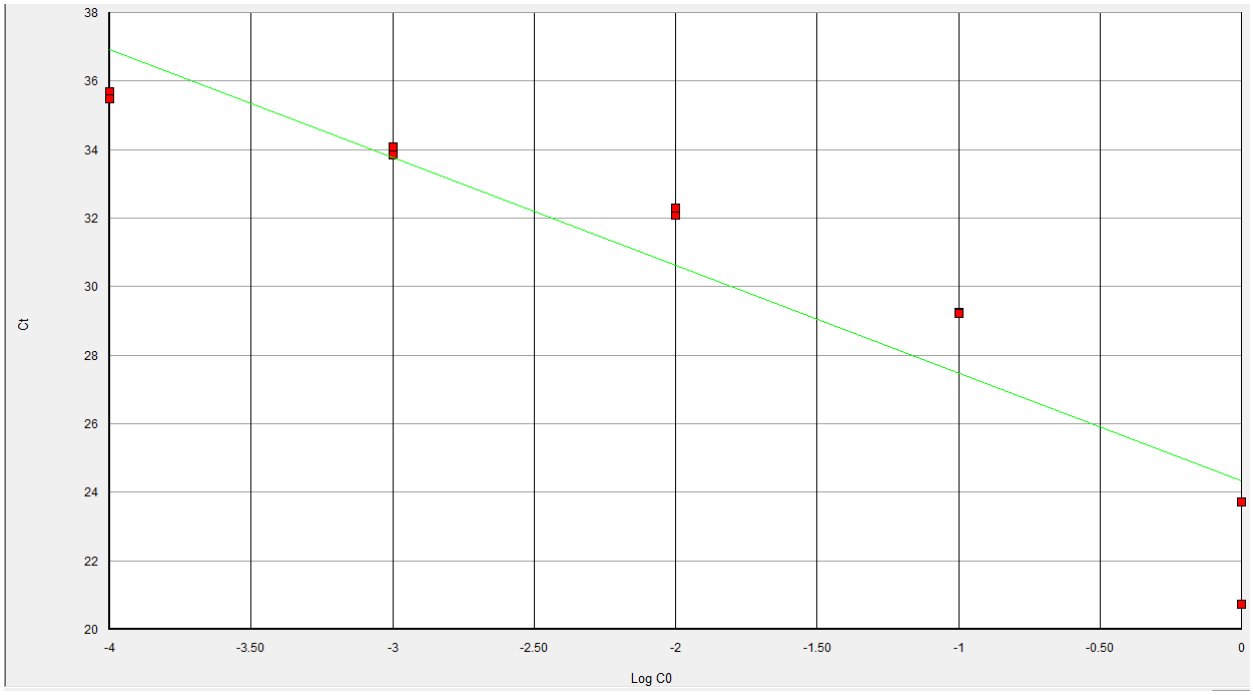

Efficiency: 110 %; slope: -3.1; R^2: 0.88

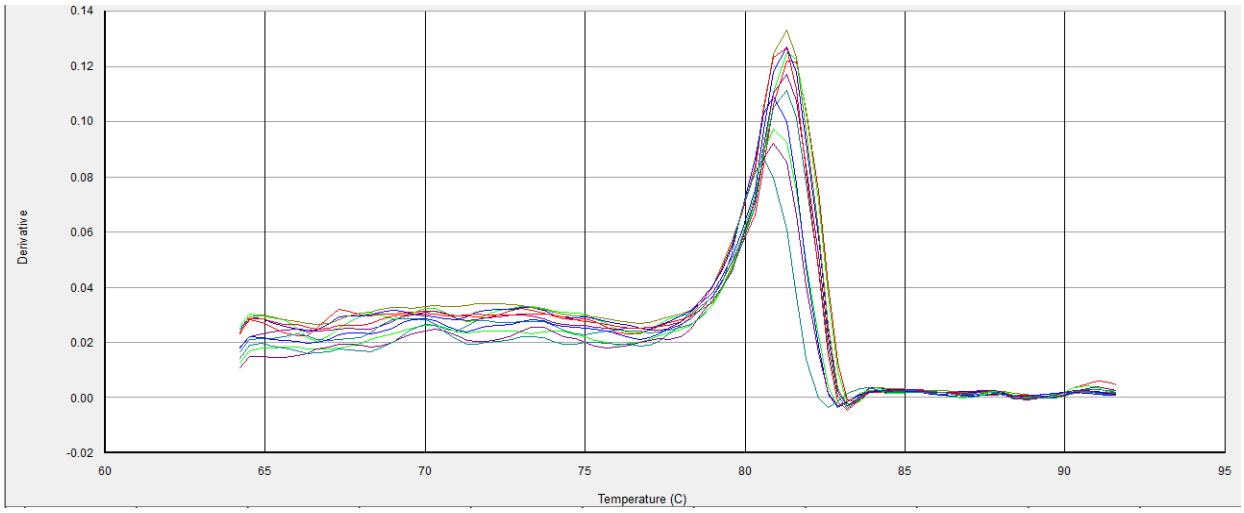

9.2.7 Haemochromatosis protein (HFE)

Standard and melting curves were drawn for HFE to ensure efficiency and specificity of amplification. See figures below.

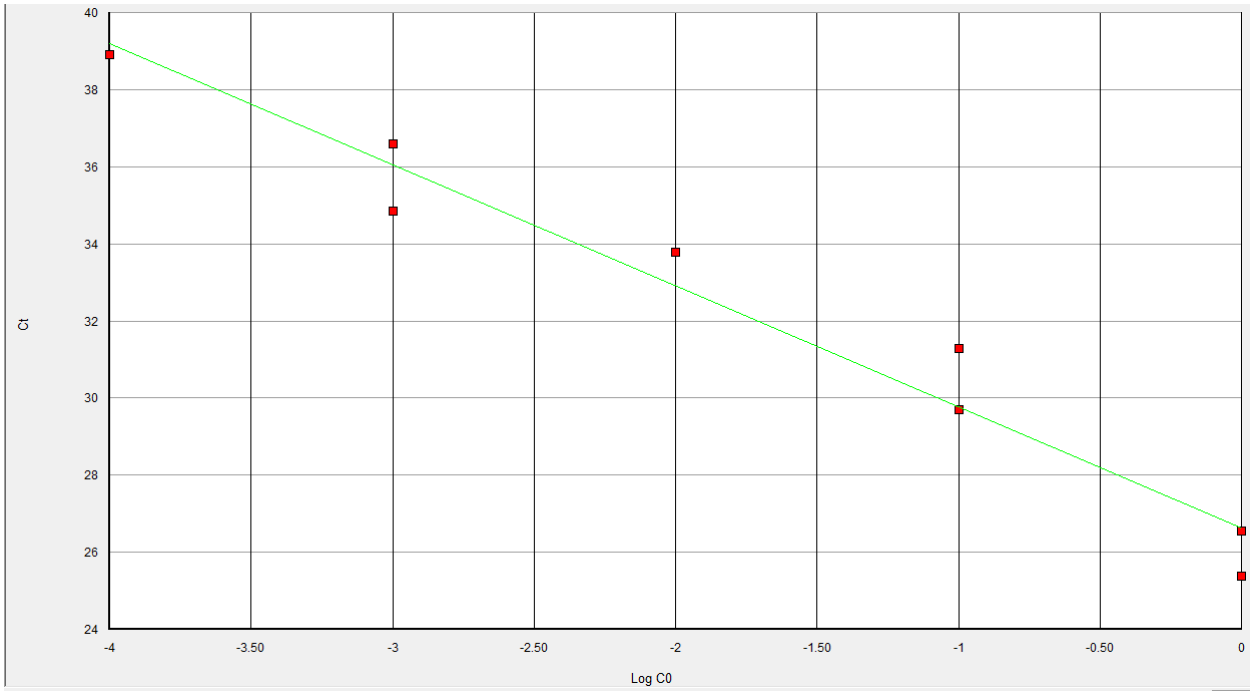

Efficiency: 110 %; slope: -3.1; R^2: 0.96

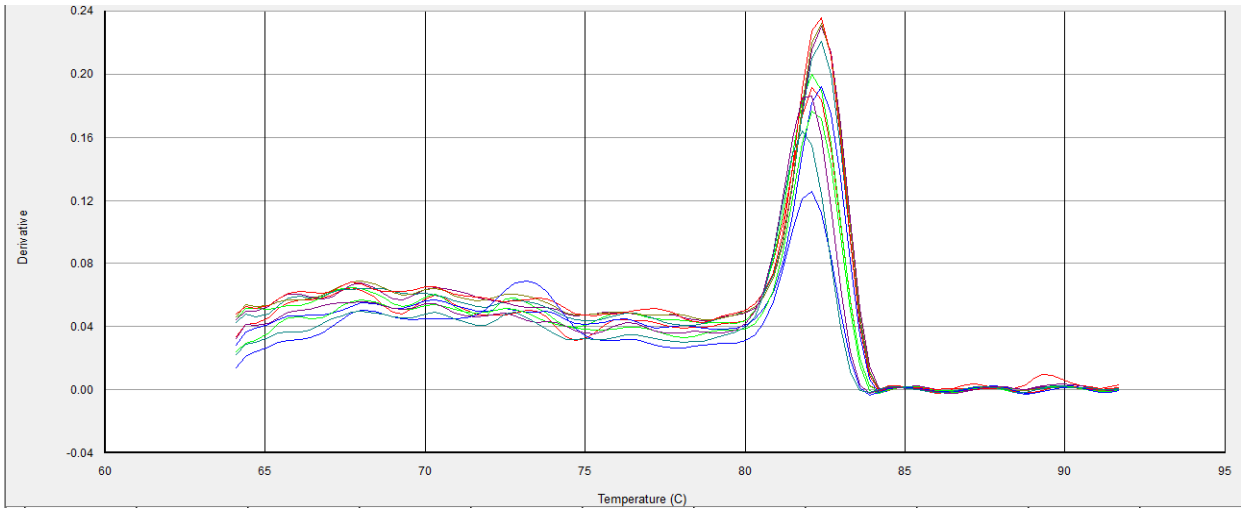

9.2.8 Transferrin receptor 1 (TfR1)

Standard and melting curves were drawn for TfR1 to ensure efficiency and specificity of amplification. See figures below.

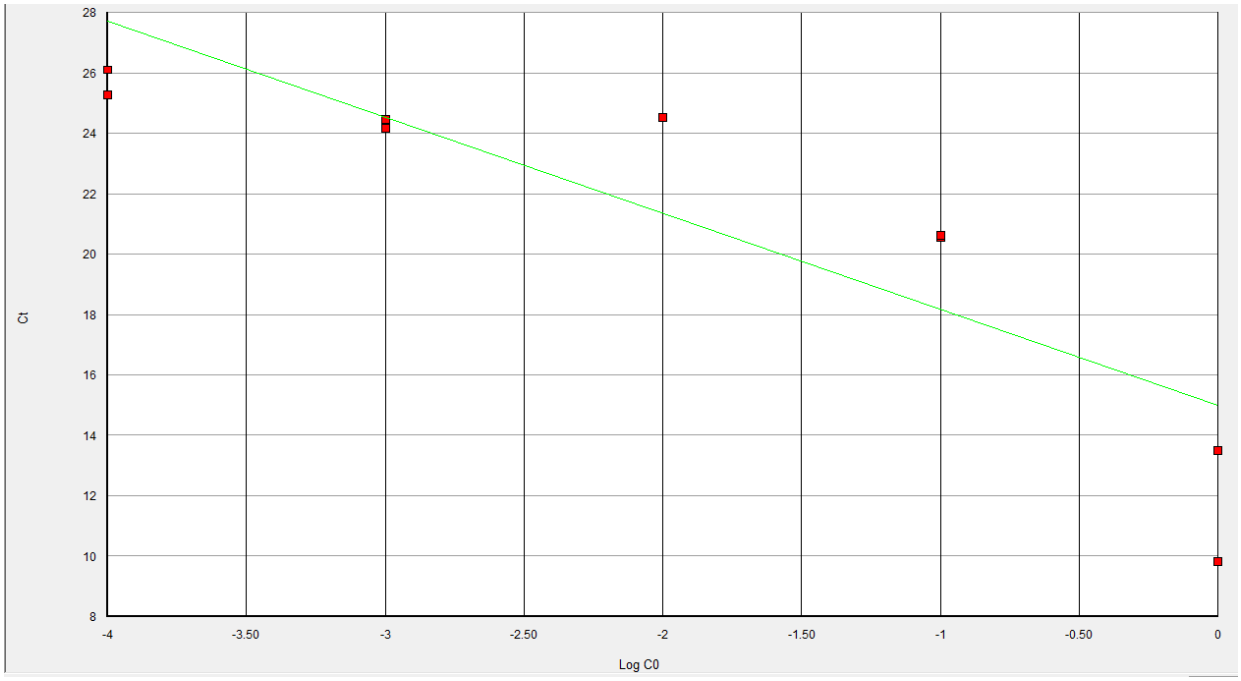

Efficiency: 105 %; slope: -3.2; R^2: 0.75

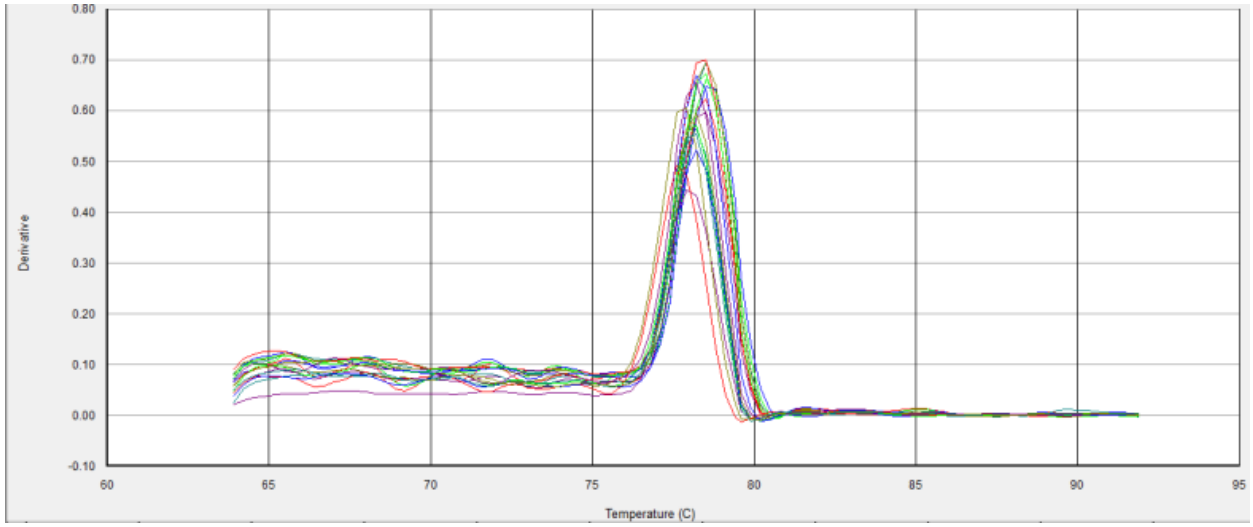

9.2.9 Ferroportin (FPN)

Standard and melting curves were drawn for FPN to ensure efficiency and specificity of amplification. See figures below.

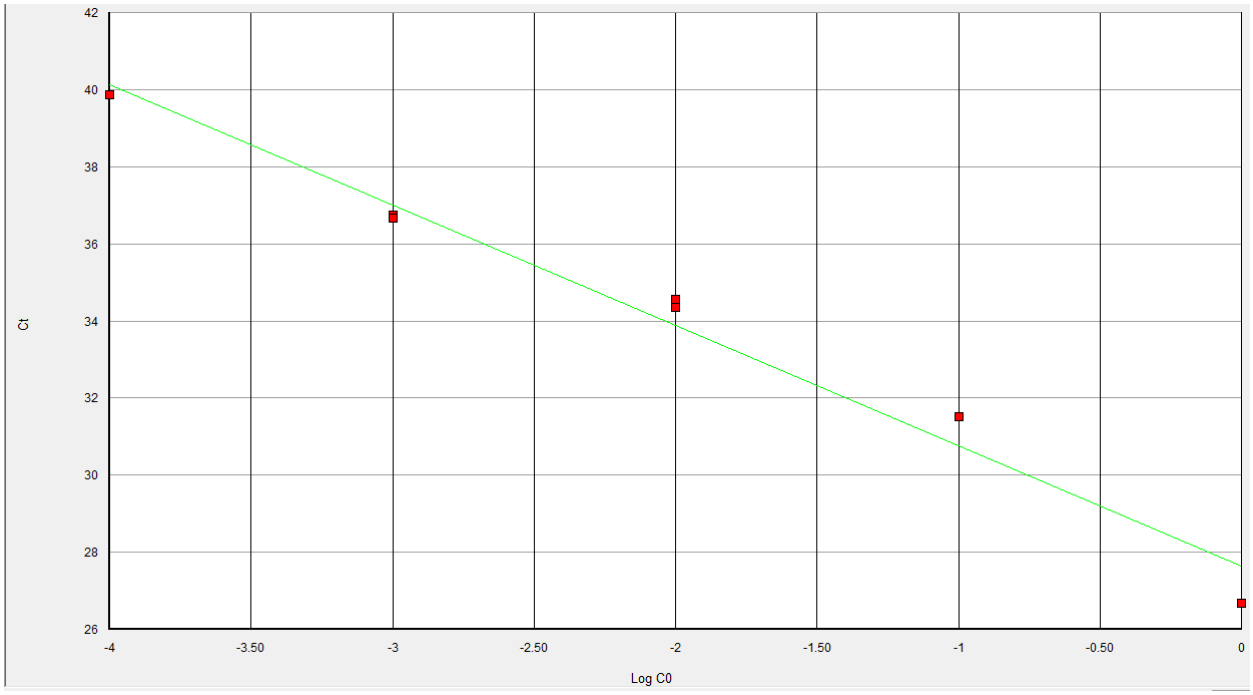

Efficiency: 110 %; slope: -3.1; R^2: 0.98

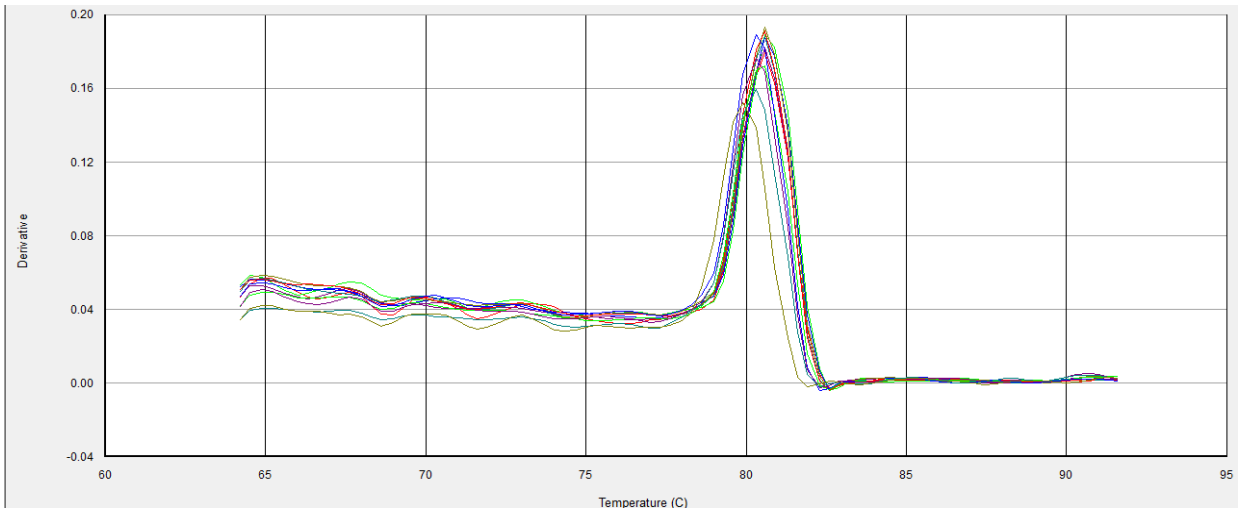

9.2.10 Hephaestin (HEPH)

Standard and melting curves were drawn for HEPH to ensure efficiency and specificity of amplification. See figures below.

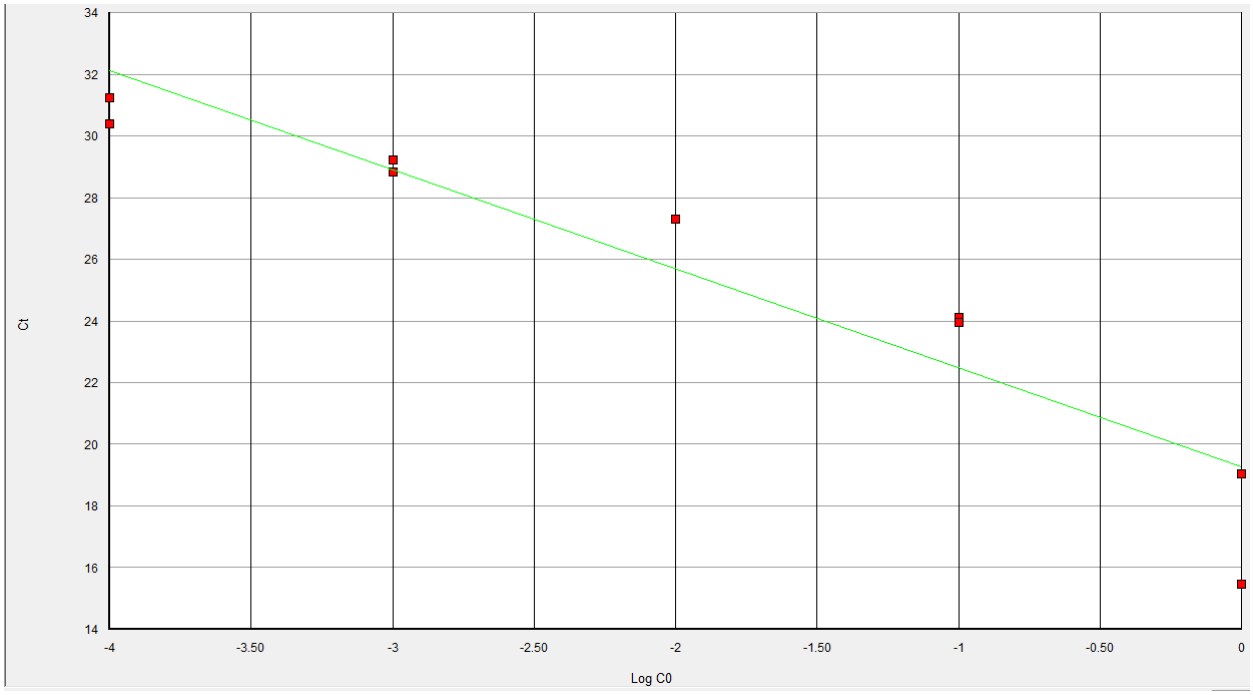

Efficiency: 105 %; slope: -3.2; R^2: 0.88

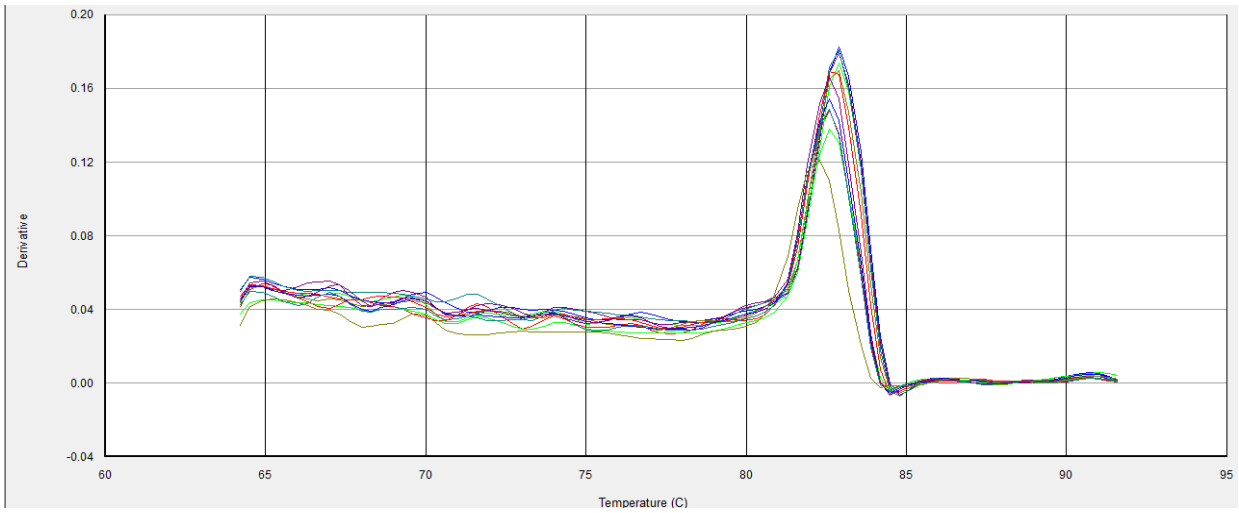

9.2.11 Copper transporter 1 (CTR1)

Standard and melting curves were drawn for CTR1 to ensure efficiency and specificity of amplification. See figures below.

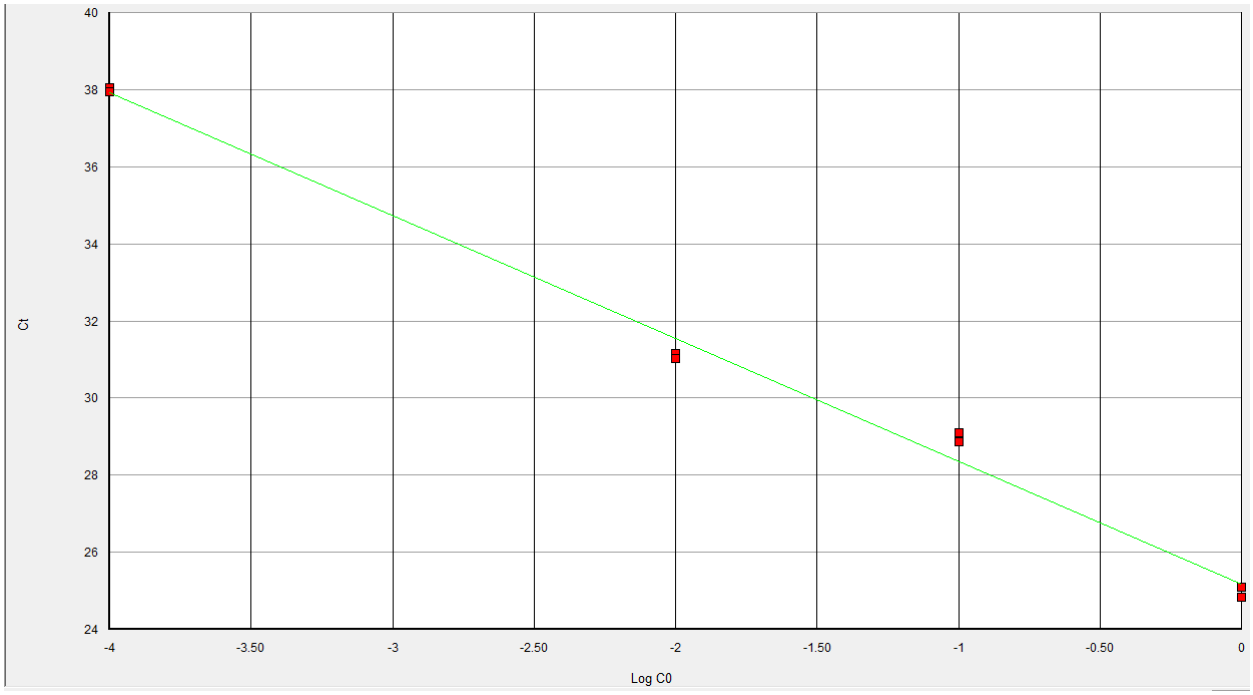

Efficiency: 105 %; slope: -3.2; R^2: 0.99

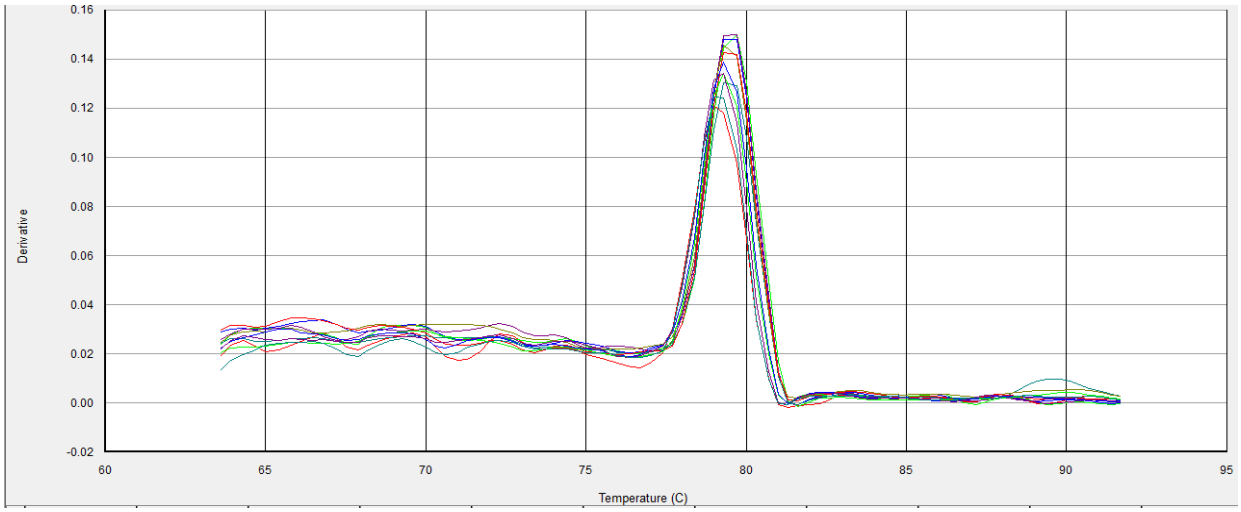

9.2.12 Human antioxidant protein homologue (HAH1)

Standard and melting curves were drawn for HAH1 to ensure efficiency and specificity of amplification. See figures below.

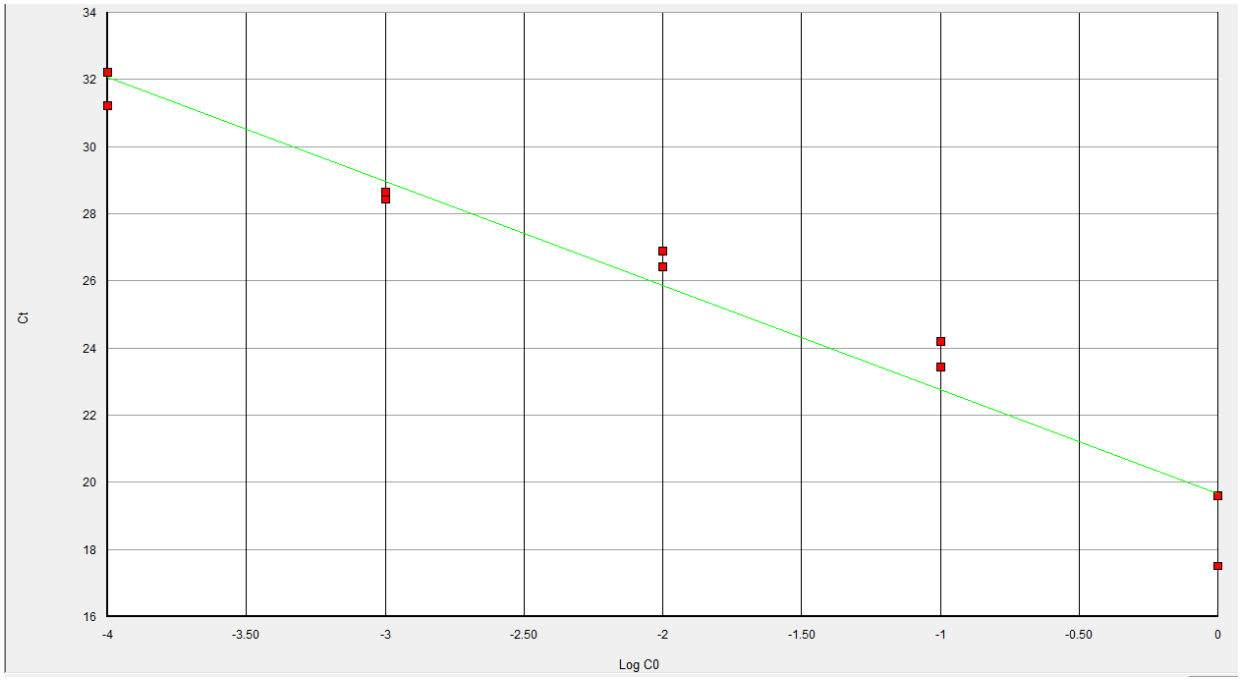

Efficiency: 110 %; slope: -3.1; R^2: 0.95

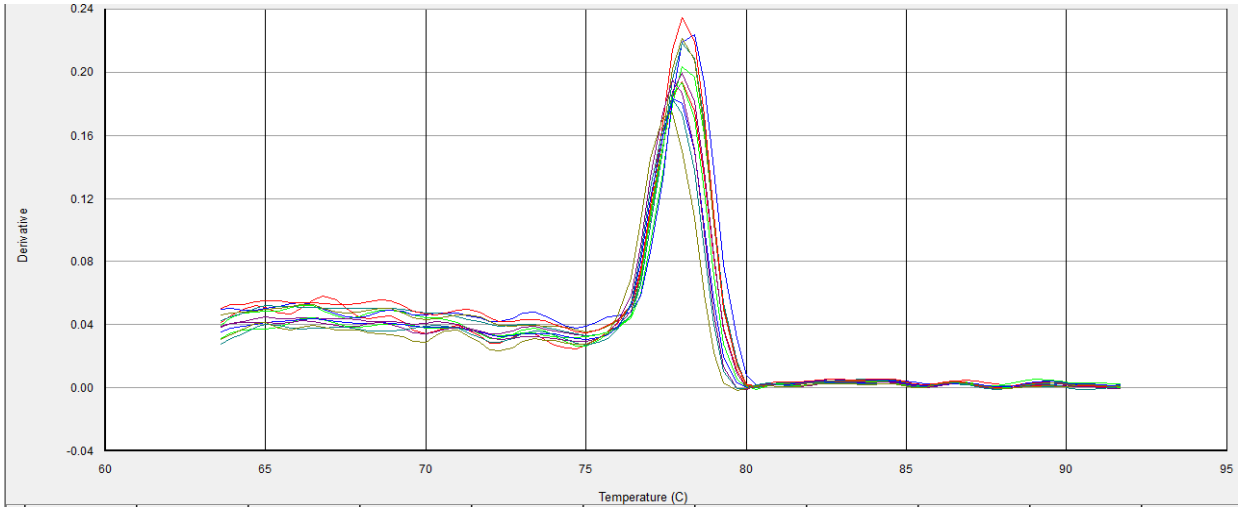

9.2.13 Copper transporting ATPase α polypeptide (ATP7A)

Standard and melting curves were drawn for ATP7A to ensure efficiency and specificity of amplification. See figures below.

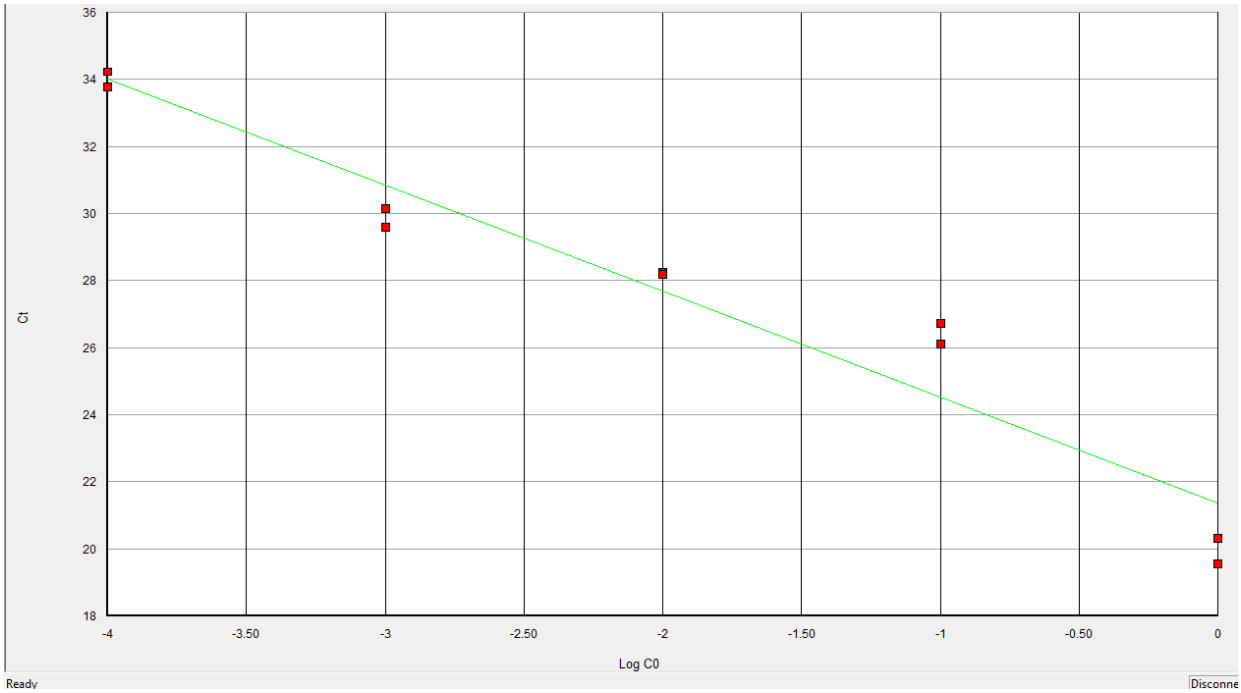

Efficiency: 105 %; slope: -3.2; R^2: 0.93

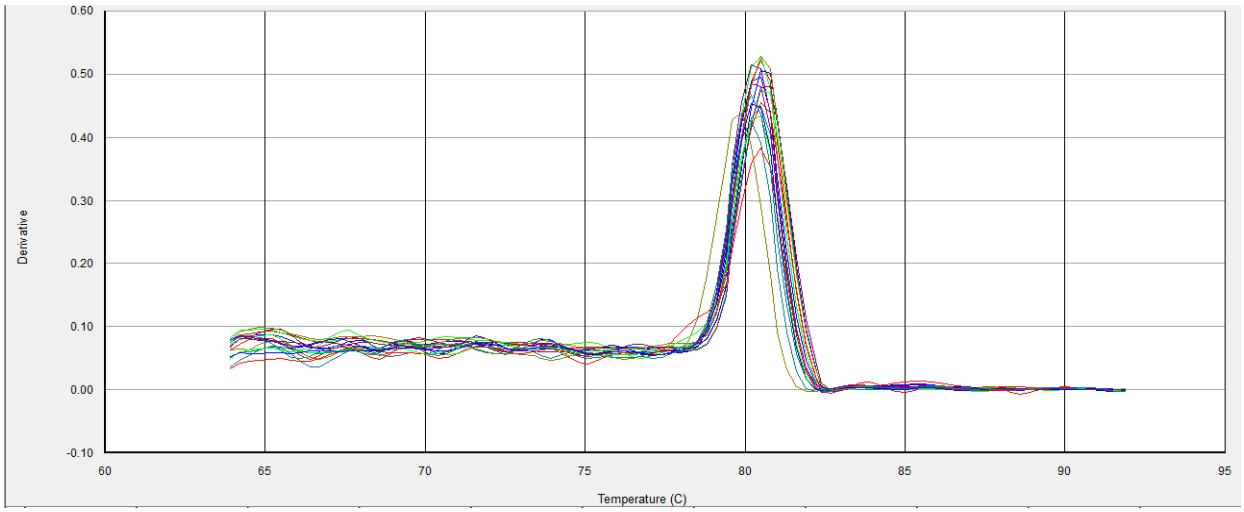

9.2.14 Copper transporting ATPase β polypeptide (ATP7B)

Standard and melting curves were drawn for ATP7B to ensure efficiency and specificity of amplification. See figures below.

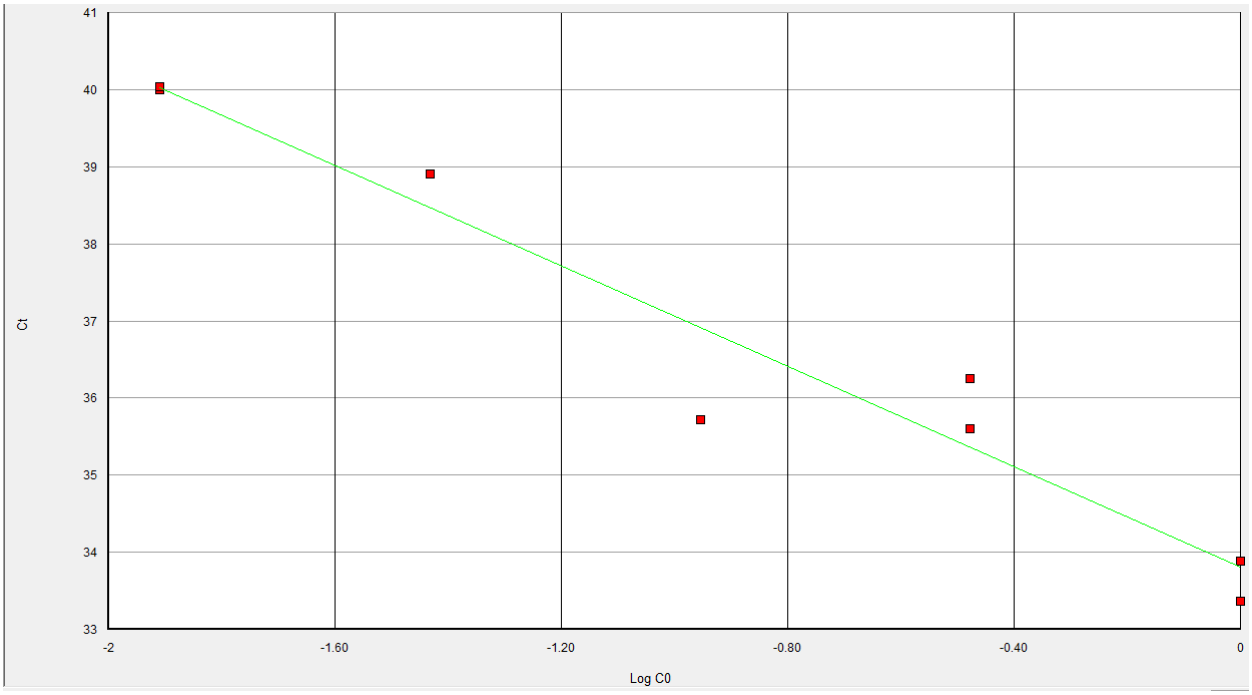

Efficiency: 101 %; slope: -3.3; R^2: 0.94

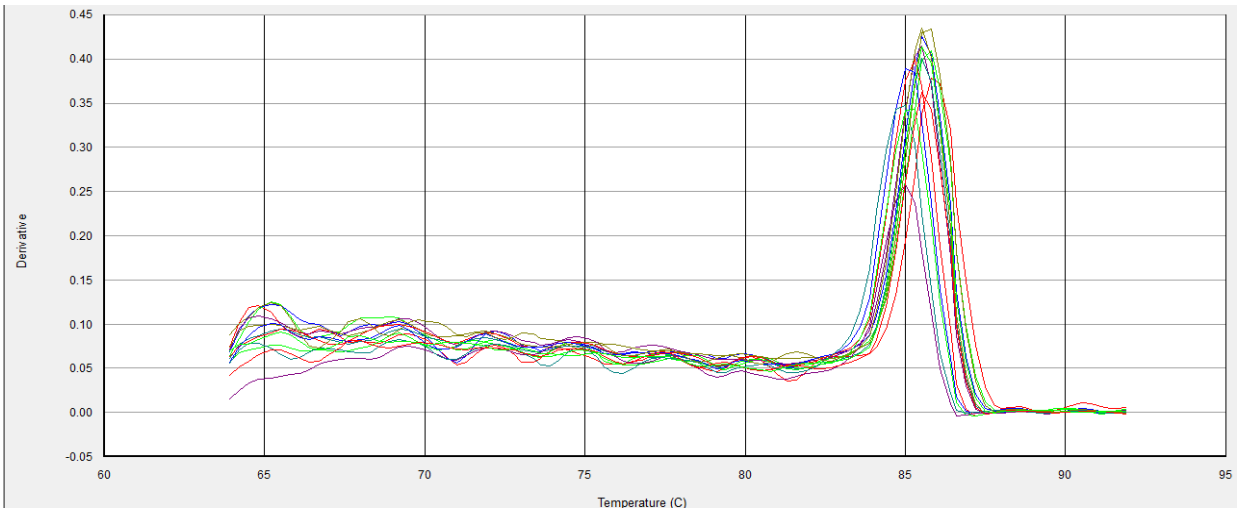

9.3 Bioinformatics analysis

Pathway analysis, ontological clustering and functional similarity clustering were applied, in **Chapter 3**, to transcriptome variation data from Caco-2 cells treated with a flavonoid-rich berry extract. Ingenuity® Pathway Analysis (IPA) software was used for pathway analysis and The DAVID Bioinformatics Resources (Ver. 6.7) were used for GO term enrichment and to find genes with a similar function to an initial gene of interest (Maaser & Borlak, 2008; Huang da *et al*, 2009). The following sections briefly describe the bioinformatics approaches applied with DAVID.

9.3.1 Pathway analysis

There are 6 steps involved in the generation of networks when using IPA software, these are described below briefly, and full descriptions are available from Ingenuity® user documentation:

1. *Focus genes* selection: "focus genes" refers to genes and gene products that are c eligible for inclusion in a network. Focus genes are considered eligible for network inclusion when they form more than one connection to other genes in the list or in the Ingenuity® knowledgebase. Focus genes are determined and sorted in decreasing order of their *triangle connectivity*, which ensures that each gene forms a connection to two other genes. The highest ranked focus gene will be the gene forming the highest number of "triangles" with neighboring genes, either from the submitted data set or from the Ingenuity® knowledgebase.

2. Networks constructed from focus genes: The highest ranked focus gene is removed to form a network, and is designated as a *seed gene*. Other focus genes are added until the maximum number of genes is included to form a network (default of 35 genes per network). Networks are grown by the assumption that "biological

functions involve locally dense interactions", thus genes are prioritised to grow a network when they form highest connections to the genes already present in the network. A metric called *specific connectivity* is applied to the genes prior to their addition to a network. Specific connectivity is the ratio between the number of genes intersecting an already present network and the total number of genes connected to the gene up for inclusion.

3. Apply *Linker genes* between small networks: This step starts with the smallest networks; they are connected to each other by *linker genes*. Linker genes are those that form connections between both networks and are more likely to be chosen for inclusion when they form denser connections. Networks are grown this way until they contain up to 35 genes (default cap to network size).

4. Introduce *Neighborhood genes:* Following network development and, where appropriate, the inclusion of linker genes; the networks are then grown by introducing *neighborhood genes*. Neighborhood genes are genes that form 2 or more connections to genes that are already on the periphery of the already present network. If no genes form 2 or more connections then genes that form a single connection are added. These neighborhood genes may be focus genes, but the probability is low, they are typically from the Ingenuity® global molecular network database.

5. Forming all *edges* between genes: All the genes selected for network inclusion in the above steps 1 to 4 are brought together and updated with annotations from the Ingenuity® knowledgebase. Connections between genes are referred to as *edges*, these include any links between genes, without discriminating the type of interaction, these include: direct interactions, indirect interactions, inhibition, stimulation, unknown interactions, etc.

6. Compute *p*-value and *network score*: After the networks are grown and the edges are formed *p*-values and the network score are calculated. The p-value is derived using a Fisher's exact test, where the number of focus genes in a given network is tested against the probability of finding the same number of "focus genes" when they are selected randomly from the global molecular network. The *network score* is then expressed as $-\log_{10}$ (*p*-value).

9.3.2 Gene ontology analysis

A Fisher's exact test is used as the statistical basis to define GO term enrichment in a given gene list. It is applied to determine if the number of genes from a GO term occurs disproportionately in one gene-list (i.e. experimental or user-submitted) relative to their occurrence in another gene-list (background) (Huang da *et al*, 2009). The example below shows a contingency table of the occurrence of *kinases* (example GO term) in an experimental gene-list, and their occurrence in a background gene list. The following examples are derived from the DAVID user documentation.

	Experimental / User-submitted gene list	Background / Human genome gene-list
Kinases	3	40
Not kinases	297	29 960

The fisher's exact *p*-value in this case would be 0.008. As $p \leq 0.05$, the experimental gene-list is said to be *enriched with Kinases*.

9.3.3 Functional similarity clustering and the Kappa score

Gene functional similarity clustering with DAVID is calculated through their "related gene searching" algorithm. This algorithm is based on the principle of overlapping GO terms between genes (Huang da *et al*, 2009).

Every gene is associated with multiple terms. If genes are associated with similar terms then they are involved in related biological mechanisms. A *Kappa* score, or *Kappa* statistic, is the outcome of the algorithm used in DAVID and this score ranges from 0 to 1. The higher the Kappa score, the stronger the agreement between the GO terms of those genes tested (Huang da *et al*, 2009). Below is a worked example to calculating the Kappa score, this examples is derived from the DAVID user documation.

Terms / Genes	Cell adhesion	Biological adhesion	Membrane	Integrin complex	Proteolysis	Apoptosis pathway
ADAM23	1	1	0	0	1	0
Itgb5	1	1	0	1	1	0

In the above contingency table, the genes to be compared are on the left-hand-side. The GO terms that either of the genes is associated with are along the top row. A binary code (1 or 0) is in place to identify if the GO term includes a gene of interest. A '1' denotes presence of the gene in the GO term and a '0' denotes its absence. In the table below is a count of the binary code, it is used to derive numerical values for the Kappa score algorithm, the parts of which are shown in brackets.

		ADAM23		Row totals
		1	0	
Itgb5	1	3 ($C_{1,1}$)	1 ($C_{0,1}$)	4 ($C_{1,*}$)
	0	0 ($C_{0,1}$)	2 ($C_{0,0}$)	2 ($C_{0,*}$)
Column totals		3 ($C_{*,1}$)	3 ($C_{*,0}$)	6 (T_{ab})

The above values can be substituted into the following equations, where K_{ab} is the Kappa score and the other alphabetical codes are represented in the contingency table above.

$$O_{ab} = \frac{C_{1,1} + C_{0,1}}{T_{ab}} = \frac{3 + 2}{6} = 0.83$$

$$A_{ab} = \frac{C_{*,1} \bullet C_{1,*} + C_{*,0} \bullet C_{0,*}}{T_{ab} \bullet T_{ab}} = \frac{3 \bullet 4 + 3 \bullet 2}{6 \bullet 6} = 0.5$$

$$K_{ab} = \frac{O_{ab} - A_{ab}}{1 - A_{ab}} = \frac{0.83 - 0.5}{1 - 0.5} = 0.66$$

If $K_{ab} < 0.25$ then genes tested have low agreement; if $K_{ab} = 0.25 - 0.5$ genes have moderate agreement; if $K_{ab} = 0.5 – 0.75$ genes have high agreement; and if $K_{ab} = 0.75 – 1$ genes have very high agreement. Therefore given the example above, $K_{ab} = 0.66$, this states that the functions of the genes ADAM23 and Itgb5 is in high agreement.

9.4 Differentially expressed genes

Following microarray analysis of Caco-2 cell mRNA following treatment with a flavonoid rich berry extract, approximately 2400 genes were found to be differentially expressed. Below is a full list of the annotated genes organised in decreasing differential expression from the control, i.e. highest fold increase to lowest fold-decrease.

Fold change	Affymetrix ID	Gene symbol	Entrez gene name
102.329	205749_at	CYP1A1	cytochrome P450, family 1, subfamily A, polypeptide 1
29.512	202859_x_at	IL8	interleukin 8
27.542	204475_at	MMP1	matrix metallopeptidase 1 (interstitial collagenase)
27.542	212190_at	SERPINE2	serpin peptidase inhibitor, clade E (nexin, plasminogen activator inhibitor type 1), member 2
23.988	211506_s_at	IL8	interleukin 8
23.988	210845_s_at	PLAUR	plasminogen activator, urokinase receptor
18.197	217678_at	SLC7A11	solute carrier family 7, (cationic amino acid transporter, y+ system) member 11
16.982	209457_at	DUSP5	dual specificity phosphatase 5
15.849	213895_at	EMP1	epithelial membrane protein 1
15.849	204420_at	FOSL1	FOS-like antigen 1
15.849	209921_at	SLC7A11	solute carrier family 7, (cationic amino acid transporter, y+ system) member 11
14.791	215034_s_at	TM4SF1	transmembrane 4 L six family member 1
13.804	207517_at	LAMC2	laminin, gamma 2
13.804	36711_at	MAFF	v-maf musculoaponeurotic fibrosarcoma oncogene homolog F (avian)
12.882	206561_s_at	AKR1B10	aldo-keto reductase family 1, member B10 (aldose reductase)
12.882	201925_s_at	CD55	CD55 molecule, decay accelerating factor for complement (Cromer blood group)
12.023	202672_s_at	ATF3	activating transcription factor 3
12.023	201325_s_at	EMP1	epithelial membrane protein 1
12.023	203108_at	GPRC5A	G protein-coupled receptor, family C, group 5, member A
12.023	218468_s_at	GREM1	gremlin 1, cysteine knot superfamily, homolog (Xenopus laevis)

Fold change	Affymetrix ID	Gene symbol	Entrez gene name
12.023	205032_at	ITGA2	integrin, alpha 2 (CD49B, alpha 2 subunit of VLA-2 receptor)
11.220	218469_at	GREM1	gremlin 1, cysteine knot superfamily, homolog (Xenopus laevis)
11.220	217996_at	PHLDA1	pleckstrin homology-like domain, family A, member 1
11.220	214866_at	PLAUR	plasminogen activator, urokinase receptor
10.471	220468_at	ARL14	ADP-ribosylation factor-like 14
10.471	219799_s_at	DHRS9	dehydrogenase/reductase (SDR family) member 9
10.471	219508_at	GCNT3	glucosaminyl (N-acetyl) transferase 3, mucin type
10.471	204286_s_at	PMAIP1	phorbol-12-myristate-13-acetate-induced protein 1
10.471	209387_s_at	TM4SF1	transmembrane 4 L six family member 1
10.471	202241_at	TRIB1	tribbles homolog 1 (Drosophila)
9.772	201926_s_at	CD55	CD55 molecule, decay accelerating factor for complement (Cromer blood group)
9.120	211889_x_at	CEACAM1	carcinoembryonic antigen-related cell adhesion molecule 1 (biliary glycoprotein)
9.120	201884_at	CEACAM5	carcinoembryonic antigen-related cell adhesion molecule 5
9.120	203821_at	HBEGF	heparin-binding EGF-like growth factor
9.120	213953_at	KRT20	keratin 20
9.120	219557_s_at	NRIP3	nuclear receptor interacting protein 3
9.120	217997_at	PHLDA1	pleckstrin homology-like domain, family A, member 1
9.120	204285_s_at	PMAIP1	phorbol-12-myristate-13-acetate-induced protein 1
8.511	206576_s_at	CEACAM1	carcinoembryonic antigen-related cell adhesion molecule 1 (biliary glycoprotein)
8.511	211883_x_at	CEACAM1	carcinoembryonic antigen-related cell adhesion molecule 1 (biliary glycoprotein)
8.511	209803_s_at	PHLDA2	pleckstrin homology-like domain, family A, member 2
8.511	201266_at	TXNRD1	thioredoxin reductase 1
7.943	209498_at	CEACAM1	carcinoembryonic antigen-related cell adhesion molecule 1 (biliary glycoprotein)
7.943	204698_at	ISG20	interferon stimulated exonuclease gene 20kDa
7.943	202267_at	LAMC2	laminin, gamma 2
7.413	201324_at	EMP1	epithelial membrane protein 1
7.413	203499_at	EPHA2	EPH receptor A2
7.413	206429_at	F2RL1	coagulation factor II (thrombin) receptor-like 1
7.413	221667_s_at	HSPB8	heat shock 22kDa protein 8
7.413	205302_at	IGFBP1	insulin-like growth factor binding protein 1

Fold change	Affymetrix ID	Gene symbol	Entrez gene name
7.413	201466_s_at	JUN	jun oncogene
7.413	210665_at	TFPI	tissue factor pathway inhibitor (lipoprotein-associated coagulation inhibitor)
7.413	212665_at	TIPARP	TCDD-inducible poly(ADP-ribose) polymerase
7.413	202504_at	TRIM29	tripartite motif-containing 29
6.918	205014_at	FGFBP1	fibroblast growth factor binding protein 1
6.918	207574_s_at	GADD45B	growth arrest and DNA-damage-inducible, beta
6.918	202831_at	GPX2	glutathione peroxidase 2 (gastrointestinal)
6.918	214056_at	MCL1	myeloid cell leukaemia sequence 1 (BCL2-related)
6.918	217999_s_at	PHLDA1	pleckstrin homology-like domain, family A, member 1
6.918	33323_r_at	SFN	stratifin
6.457	210538_s_at	BIRC3	baculoviral IAP repeat-containing 3
6.457	209304_x_at	GADD45B	growth arrest and DNA-damage-inducible, beta
6.457	203925_at	GCLM	glutamate-cysteine ligase, modifier subunit
6.457	38037_at	HBEGF	heparin-binding EGF-like growth factor
6.457	33304_at	ISG20	interferon stimulated exonuclease gene 20kDa
6.457	208960_s_at	KLF6	Kruppel-like factor 6
6.457	216248_s_at	NR4A2	nuclear receptor subfamily 4, group A, member 2
6.457	210664_s_at	TFPI	tissue factor pathway inhibitor (lipoprotein-associated coagulation inhibitor)
6.457	218368_s_at	TNFRSF12A	tumor necrosis factor receptor superfamily, member 12A
6.457	221962_s_at	UBE2H	ubiquitin-conjugating enzyme E2H (UBC8 homolog, yeast)
6.026	201041_s_at	DUSP1	dual specificity phosphatase 1
6.026	215177_s_at	ITGA6	integrin, alpha 6
6.026	213281_at	JUN	jun oncogene
6.026	33322_i_at	SFN	stratifin
6.026	209386_at	TM4SF1	transmembrane 4 L six family member 1
5.623	209735_at	ABCG2	ATP-binding cassette, sub-family G (WHITE), member 2
5.623	215913_s_at	GULP1	GULP, engulfment adaptor PTB domain containing 1
5.623	200798_x_at	MCL1	myeloid cell leukaemia sequence 1 (BCL2-related)
5.623	201939_at	PLK2	polo-like kinase 2 (Drosophila)
5.623	217741_s_at	ZFAND5	zinc finger, AN1-type domain 5

Fold change	Affymetrix ID	Gene symbol	Entrez gene name
5.248	204602_at	DKK1	dickkopf homolog 1 (Xenopus laevis)
5.248	221577_x_at	GDF15	growth differentiation factor 15
5.248	208961_s_at	KLF6	Kruppel-like factor 6
5.248	212099_at	RHOB	ras homolog gene family, member B
5.248	210260_s_at	TNFAIP8	tumor necrosis factor, alpha-induced protein 8
4.898	219474_at	C3ORF52	chromosome 3 open reading frame 52
4.898	207147_at	DLX2	distal-less homeobox 2
4.898	218498_s_at	ERO1L	ERO1-like (S. cerevisiae)
4.898	204472_at	GEM	GTP binding protein overexpressed in skeletal muscle
4.898	207160_at	IL12A	interleukin 12A (natural killer cell stimulatory factor 1, cytotoxic lymphocyte maturation factor 1, p35)
4.898	203144_s_at	KIAA0040	KIAA0040
4.898	204622_x_at	NR4A2	nuclear receptor subfamily 4, group A, member 2
4.898	204435_at	NUPL1	nucleoporin like 1
4.898	202627_s_at	SERPINE1	serpin peptidase inhibitor, clade E (nexin, plasminogen activator inhibitor type 1), member 1
4.898	204011_at	SPRY2	sprouty homolog 2 (Drosophila)
4.898	208296_x_at	TNFAIP8	tumor necrosis factor, alpha-induced protein 8
4.898	214581_x_at	TNFRSF21	tumor necrosis factor receptor superfamily, member 21
4.898	221765_at	UGCG	UDP-glucose ceramide glucosyltransferase
4.898	204881_s_at	UGCG	UDP-glucose ceramide glucosyltransferase
4.571	218723_s_at	C13ORF15	chromosome 13 open reading frame 15
4.571	203757_s_at	CEACAM6	carcinoembryonic antigen-related cell adhesion molecule 6 (non-specific cross reacting antigen)
4.571	219500_at	CLCF1	cardiotrophin-like cytokine factor 1
4.571	201428_at	CLDN4	claudin 4
4.571	209967_s_at	CREM	cAMP responsive element modulator
4.571	202669_s_at	EFNB2	ephrin-B2
4.571	202949_s_at	FHL2	four and a half LIM domains 2
4.571	209305_s_at	GADD45B	growth arrest and DNA-damage-inducible, beta
4.571	201464_x_at	JUN	jun oncogene
4.571	202067_s_at	LDLR	low density lipoprotein receptor
4.571	205479_s_at	PLAU	plasminogen activator, urokinase

Fold change	Affymetrix ID	Gene symbol	Entrez gene name
4.571	202014_at	PPP1R15A	protein phosphatase 1, regulatory (inhibitor) subunit 15A
4.571	202786_at	STK39	serine threonine kinase 39 (STE20/SPS1 homolog, yeast)
4.571	213258_at	TFPI	tissue factor pathway inhibitor (lipoprotein-associated coagulation inhibitor)
4.571	203167_at	TIMP2	TIMP metallopeptidase inhibitor 2
4.571	203234_at	UPP1	uridine phosphorylase 1
4.571	215150_at	YOD1	YOD1 OTU deubiquinating enzyme 1 homolog (S. cerevisiae)
4.571	201531_at	ZFP36	zinc finger protein 36, C3H type, homolog (mouse)
4.266	205239_at	AREG	amphiregulin
4.266	211848_s_at	CEACAM7	carcinoembryonic antigen-related cell adhesion molecule 7
4.266	202668_at	EFNB2	ephrin-B2
4.266	210007_s_at	GPD2	glycerol-3-phosphate dehydrogenase 2 (mitochondrial)
4.266	204137_at	GPR137B	G protein-coupled receptor 137B
4.266	201656_at	ITGA6	integrin, alpha 6
4.266	201473_at	JUNB	jun B proto-oncogene
4.266	203143_s_at	KIAA0040	KIAA0040
4.266	210365_at	RUNX1	runt-related transcription factor 1
4.266	201249_at	SLC2A1	solute carrier family 2 (facilitated glucose transporter), member 1
4.266	204526_s_at	TBC1D8	TBC1 domain family, member 8 (with GRAM domain)
4.266	214168_s_at	TJP1	tight junction protein 1 (zona occludens 1)
4.266	218856_at	TNFRSF21	tumor necrosis factor receptor superfamily, member 21
3.981	205566_at	ABHD2	abhydrolase domain containing 2
3.981	214696_at	C17ORF91	chromosome 17 open reading frame 91
3.981	206199_at	CEACAM7	carcinoembryonic antigen-related cell adhesion molecule 7
3.981	207630_s_at	CREM	cAMP responsive element modulator
3.981	208893_s_at	DUSP6	dual specificity phosphatase 6
3.981	201313_at	ENO2	enolase 2 (gamma, neuronal)
3.981	209189_at	FOS	v-fos FBJ murine osteosarcoma viral oncogene homolog
3.981	208868_s_at	GABARAPL1	GABA(A) receptor-associated protein like 1
3.981	202923_s_at	GCLC	glutamate-cysteine ligase, catalytic subunit
3.981	214157_at	GNAS	GNAS complex locus

Fold change	Affymetrix ID	Gene symbol	Entrez gene name
3.981	201389_at	ITGA5	integrin, alpha 5 (fibronectin receptor, alpha polypeptide)
3.981	217173_s_at	LDLR	low density lipoprotein receptor
3.981	202674_s_at	LMO7	LIM domain 7
3.981	213909_at	LRRC15	leucine rich repeat containing 15
3.981	214827_at	PARD6B	par-6 partitioning defective 6 homolog beta (C. elegans)
3.981	37028_at	PPP1R15A	protein phosphatase 1, regulatory (inhibitor) subunit 15A
3.981	202388_at	RGS2	regulator of G-protein signaling 2, 24kDa
3.981	202129_s_at	RIOK3	RIO kinase 3 (yeast)
3.981	219614_s_at	SLC6A20	solute carrier family 6 (proline IMINO transporter), member 20
3.981	204368_at	SLCO2A1	solute carrier organic anion transporter family, member 2A1
3.981	221489_s_at	SPRY4	sprouty homolog 4 (Drosophila)
3.715	213497_at	ABTB2	ankyrin repeat and BTB (POZ) domain containing 2
3.715	203065_s_at	CAV1	caveolin 1, caveolae protein, 22kDa
3.715	203324_s_at	CAV2	caveolin 2
3.715	211657_at	CEACAM6	carcinoembryonic antigen-related cell adhesion molecule 6 (non-specific cross reacting antigen)
3.715	206198_s_at	CEACAM7	carcinoembryonic antigen-related cell adhesion molecule 7
3.715	203729_at	EMP3	epithelial membrane protein 3
3.715	220124_at	GAN	gigaxonin
3.715	220585_at	HKDC1	hexokinase domain containing 1
3.715	209185_s_at	IRS2	insulin receptor substrate 2
3.715	203068_at	KLHL21	kelch-like 21 (Drosophila)
3.715	208934_s_at	LGALS8	lectin, galactoside-binding, soluble, 8
3.715	213684_s_at	PDLIM5	PDZ and LIM domain 5
3.715	208300_at	PTPRH	protein tyrosine phosphatase, receptor type, H
3.715	210675_s_at	PTPRR	protein tyrosine phosphatase, receptor type, R
3.715	205205_at	RELB	v-rel reticuloendotheliosis viral oncogene homolog B
3.715	219710_at	SH3TC2	SH3 domain and tetratricopeptide repeats 2
3.715	219911_s_at	SLCO4A1	solute carrier organic anion transporter family, member 4A1
3.715	209676_at	TFPI	tissue factor pathway inhibitor (lipoprotein-associated coagulation inhibitor)
3.715	213349_at	TMCC1	transmembrane and coiled-coil domain family 1

Fold change	Affymetrix ID	Gene symbol	Entrez gene name
3.715	218647_s_at	YRDC	yrdC domain containing (E. coli)
3.715	210275_s_at	ZFAND5	zinc finger, AN1-type domain 5
3.467	204455_at	DST	dystonin
3.467	208891_at	DUSP6	dual specificity phosphatase 6
3.467	210999_s_at	GRB10	growth factor receptor-bound protein 10
3.467	209098_s_at	JAG1	jagged 1 (Alagille syndrome)
3.467	204401_at	KCNN4	potassium intermediate/small conductance calcium-activated channel, subfamily N, member 4
3.467	210732_s_at	LGALS8	lectin, galactoside-binding, soluble, 8
3.467	221994_at	PDLIM5	PDZ and LIM domain 5
3.467	216804_s_at	PDLIM5	PDZ and LIM domain 5
3.467	202458_at	PRSS23	protease, serine, 23
3.467	212311_at	SERINC2	serine incorporator 2
3.467	219682_s_at	TBX3	T-box 3
3.467	219058_x_at	TINAGL1	tubulointerstitial nephritis antigen-like 1
3.467	218999_at	TMEM140	transmembrane protein 140
3.236	203946_s_at	ARG2	arginase, type II
3.236	206665_s_at	BCL2L1	BCL2-like 1
3.236	212097_at	CAV1	caveolin 1, caveolae protein, 22kDa
3.236	209850_s_at	CDC42EP2	CDC42 effector protein (Rho GTPase binding) 2
3.236	202284_s_at	CDKN1A	cyclin-dependent kinase inhibitor 1A (p21, Cip1)
3.236	213554_s_at	CDV3	CDV3 homolog (mouse)
3.236	202536_at	CHMP2B	chromatin modifying protein 2B
3.236	201693_s_at	EGR1	early growth response 1
3.236	211603_s_at	ETV4	ets variant 4
3.236	213341_at	FEM1C	fem-1 homolog c (C. elegans)
3.236	211458_s_at	GABARAPL1	GABA(A) receptor-associated protein like 1
3.236	208138_at	GAST	gastrin
3.236	202922_at	GCLC	glutamate-cysteine ligase, catalytic subunit
3.236	209410_s_at	GRB10	growth factor receptor-bound protein 10
3.236	206342_x_at	IDS	iduronate 2-sulfatase

Fold change	Affymetrix ID	Gene symbol	Entrez gene name
3.236	201631_s_at	IER3	immediate early response 3
3.236	202146_at	IFRD1	interferon-related developmental regulator 1
3.236	202147_s_at	IFRD1	interferon-related developmental regulator 1
3.236	209184_s_at	IRS2	insulin receptor substrate 2
3.236	218474_s_at	KCTD5	potassium channel tetramerisation domain containing 5
3.236	218823_s_at	KCTD9	potassium channel tetramerisation domain containing 9
3.236	203390_s_at	KIF3C	kinesin family member 3C
3.236	208785_s_at	MAP1LC3B	microtubule-associated protein 1 light chain 3 beta
3.236	212473_s_at	MICAL2	microtubule associated monooxygenase, calponin and LIM domain containing 2
3.236	212472_at	MICAL2	microtubule associated monooxygenase, calponin and LIM domain containing 2
3.236	200787_s_at	PEA15	phosphoprotein enriched in astrocytes 15
3.236	206636_at	RASA2	RAS p21 protein activator 2
3.236	212724_at	RND3	Rho family GTPase 3
3.236	202684_s_at	RNMT	RNA (guanine-7-) methyltransferase
3.236	204351_at	S100P	S100 calcium binding protein P
3.236	205691_at	SYNGR3	synaptogyrin 3
3.236	209191_at	TUBB6	tubulin, beta 6
3.236	211764_s_at	UBE2D1	ubiquitin-conjugating enzyme E2D 1 (UBC4/5 homolog, yeast)
3.020	218964_at	ARID3B	AT rich interactive domain 3B (BRIGHT-like)
3.020	205780_at	BIK	BCL2-interacting killer (apoptosis-inducing)
3.020	208653_s_at	CD164	CD164 molecule, sialomucin
3.020	201694_s_at	EGR1	early growth response 1
3.020	45297_at	EHD2	EH-domain containing 2
3.020	213506_at	F2RL1	coagulation factor II (thrombin) receptor-like 1
3.020	208869_s_at	GABARAPL1	GABA(A) receptor-associated protein like 1
3.020	202543_s_at	GMFB	glia maturation factor, beta
3.020	204235_s_at	GULP1	GULP, engulfment adaptor PTB domain containing 1
3.020	204237_at	GULP1	GULP, engulfment adaptor PTB domain containing 1
3.020	220266_s_at	KLF4	Kruppel-like factor 4 (gut)
3.020	202068_s_at	LDLR	low density lipoprotein receptor

Fold change	Affymetrix ID	Gene symbol	Entrez gene name
3.020	202679_at	NPC1	Niemann-Pick disease, type C1
3.020	213372_at	PAQR3	progestin and adipoQ receptor family member III
3.020	208383_s_at	PCK1	phosphoenolpyruvate carboxykinase 1 (soluble)
3.020	218951_s_at	PLCXD1	phosphatidylinositol-specific phospholipase C, X domain containing 1
3.020	207223_s_at	ROD1	ROD1 regulator of differentiation 1 (S. pombe)
3.020	218928_s_at	SLC37A1	solute carrier family 37 (glycerol-3-phosphate transporter), member 1
3.020	205016_at	TGFA	transforming growth factor, alpha
3.020	213191_at	TICAM1	toll-like receptor adaptor molecule 1
3.020	209118_s_at	TUBA1A	tubulin, alpha 1a
3.020	214590_s_at	UBE2D1	ubiquitin-conjugating enzyme E2D 1 (UBC4/5 homolog, yeast)
3.020	217785_s_at	YKT6	YKT6 v-SNARE homolog (S. cerevisiae)
2.818	200615_s_at	AP2B1	adaptor-related protein complex 2, beta 1 subunit
2.818	210896_s_at	ASPH	aspartate beta-hydroxylase
2.818	200921_s_at	BTG1	B-cell translocation gene 1, anti-proliferative
2.818	219720_s_at	C14ORF118	chromosome 14 open reading frame 118
2.818	213548_s_at	CDV3	CDV3 homolog (mouse)
2.818	217028_at	CXCR4	chemokine (C-X-C motif) receptor 4
2.818	208892_s_at	DUSP6	dual specificity phosphatase 6
2.818	213310_at	EIF2C2	eukaryotic translation initiation factor 2C, 2
2.818	211535_s_at	FGFR1	fibroblast growth factor receptor 1
2.818	206074_s_at	HMGA1	high mobility group AT-hook 1
2.818	218611_at	IER5	immediate early response 5
2.818	204990_s_at	ITGB4	integrin, beta 4
2.818	209099_x_at	JAG1	jagged 1 (Alagille syndrome)
2.818	216268_s_at	JAG1	jagged 1 (Alagille syndrome)
2.818	221841_s_at	KLF4	Kruppel-like factor 4 (gut)
2.818	208936_x_at	LGALS8	lectin, galactoside-binding, soluble, 8
2.818	208786_s_at	MAP1LC3B	microtubule-associated protein 1 light chain 3 beta
2.818	218295_s_at	NUP50	nucleoporin 50kDa
2.818	200788_s_at	PEA15	phosphoprotein enriched in astrocytes 15

Fold change	Affymetrix ID	Gene symbol	Entrez gene name
2.818	219045_at	RHOF	ras homolog gene family, member F (in filopodia)
2.818	221269_s_at	SH3BGRL3	SH3 domain binding glutamic acid-rich protein like 3
2.818	213843_x_at	SLC6A8	solute carrier family 6 (neurotransmitter transporter, creatine), member 8
2.818	205547_s_at	TAGLN	transgelin
2.818	201208_s_at	TNFAIP1	tumor necrosis factor, alpha-induced protein 1 (endothelial)
2.818	202643_s_at	TNFAIP3	tumor necrosis factor, alpha-induced protein 3
2.818	203672_x_at	TPMT	thiopurine S-methyltransferase
2.818	204141_at	TUBB2A	tubulin, beta 2A
2.818	221291_at	ULBP2	UL16 binding protein 2
2.818	210935_s_at	WDR1	WD repeat domain 1
2.630	221927_s_at	ABHD11	abhydrolase domain containing 11
2.630	207992_s_at	AMPD3	adenosine monophosphate deaminase (isoform E)
2.630	201012_at	ANXA1	annexin A1
2.630	203910_at	ARHGAP29	Rho GTPase activating protein 29
2.630	211716_x_at	ARHGDIA	Rho GDP dissociation inhibitor (GDI) alpha
2.630	213606_s_at	ARHGDIA	Rho GDP dissociation inhibitor (GDI) alpha
2.630	201168_x_at	ARHGDIA	Rho GDP dissociation inhibitor (GDI) alpha
2.630	215037_s_at	BCL2L1	BCL2-like 1
2.630	200920_s_at	BTG1	B-cell translocation gene 1, anti-proliferative
2.630	213134_x_at	BTG3	BTG family, member 3
2.630	205548_s_at	BTG3	BTG family, member 3
2.630	200776_s_at	BZW1	basic leucine zipper and W2 domains 1
2.630	219856_at	C1ORF116	chromosome 1 open reading frame 116
2.630	202575_at	CRABP2	cellular retinoic acid binding protein 2
2.630	206374_at	DUSP8	dual specificity phosphatase 8
2.630	219207_at	EDC3	enhancer of mRNA decapping 3 homolog (S. cerevisiae)
2.630	205767_at	EREG	epiregulin
2.630	200859_x_at	FLNA	filamin A, alpha (actin binding protein 280)
2.630	213746_s_at	FLNA	filamin A, alpha (actin binding protein 280)
2.630	214752_x_at	FLNA	filamin A, alpha (actin binding protein 280)

Fold change	Affymetrix ID	Gene symbol	Entrez gene name
2.630	215243_s_at	GJB3	gap junction protein, beta 3, 31kDa
2.630	205770_at	GSR	glutathione reductase
2.630	202558_s_at	HSPA13	heat shock protein 70kDa family, member 13
2.630	202439_s_at	IDS	iduronate 2-sulfatase
2.630	203627_at	IGF1R	insulin-like growth factor 1 receptor
2.630	204116_at	IL2RG	interleukin 2 receptor, gamma (severe combined immunodeficiency)
2.630	208540_x_at	LOC729659	S100 calcium binding protein A11 pseudogene
2.630	214057_at	MCL1	myeloid cell leukaemia sequence 1 (BCL2-related)
2.630	207233_s_at	MITF	microphthalmia-associated transcription factor
2.630	211071_s_at	MLLT11	myeloid/lymphoid or mixed-lineage leukaemia (trithorax homolog, Drosophila); translocated to, 11
2.630	210048_at	NAPG	N-ethylmaleimide-sensitive factor attachment protein, gamma
2.630	207543_s_at	P4HA1	prolyl 4-hydroxylase, alpha polypeptide I
2.630	203242_s_at	PDLIM5	PDZ and LIM domain 5
2.630	209193_at	PIM1	pim-1 oncogene
2.630	635_s_at	PPP2R5B	protein phosphatase 2, regulatory subunit B', beta isoform
2.630	215707_s_at	PRNP	prion protein
2.630	206084_at	PTPRR	protein tyrosine phosphatase, receptor type, R
2.630	209882_at	RIT1	Ras-like without CAAX 1
2.630	204668_at	RNF24	ring finger protein 24
2.630	200660_at	S100A11	S100 calcium binding protein A11
2.630	201543_s_at	SAR1A	SAR1 homolog A (S. cerevisiae)
2.630	200958_s_at	SDCBP	syndecan binding protein (syntenin)
2.630	212314_at	SERINC2	serine incorporator 2
2.630	202856_s_at	SLC16A3	solute carrier family 16, member 3 (monocarboxylic acid transporter 4)
2.630	202855_s_at	SLC16A3	solute carrier family 16, member 3 (monocarboxylic acid transporter 4)
2.630	201250_s_at	SLC2A1	solute carrier family 2 (facilitated glucose transporter), member 1
2.630	216202_s_at	SPTLC2	serine palmitoyltransferase, long chain base subunit 2
2.630	201471_s_at	SQSTM1	sequestosome 1
2.630	208322_s_at	ST3GAL1	ST3 beta-galactoside alpha-2,3-sialyltransferase 1
2.630	203439_s_at	STC2	stanniocalcin 2

Fold change	Affymetrix ID	Gene symbol	Entrez gene name
2.630	221592_at	TBC1D8	TBC1 domain family, member 8 (with GRAM domain)
2.630	203085_s_at	TGFB1	transforming growth factor, beta 1
2.630	217730_at	TMBIM1	transmembrane BAX inhibitor motif containing 1
2.630	208596_s_at	UGT1A7	UDP glucuronosyltransferase 1 family, polypeptide A7
2.630	210064_s_at	UPK1B	uroplakin 1B
2.630	212533_at	WEE1	WEE1 homolog (S. pombe)
2.630	212860_at	ZDHHC18	zinc finger, DHHC-type containing 18
2.455	209994_s_at	ABCB4	ATP-binding cassette, sub-family B (MDR/TAP), member 4
2.455	202912_at	ADM	adrenomedullin
2.455	205263_at	BCL10	B-cell CLL/lymphoma 10
2.455	212312_at	BCL2L1	BCL2-like 1
2.455	200985_s_at	CD59	CD59 molecule, complement regulatory protein
2.455	218178_s_at	CHMP1B	chromatin modifying protein 1B
2.455	208925_at	CLDND1	claudin domain containing 1
2.455	221676_s_at	CORO1C	coronin, actin binding protein, 1C
2.455	204751_x_at	DSC2	desmocollin 2
2.455	201538_s_at	DUSP3	dual specificity phosphatase 3
2.455	204540_at	EEF1A2	eukaryotic translation elongation factor 1 alpha 2
2.455	209037_s_at	EHD1	EH-domain containing 1
2.455	212527_at	FAM152B	family with sequence similarity 152, member B
2.455	208613_s_at	FLNB	filamin B, beta (actin binding protein 278)
2.455	207180_s_at	HTATIP2	HIV-1 Tat interactive protein 2, 30kDa
2.455	202637_s_at	ICAM1	intercellular adhesion molecule 1
2.455	205992_s_at	IL15	interleukin 15
2.455	201627_s_at	INSIG1	insulin induced gene 1
2.455	221877_at	IRGQ	immunity-related GTPase family, Q
2.455	64488_at	IRGQ	immunity-related GTPase family, Q
2.455	209743_s_at	ITCH	itchy E3 ubiquitin protein ligase homolog (mouse)
2.455	209653_at	KPNA4	karyopherin alpha 4 (importin alpha 3)
2.455	204734_at	KRT15	keratin 15

Fold change	Affymetrix ID	Gene symbol	Entrez gene name
2.455	208433_s_at	LRP8	low density lipoprotein receptor-related protein 8, apolipoprotein e receptor
2.455	200797_s_at	MCL1	myeloid cell leukaemia sequence 1 (BCL2-related)
2.455	204702_s_at	NFE2L3	nuclear factor (erythroid-derived 2)-like 3
2.455	203918_at	PCDH1	protocadherin 1
2.455	218472_s_at	PELO	pelota homolog (Drosophila)
2.455	203879_at	PIK3CD	phosphoinositide-3-kinase, catalytic, delta polypeptide
2.455	207469_s_at	PIR	pirin (iron-binding nuclear protein)
2.455	217875_s_at	PMEPA1	prostate transmembrane protein, androgen induced 1
2.455	203997_at	PTPN3	protein tyrosine phosphatase, non-receptor type 3
2.455	210101_x_at	SH3GLB1	SH3-domain GRB2-like endophilin B1
2.455	210854_x_at	SLC6A8	solute carrier family 6 (neurotransmitter transporter, creatine), member 8
2.455	215812_s_at	SLC6A8	solute carrier family 6 (neurotransmitter transporter, creatine), member 8
2.455	210357_s_at	SMOX	spermine oxidase
2.455	203127_s_at	SPTLC2	serine palmitoyltransferase, long chain base subunit 2
2.455	202644_s_at	TNFAIP3	tumor necrosis factor, alpha-induced protein 3
2.455	212481_s_at	TPM4	tropomyosin 4
2.455	203343_at	UGDH	UDP-glucose dehydrogenase
2.455	221704_s_at	VPS37B	vacuolar protein sorting 37 homolog B (S. cerevisiae)
2.455	200611_s_at	WDR1	WD repeat domain 1
2.455	210812_at	XRCC4	X-ray repair complementing defective repair in Chinese hamster cells 4
2.455	211962_s_at	ZFP36L1	zinc finger protein 36, C3H type-like 1
2.291	209993_at	ABCB1	ATP-binding cassette, sub-family B (MDR/TAP), member 1
2.291	206155_at	ABCC2	ATP-binding cassette, sub-family C (CFTR/MRP), member 2
2.291	219496_at	ANKRD57	ankyrin repeat domain 57
2.291	205047_s_at	ASNS	asparagine synthetase
2.291	209135_at	ASPH	aspartate beta-hydroxylase
2.291	218608_at	ATP13A2	ATPase type 13A2
2.291	203612_at	BYSL	bystin-like
2.291	200777_s_at	BZW1	basic leucine zipper and W2 domains 1
2.291	219023_at	C4ORF16	chromosome 4 open reading frame 16

Fold change	Affymetrix ID	Gene symbol	Entrez gene name
2.291	218008_at	C7ORF42	chromosome 7 open reading frame 42
2.291	221040_at	CAPN10	calpain 10
2.291	204610_s_at	CCDC85B	coiled-coil domain containing 85B
2.291	208712_at	CCND1	cyclin D1
2.291	209772_s_at	CD24	CD24 molecule
2.291	208650_s_at	CD24	CD24 molecule
2.291	212463_at	CD59	CD59 molecule, complement regulatory protein
2.291	200984_s_at	CD59	CD59 molecule, complement regulatory protein
2.291	219492_at	CHIC2	cysteine-rich hydrophobic domain 2
2.291	202538_s_at	CHMP2B	chromatin modifying protein 2B
2.291	209156_s_at	COL6A2	collagen, type VI, alpha 2
2.291	222235_s_at	CSGALNACT2	chondroitin sulfate N-acetylgalactosaminyltransferase 2
2.291	209158_s_at	CYTH2	cytohesin 2
2.291	203367_at	DUSP14	dual specificity phosphatase 14
2.291	201537_s_at	DUSP3	dual specificity phosphatase 3
2.291	209536_s_at	EHD4	EH-domain containing 4
2.291	91826_at	EPS8L1	EPS8-like 1
2.291	208622_s_at	EZR	ezrin
2.291	212400_at	FAM102A	family with sequence similarity 102, member A
2.291	204232_at	FCER1G	Fc fragment of IgE, high affinity I, receptor for; gamma polypeptide
2.291	214240_at	GAL	galanin prepropeptide
2.291	214430_at	GLA	galactosidase, alpha
2.291	202755_s_at	GPC1	glypican 1
2.291	208308_s_at	GPI	glucose phosphate isomerase
2.291	219357_at	GTPBP1	GTP binding protein 1
2.291	202934_at	HK2	hexokinase 2
2.291	202557_at	HSPA13	heat shock protein 70kDa family, member 13
2.291	219998_at	HSPC159	galectin-related protein
2.291	211676_s_at	IFNGR1	interferon gamma receptor 1
2.291	203828_s_at	IL32	interleukin 32

Fold change	Affymetrix ID	Gene symbol	Entrez gene name
2.291	201625_s_at	INSIG1	insulin induced gene 1
2.291	209744_x_at	ITCH	itchy E3 ubiquitin protein ligase homolog (mouse)
2.291	217094_s_at	ITCH	itchy E3 ubiquitin protein ligase homolog (mouse)
2.291	201751_at	JOSD1	Josephin domain containing 1
2.291	215515_at	KIRREL	kin of IRRE like (Drosophila)
2.291	219399_at	LIN7C	lin-7 homolog C (C. elegans)
2.291	204970_s_at	MAFG	v-maf musculoaponeurotic fibrosarcoma oncogene homolog G (avian)
2.291	206247_at	MICB	MHC class I polypeptide-related sequence B
2.291	201297_s_at	MOBKL1B	MOB1, Mps One Binder kinase activator-like 1B (yeast)
2.291	201761_at	MTHFD2	methylenetetrahydrofolate dehydrogenase (NADP+ dependent) 2, methenyltetrahydrofolate cyclohydrolase
2.291	37005_at	NBL1	neuroblastoma, suppression of tumorigenicity 1
2.291	211681_s_at	PDLIM5	PDZ and LIM domain 5
2.291	201037_at	PFKP	phosphofructokinase, platelet
2.291	213030_s_at	PLXNA2	plexin A2
2.291	205618_at	PRRG1	proline rich Gla (G-carboxyglutamic acid) 1
2.291	209885_at	RHOD	ras homolog gene family, member D
2.291	213038_at	RNF19B	ring finger protein 19B
2.291	36564_at	RNF19B	ring finger protein 19B
2.291	214697_s_at	ROD1	ROD1 regulator of differentiation 1 (S. pombe)
2.291	218209_s_at	RPRD1A	regulation of nuclear pre-mRNA domain containing 1A
2.291	204541_at	SEC14L2	SEC14-like 2 (S. cerevisiae)
2.291	208381_s_at	SGPL1	sphingosine-1-phosphate lyase 1
2.291	209091_s_at	SH3GLB1	SH3-domain GRB2-like endophilin B1
2.291	202234_s_at	SLC16A1	solute carrier family 16, member 1 (monocarboxylic acid transporter 1)
2.291	202497_x_at	SLC2A3	solute carrier family 2 (facilitated glucose transporter), member 3
2.291	220123_at	SLC35F5	solute carrier family 35, member F5
2.291	212295_s_at	SLC7A1	solute carrier family 7 (cationic amino acid transporter, y+ system), member 1
2.291	219677_at	SPSB1	splA/ryanodine receptor domain and SOCS box containing 1
2.291	40420_at	STK10	serine/threonine kinase 10
2.291	220800_s_at	TMOD3	tropomodulin 3 (ubiquitous)

Fold change	Affymetrix ID	Gene symbol	Entrez gene name
2.291	210405_x_at	TNFRSF10B	tumor necrosis factor receptor superfamily, member 10b
2.291	209372_x_at	TUBB2B	tubulin, beta 2B
2.291	217799_x_at	UBE2H	ubiquitin-conjugating enzyme E2H (UBC8 homolog, yeast)
2.291	210065_s_at	UPK1B	uroplakin 1B
2.291	202205_at	VASP	vasodilator-stimulated phosphoprotein
2.291	211527_x_at	VEGFA	vascular endothelial growth factor A
2.291	209822_s_at	VLDLR	very low density lipoprotein receptor
2.291	209216_at	WDR45	WD repeat domain 45
2.291	219540_at	ZNF267	zinc finger protein 267
2.138	213017_at	ABHD3	abhydrolase domain containing 3
2.138	218581_at	ABHD4	abhydrolase domain containing 4
2.138	211653_x_at	AKR1C2	aldo-keto reductase family 1, member C2 (dihydrodiol dehydrogenase 2; bile acid binding protein; 3-alpha hydroxysteroid dehydrogenase, type III)
2.138	222108_at	AMIGO2	adhesion molecule with Ig-like domain 2
2.138	206632_s_at	APOBEC3B	apolipoprotein B mRNA editing enzyme, catalytic polypeptide-like 3B
2.138	221031_s_at	APOLD1	apolipoprotein L domain containing 1
2.138	201772_at	AZIN1	antizyme inhibitor 1
2.138	221190_s_at	C18ORF8	chromosome 18 open reading frame 8
2.138	221764_at	C19ORF22	chromosome 19 open reading frame 22
2.138	206788_s_at	CBFB	core-binding factor, beta subunit
2.138	202537_s_at	CHMP2B	chromatin modifying protein 2B
2.138	205474_at	CRLF3	cytokine receptor-like factor 3
2.138	202887_s_at	DDIT4	DNA-damage-inducible transcript 4
2.138	203810_at	DNAJB4	DnaJ (Hsp40) homolog, subfamily B, member 4
2.138	208810_at	DNAJB6	DnaJ (Hsp40) homolog, subfamily B, member 6
2.138	203258_at	DRAP1	DR1-associated protein 1 (negative cofactor 2 alpha)
2.138	217901_at	DSG2	desmoglein 2
2.138	208708_x_at	EIF5	eukaryotic translation initiation factor 5
2.138	221665_s_at	EPS8L1	EPS8-like 1
2.138	221655_x_at	EPS8L1	EPS8-like 1
2.138	208621_s_at	EZR	ezrin

Fold change	Affymetrix ID	Gene symbol	Entrez gene name
2.138	218898_at	FAM57A	family with sequence similarity 57, member A
2.138	219901_at	FGD6	FYVE, RhoGEF and PH domain containing 6
2.138	210187_at	FKBP1A	FK506 binding protein 1A, 12kDa
2.138	207178_s_at	FRK	fyn-related kinase
2.138	218193_s_at	GOLT1B	Golgi transport 1 homolog B (S. cerevisiae)
2.138	209409_at	GRB10	growth factor receptor-bound protein 10
2.138	202042_at	HARS	histidyl-tRNA synthetase
2.138	221896_s_at	HIGD1A	HIG1 domain family, member 1A
2.138	205466_s_at	HS3ST1	heparan sulfate (glucosamine) 3-O-sulfotransferase 1
2.138	202638_s_at	ICAM1	intercellular adhesion molecule 1
2.138	212223_at	IDS	iduronate 2-sulfatase
2.138	203233_at	IL4R	interleukin 4 receptor
2.138	202794_at	INPP1	inositol polyphosphate-1-phosphatase
2.138	201626_at	INSIG1	insulin induced gene 1
2.138	213076_at	ITPKC	inositol 1,4,5-trisphosphate 3-kinase C
2.138	217938_s_at	KCMF1	potassium channel modulatory factor 1
2.138	201776_s_at	KIAA0494	KIAA0494
2.138	221502_at	KPNA3	karyopherin alpha 3 (importin alpha 4)
2.138	218651_s_at	LARP6	La ribonucleoprotein domain family, member 6
2.138	218816_at	LRRC1	leucine rich repeat containing 1
2.138	200712_s_at	MAPRE1	microtubule-associated protein, RP/EB family, member 1
2.138	209200_at	MEF2C	myocyte enhancer factor 2C
2.138	209199_s_at	MEF2C	myocyte enhancer factor 2C
2.138	218853_s_at	MOSPD1	motile sperm domain containing 1
2.138	217739_s_at	NAMPT	nicotinamide phosphoribosyltransferase
2.138	217738_at	NAMPT	nicotinamide phosphoribosyltransferase
2.138	220731_s_at	NECAP2	NECAP endocytosis associated 2
2.138	201502_s_at	NFKBIA	nuclear factor of kappa light polypeptide gene enhancer in B-cells inhibitor, alpha
2.138	218215_s_at	NR1H2	nuclear receptor subfamily 1, group H, member 2
2.138	208875_s_at	PAK2	p21 protein (Cdc42/Rac)-activated kinase 2

Fold change	Affymetrix ID	Gene symbol	Entrez gene name
2.138	204715_at	PANX1	pannexin 1
2.138	209552_at	PAX8	paired box 8
2.138	206686_at	PDK1	pyruvate dehydrogenase kinase, isozyme 1
2.138	203243_s_at	PDLIM5	PDZ and LIM domain 5
2.138	218644_at	PLEK2	pleckstrin 2
2.138	201490_s_at	PPIF	peptidylprolyl isomerase F
2.138	201489_at	PPIF	peptidylprolyl isomerase F
2.138	201375_s_at	PPP2CB	protein phosphatase 2 (formerly 2A), catalytic subunit, beta isoform
2.138	201300_s_at	PRNP	prion protein
2.138	200833_s_at	RAP1B	RAP1B, member of RAS oncogene family
2.138	201783_s_at	RELA	v-rel reticuloendotheliosis viral oncogene homolog A (avian)
2.138	203175_at	RHOG	ras homolog gene family, member G (rho G)
2.138	212647_at	RRAS	related RAS viral (r-ras) oncogene homolog
2.138	210790_s_at	SAR1A	SAR1 homolog A (S. cerevisiae)
2.138	213988_s_at	SAT1	spermidine/spermine N1-acetyltransferase 1
2.138	202071_at	SDC4	syndecan 4
2.138	57703_at	SENP5	SUMO1/sentrin specific peptidase 5
2.138	201739_at	SGK1	serum/glucocorticoid regulated kinase 1
2.138	202236_s_at	SLC16A1	solute carrier family 16, member 1 (monocarboxylic acid transporter 1)
2.138	216236_s_at	SLC2A3	solute carrier family 2 (facilitated glucose transporter), member 3
2.138	219409_at	SNIP1	Smad nuclear interacting protein 1
2.138	209481_at	SNRK	SNF related kinase
2.138	212458_at	SPRED2	sprouty-related, EVH1 domain containing 2
2.138	206907_at	TNFSF9	tumor necrosis factor (ligand) superfamily, member 9
2.138	203671_at	TPMT	thiopurine S-methyltransferase
2.138	215125_s_at	UGT1A7	UDP glucuronosyltransferase 1 family, polypeptide A7
2.138	210513_s_at	VEGFA	vascular endothelial growth factor A
2.138	209217_s_at	WDR45	WD repeat domain 45
2.138	222357_at	ZBTB20	zinc finger and BTB domain containing 20
2.138	204181_s_at	ZBTB43	zinc finger and BTB domain containing 43

Fold change	Affymetrix ID	Gene symbol	Entrez gene name
2.138	206683_at	ZNF165	zinc finger protein 165
2.138	219376_at	ZNF322B	zinc finger protein 322B
1.995	209380_s_at	ABCC5	ATP-binding cassette, sub-family C (CFTR/MRP), member 5
1.995	217626_at	AKR1C1	aldo-keto reductase family 1, member C1 (dihydrodiol dehydrogenase 1; 20-alpha (3-alpha)-hydroxysteroid dehydrogenase)
1.995	209699_x_at	AKR1C2	aldo-keto reductase family 1, member C2 (dihydrodiol dehydrogenase 2; bile acid binding protein; 3-alpha hydroxysteroid dehydrogenase, type III)
1.995	201096_s_at	ARF4	ADP-ribosylation factor 4
1.995	203945_at	ARG2	arginase, type II
1.995	219973_at	ARSJ	arylsulfatase family, member J
1.995	209186_at	ATP2A2	ATPase, Ca++ transporting, cardiac muscle, slow twitch 2
1.995	217835_x_at	C20ORF24	chromosome 20 open reading frame 24
1.995	213798_s_at	CAP1	CAP, adenylate cyclase-associated protein 1 (yeast)
1.995	211434_s_at	CCRL2	chemokine (C-C motif) receptor-like 2
1.995	200983_x_at	CD59	CD59 molecule, complement regulatory protein
1.995	205627_at	CDA	cytidine deaminase
1.995	209939_x_at	CFLAR	CASP8 and FADD-like apoptosis regulator
1.995	210563_x_at	CFLAR	CASP8 and FADD-like apoptosis regulator
1.995	218177_at	CHMP1B	chromatin modifying protein 1B
1.995	203954_x_at	CLDN3	claudin 3
1.995	203634_s_at	CPT1A	carnitine palmitoyltransferase 1A (liver)
1.995	208735_s_at	CTDSP2	CTD (carboxy-terminal domain, RNA polymerase II, polypeptide A) small phosphatase 2
1.995	218260_at	DDA1	DET1 and DDB1 associated 1
1.995	203811_s_at	DNAJB4	DnaJ (Hsp40) homolog, subfamily B, member 4
1.995	212792_at	DPY19L1	dpy-19-like 1 (C. elegans)
1.995	218995_s_at	EDN1	endothelin 1
1.995	201984_s_at	EGFR	epidermal growth factor receptor (erythroblastic leukaemia viral (v-erb-b) oncogene homolog, avian)
1.995	202021_x_at	EIF1	eukaryotic translation initiation factor 1
1.995	212227_x_at	EIF1	eukaryotic translation initiation factor 1
1.995	201144_s_at	EIF2S1	eukaryotic translation initiation factor 2, subunit 1 alpha, 35kDa
1.995	208290_s_at	EIF5	eukaryotic translation initiation factor 5

Fold change	Affymetrix ID	Gene symbol	Entrez gene name
1.995	220198_s_at	EIF5A2	eukaryotic translation initiation factor 5A2
1.995	203349_s_at	ETV5	ets variant 5
1.995	208623_s_at	EZR	ezrin
1.995	219429_at	FA2H	fatty acid 2-hydroxylase
1.995	212373_at	FEM1B	fem-1 homolog b (C. elegans)
1.995	208840_s_at	G3BP2	GTPase activating protein (SH3 domain) binding protein 2
1.995	204224_s_at	GCH1	GTP cyclohydrolase 1
1.995	219473_at	GDAP2	ganglioside induced differentiation associated protein 2
1.995	218913_s_at	GMIP	GEM interacting protein
1.995	201179_s_at	GNAI3	guanine nucleotide binding protein (G protein), alpha inhibiting activity polypeptide 3
1.995	202756_s_at	GPC1	glypican 1
1.995	218238_at	GTPBP4	GTP binding protein 4
1.995	200800_s_at	HSPA1A	heat shock 70kDa protein 1A
1.995	209448_at	HTATIP2	HIV-1 Tat interactive protein 2, 30kDa
1.995	202081_at	IER2	immediate early response 2
1.995	217371_s_at	IL15	interleukin 15
1.995	200995_at	IPO7	importin 7
1.995	221503_s_at	KPNA3	karyopherin alpha 3 (importin alpha 4)
1.995	202651_at	LPGAT1	lysophosphatidylglycerol acyltransferase 1
1.995	201412_at	LRP10	low density lipoprotein receptor-related protein 10
1.995	212978_at	LRRC8B	leucine rich repeat containing 8 family, member B
1.995	211686_s_at	MAK16	MAK16 homolog (S. cerevisiae)
1.995	218522_s_at	MAP1S	microtubule-associated protein 1S
1.995	202670_at	MAP2K1	mitogen-activated protein kinase kinase 1
1.995	212497_at	MAPK1IP1L	mitogen-activated protein kinase 1 interacting protein 1-like
1.995	200898_s_at	MGEA5	meningioma expressed antigen 5 (hyaluronidase)
1.995	201298_s_at	MOBKL1B	MOB1, Mps One Binder kinase activator-like 1B (yeast)
1.995	218687_s_at	MUC13	mucin 13, cell surface associated
1.995	202431_s_at	MYC	v-myc myelocytomatosis viral oncogene homolog (avian)
1.995	222206_s_at	NCLN	nicalin homolog (zebrafish)

Fold change	Affymetrix ID	Gene symbol	Entrez gene name
1.995	218678_at	NES	nestin
1.995	219100_at	OBFC1	oligonucleotide/oligosaccharide-binding fold containing 1
1.995	218556_at	ORMDL2	ORM1-like 2 (S. cerevisiae)
1.995	218319_at	PELI1	pellino homolog 1 (Drosophila)
1.995	204369_at	PIK3CA	phosphoinositide-3-kinase, catalytic, alpha polypeptide
1.995	211697_x_at	PNO1	partner of NOB1 homolog (S. cerevisiae)
1.995	218292_s_at	PRKAG2	protein kinase, AMP-activated, gamma 2 non-catalytic subunit
1.995	203650_at	PROCR	protein C receptor, endothelial (EPCR)
1.995	209694_at	PTS	6-pyruvoyltetrahydropterin synthase
1.995	203885_at	RAB21	RAB21, member RAS oncogene family
1.995	205924_at	RAB3B	RAB3B, member RAS oncogene family
1.995	210127_at	RAB6B	RAB6B, member RAS oncogene family
1.995	214435_x_at	RALA	v-ral simian leukaemia viral oncogene homolog A (ras related)
1.995	213923_at	RAP2B	RAP2B, member of RAS oncogene family
1.995	209878_s_at	RELA	v-rel reticuloendotheliosis viral oncogene homolog A (avian)
1.995	202636_at	RNF103	ring finger protein 103
1.995	204665_at	RP5-1000E10.4	suppressor of IKK epsilon
1.995	212590_at	RRAS2	related RAS viral (r-ras) oncogene homolog 2
1.995	208456_s_at	RRAS2	related RAS viral (r-ras) oncogene homolog 2
1.995	214838_at	SFT2D2	SFT2 domain containing 2
1.995	209884_s_at	SLC4A7	solute carrier family 4, sodium bicarbonate cotransporter, member 7
1.995	208078_s_at	SNF1LK	salt-inducible kinase 1
1.995	220140_s_at	SNX11	sorting nexin 11
1.995	218817_at	SPCS3	signal peptidase complex subunit 3 homolog (S. cerevisiae)
1.995	219257_s_at	SPHK1	sphingosine kinase 1
1.995	202506_at	SSFA2	sperm specific antigen 2
1.995	201060_x_at	STOM	stomatin
1.995	220030_at	STYK1	serine/threonine/tyrosine kinase 1
1.995	212457_at	TFE3	transcription factor binding to IGHM enhancer 3
1.995	203313_s_at	TGIF1	TGFB-induced factor homeobox 1

Fold change	Affymetrix ID	Gene symbol	Entrez gene name
1.995	202011_at	TJP1	tight junction protein 1 (zona occludens 1)
1.995	213285_at	TMEM30B	transmembrane protein 30B
1.995	209294_x_at	TNFRSF10B	tumor necrosis factor receptor superfamily, member 10b
1.995	209295_at	TNFRSF10B	tumor necrosis factor receptor superfamily, member 10b
1.995	207536_s_at	TNFRSF9	tumor necrosis factor receptor superfamily, member 9
1.995	206911_at	TRIM25	tripartite motif-containing 25
1.995	210541_s_at	TRIM27	tripartite motif-containing 27
1.995	213476_x_at	TUBB3	tubulin, beta 3
1.995	218340_s_at	UBA6	ubiquitin-like modifier activating enzyme 6
1.995	201001_s_at	UBE2V1	ubiquitin-conjugating enzyme E2 variant 1
1.995	206094_x_at	UGT1A7	UDP glucuronosyltransferase 1 family, polypeptide A7
1.995	211662_s_at	VDAC2	voltage-dependent anion channel 2
1.995	204507_s_at	WDR92	WD repeat domain 92
1.995	201760_s_at	WSB2	WD repeat and SOCS box-containing 2
1.995	209551_at	YIPF4	Yip1 domain family, member 4
1.995	200640_at	YWHAZ	tyrosine 3-monooxygenase/tryptophan 5-monooxygenase activation protein, zeta polypeptide
-1.995	214033_at	ABCC6	ATP-binding cassette, sub-family C (CFTR/MRP), member 6
-1.995	219986_s_at	ACAD10	acyl-Coenzyme A dehydrogenase family, member 10
-1.995	219413_at	ACBD4	acyl-Coenzyme A binding domain containing 4
-1.995	204393_s_at	ACPP	acid phosphatase, prostate
-1.995	208636_at	ACTN1	actinin, alpha 1
-1.995	208637_x_at	ACTN1	actinin, alpha 1
-1.995	203865_s_at	ADARB1	adenosine deaminase, RNA-specific, B1 (RED1 homolog rat)
-1.995	218480_at	AGBL5	ATP/GTP binding protein-like 5
-1.995	212175_s_at	AK2	adenylate kinase 2
-1.995	218373_at	AKTIP	AKT interacting protein
-1.995	212798_s_at	ANKMY2	ankyrin repeat and MYND domain containing 2
-1.995	213035_at	ANKRD28	ankyrin repeat domain 28
-1.995	213419_at	APBB2	amyloid beta (A4) precursor protein-binding, family B, member 2
-1.995	212970_at	APBB2	amyloid beta (A4) precursor protein-binding, family B, member 2

Fold change	Affymetrix ID	Gene symbol	Entrez gene name
-1.995	206955_at	AQP7	aquaporin 7
-1.995	214102_at	ARAP2	ArfGAP with RhoGAP domain, ankyrin repeat and PH domain 2
-1.995	212234_at	ASXL1	additional sex combs like 1 (Drosophila)
-1.995	203168_at	ATF6B	activating transcription factor 6 beta
-1.995	205052_at	AUH	AU RNA binding protein/enoyl-Coenzyme A hydratase
-1.995	210534_s_at	B9D1	B9 protein domain 1
-1.995	211947_s_at	BAT2D1	BAT2 domain containing 1
-1.995	221241_s_at	BCL2L14	BCL2-like 14 (apoptosis facilitator)
-1.995	210334_x_at	BIRC5	baculoviral IAP repeat-containing 5
-1.995	202179_at	BLMH	bleomycin hydrolase
-1.995	59644_at	BMP2K	BMP2 inducible kinase
-1.995	207186_s_at	BPTF	bromodomain PHD finger transcription factor
-1.995	209271_at	BPTF	bromodomain PHD finger transcription factor
-1.995	212645_x_at	BRE	brain and reproductive organ-expressed (TNFRSF1A modulator)
-1.995	211566_x_at	BRE	brain and reproductive organ-expressed (TNFRSF1A modulator)
-1.995	218024_at	BRP44L	brain protein 44-like
-1.995	220060_s_at	C12ORF48	chromosome 12 open reading frame 48
-1.995	219757_s_at	C14ORF101	chromosome 14 open reading frame 101
-1.995	219009_at	C14ORF93	chromosome 14 open reading frame 93
-1.995	217640_x_at	C18ORF24	chromosome 18 open reading frame 24
-1.995	218429_s_at	C19ORF66	chromosome 19 open reading frame 66
-1.995	218546_at	C1ORF115	chromosome 1 open reading frame 115
-1.995	207711_at	C20ORF117	chromosome 20 open reading frame 117
-1.995	219004_s_at	C21ORF45	chromosome 21 open reading frame 45
-1.995	201677_at	C3ORF37	chromosome 3 open reading frame 37
-1.995	219450_at	C4ORF19	chromosome 4 open reading frame 19
-1.995	39817_s_at	C6ORF108	chromosome 6 open reading frame 108
-1.995	213322_at	C6ORF130	chromosome 6 open reading frame 130
-1.995	213596_at	CASP4	caspase 4, apoptosis-related cysteine peptidase
-1.995	211464_x_at	CASP6	caspase 6, apoptosis-related cysteine peptidase

Fold change	Affymetrix ID	Gene symbol	Entrez gene name
-1.995	208908_s_at	CAST	calpastatin
-1.995	207467_x_at	CAST	calpastatin
-1.995	209682_at	CBLB	Cas-Br-M (murine) ecotropic retroviral transforming sequence b
-1.995	219130_at	CCDC76	coiled-coil domain containing 76
-1.995	205167_s_at	CDC25C	cell division cycle 25 homolog C (S. pombe)
-1.995	204126_s_at	CDC45L	CDC45 cell division cycle 45-like (S. cerevisiae)
-1.995	221436_s_at	CDCA3	cell division cycle associated 3
-1.995	210821_x_at	CENPA	centromere protein A
-1.995	203492_x_at	CEP57	centrosomal protein 57kDa
-1.995	203975_s_at	CHAF1A	chromatin assembly factor 1, subunit A (p150)
-1.995	204193_at	CHKB	choline kinase beta
-1.995	217501_at	CIAO1	cytosolic iron-sulfur protein assembly 1 homolog (S. cerevisiae)
-1.995	213839_at	CLMN	calmin (calponin-like, transmembrane)
-1.995	220739_s_at	CNNM3	cyclin M3
-1.995	219302_s_at	CNTNAP2	contactin associated protein-like 2
-1.995	218760_at	COQ6	coenzyme Q6 homolog, monooxygenase (S. cerevisiae)
-1.995	206256_at	CPN1	carboxypeptidase N, polypeptide 1
-1.995	215930_s_at	CTAGE5	CTAGE family, member 5
-1.995	201904_s_at	CTDSPL	CTD (carboxy-terminal domain, RNA polymerase II, polypeptide A) small phosphatase-like
-1.995	202613_at	CTPS	CTP synthase
-1.995	36084_at	CUL7	cullin 7
-1.995	823_at	CX3CL1	chemokine (C-X3-C motif) ligand 1
-1.995	207843_x_at	CYB5A	cytochrome b5 type A (microsomal)
-1.995	209366_x_at	CYB5A	cytochrome b5 type A (microsomal)
-1.995	39582_at	CYLD	cylindromatosis (turban tumor syndrome)
-1.995	205502_at	CYP17A1	cytochrome P450, family 17, subfamily A, polypeptide 1
-1.995	219664_s_at	DECR2	2,4-dienoyl CoA reductase 2, peroxisomal
-1.995	214079_at	DHRS2	dehydrogenase/reductase (SDR family) member 2
-1.995	212503_s_at	DIP2C	DIP2 disco-interacting protein 2 homolog C (Drosophila)
-1.995	201681_s_at	DLG5	discs, large homolog 5 (Drosophila)

Fold change	Affymetrix ID	Gene symbol	Entrez gene name
-1.995	222360_at	DPH5	DPH5 homolog (S. cerevisiae)
-1.995	208955_at	DUT	deoxyuridine triphosphatase
-1.995	209701_at	ERAP1	endoplasmic reticulum aminopeptidase 1
-1.995	204817_at	ESPL1	extra spindle pole bodies homolog 1 (S. cerevisiae)
-1.995	204231_s_at	FAAH	fatty acid amide hydrolase
-1.995	212981_s_at	FAM115A	family with sequence similarity 115, member A
-1.995	213463_s_at	FAM149B1	family with sequence similarity 149, member B1
-1.995	36612_at	FAM168A	family with sequence similarity 168, member A
-1.995	212357_at	FAM168A	family with sequence similarity 168, member A
-1.995	213689_x_at	FAM69A	family with sequence similarity 69, member A
-1.995	204283_at	FARS2	phenylalanyl-tRNA synthetase 2, mitochondrial
-1.995	210638_s_at	FBXO9	F-box protein 9
-1.995	203620_s_at	FCHSD2	FCH and double SH3 domains 2
-1.995	218454_at	FLJ22662	hypothetical protein FLJ22662
-1.995	218885_s_at	GALNT12	UDP-N-acetyl-alpha-D-galactosamine:polypeptide N-acetylgalactosaminyltransferase 12 (GalNAc-T12)
-1.995	213280_at	GARNL4	GTPase activating Rap/RanGAP domain-like 4
-1.995	204867_at	GCHFR	GTP cyclohydrolase I feedback regulator
-1.995	219078_at	GPATCH2	G patch domain containing 2
-1.995	212205_at	H2AFV	H2A histone family, member V
-1.995	205657_at	HAAO	3-hydroxyanthranilate 3,4-dioxygenase
-1.995	220801_s_at	HAO2	hydroxyacid oxidase 2 (long chain)
-1.995	219484_at	HCFC2	host cell factor C2
-1.995	218306_s_at	HERC1	hect (homologous to the E6-AP (UBE3A) carboxyl terminus) domain and RCC1 (CHC1)-like domain (RLD) 1
-1.995	217902_s_at	HERC2	hect domain and RLD 2
-1.995	211330_s_at	HFE	hemochromatosis
-1.995	203711_s_at	HIBCH	3-hydroxyisobutyryl-Coenzyme A hydrolase
-1.995	214472_at	HIST1H3D	histone cluster 1, H3d
-1.995	216548_x_at	HMG4L	high-mobility group (nonhistone chromosomal) protein 4-like
-1.995	219976_at	HOOK1	hook homolog 1 (Drosophila)

Fold change	Affymetrix ID	Gene symbol	Entrez gene name
-1.995	209844_at	HOXB13	homeobox B13
-1.995	216450_x_at	HSP90B1	heat shock protein 90kDa beta (Grp94), member 1
-1.995	201193_at	IDH1	isocitrate dehydrogenase 1 (NADP+), soluble
-1.995	205059_s_at	IDUA	iduronidase, alpha-L-
-1.995	218709_s_at	IFT52	intraflagellar transport 52 homolog (Chlamydomonas)
-1.995	218100_s_at	IFT57	intraflagellar transport 57 homolog (Chlamydomonas)
-1.995	202410_x_at	IGF2	insulin-like growth factor 2 (somatomedin A)
-1.995	205376_at	INPP4B	inositol polyphosphate-4-phosphatase, type II, 105kDa
-1.995	218905_at	INTS8	integrator complex subunit 8
-1.995	205176_s_at	ITGB3BP	integrin beta 3 binding protein (beta3-endonexin)
-1.995	217894_at	KCTD3	potassium channel tetramerisation domain containing 3
-1.995	202181_at	KIAA0247	KIAA0247
-1.995	212946_at	KIAA0564	KIAA0564
-1.995	36888_at	KIAA0841	KIAA0841
-1.995	204709_s_at	KIF23	kinesin family member 23
-1.995	209408_at	KIF2C	kinesin family member 2C
-1.995	221838_at	KLHL22	kelch-like 22 (Drosophila)
-1.995	201505_at	LAMB1	laminin, beta 1
-1.995	220158_at	LGALS14	lectin, galactoside-binding, soluble, 14
-1.995	209205_s_at	LMO4	LIM domain only 4
-1.995	213605_s_at	LOC100134401	hypothetical protein LOC100134401
-1.995	211996_s_at	LOC23117	PI-3-kinase-related kinase SMG-1 isoform 1 homolog
-1.995	220770_s_at	LOC63920	transposon-derived Buster3 transposase-like
-1.995	215123_at	LOC729602	NPIP-like protein ENSP00000283050
-1.995	215667_x_at	LOC730324	similar to postmeiotic segregation increased 2-like 2
-1.995	216908_x_at	LOC94431	RRN3 RNA polymerase I transcription factor homolog (S. cerevisiae) pseudogene
-1.995	212692_s_at	LRBA	LPS-responsive vesicle trafficking, beach and anchor containing
-1.995	214109_at	LRBA	LPS-responsive vesicle trafficking, beach and anchor containing
-1.995	219573_at	LRRC16A	leucine rich repeat containing 16A
-1.995	202245_at	LSS	lanosterol synthase (2,3-oxidosqualene-lanosterol cyclase)

Fold change	Affymetrix ID	Gene symbol	Entrez gene name
-1.995	209014_at	MAGED1	melanoma antigen family D, 1
-1.995	65884_at	MAN1B1	mannosidase, alpha, class 1B, member 1
-1.995	219814_at	MBNL3	muscleblind-like 3 (Drosophila)
-1.995	209623_at	MCCC2	methylcrotonoyl-Coenzyme A carboxylase 2 (beta)
-1.995	220651_s_at	MCM10	minichromosome maintenance complex component 10
-1.995	222037_at	MCM4	minichromosome maintenance complex component 4
-1.995	212945_s_at	MGA	MAX gene associated
-1.995	204918_s_at	MLLT3	myeloid/lymphoid or mixed-lineage leukaemia (trithorax homolog, Drosophila); translocated to, 3
-1.995	218773_s_at	MSRB2	methionine sulfoxide reductase B2
-1.995	204871_at	MTERF	mitochondrial transcription termination factor
-1.995	218506_x_at	N-PAC	cytokine-like nuclear factor n-pac
-1.995	219378_at	NARG1L	NMDA receptor regulated 1-like
-1.995	206453_s_at	NDRG2	NDRG family member 2
-1.995	213012_at	NEDD4	neural precursor cell expressed, developmentally down-regulated 4
-1.995	204641_at	NEK2	NIMA (never in mitosis gene a)-related kinase 2
-1.995	212299_at	NEK9	NIMA (never in mitosis gene a)- related kinase 9
-1.995	217527_s_at	NFATC2IP	nuclear factor of activated T-cells, cytoplasmic, calcineurin-dependent 2 interacting protein
-1.995	215743_at	NMT2	N-myristoyltransferase 2
-1.995	202783_at	NNT	nicotinamide nucleotide transhydrogenase
-1.995	218244_at	NOL8	nucleolar protein 8
-1.995	207217_s_at	NOX1	NADPH oxidase 1
-1.995	206418_at	NOX1	NADPH oxidase 1
-1.995	200747_s_at	NUMA1	nuclear mitotic apparatus protein 1
-1.995	213599_at	OIP5	Opa interacting protein 5
-1.995	213204_at	PARC	p53-associated parkin-like cytoplasmic protein
-1.995	219639_x_at	PARP6	poly (ADP-ribose) polymerase family, member 6
-1.995	202876_s_at	PBX2	pre-B-cell leukaemia homeobox 2
-1.995	214177_s_at	PBXIP1	pre-B-cell leukaemia homeobox interacting protein 1
-1.995	204476_s_at	PC	pyruvate carboxylase
-1.995	39650_s_at	PCNXL2	pecanex-like 2 (Drosophila)

Fold change	Affymetrix ID	Gene symbol	Entrez gene name
-1.995	218953_s_at	PCYOX1L	prenylcysteine oxidase 1 like
-1.995	210825_s_at	PEBP1	phosphatidylethanolamine binding protein 1
-1.995	211941_s_at	PEBP1	phosphatidylethanolamine binding protein 1
-1.995	202108_at	PEPD	peptidase D
-1.995	55616_at	PERLD1	per1-like domain containing 1
-1.995	204873_at	PEX1	peroxisomal biogenesis factor 1
-1.995	205160_at	PEX11A	peroxisomal biogenesis factor 11 alpha
-1.995	204545_at	PEX6	peroxisomal biogenesis factor 6
-1.995	219235_s_at	PHACTR4	phosphatase and actin regulator 4
-1.995	217953_at	PHF3	PHD finger protein 3
-1.995	213407_at	PHLPPL	PH domain and leucine rich repeat protein phosphatase-like
-1.995	219093_at	PID1	phosphotyrosine interaction domain containing 1
-1.995	213889_at	PIGL	phosphatidylinositol glycan anchor biosynthesis, class L
-1.995	219048_at	PIGN	phosphatidylinositol glycan anchor biosynthesis, class N
-1.995	202732_at	PKIG	protein kinase (cAMP-dependent, catalytic) inhibitor gamma
-1.995	219702_at	PLAC1	placenta-specific 1
-1.995	220157_x_at	PLEKHA9	pleckstrin homology domain containing, family A (phosphoinositide binding specific) member 9
-1.995	215412_x_at	PMS2L2	postmeiotic segregation increased 2-like 2 pseudogene
-1.995	216525_x_at	PMS2L3	postmeiotic segregation increased 2-like 3
-1.995	201578_at	PODXL	podocalyxin-like
-1.995	212836_at	POLD3	polymerase (DNA-directed), delta 3, accessory subunit
-1.995	207746_at	POLQ	polymerase (DNA directed), theta
-1.995	208469_s_at	PPT2	palmitoyl-protein thioesterase 2
-1.995	218009_s_at	PRC1	protein regulator of cytokinesis 1
-1.995	206346_at	PRLR	prolactin receptor
-1.995	219392_x_at	PRR11	proline rich 11
-1.995	207011_s_at	PTK7	PTK7 protein tyrosine kinase 7
-1.995	211737_x_at	PTN	pleiotrophin
-1.995	213313_at	RABGAP1	RAB GTPase activating protein 1
-1.995	204028_s_at	RABGAP1	RAB GTPase activating protein 1

Fold change	Affymetrix ID	Gene symbol	Entrez gene name
-1.995	204828_at	RAD9A	RAD9 homolog A (S. pombe)
-1.995	201394_s_at	RBM5	RNA binding motif protein 5
-1.995	216215_s_at	RBM9	RNA binding motif protein 9
-1.995	204969_s_at	RDX	radixin
-1.995	212398_at	RDX	radixin
-1.995	208021_s_at	RFC1	replication factor C (activator 1) 1, 145kDa
-1.995	203210_s_at	RFC5	replication factor C (activator 1) 5, 36.5kDa
-1.995	219154_at	RHOF	ras homolog gene family, member F (in filopodia)
-1.995	213397_x_at	RNASE4	ribonuclease, RNase A family, 4
-1.995	204040_at	RNF144A	ring finger protein 144A
-1.995	219739_at	RNF186	ring finger protein 186
-1.995	205806_at	ROM1	retinal outer segment membrane protein 1
-1.995	218307_at	RSAD1	radical S-adenosyl methionine domain containing 1
-1.995	204030_s_at	SCHIP1	schwannomin interacting protein 1
-1.995	221216_s_at	SCMH1	sex comb on midleg homolog 1 (Drosophila)
-1.995	200961_at	SEPHS2	selenophosphate synthetase 2
-1.995	212493_s_at	SETD2	SET domain containing 2
-1.995	210172_at	SF1	splicing factor 1
-1.995	215699_x_at	SFI1	Sfi1 homolog, spindle assembly associated (yeast)
-1.995	212721_at	SFRS12	splicing factor, arginine/serine-rich 12
-1.995	212266_s_at	SFRS5	splicing factor, arginine/serine-rich 5
-1.995	213649_at	SFRS7	splicing factor, arginine/serine-rich 7, 35kDa
-1.995	220038_at	SGK3	serum/glucocorticoid regulated kinase family, member 3
-1.995	203014_x_at	SGSM3	small G protein signaling modulator 3
-1.995	40149_at	SH2B1	SH2B adaptor protein 1
-1.995	204967_at	SHROOM2	shroom family member 2
-1.995	203125_x_at	SLC11A2	solute carrier family 11 (proton-coupled divalent metal ion transporters), member 2
-1.995	210686_x_at	SLC25A16	solute carrier family 25 (mitochondrial carrier; Graves disease autoantigen), member 16
-1.995	221920_s_at	SLC25A37	solute carrier family 25, member 37
-1.995	203164_at	SLC33A1	solute carrier family 33 (acetyl-CoA transporter), member 1

Fold change	Affymetrix ID	Gene symbol	Entrez gene name
-1.995	217828_at	SLTM	SAFB-like, transcription modulator
-1.995	210993_s_at	SMAD1	SMAD family member 1
-1.995	215294_s_at	SMARCA1	SWI/SNF related, matrix associated, actin dependent regulator of chromatin, subfamily a, member 1
-1.995	217792_at	SNX5	sorting nexin 5
-1.995	209437_s_at	SPON1	spondin 1, extracellular matrix protein
-1.995	208920_at	SRI	sorcin
-1.995	221554_at	STRADA	STE20-related kinase adaptor alpha
-1.995	203767_s_at	STS	steroid sulfatase (microsomal), isozyme S
-1.995	210612_s_at	SYNJ2	synaptojanin 2
-1.995	204045_at	TCEAL1	transcription elongation factor A (SII)-like 1
-1.995	209153_s_at	TCF3	transcription factor 3 (E2A immunoglobulin enhancer binding factors E12/E47)
-1.995	205210_at	TGFBRAP1	transforming growth factor, beta receptor associated protein 1
-1.995	216262_s_at	TGIF2	TGFB-induced factor homeobox 2
-1.995	204565_at	THEM2	thioesterase superfamily member 2
-1.995	204064_at	THOC1	THO complex 1
-1.995	222122_s_at	THOC2	THO complex 2
-1.995	205217_at	TIMM8A	translocase of inner mitochondrial membrane 8 homolog A (yeast)
-1.995	204340_at	TMEM187	transmembrane protein 187
-1.995	212621_at	TMEM194A	transmembrane protein 194A
-1.995	203050_at	TP53BP1	tumor protein p53 binding protein 1
-1.995	217914_at	TPCN1	two pore segment channel 1
-1.995	214196_s_at	TPP1	tripeptidyl peptidase I
-1.995	204352_at	TRAF5	TNF receptor-associated factor 5
-1.995	202368_s_at	TRAM2	translocation associated membrane protein 2
-1.995	221627_at	TRIM10	tripartite motif-containing 10
-1.995	203148_s_at	TRIM14	tripartite motif-containing 14
-1.995	203567_s_at	TRIM38	tripartite motif-containing 38
-1.995	221952_x_at	TRMT5	TRM5 tRNA methyltransferase 5 homolog (S. cerevisiae)
-1.995	208663_s_at	TTC3	tetratricopeptide repeat domain 3
-1.995	208664_s_at	TTC3	tetratricopeptide repeat domain 3

Fold change	Affymetrix ID	Gene symbol	Entrez gene name
-1.995	203584_at	TTC35	tetratricopeptide repeat domain 35
-1.995	203048_s_at	TTC37	tetratricopeptide repeat domain 37
-1.995	214672_at	TTLL5	tubulin tyrosine ligase-like family, member 5
-1.995	219948_x_at	UGT2A3	UDP glucuronosyltransferase 2 family, polypeptide A3
-1.995	206405_x_at	USP6	ubiquitin specific peptidase 6 (Tre-2 oncogene)
-1.995	211571_s_at	VCAN	versican
-1.995	203564_at	VCP	valosin-containing protein
-1.995	205019_s_at	VIPR1	vasoactive intestinal peptide receptor 1
-1.995	203106_s_at	VPS41	vacuolar protein sorting 41 homolog (S. cerevisiae)
-1.995	213031_s_at	WDR73	WD repeat domain 73
-1.995	203043_at	ZBED1	zinc finger, BED-type containing 1
-1.995	218348_s_at	ZC3H7A	zinc finger CCCH-type containing 7A
-1.995	222237_s_at	ZFP112	zinc finger protein 112 homolog (mouse)
-1.995	37943_at	ZFYVE26	zinc finger, FYVE domain containing 26
-1.995	214670_at	ZKSCAN1	zinc finger with KRAB and SCAN domains 1
-1.995	37254_at	ZNF133	zinc finger protein 133
-1.995	215359_x_at	ZNF44	zinc finger protein 44
-2.138	221669_s_at	ACAD8	acyl-Coenzyme A dehydrogenase family, member 8
-2.138	206833_s_at	ACYP2	acylphosphatase 2, muscle type
-2.138	201752_s_at	ADD3	adducin 3 (gamma)
-2.138	201924_at	AFF1	AF4/FMR2 family, member 1
-2.138	212543_at	AIM1	absent in melanoma 1
-2.138	218064_s_at	AKAP8L	A kinase (PRKA) anchor protein 8-like
-2.138	213591_at	ALDH7A1	aldehyde dehydrogenase 7 family, member A1
-2.138	204704_s_at	ALDOB	aldolase B, fructose-bisphosphate
-2.138	205583_s_at	ALG13	asparagine-linked glycosylation 13 homolog (S. cerevisiae)
-2.138	207140_at	ALPI	alkaline phosphatase, intestinal
-2.138	216550_x_at	ANKRD12	ankyrin repeat domain 12
-2.138	218950_at	ARAP3	ArfGAP with RhoGAP domain, ankyrin repeat and PH domain 3
-2.138	211852_s_at	ATRN	attractin

Fold change	Affymetrix ID	Gene symbol	Entrez gene name
-2.138	208860_s_at	ATRX	alpha thalassemia/mental retardation syndrome X-linked (RAD54 homolog, S. cerevisiae)
-2.138	220580_at	BICC1	bicaudal C homolog 1 (Drosophila)
-2.138	202095_s_at	BIRC5	baculoviral IAP repeat-containing 5
-2.138	205750_at	BPHL	biphenyl hydrolase-like (serine hydrolase)
-2.138	38241_at	BTN3A3	butyrophilin, subfamily 3, member A3
-2.138	209642_at	BUB1	budding uninhibited by benzimidazoles 1 homolog (yeast)
-2.138	204073_s_at	C11ORF9	chromosome 11 open reading frame 9
-2.138	211034_s_at	C12ORF51	chromosome 12 open reading frame 51
-2.138	219617_at	C2ORF34	chromosome 2 open reading frame 34
-2.138	219455_at	C7ORF63	chromosome 7 open reading frame 63
-2.138	218168_s_at	CABC1	chaperone, ABC1 activity of bc1 complex homolog (S. pombe)
-2.138	222201_s_at	CASP8AP2	caspase 8 associated protein 2
-2.138	203799_at	CD302	CD302 molecule
-2.138	206387_at	CDX2	caudal type homeobox 2
-2.138	222151_s_at	CEP63	centrosomal protein 63kDa
-2.138	209194_at	CETN2	centrin, EF-hand protein, 2
-2.138	203950_s_at	CLCN6	chloride channel 6
-2.138	209164_s_at	CYB561	cytochrome b-561
-2.138	218021_at	DHRS4	dehydrogenase/reductase (SDR family) member 4
-2.138	209916_at	DHTKD1	dehydrogenase E1 and transketolase domain containing 1
-2.138	205726_at	DIAPH2	diaphanous homolog 2 (Drosophila)
-2.138	212504_at	DIP2C	DIP2 disco-interacting protein 2 homolog C (Drosophila)
-2.138	212611_at	DTX4	deltex 4 homolog (Drosophila)
-2.138	209932_s_at	DUT	deoxyuridine triphosphatase
-2.138	208956_x_at	DUT	deoxyuridine triphosphatase
-2.138	206101_at	ECM2	extracellular matrix protein 2, female organ and adipocyte specific
-2.138	217735_s_at	EIF2AK1	eukaryotic translation initiation factor 2-alpha kinase 1
-2.138	201935_s_at	EIF4G3	eukaryotic translation initiation factor 4 gamma, 3
-2.138	201027_s_at	EIF5B	eukaryotic translation initiation factor 5B
-2.138	202414_at	ERCC5	excision repair cross-complementing rodent repair deficiency, complementation group 5

Fold change	Affymetrix ID	Gene symbol	Entrez gene name
-2.138	212979_s_at	FAM115A	family with sequence similarity 115, member A
-2.138	218397_at	FANCL	Fanconi anemia, complementation group L
-2.138	203032_s_at	FH	fumarate hydratase
-2.138	206857_s_at	FKBP1B	FK506 binding protein 1B, 12.6 kDa
-2.138	215293_s_at	FRAG1	FGF receptor activating protein 1
-2.138	208475_at	FRMD4A	FERM domain containing 4A
-2.138	204374_s_at	GALK1	galactokinase 1
-2.138	209729_at	GAS2L1	growth arrest-specific 2 like 1
-2.138	213018_at	GATAD1	GATA zinc finger domain containing 1
-2.138	219722_s_at	GDPD3	glycerophosphodiester phosphodiesterase domain containing 3
-2.138	208914_at	GGA2	Golgi associated, gamma adaptin ear containing, ARF binding protein 2
-2.138	211767_at	GINS4	GINS complex subunit 4 (Sld5 homolog)
-2.138	218350_s_at	GMNN	geminin, DNA replication inhibitor
-2.138	201956_s_at	GNPAT	glyceronephosphate O-acyltransferase
-2.138	215470_at	GTF2H2B	general transcription factor IIH, polypeptide 2B
-2.138	218412_s_at	GTF2IRD1	GTF2I repeat domain containing 1
-2.138	204317_at	GTSE1	G-2 and S-phase expressed 1
-2.138	215942_s_at	GTSE1	G-2 and S-phase expressed 1
-2.138	212206_s_at	H2AFV	H2A histone family, member V
-2.138	218460_at	HEATR2	HEAT repeat containing 2
-2.138	205313_at	HNF1B	HNF1 homeobox B
-2.138	221919_at	HNRNPA1	heterogeneous nuclear ribonucleoprotein A1
-2.138	208814_at	HSPA4	heat shock 70kDa protein 4
-2.138	220322_at	IL1F9	interleukin 1 family, member 9
-2.138	214705_at	INADL	InaD-like (Drosophila)
-2.138	201124_at	ITGB5	integrin, beta 5
-2.138	202182_at	KAT2A	K(lysine) acetyltransferase 2A
-2.138	211713_x_at	KIAA0101	KIAA0101
-2.138	212943_at	KIAA0528	KIAA0528
-2.138	204155_s_at	KIAA0999	KIAA0999 protein

Fold change	Affymetrix ID	Gene symbol	Entrez gene name
-2.138	222039_at	KIF18B	kinesin family member 18B
-2.138	209680_s_at	KIFC1	kinesin family member C1
-2.138	206054_at	KNG1	kininogen 1
-2.138	212785_s_at	LARP7	La ribonucleoprotein domain family, member 7
-2.138	204016_at	LARS2	leucyl-tRNA synthetase 2, mitochondrial
-2.138	206606_at	LIPC	lipase, hepatic
-2.138	217506_at	LOC400642	hypothetical LOC400642
-2.138	204298_s_at	LOX	lysyl oxidase
-2.138	203495_at	LRRC14	leucine rich repeat containing 14
-2.138	222036_s_at	MCM4	minichromosome maintenance complex component 4
-2.138	216237_s_at	MCM5	minichromosome maintenance complex component 5
-2.138	203062_s_at	MDC1	mediator of DNA damage checkpoint 1
-2.138	212693_at	MDN1	MDN1, midasin homolog (yeast)
-2.138	204305_at	MIPEP	mitochondrial intermediate peptidase
-2.138	36830_at	MIPEP	mitochondrial intermediate peptidase
-2.138	211673_s_at	MOCS1	molybdenum cofactor synthesis 1
-2.138	213924_at	MPPE1	metallophosphoesterase 1
-2.138	218536_at	MRS2	MRS2 magnesium homeostasis factor homolog (S. cerevisiae)
-2.138	219451_at	MSRB2	methionine sulfoxide reductase B2
-2.138	216862_s_at	MTCP1	mature T-cell proliferation 1
-2.138	203037_s_at	MTSS1	metastasis suppressor 1
-2.138	212093_s_at	MTUS1	mitochondrial tumor suppressor 1
-2.138	204139_x_at	MZF1	myeloid zinc finger 1
-2.138	218330_s_at	NAV2	neuron navigator 2
-2.138	212854_x_at	NBPF10	neuroblastoma breakpoint family, member 10
-2.138	204321_at	NEO1	neogenin homolog 1 (chicken)
-2.138	212808_at	NFATC2IP	nuclear factor of activated T-cells, cytoplasmic, calcineurin-dependent 2 interacting protein
-2.138	218318_s_at	NLK	nemo-like kinase
-2.138	209262_s_at	NR2F6	nuclear receptor subfamily 2, group F, member 6
-2.138	204105_s_at	NRCAM	neuronal cell adhesion molecule

Fold change	Affymetrix ID	Gene symbol	Entrez gene name
-2.138	217802_s_at	NUCKS1	nuclear casein kinase and cyclin-dependent kinase substrate 1
-2.138	213945_s_at	NUP210	nucleoporin 210kDa
-2.138	209240_at	OGT	O-linked N-acetylglucosamine (GlcNAc) transferase (UDP-N-acetylglucosamine:polypeptide-N-acetylglucosaminyl transferase)
-2.138	211778_s_at	OVOL2	ovo-like 2 (Drosophila)
-2.138	219461_at	PAK6	p21 protein (Cdc42/Rac)-activated kinase 6
-2.138	204752_x_at	PARP2	poly (ADP-ribose) polymerase 2
-2.138	203860_at	PCCA	propionyl Coenzyme A carboxylase, alpha polypeptide
-2.138	214797_s_at	PCTK3	PCTAIRE protein kinase 3
-2.138	203803_at	PCYOX1	prenylcysteine oxidase 1
-2.138	209577_at	PCYT2	phosphate cytidylyltransferase 2, ethanolamine
-2.138	219304_s_at	PDGFD	platelet derived growth factor D
-2.138	205353_s_at	PEBP1	phosphatidylethanolamine binding protein 1
-2.138	220576_at	PGAP1	post-GPI attachment to proteins 1
-2.138	219394_at	PGS1	phosphatidylglycerophosphate synthase 1
-2.138	203278_s_at	PHF21A	PHD finger protein 21A
-2.138	212719_at	PHLPP	PH domain and leucine rich repeat protein phosphatase
-2.138	201080_at	PIP4K2B	phosphatidylinositol-5-phosphate 4-kinase, type II, beta
-2.138	214874_at	PKP4	plakophilin 4
-2.138	220952_s_at	PLEKHA5	pleckstrin homology domain containing, family A member 5
-2.138	219510_at	POLQ	polymerase (DNA directed), theta
-2.138	209337_at	PSIP1	PC4 and SFRS1 interacting protein 1
-2.138	219938_s_at	PSTPIP2	proline-serine-threonine phosphatase interacting protein 2
-2.138	203038_at	PTPRK	protein tyrosine phosphatase, receptor type, K
-2.138	219428_s_at	PXMP4	peroxisomal membrane protein 4, 24kDa
-2.138	217597_x_at	RAB40B	RAB40B, member RAS oncogene family
-2.138	208393_s_at	RAD50	RAD50 homolog (S. cerevisiae)
-2.138	209849_s_at	RAD51C	RAD51 homolog C (S. cerevisiae)
-2.138	205647_at	RAD52	RAD52 homolog (S. cerevisiae)
-2.138	212031_at	RBM25	RNA binding motif protein 25
-2.138	204365_s_at	REEP1	receptor accessory protein 1

Fold change	Affymetrix ID	Gene symbol	Entrez gene name
-2.138	204023_at	RFC4	replication factor C (activator 1) 4, 37kDa
-2.138	209110_s_at	RGL2	ral guanine nucleotide dissociation stimulator-like 2
-2.138	220329_s_at	RMND1	required for meiotic nuclear division 1 homolog (S. cerevisiae)
-2.138	205158_at	RNASE4	ribonuclease, RNase A family, 4
-2.138	209111_at	RNF5	ring finger protein 5
-2.138	207624_s_at	RPGR	retinitis pigmentosa GTPase regulator
-2.138	221989_at	RPL10	ribosomal protein L10
-2.138	208607_s_at	SAA1	serum amyloid A1
-2.138	215848_at	SCAPER	S phase cyclin A-associated protein in the ER
-2.138	201427_s_at	SEPP1	selenoprotein P, plasma, 1
-2.138	212414_s_at	SEPT6	septin 6
-2.138	209443_at	SERPINA5	serpin peptidase inhibitor, clade A (alpha-1 antiproteinase, antitrypsin), member 5
-2.138	218346_s_at	SESN1	sestrin 1
-2.138	215038_s_at	SETD2	SET domain containing 2
-2.138	219749_at	SH2D4A	SH2 domain containing 4A
-2.138	201311_s_at	SH3BGRL	SH3 domain binding glutamic acid-rich protein like
-2.138	213600_at	SIPA1L3	signal-induced proliferation-associated 1 like 3
-2.138	203761_at	SLA	Src-like-adaptor
-2.138	206081_at	SLC24A1	solute carrier family 24 (sodium/potassium/calcium exchanger), member 1
-2.138	201349_at	SLC9A3R1	solute carrier family 9 (sodium/hydrogen exchanger), member 3 regulator 1
-2.138	203875_at	SMARCA1	SWI/SNF related, matrix associated, actin dependent regulator of chromatin, subfamily a, member 1
-2.138	203874_s_at	SMARCA1	SWI/SNF related, matrix associated, actin dependent regulator of chromatin, subfamily a, member 1
-2.138	205658_s_at	SNAPC4	small nuclear RNA activating complex, polypeptide 4, 190kDa
-2.138	218324_s_at	SPATS2	spermatogenesis associated, serine-rich 2
-2.138	205185_at	SPINK5	serine peptidase inhibitor, Kazal type 5
-2.138	213355_at	ST3GAL6	ST3 beta-galactoside alpha-2,3-sialyltransferase 6
-2.138	221191_at	STAG3L1	stromal antigen 3-like 1
-2.138	209969_s_at	STAT1	signal transducer and activator of transcription 1, 91kDa
-2.138	205339_at	STIL	SCL/TAL1 interrupting locus
-2.138	204287_at	SYNGR1	synaptogyrin 1

Fold change	Affymetrix ID	Gene symbol	Entrez gene name
-2.138	219992_at	TAC3	tachykinin 3
-2.138	219771_at	TBC1D8B	TBC1 domain family, member 8B (with GRAM domain)
-2.138	204731_at	TGFBR3	transforming growth factor, beta receptor III
-2.138	217974_at	TM7SF3	transmembrane 7 superfamily member 3
-2.138	218815_s_at	TMEM51	transmembrane protein 51
-2.138	217853_at	TNS3	tensin 3
-2.138	210052_s_at	TPX2	TPX2, microtubule-associated, homolog (Xenopus laevis)
-2.138	202369_s_at	TRAM2	translocation associated membrane protein 2
-2.138	219351_at	TRAPPC2	trafficking protein particle complex 2
-2.138	206308_at	TRDMT1	tRNA aspartic acid methyltransferase 1
-2.138	203049_s_at	TTC37	tetratricopeptide repeat domain 37
-2.138	202589_at	TYMS	thymidylate synthetase
-2.138	208760_at	UBE2I	ubiquitin-conjugating enzyme E2I (UBC9 homolog, yeast)
-2.138	212403_at	UBE3B	ubiquitin protein ligase E3B
-2.138	202317_s_at	UBE4B	ubiquitination factor E4B (UFD2 homolog, yeast)
-2.138	218108_at	UBR7	ubiquitin protein ligase E3 component n-recognin 7 (putative)
-2.138	220079_s_at	USP48	ubiquitin specific peptidase 48
-2.138	201886_at	WDR23	WD repeat domain 23
-2.138	202250_s_at	WDR42A	WD repeat domain 42A
-2.138	218505_at	WDR59	WD repeat domain 59
-2.138	219251_s_at	WDR60	WD repeat domain 60
-2.138	205340_at	ZBTB24	zinc finger and BTB domain containing 24
-2.138	213064_at	ZC3H14	zinc finger CCCH-type containing 14
-2.138	210281_s_at	ZMYM2	zinc finger, MYM-type 2
-2.138	202051_s_at	ZMYM4	zinc finger, MYM-type 4
-2.138	219854_at	ZNF14	zinc finger protein 14
-2.138	219314_s_at	ZNF219	zinc finger protein 219
-2.138	209538_at	ZNF32	zinc finger protein 32
-2.138	215012_at	ZNF451	zinc finger protein 451
-2.138	213775_x_at	ZNF638	zinc finger protein 638

Fold change	Affymetrix ID	Gene symbol	Entrez gene name
-2.138	205594_at	ZNF652	zinc finger protein 652
-2.138	219627_at	ZNF767	zinc finger family member 767
-2.138	204026_s_at	ZWINT	ZW10 interactor
-2.291	203196_at	ABCC4	ATP-binding cassette, sub-family C (CFTR/MRP), member 4
-2.291	212186_at	ACACA	acetyl-Coenzyme A carboxylase alpha
-2.291	215728_s_at	ACOT7	acyl-CoA thioesterase 7
-2.291	209195_s_at	ADCY6	adenylate cyclase 6
-2.291	205882_x_at	ADD3	adducin 3 (gamma)
-2.291	207544_s_at	ADH6	alcohol dehydrogenase 6 (class V)
-2.291	212174_at	AK2	adenylate kinase 2
-2.291	209424_s_at	AMACR	alpha-methylacyl-CoA racemase
-2.291	212289_at	ANKRD12	ankyrin repeat domain 12
-2.291	201613_s_at	AP1G2	adaptor-related protein complex 1, gamma 2 subunit
-2.291	40148_at	APBB2	amyloid beta (A4) precursor protein-binding, family B, member 2
-2.291	218917_s_at	ARID1A	AT rich interactive domain 1A (SWI-like)
-2.291	205865_at	ARID3A	AT rich interactive domain 3A (BRIGHT-like)
-2.291	212614_at	ARID5B	AT rich interactive domain 5B (MRF1-like)
-2.291	213587_s_at	ATP6V0E2	ATPase, H+ transporting V0 subunit e2
-2.291	204624_at	ATP7B	ATPase, Cu++ transporting, beta polypeptide
-2.291	213106_at	ATP8A1	ATPase, aminophospholipid transporter (APLT), class I, type 8A, member 1
-2.291	214342_at	ATXN7L1	ataxin 7-like 1
-2.291	209464_at	AURKB	aurora kinase B
-2.291	202094_at	BIRC5	baculoviral IAP repeat-containing 5
-2.291	218789_s_at	C11ORF71	chromosome 11 open reading frame 71
-2.291	214264_s_at	C14ORF143	chromosome 14 open reading frame 143
-2.291	214357_at	C1ORF105	chromosome 1 open reading frame 105
-2.291	218646_at	C4ORF27	chromosome 4 open reading frame 27
-2.291	218179_s_at	C4ORF41	chromosome 4 open reading frame 41
-2.291	221879_at	CALML4	calmodulin-like 4
-2.291	222137_at	CC2D1A	coiled-coil and C2 domain containing 1A

Fold change	Affymetrix ID	Gene symbol	Entrez gene name
-2.291	218175_at	CCDC92	coiled-coil domain containing 92
-2.291	212899_at	CDC2L6	cell division cycle 2-like 6 (CDK8-like)
-2.291	204739_at	CENPC1	centromere protein C 1
-2.291	203491_s_at	CEP57	centrosomal protein 57kDa
-2.291	204266_s_at	CHKA	choline kinase alpha
-2.291	209571_at	CIR	CBF1 interacting corepressor
-2.291	213499_at	CLCN2	chloride channel 2
-2.291	213050_at	COBL	cordon-bleu homolog (mouse)
-2.291	208817_at	COMT	catechol-O-methyltransferase
-2.291	218328_at	COQ4	coenzyme Q4 homolog (S. cerevisiae)
-2.291	220044_x_at	CROP	cisplatin resistance-associated overexpressed protein
-2.291	220753_s_at	CRYL1	crystallin, lambda 1
-2.291	209163_at	CYB561	cytochrome b-561
-2.291	201279_s_at	DAB2	disabled homolog 2, mitogen-responsive phosphoprotein (Drosophila)
-2.291	208718_at	DDX17	DEAD (Asp-Glu-Ala-Asp) box polypeptide 17
-2.291	218756_s_at	DHRS11	dehydrogenase/reductase (SDR family) member 11
-2.291	213647_at	DNA2	DNA replication helicase 2 homolog (yeast)
-2.291	205554_s_at	DNASE1L3	deoxyribonuclease I-like 3
-2.291	218457_s_at	DNMT3A	DNA (cytosine-5-)-methyltransferase 3 alpha
-2.291	213267_at	DOPEY1	dopey family member 1
-2.291	205248_at	DOPEY2	dopey family member 2
-2.291	203762_s_at	DYNC2LI1	dynein, cytoplasmic 2, light intermediate chain 1
-2.291	207231_at	DZIP3	DAZ interacting protein 3, zinc finger
-2.291	221586_s_at	E2F5	E2F transcription factor 5, p130-binding
-2.291	202326_at	EHMT2	euchromatic histone-lysine N-methyltransferase 2
-2.291	201026_at	EIF5B	eukaryotic translation initiation factor 5B
-2.291	204142_at	ENOSF1	enolase superfamily member 1
-2.291	220524_at	EPB41L4B	erythrocyte membrane protein band 4.1 like 4B
-2.291	219905_at	ERMAP	erythroblast membrane-associated protein (Scianna blood group)
-2.291	214802_at	EXOC7	exocyst complex component 7

Fold change	Affymetrix ID	Gene symbol	Entrez gene name
-2.291	204714_s_at	F5	coagulation factor V (proaccelerin, labile factor)
-2.291	218518_at	FAM13B1	family with sequence similarity 13, member B1
-2.291	221591_s_at	FAM64A	family with sequence similarity 64, member A
-2.291	213007_at	FANCI	Fanconi anemia, complementation group I
-2.291	213008_at	FANCI	Fanconi anemia, complementation group I
-2.291	212987_at	FBXO9	F-box protein 9
-2.291	215645_at	FLCN	folliculin
-2.291	216442_x_at	FN1	fibronectin 1
-2.291	212464_s_at	FN1	fibronectin 1
-2.291	210495_x_at	FN1	fibronectin 1
-2.291	211719_x_at	FN1	fibronectin 1
-2.291	207014_at	GABRA2	gamma-aminobutyric acid (GABA) A receptor, alpha 2
-2.291	216411_s_at	GALK2	galactokinase 2
-2.291	205354_at	GAMT	guanidinoacetate N-methyltransferase
-2.291	209604_s_at	GATA3	GATA binding protein 3
-2.291	206102_at	GINS1	GINS complex subunit 1 (Psf1 homolog)
-2.291	222034_at	GNB2L1	guanine nucleotide binding protein (G protein), beta polypeptide 2-like 1
-2.291	222102_at	GSTA3	glutathione S-transferase alpha 3
-2.291	202967_at	GSTA4	glutathione S-transferase alpha 4
-2.291	215333_x_at	GSTM1	glutathione S-transferase mu 1
-2.291	204550_x_at	GSTM1	glutathione S-transferase mu 1
-2.291	205439_at	GSTT2	glutathione S-transferase theta 2
-2.291	206312_at	GUCY2C	guanylate cyclase 2C (heat stable enterotoxin receptor)
-2.291	219352_at	HERC6	hect domain and RLD 6
-2.291	204578_at	HISPPD2A	histidine acid phosphatase domain containing 2A
-2.291	215071_s_at	HIST1H2AC	histone cluster 1, H2ac
-2.291	208025_s_at	HMGA2	high mobility group AT-hook 2
-2.291	207165_at	HMMR	hyaluronan-mediated motility receptor (RHAMM)
-2.291	211930_at	HNRNPA3	heterogeneous nuclear ribonucleoprotein A3
-2.291	212203_x_at	IFITM3	interferon induced transmembrane protein 3 (1-8U)

Fold change	Affymetrix ID	Gene symbol	Entrez gene name
-2.291	209342_s_at	IKBKB	inhibitor of kappa light polypeptide gene enhancer in B-cells, kinase beta
-2.291	213447_at	IPW	imprinted in Prader-Willi syndrome (non-protein coding)
-2.291	205874_at	ITPKA	inositol 1,4,5-trisphosphate 3-kinase A
-2.291	213005_s_at	KANK1	KN motif and ankyrin repeat domains 1
-2.291	203845_at	KAT2B	K(lysine) acetyltransferase 2B
-2.291	213034_at	KIAA0999	KIAA0999 protein
-2.291	212779_at	KIAA1109	KIAA1109
-2.291	220777_at	KIF13A	kinesin family member 13A
-2.291	203943_at	KIF3B	kinesin family member 3B
-2.291	205306_x_at	KMO	kynurenine 3-monooxygenase (kynurenine 3-hydroxylase)
-2.291	206316_s_at	KNTC1	kinetochore associated 1
-2.291	34764_at	LARS2	leucyl-tRNA synthetase 2, mitochondrial
-2.291	213195_at	LOC201229	hypothetical protein LOC201229
-2.291	213510_x_at	LOC220594	TL132 protein
-2.291	215247_at	LOC440895	LIM and senescent cell antigen-like domains 3-like
-2.291	221640_s_at	LRDD	leucine-rich repeats and death domain containing
-2.291	205606_at	LRP6	low density lipoprotein receptor-related protein 6
-2.291	220143_x_at	LUC7L	LUC7-like (S. cerevisiae)
-2.291	203778_at	MANBA	mannosidase, beta A, lysosomal
-2.291	206249_at	MAP3K13	mitogen-activated protein kinase kinase kinase 13
-2.291	221824_s_at	MARCH8	membrane-associated ring finger (C3HC4) 8
-2.291	202350_s_at	MATN2	matrilin 2
-2.291	201555_at	MCM3	minichromosome maintenance complex component 3
-2.291	219673_at	MCM9	minichromosome maintenance complex component 9
-2.291	218883_s_at	MLF1IP	MLF1 interacting protein
-2.291	212079_s_at	MLL	myeloid/lymphoid or mixed-lineage leukaemia (trithorax homolog, Drosophila)
-2.291	210212_x_at	MTCP1	mature T-cell proliferation 1
-2.291	218663_at	NCAPG	non-SMC condensin I complex, subunit G
-2.291	219588_s_at	NCAPG2	non-SMC condensin II complex, subunit G2
-2.291	209105_at	NCOA1	nuclear receptor coactivator 1

Fold change	Affymetrix ID	Gene symbol	Entrez gene name
-2.291	209107_x_at	NCOA1	nuclear receptor coactivator 1
-2.291	214657_s_at	NCRNA00084	non-protein coding RNA 84
-2.291	219961_s_at	NCRNA00153	non-protein coding RNA 153
-2.291	202607_at	NDST1	N-deacetylase/N-sulfotransferase (heparan glucosaminyl) 1
-2.291	213331_s_at	NEK1	NIMA (never in mitosis gene a)-related kinase 1
-2.291	217526_at	NFATC2IP	nuclear factor of activated T-cells, cytoplasmic, calcineurin-dependent 2 interacting protein
-2.291	201708_s_at	NIPSNAP1	nipsnap homolog 1 (C. elegans)
-2.291	206340_at	NR1H4	nuclear receptor subfamily 1, group H, member 4
-2.291	201865_x_at	NR3C1	nuclear receptor subfamily 3, group C, member 1 (glucocorticoid receptor)
-2.291	219067_s_at	NSMCE4A	non-SMC element 4 homolog A (S. cerevisiae)
-2.291	211376_s_at	NSMCE4A	non-SMC element 4 homolog A (S. cerevisiae)
-2.291	203675_at	NUCB2	nucleobindin 2
-2.291	204766_s_at	NUDT1	nudix (nucleoside diphosphate linked moiety X)-type motif 1
-2.291	214136_at	NUDT13	nudix (nucleoside diphosphate linked moiety X)-type motif 13
-2.291	220035_at	NUP210	nucleoporin 210kDa
-2.291	218162_at	OLFML3	olfactomedin-like 3
-2.291	207576_x_at	OXT	oxytocin, prepropeptide
-2.291	222317_at	PDE3B	phosphodiesterase 3B, cGMP-inhibited
-2.291	205251_at	PER2	period homolog 2 (Drosophila)
-2.291	218410_s_at	PGP	phosphoglycolate phosphatase
-2.291	218517_at	PHF17	PHD finger protein 17
-2.291	209438_at	PHKA2	phosphorylase kinase, alpha 2 (liver)
-2.291	202738_s_at	PHKB	phosphorylase kinase, beta
-2.291	209780_at	PHTF2	putative homeodomain transcription factor 2
-2.291	212239_at	PIK3R1	phosphoinositide-3-kinase, regulatory subunit 1 (alpha)
-2.291	212249_at	PIK3R1	phosphoinositide-3-kinase, regulatory subunit 1 (alpha)
-2.291	212240_s_at	PIK3R1	phosphoinositide-3-kinase, regulatory subunit 1 (alpha)
-2.291	204572_s_at	PIN4	protein (peptidylprolyl cis/trans isomerase) NIMA-interacting, 4 (parvulin)
-2.291	220686_s_at	PIWIL2	piwi-like 2 (Drosophila)
-2.291	213222_at	PLCB1	phospholipase C, beta 1 (phosphoinositide-specific)

Fold change	Affymetrix ID	Gene symbol	Entrez gene name
-2.291	202789_at	PLCG1	phospholipase C, gamma 1
-2.291	204887_s_at	PLK4	polo-like kinase 4 (Drosophila)
-2.291	204519_s_at	PLLP	plasma membrane proteolipid (plasmolipin)
-2.291	206956_at	PMF1	polyamine-modulated factor 1
-2.291	203515_s_at	PMVK	phosphomevalonate kinase
-2.291	212349_at	POFUT1	protein O-fucosyltransferase 1
-2.291	204835_at	POLA1	polymerase (DNA directed), alpha 1, catalytic subunit
-2.291	216026_s_at	POLE	polymerase (DNA directed), epsilon
-2.291	205909_at	POLE2	polymerase (DNA directed), epsilon 2 (p59 subunit)
-2.291	219317_at	POLI	polymerase (DNA directed) iota
-2.291	214144_at	POLR2D	polymerase (RNA) II (DNA directed) polypeptide D
-2.291	212686_at	PPM1H	protein phosphatase 1H (PP2C domain containing)
-2.291	218045_x_at	PTMS	parathymosin
-2.291	209515_s_at	RAB27A	RAB27A, member RAS oncogene family
-2.291	206066_s_at	RAD51C	RAD51 homolog C (S. cerevisiae)
-2.291	204558_at	RAD54L	RAD54-like (S. cerevisiae)
-2.291	210552_s_at	RALGPS1	Ral GEF with PH domain and SH3 binding motif 1
-2.291	221872_at	RARRES1	retinoic acid receptor responder (tazarotene induced) 1
-2.291	212783_at	RBBP6	retinoblastoma binding protein 6
-2.291	212027_at	RBM25	RNA binding motif protein 25
-2.291	212030_at	RBM25	RNA binding motif protein 25
-2.291	212033_at	RBM25	RNA binding motif protein 25
-2.291	203696_s_at	RFC2	replication factor C (activator 1) 2, 40kDa
-2.291	60471_at	RIN3	Ras and Rab interactor 3
-2.291	219457_s_at	RIN3	Ras and Rab interactor 3
-2.291	219263_at	RNF128	ring finger protein 128
-2.291	220991_s_at	RNF32	ring finger protein 32
-2.291	213973_at	RRBP1	ribosome binding protein 1 homolog 180kDa (dog)
-2.291	212301_at	RTF1	Rtf1, Paf1/RNA polymerase II complex component, homolog (S. cerevisiae)
-2.291	218243_at	RUFY1	RUN and FYVE domain containing 1

Fold change	Affymetrix ID	Gene symbol	Entrez gene name
-2.291	202792_s_at	SAPS2	SAPS domain family, member 2
-2.291	213874_at	SERPINA4	serpin peptidase inhibitor, clade A (alpha-1 antiproteinase, antitrypsin), member 4
-2.291	221562_s_at	SIRT3	sirtuin (silent mating type information regulation 2 homolog) 3 (S. cerevisiae)
-2.291	221913_at	SIRT3	sirtuin (silent mating type information regulation 2 homolog) 3 (S. cerevisiae)
-2.291	210047_at	SLC11A2	solute carrier family 11 (proton-coupled divalent metal ion transporters), member 2
-2.291	205074_at	SLC22A5	solute carrier family 22 (organic cation/carnitine transporter), member 5
-2.291	218136_s_at	SLC25A37	solute carrier family 25, member 37
-2.291	212890_at	SLC38A10	solute carrier family 38, member 10
-2.291	222364_at	SLC44A1	solute carrier family 44, member 1
-2.291	215623_x_at	SMC4	structural maintenance of chromosomes 4
-2.291	214494_s_at	SPG7	spastic paraplegia 7 (pure and complicated autosomal recessive)
-2.291	202104_s_at	SPG7	spastic paraplegia 7 (pure and complicated autosomal recessive)
-2.291	213329_at	SRGAP2	SLIT-ROBO Rho GTPase activating protein 2
-2.291	212625_at	STX10	syntaxin 10
-2.291	207601_at	SULT1B1	sulfotransferase family, cytosolic, 1B, member 1
-2.291	218308_at	TACC3	transforming, acidic coiled-coil containing protein 3
-2.291	201814_at	TBC1D5	TBC1 domain family, member 5
-2.291	202371_at	TCEAL4	transcription elongation factor A (SII)-like 4
-2.291	212387_at	TCF4	transcription factor 4
-2.291	212382_at	TCF4	transcription factor 4
-2.291	219800_s_at	THNSL1	threonine synthase-like 1 (S. cerevisiae)
-2.291	212994_at	THOC2	THO complex 2
-2.291	213135_at	TIAM1	T-cell lymphoma invasion and metastasis 1
-2.291	212770_at	TLE3	transducin-like enhancer of split 3 (E(sp1) homolog, Drosophila)
-2.291	203839_s_at	TNK2	tyrosine kinase, non-receptor, 2
-2.291	219587_at	TTC12	tetratricopeptide repeat domain 12
-2.291	219481_at	TTC13	tetratricopeptide repeat domain 13
-2.291	218838_s_at	TTC31	tetratricopeptide repeat domain 31
-2.291	204822_at	TTK	TTK protein kinase
-2.291	205854_at	TULP3	tubby like protein 3

Fold change	Affymetrix ID	Gene symbol	Entrez gene name
-2.291	202365_at	UNC119B	unc-119 homolog B (C. elegans)
-2.291	203519_s_at	UPF2	UPF2 regulator of nonsense transcripts homolog (yeast)
-2.291	214323_s_at	UPF3A	UPF3 regulator of nonsense transcripts homolog A (yeast)
-2.291	203241_at	UVRAG	UV radiation resistance associated gene
-2.291	219538_at	WDR5B	WD repeat domain 5B
-2.291	203958_s_at	ZBTB40	zinc finger and BTB domain containing 40
-2.291	213063_at	ZC3H14	zinc finger CCCH-type containing 14
-2.291	201368_at	ZFP36L2	zinc finger protein 36, C3H type-like 2
-2.291	203556_at	ZHX2	zinc fingers and homeoboxes 2
-2.291	207394_at	ZNF137	zinc finger protein 137
-2.291	207513_s_at	ZNF189	zinc finger protein 189
-2.291	219228_at	ZNF331	zinc finger protein 331
-2.291	215358_x_at	ZNF37B	zinc finger protein 37B
-2.291	211257_x_at	ZNF638	zinc finger protein 638
-2.291	222120_at	ZNF764	zinc finger protein 764
-2.455	203981_s_at	ABCD4	ATP-binding cassette, sub-family D (ALD), member 4
-2.455	213198_at	ACVR1B	activin A receptor, type IB
-2.455	213245_at	ADCY1	adenylate cyclase 1 (brain)
-2.455	205996_s_at	AK2	adenylate kinase 2
-2.455	211004_s_at	ALDH3B1	aldehyde dehydrogenase 3 family, member B1
-2.455	209426_s_at	AMACR	alpha-methylacyl-CoA racemase
-2.455	204294_at	AMT	aminomethyltransferase
-2.455	216195_at	ANK2	ankyrin 2, neuronal
-2.455	214723_x_at	ANKRD36B	ankyrin repeat domain 36B
-2.455	208861_s_at	ATRX	alpha thalassemia/mental retardation syndrome X-linked (RAD54 homolog, S. cerevisiae)
-2.455	205363_at	BBOX1	butyrobetaine (gamma), 2-oxoglutarate dioxygenase (gamma-butyrobetaine hydroxylase) 1
-2.455	214452_at	BCAT1	branched chain aminotransferase 1, cytosolic
-2.455	213709_at	BHLHB9	basic helix-loop-helix domain containing, class B, 9
-2.455	216521_s_at	BRCC3	BRCA1/BRCA2-containing complex, subunit 3
-2.455	221196_x_at	BRCC3	BRCA1/BRCA2-containing complex, subunit 3

Fold change	Affymetrix ID	Gene symbol	Entrez gene name
-2.455	218983_at	C1RL	complement component 1, r subcomponent-like
-2.455	220943_s_at	C2ORF56	chromosome 2 open reading frame 56
-2.455	204238_s_at	C6ORF108	chromosome 6 open reading frame 108
-2.455	64408_s_at	CALML4	calmodulin-like 4
-2.455	214322_at	CAMK2G	calcium/calmodulin-dependent protein kinase II gamma
-2.455	212554_at	CAP2	CAP, adenylate cyclase-associated protein, 2 (yeast)
-2.455	212551_at	CAP2	CAP, adenylate cyclase-associated protein, 2 (yeast)
-2.455	210944_s_at	CAPN3	calpain 3, (p94)
-2.455	209790_s_at	CASP6	caspase 6, apoptosis-related cysteine peptidase
-2.455	201432_at	CAT	catalase
-2.455	207625_s_at	CBFA2T2	core-binding factor, runt domain, alpha subunit 2; translocated to, 2
-2.455	219644_at	CCDC41	coiled-coil domain containing 41
-2.455	214710_s_at	CCNB1	cyclin B1
-2.455	205271_s_at	CCRK	cell cycle related kinase
-2.455	204962_s_at	CENPA	centromere protein A
-2.455	207590_s_at	CENPI	centromere protein I
-2.455	206003_at	CEP135	centrosomal protein 135kDa
-2.455	204251_s_at	CEP164	centrosomal protein 164kDa
-2.455	210859_x_at	CLN3	ceroid-lipofuscinosis, neuronal 3
-2.455	204576_s_at	CLUAP1	clusterin associated protein 1
-2.455	219300_s_at	CNTNAP2	contactin associated protein-like 2
-2.455	212228_s_at	COQ9	coenzyme Q9 homolog (S. cerevisiae)
-2.455	205538_at	CORO2A	coronin, actin binding protein, 2A
-2.455	204662_at	CP110	CP110 protein
-2.455	207030_s_at	CSRP2	cysteine and glycine-rich protein 2
-2.455	201906_s_at	CTDSPL	CTD (carboxy-terminal domain, RNA polymerase II, polypeptide A) small phosphatase-like
-2.455	221850_x_at	CTGLF1	centaurin, gamma-like family, member 1
-2.455	203979_at	CYP27A1	cytochrome P450, family 27, subfamily A, polypeptide 1
-2.455	212855_at	DCUN1D4	DCN1, defective in cullin neddylation 1, domain containing 4 (S. cerevisiae)
-2.455	208149_x_at	DDX11	DEAD/H (Asp-Glu-Ala-Asp/His) box polypeptide 11 (CHL1-like helicase homolog, S. cerevisiae)

Fold change	Affymetrix ID	Gene symbol	Entrez gene name
-2.455	213998_s_at	DDX17	DEAD (Asp-Glu-Ala-Asp) box polypeptide 17
-2.455	48808_at	DHFR	dihydrofolate reductase
-2.455	202532_s_at	DHFR	dihydrofolate reductase
-2.455	202534_x_at	DHFR	dihydrofolate reductase
-2.455	208216_at	DLX4	distal-less homeobox 4
-2.455	220372_at	DNAJC28	DnaJ (Hsp40) homolog, subfamily C, member 28
-2.455	201431_s_at	DPYSL3	dihydropyrimidinase-like 3
-2.455	218854_at	DSE	dermatan sulfate epimerase
-2.455	207232_s_at	DZIP3	DAZ interacting protein 3, zinc finger
-2.455	209963_s_at	EPOR	erythropoietin receptor
-2.455	218180_s_at	EPS8L2	EPS8-like 2
-2.455	219629_at	FAM118A	family with sequence similarity 118, member A
-2.455	222245_s_at	FER1L4	fer-1-like 4 (C. elegans)
-2.455	213737_x_at	FLJ35785	Golgi autoantigen, golgin subfamily a, 9 pseudogene
-2.455	203146_s_at	GABBR1	gamma-aminobutyric acid (GABA) B receptor, 1
-2.455	210002_at	GATA6	GATA binding protein 6
-2.455	221521_s_at	GINS2	GINS complex subunit 2 (Psf2 homolog)
-2.455	218146_at	GLT8D1	glycosyltransferase 8 domain containing 1
-2.455	220773_s_at	GPHN	gephyrin
-2.455	219313_at	GRAMD1C	GRAM domain containing 1C
-2.455	206712_at	GRTP1	growth hormone regulated TBC protein 1
-2.455	204418_x_at	GSTM2	glutathione S-transferase mu 2 (muscle)
-2.455	204318_s_at	GTSE1	G-2 and S-phase expressed 1
-2.455	204315_s_at	GTSE1	G-2 and S-phase expressed 1
-2.455	210387_at	HIST1H2BG	histone cluster 1, H2bg
-2.455	209709_s_at	HMMR	hyaluronan-mediated motility receptor (RHAMM)
-2.455	210881_s_at	IGF2	insulin-like growth factor 2 (somatomedin A)
-2.455	212813_at	JAM3	junctional adhesion molecule 3
-2.455	214861_at	JMJD2C	jumonji domain containing 2C
-2.455	216762_at	KANK1	KN motif and ankyrin repeat domains 1

Fold change	Affymetrix ID	Gene symbol	Entrez gene name
-2.455	213358_at	KIAA0802	KIAA0802
-2.455	209760_at	KIAA0922	KIAA0922
-2.455	204444_at	KIF11	kinesin family member 11
-2.455	221258_s_at	KIF18A	kinesin family member 18A
-2.455	217906_at	KLHDC2	kelch domain containing 2
-2.455	214045_at	LIAS	lipoic acid synthetase
-2.455	202193_at	LIMK2	LIM domain kinase 2
-2.455	209204_at	LMO4	LIM domain only 4
-2.455	212850_s_at	LRP4	low density lipoprotein receptor-related protein 4
-2.455	221740_x_at	LRRC37A2	leucine rich repeat containing 37, member A2
-2.455	211018_at	LSS	lanosterol synthase (2,3-oxidosqualene-lanosterol cyclase)
-2.455	204069_at	MEIS1	Meis homeobox 1
-2.455	218251_at	MID1IP1	MID1 interacting protein 1 (gastrulation specific G12 homolog (zebrafish))
-2.455	218630_at	MKS1	Meckel syndrome, type 1
-2.455	219527_at	MOSC2	MOCO sulphurase C-terminal domain containing 2
-2.455	202974_at	MPP1	membrane protein, palmitoylated 1, 55kDa
-2.455	214268_s_at	MTMR4	myotubularin related protein 4
-2.455	212372_at	MYH10	myosin, heavy chain 10, non-muscle
-2.455	220319_s_at	MYLIP	myosin regulatory light chain interacting protein
-2.455	213375_s_at	N4BP2L1	NEDD4 binding protein 2-like 1
-2.455	221899_at	N4BP2L2	NEDD4 binding protein 2-like 2
-2.455	204162_at	NDC80	NDC80 homolog, kinetochore complex component (S. cerevisiae)
-2.455	212448_at	NEDD4L	neural precursor cell expressed, developmentally down-regulated 4-like
-2.455	219542_at	NEK11	NIMA (never in mitosis gene a)- related kinase 11
-2.455	202007_at	NID1	nidogen 1
-2.455	214722_at	NOTCH2NL	Notch homolog 2 (Drosophila) N-terminal like
-2.455	214870_x_at	NPIP	nuclear pore complex interacting protein
-2.455	211671_s_at	NR3C1	nuclear receptor subfamily 3, group C, member 1 (glucocorticoid receptor)
-2.455	220176_at	NUBPL	nucleotide binding protein-like
-2.455	222027_at	NUCKS1	nuclear casein kinase and cyclin-dependent kinase substrate 1

Fold change	Affymetrix ID	Gene symbol	Entrez gene name
-2.455	212775_at	OBSL1	obscurin-like 1
-2.455	202780_at	OXCT1	3-oxoacid CoA transferase 1
-2.455	214086_s_at	PARP2	poly (ADP-ribose) polymerase 2
-2.455	214239_x_at	PCGF2	polycomb group ring finger 2
-2.455	214937_x_at	PCM1	pericentriolar material 1
-2.455	214118_x_at	PCM1	pericentriolar material 1
-2.455	212594_at	PDCD4	programmed cell death 4 (neoplastic transformation inhibitor)
-2.455	214582_at	PDE3B	phosphodiesterase 3B, cGMP-inhibited
-2.455	212092_at	PEG10	paternally expressed 10
-2.455	212660_at	PHF15	PHD finger protein 15
-2.455	203688_at	PKD2	polycystic kidney disease 2 (autosomal dominant)
-2.455	201928_at	PKP4	plakophilin 4
-2.455	209504_s_at	PLEKHB1	pleckstrin homology domain containing, family B (evectins) member 1
-2.455	218901_at	PLSCR4	phospholipid scramblase 4
-2.455	212036_s_at	PNN	pinin, desmosome associated protein
-2.455	220675_s_at	PNPLA3	patatin-like phospholipase domain containing 3
-2.455	210433_at	POFUT1	protein O-fucosyltransferase 1
-2.455	203422_at	POLD1	polymerase (DNA directed), delta 1, catalytic subunit 125kDa
-2.455	209355_s_at	PPAP2B	phosphatidic acid phosphatase type 2B
-2.455	213849_s_at	PPP2R2B	protein phosphatase 2 (formerly 2A), regulatory subunit B, beta isoform
-2.455	213483_at	PPWD1	peptidylprolyl isomerase domain and WD repeat containing 1
-2.455	205194_at	PSPH	phosphoserine phosphatase
-2.455	209815_at	PTCH1	patched homolog 1 (Drosophila)
-2.455	219076_s_at	PXMP2	peroxisomal membrane protein 2, 22kDa
-2.455	203933_at	RAB11FIP3	RAB11 family interacting protein 3 (class II)
-2.455	212781_at	RBBP6	retinoblastoma binding protein 6
-2.455	212028_at	RBM25	RNA binding motif protein 25
-2.455	218352_at	RCBTB1	regulator of chromosome condensation (RCC1) and BTB (POZ) domain containing protein 1
-2.455	214433_s_at	SELENBP1	selenium binding protein 1
-2.455	219194_at	SEMA4G	sema domain, immunoglobulin domain (Ig), transmembrane domain (TM) and short cytoplasmic domain, (semaphorin) 4G

Fold change	Affymetrix ID	Gene symbol	Entrez gene name
-2.455	220626_at	SERPINA10	serpin peptidase inhibitor, clade A (alpha-1 antiproteinase, antitrypsin), member 10
-2.455	214092_x_at	SFRS14	splicing factor, arginine/serine-rich 14
-2.455	220974_x_at	SFXN3	sideroflexin 3
-2.455	219493_at	SHCBP1	SHC SH2-domain binding protein 1
-2.455	207095_at	SLC10A2	solute carrier family 10 (sodium/bile acid cotransporter family), member 2
-2.455	202800_at	SLC1A3	solute carrier family 1 (glial high affinity glutamate transporter), member 3
-2.455	204587_at	SLC25A14	solute carrier family 25 (mitochondrial carrier, brain), member 14
-2.455	214140_at	SLC25A16	solute carrier family 25 (mitochondrial carrier; Graves disease autoantigen), member 16
-2.455	203658_at	SLC25A20	solute carrier family 25 (carnitine/acylcarnitine translocase), member 20
-2.455	218494_s_at	SLC2A4RG	SLC2A4 regulator
-2.455	205799_s_at	SLC3A1	solute carrier family 3 (cystine, dibasic and neutral amino acid transporters, activator of cystine, dibasic and neutral amino acid transport), member 1
-2.455	206565_x_at	SMA4	glucuronidase, beta pseudogene
-2.455	213253_at	SMC2	structural maintenance of chromosomes 2
-2.455	219583_s_at	SPATA7	spermatogenesis associated 7
-2.455	217813_s_at	SPIN1	spindlin 1
-2.455	211704_s_at	SPIN2B	spindlin family, member 2B
-2.455	222173_s_at	TBC1D2	TBC1 domain family, member 2
-2.455	212796_s_at	TBC1D2B	TBC1 domain family, member 2B
-2.455	201813_s_at	TBC1D5	TBC1 domain family, member 5
-2.455	203753_at	TCF4	transcription factor 4
-2.455	218584_at	TCTN1	tectonic family member 1
-2.455	218724_s_at	TGIF2	TGFB-induced factor homeobox 2
-2.455	219423_x_at	TNFRSF25	tumor necrosis factor receptor superfamily, member 25
-2.455	210372_s_at	TPD52L1	tumor protein D52-like 1
-2.455	201731_s_at	TPR	translocated promoter region (to activated MET oncogene)
-2.455	213679_at	TTC30A	tetratricopeptide repeat domain 30A
-2.455	220507_s_at	UPB1	ureidopropionase, beta
-2.455	206958_s_at	UPF3A	UPF3 regulator of nonsense transcripts homolog A (yeast)
-2.455	212606_at	WDFY3	WD repeat and FYVE domain containing 3
-2.455	209053_s_at	WHSC1	Wolf-Hirschhorn syndrome candidate 1

Fold change	Affymetrix ID	Gene symbol	Entrez gene name
-2.455	209375_at	XPC	xeroderma pigmentosum, complementation group C
-2.455	201369_s_at	ZFP36L2	zinc finger protein 36, C3H type-like 2
-2.455	213073_at	ZFYVE26	zinc finger, FYVE domain containing 26
-2.455	205739_x_at	ZNF107	zinc finger protein 107
-2.455	205514_at	ZNF415	zinc finger protein 415
-2.455	221625_at	ZNF506	zinc finger protein 506
-2.455	220617_s_at	ZNF532	zinc finger protein 532
-2.455	220661_s_at	ZNF692	zinc finger protein 692
-2.455	57516_at	ZNF764	zinc finger protein 764
-2.455	219676_at	ZSCAN16	zinc finger and SCAN domain containing 16
-2.630	205512_s_at	AIFM1	apoptosis-inducing factor, mitochondrion-associated, 1
-2.630	208950_s_at	ALDH7A1	aldehyde dehydrogenase 7 family, member A1
-2.630	214221_at	ALMS1	Alstrom syndrome 1
-2.630	212985_at	APBB2	amyloid beta (A4) precursor protein-binding, family B, member 2
-2.630	201288_at	ARHGDIB	Rho GDP dissociation inhibitor (GDI) beta
-2.630	203264_s_at	ARHGEF9	Cdc42 guanine nucleotide exchange factor (GEF) 9
-2.630	210649_s_at	ARID1A	AT rich interactive domain 1A (SWI-like)
-2.630	219218_at	BAHCC1	BAH domain and coiled-coil containing 1
-2.630	212745_s_at	BBS4	Bardet-Biedl syndrome 4
-2.630	218285_s_at	BDH2	3-hydroxybutyrate dehydrogenase, type 2
-2.630	217207_s_at	BTNL3	butyrophilin-like 3
-2.630	203257_s_at	C11ORF49	chromosome 11 open reading frame 49
-2.630	203173_s_at	C16ORF62	chromosome 16 open reading frame 62
-2.630	209007_s_at	C1ORF63	chromosome 1 open reading frame 63
-2.630	65472_at	C2ORF68	chromosome 2 open reading frame 68
-2.630	209030_s_at	CADM1	cell adhesion molecule 1
-2.630	201617_x_at	CALD1	caldesmon 1
-2.630	201616_s_at	CALD1	caldesmon 1
-2.630	212077_at	CALD1	caldesmon 1
-2.630	216598_s_at	CCL2	chemokine (C-C motif) ligand 2

Fold change	Affymetrix ID	Gene symbol	Entrez gene name
-2.630	212897_at	CDC2L6	cell division cycle 2-like 6 (CDK8-like)
-2.630	210622_x_at	CDK10	cyclin-dependent kinase 10
-2.630	218740_s_at	CDK5RAP3	CDK5 regulatory subunit associated protein 3
-2.630	213492_at	COL2A1	collagen, type II, alpha 1
-2.630	210070_s_at	CPT1B	carnitine palmitoyltransferase 1B (muscle)
-2.630	210757_x_at	DAB2	disabled homolog 2, mitogen-responsive phosphoprotein (Drosophila)
-2.630	205472_s_at	DACH1	dachshund homolog 1 (Drosophila)
-2.630	210397_at	DEFB1	defensin, beta 1
-2.630	215058_at	DENND5B	DENN/MADD domain containing 5B
-2.630	220295_x_at	DEPDC1	DEP domain containing 1
-2.630	205223_at	DEPDC5	DEP domain containing 5
-2.630	206752_s_at	DFFB	DNA fragmentation factor, 40kDa, beta polypeptide (caspase-activated DNase)
-2.630	205744_at	DOC2A	double C2-like domains, alpha
-2.630	203358_s_at	EZH2	enhancer of zeste homolog 2 (Drosophila)
-2.630	210445_at	FABP6	fatty acid binding protein 6, ileal
-2.630	203482_at	FAM178A	family with sequence similarity 178, member A
-2.630	216044_x_at	FAM69A	family with sequence similarity 69, member A
-2.630	203806_s_at	FANCA	Fanconi anemia, complementation group A
-2.630	58780_s_at	FLJ10357	hypothetical protein FLJ10357
-2.630	219316_s_at	FLVCR2	feline leukaemia virus subgroup C cellular receptor family, member 2
-2.630	202580_x_at	FOXM1	forkhead box M1
-2.630	41858_at	FRAG1	FGF receptor activating protein 1
-2.630	1598_g_at	GAS6	growth arrest-specific 6
-2.630	205498_at	GHR	growth hormone receptor
-2.630	203384_s_at	GOLGA1	Golgi autoantigen, golgin subfamily a, 1
-2.630	201057_s_at	GOLGB1	golgin B1, Golgi integral membrane protein
-2.630	215554_at	GPLD1	glycosylphosphatidylinositol specific phospholipase D1
-2.630	206204_at	GRB14	growth factor receptor-bound protein 14
-2.630	219233_s_at	GSDMB	gasdermin B
-2.630	215659_at	GSDMB	gasdermin B

Fold change	Affymetrix ID	Gene symbol	Entrez gene name
-2.630	201035_s_at	HADH	hydroxyacyl-Coenzyme A dehydrogenase
-2.630	206846_s_at	HDAC6	histone deacetylase 6
-2.630	203744_at	HMGB3	high-mobility group box 3
-2.630	214434_at	HSPA12A	heat shock 70kDa protein 12A
-2.630	219284_at	HSPBAP1	HSPB (heat shock 27kDa) associated protein 1
-2.630	201163_s_at	IGFBP7	insulin-like growth factor binding protein 7
-2.630	201162_at	IGFBP7	insulin-like growth factor binding protein 7
-2.630	221974_at	IPW	imprinted in Prader-Willi syndrome (non-protein coding)
-2.630	213392_at	IQCK	IQ motif containing K
-2.630	216958_s_at	IVD	isovaleryl Coenzyme A dehydrogenase
-2.630	212523_s_at	KIAA0146	KIAA0146
-2.630	204156_at	KIAA0999	KIAA0999 protein
-2.630	218355_at	KIF4A	kinesin family member 4A
-2.630	211651_s_at	LAMB1	laminin, beta 1
-2.630	214035_x_at	LOC399491	LOC399491 protein
-2.630	211596_s_at	LRIG1	leucine-rich repeats and immunoglobulin-like domains 1
-2.630	203668_at	MAN2C1	mannosidase, alpha, class 2C, member 1
-2.630	218366_x_at	METT11D1	methyltransferase 11 domain containing 1
-2.630	205442_at	MFAP3L	microfibrillar-associated protein 3-like
-2.630	211038_s_at	MGC12760	ciliary rootlet coiled-coil, rootletin-like 1
-2.630	221771_s_at	MPHOSPH8	M-phase phosphoprotein 8
-2.630	214071_at	MPPE1	metallophosphoesterase 1
-2.630	203678_at	MTMR15	myotubularin related protein 15
-2.630	212277_at	MTMR4	myotubularin related protein 4
-2.630	212096_s_at	MTUS1	mitochondrial tumor suppressor 1
-2.630	210778_s_at	MXD4	MAX dimerisation protein 4
-2.630	214765_s_at	NAAA	N-acylethanolamine acid amidase
-2.630	201970_s_at	NASP	nuclear autoantigenic sperm protein (histone-binding)
-2.630	214693_x_at	NBPF8	neuroblastoma breakpoint family, member 8
-2.630	201774_s_at	NCAPD2	non-SMC condensin I complex, subunit D2

Fold change	Affymetrix ID	Gene symbol	Entrez gene name
-2.630	212789_at	NCAPD3	non-SMC condensin II complex, subunit D3
-2.630	212949_at	NCAPH	non-SMC condensin I complex, subunit H
-2.630	210249_s_at	NCOA1	nuclear receptor coactivator 1
-2.630	210174_at	NR5A2	nuclear receptor subfamily 5, group A, member 2
-2.630	207877_s_at	NVL	nuclear VCP-like
-2.630	201599_at	OAT	ornithine aminotransferase (gyrate atrophy)
-2.630	212307_s_at	OGT	O-linked N-acetylglucosamine (GlcNAc) transferase (UDP-N-acetylglucosamine:polypeptide-N-acetylglucosaminyl transferase)
-2.630	207564_x_at	OGT	O-linked N-acetylglucosamine (GlcNAc) transferase (UDP-N-acetylglucosamine:polypeptide-N-acetylglucosaminyl transferase)
-2.630	205040_at	ORM1	orosomucoid 1
-2.630	207838_x_at	PBXIP1	pre-B-cell leukaemia homeobox interacting protein 1
-2.630	213517_at	PCBP2	poly(rC) binding protein 2
-2.630	202174_s_at	PCM1	pericentriolar material 1
-2.630	221142_s_at	PECR	peroxisomal trans-2-enoyl-CoA reductase
-2.630	201701_s_at	PGRMC2	progesterone receptor membrane component 2
-2.630	222150_s_at	PION	pigeon homolog (Drosophila)
-2.630	177_at	PLD1	phospholipase D1, phosphatidylcholine-specific
-2.630	212841_s_at	PPFIBP2	PTPRF interacting protein, binding protein 2 (liprin beta 2)
-2.630	204788_s_at	PPOX	protoporphyrinogen oxidase
-2.630	216347_s_at	PPP1R13B	protein phosphatase 1, regulatory (inhibitor) subunit 13B
-2.630	211090_s_at	PRPF4B	PRP4 pre-mRNA processing factor 4 homolog B (yeast)
-2.630	208165_s_at	PRSS16	protease, serine, 16 (thymus)
-2.630	205961_s_at	PSIP1	PC4 and SFRS1 interacting protein 1
-2.630	205048_s_at	PSPH	phosphoserine phosphatase
-2.630	220500_s_at	RABL2A	RAB, member of RAS oncogene family-like 2A
-2.630	209349_at	RAD50	RAD50 homolog (S. cerevisiae)
-2.630	219494_at	RAD54B	RAD54 homolog B (S. cerevisiae)
-2.630	210106_at	RDH5	retinol dehydrogenase 5 (11-cis/9-cis)
-2.630	215201_at	REPS1	RALBP1 associated Eps domain containing 1
-2.630	218370_s_at	S100PBP	S100P binding protein

Fold change	Affymetrix ID	Gene symbol	Entrez gene name
-2.630	209741_x_at	SCAPER	S phase cyclin A-associated protein in the ER
-2.630	216399_s_at	SCAPER	S phase cyclin A-associated protein in the ER
-2.630	212158_at	SDC2	syndecan 2
-2.630	218649_x_at	SDCCAG1	serologically defined colon cancer antigen 1
-2.630	219751_at	SETD6	SET domain containing 6
-2.630	36129_at	SGSM2	small G protein signaling modulator 2
-2.630	213308_at	SHANK2	SH3 and multiple ankyrin repeat domains 2
-2.630	206664_at	SI	sucrase-isomaltase (alpha-glucosidase)
-2.630	202254_at	SIPA1L1	signal-induced proliferation-associated 1 like 1
-2.630	204404_at	SLC12A2	solute carrier family 12 (sodium/potassium/chloride transporters), member 2
-2.630	211855_s_at	SLC25A14	solute carrier family 25 (mitochondrial carrier, brain), member 14
-2.630	218978_s_at	SLC25A37	solute carrier family 25, member 37
-2.630	222217_s_at	SLC27A3	solute carrier family 27 (fatty acid transporter), member 3
-2.630	217122_s_at	SLC35E2	solute carrier family 35, member E2
-2.630	202830_s_at	SLC37A4	solute carrier family 37 (glucose-6-phosphate transporter), member 4
-2.630	204240_s_at	SMC2	structural maintenance of chromosomes 2
-2.630	219109_at	SPAG16	sperm associated antigen 16
-2.630	203145_at	SPAG5	sperm associated antigen 5
-2.630	202440_s_at	ST5	suppression of tumorigenicity 5
-2.630	221264_s_at	TARDBP	TAR DNA binding protein
-2.630	222116_s_at	TBC1D16	TBC1 domain family, member 16
-2.630	211052_s_at	TBCD	tubulin folding cofactor D
-2.630	221016_s_at	TCF7L1	transcription factor 7-like 1 (T-cell specific, HMG-box)
-2.630	201042_at	TGM2	transglutaminase 2 (C polypeptide, protein-glutamine-gamma-glutamyltransferase)
-2.630	54632_at	THADA	thyroid adenoma associated
-2.630	201450_s_at	TIA1	TIA1 cytotoxic granule-associated RNA binding protein
-2.630	210166_at	TLR5	toll-like receptor 5
-2.630	219410_at	TMEM45A	transmembrane protein 45A
-2.630	210886_x_at	TP53TG1	TP53 target 1 (non-protein coding)
-2.630	201730_s_at	TPR	translocated promoter region (to activated MET oncogene)

Fold change	Affymetrix ID	Gene symbol	Entrez gene name
-2.630	209660_at	TTR	transthyretin
-2.630	218289_s_at	UBA5	ubiquitin-like modifier activating enzyme 5
-2.630	206959_s_at	UPF3A	UPF3 regulator of nonsense transcripts homolog A (yeast)
-2.630	212980_at	USP34	ubiquitin specific peptidase 34
-2.630	204255_s_at	VDR	vitamin D (1,25- dihydroxyvitamin D3) receptor
-2.630	204254_s_at	VDR	vitamin D (1,25- dihydroxyvitamin D3) receptor
-2.630	218396_at	VPS13C	vacuolar protein sorting 13 homolog C (S. cerevisiae)
-2.630	221103_s_at	WDR52	WD repeat domain 52
-2.630	209054_s_at	WHSC1	Wolf-Hirschhorn syndrome candidate 1
-2.630	201294_s_at	WSB1	WD repeat and SOCS box-containing 1
-2.630	203959_s_at	ZBTB40	zinc finger and BTB domain containing 40
-2.630	222186_at	ZFAND6	zinc finger, AN1-type domain 6
-2.630	201367_s_at	ZFP36L2	zinc finger protein 36, C3H type-like 2
-2.630	207605_x_at	ZNF117	zinc finger protein 117
-2.630	221645_s_at	ZNF83	zinc finger protein 83
-2.818	220841_s_at	AHI1	Abelson helper integration site 1
-2.818	205640_at	ALDH3B1	aldehyde dehydrogenase 3 family, member B1
-2.818	208951_at	ALDH7A1	aldehyde dehydrogenase 7 family, member A1
-2.818	216563_at	ANKRD12	ankyrin repeat domain 12
-2.818	220940_at	ANKRD36B	ankyrin repeat domain 36B
-2.818	219842_at	ARL15	ADP-ribosylation factor-like 15
-2.818	219164_s_at	ATG2B	ATG2 autophagy related 2 homolog B (S. cerevisiae)
-2.818	210858_x_at	ATM	ataxia telangiectasia mutated
-2.818	214132_at	ATP5C1	ATP synthase, H+ transporting, mitochondrial F1 complex, gamma polypeptide 1
-2.818	214742_at	AZI1	5-azacytidine induced 1
-2.818	211715_s_at	BDH1	3-hydroxybutyrate dehydrogenase, type 1
-2.818	204531_s_at	BRCA1	breast cancer 1, early onset
-2.818	221208_s_at	C11ORF61	chromosome 11 open reading frame 61
-2.818	53720_at	C19ORF66	chromosome 19 open reading frame 66
-2.818	220149_at	C2ORF54	chromosome 2 open reading frame 54

Fold change	Affymetrix ID	Gene symbol	Entrez gene name
-2.818	209285_s_at	C3ORF63	chromosome 3 open reading frame 63
-2.818	220234_at	CA8	carbonic anhydrase VIII
-2.818	218456_at	CAPRIN2	caprin family member 2
-2.818	211922_s_at	CAT	catalase
-2.818	203469_s_at	CDK10	cyclin-dependent kinase 10
-2.818	209172_s_at	CENPF	centromere protein F, 350/400ka (mitosin)
-2.818	219242_at	CEP63	centrosomal protein 63kDa
-2.818	219301_s_at	CNTNAP2	contactin associated protein-like 2
-2.818	221971_x_at	CTGLF1	centaurin, gamma-like family, member 1
-2.818	216058_s_at	CYP2C19	cytochrome P450, family 2, subfamily C, polypeptide 19
-2.818	220562_at	CYP2W1	cytochrome P450, family 2, subfamily W, polypeptide 1
-2.818	203409_at	DDB2	damage-specific DNA binding protein 2, 48kDa
-2.818	206457_s_at	DIO1	deiodinase, iodothyronine, type I
-2.818	220572_at	DKFZP547G183	hypothetical LOC55525
-2.818	203764_at	DLGAP5	discs, large (Drosophila) homolog-associated protein 5
-2.818	203763_at	DYNC2LI1	dynein, cytoplasmic 2, light intermediate chain 1
-2.818	219990_at	E2F8	E2F transcription factor 8
-2.818	209696_at	FBP1	fructose-1,6-bisphosphatase 1
-2.818	218920_at	FLJ10404	hypothetical protein FLJ10404
-2.818	214093_s_at	FUBP1	far upstream element (FUSE) binding protein 1
-2.818	203179_at	GALT	galactose-1-phosphate uridylyltransferase
-2.818	213552_at	GLCE	glucuronic acid epimerase
-2.818	205531_s_at	GLS2	glutaminase 2 (liver, mitochondrial)
-2.818	218147_s_at	GLT8D1	glycosyltransferase 8 domain containing 1
-2.818	201567_s_at	GOLGA4	Golgi autoantigen, golgin subfamily a, 4
-2.818	213706_at	GPD1	glycerol-3-phosphate dehydrogenase 1 (soluble)
-2.818	212070_at	GPR56	G protein-coupled receptor 56
-2.818	204793_at	GPRASP1	G protein-coupled receptor associated sorting protein 1
-2.818	209377_s_at	HMGN3	high mobility group nucleosomal binding domain 3
-2.818	218780_at	HOOK2	hook homolog 2 (Drosophila)

Fold change	Affymetrix ID	Gene symbol	Entrez gene name
-2.818	204792_s_at	IFT140	intraflagellar transport 140 homolog (Chlamydomonas)
-2.818	204703_at	IFT88	intraflagellar transport 88 homolog (Chlamydomonas)
-2.818	213804_at	INPP5B	inositol polyphosphate-5-phosphatase, 75kDa
-2.818	203906_at	IQSEC1	IQ motif and Sec7 domain 1
-2.818	221125_s_at	KCNMB3	potassium large conductance calcium-activated channel, subfamily M beta member 3
-2.818	219479_at	KDELC1	KDEL (Lys-Asp-Glu-Leu) containing 1
-2.818	216969_s_at	KIF22	kinesin family member 22
-2.818	208450_at	LGALS2	lectin, galactoside-binding, soluble, 2
-2.818	202726_at	LIG1	ligase I, DNA, ATP-dependent
-2.818	221501_x_at	LOC339047	hypothetical protein LOC339047
-2.818	215920_s_at	LOC440350	similar to nuclear pore complex interacting protein
-2.818	37796_at	LRCH4	leucine-rich repeats and calponin homology (CH) domain containing 4
-2.818	219999_at	MAN2A2	mannosidase, alpha, class 2A, member 2
-2.818	204041_at	MAOB	monoamine oxidase B
-2.818	35147_at	MCF2L	MCF.2 cell line derived transforming sequence-like
-2.818	221636_s_at	MOSC2	MOCO sulphurase C-terminal domain containing 2
-2.818	222369_at	NAT11	N-acetyltransferase 11 (GCN5-related, putative)
-2.818	207631_at	NBR2	neighbor of BRCA1 gene 2
-2.818	218662_s_at	NCAPG	non-SMC condensin I complex, subunit G
-2.818	209106_at	NCOA1	nuclear receptor coactivator 1
-2.818	209289_at	NFIB	nuclear factor I/B
-2.818	201591_s_at	NISCH	nischarin
-2.818	219553_at	NME7	non-metastatic cells 7, protein expressed in (nucleoside-diphosphate kinase)
-2.818	213471_at	NPHP4	nephronophthisis 4
-2.818	204538_x_at	NPIP	nuclear pore complex interacting protein
-2.818	216321_s_at	NR3C1	nuclear receptor subfamily 3, group C, member 1 (glucocorticoid receptor)
-2.818	212776_s_at	OBSL1	obscurin-like 1
-2.818	220133_at	ODAM	odontogenic, ameloblast asssociated
-2.818	205564_at	PAGE4	P antigen family, member 4 (prostate associated)
-2.818	203117_s_at	PAN2	PAN2 polyA specific ribonuclease subunit homolog (S. cerevisiae)

Fold change	Affymetrix ID	Gene symbol	Entrez gene name
-2.818	209439_s_at	PHKA2	phosphorylase kinase, alpha 2 (liver)
-2.818	207081_s_at	PI4KA	phosphatidylinositol 4-kinase, catalytic, alpha
-2.818	201929_s_at	PKP4	plakophilin 4
-2.818	221088_s_at	PPP1R9A	protein phosphatase 1, regulatory (inhibitor) subunit 9A
-2.818	205037_at	RABL4	RAB, member of RAS oncogene family-like 4
-2.818	205178_s_at	RBBP6	retinoblastoma binding protein 6
-2.818	219754_at	RBM41	RNA binding motif protein 41
-2.818	209497_s_at	RBM4B	RNA binding motif protein 4B
-2.818	204364_s_at	REEP1	receptor accessory protein 1
-2.818	219610_at	RGNEF	Rho-guanine nucleotide exchange factor
-2.818	213555_at	RWDD2A	RWD domain containing 2A
-2.818	206325_at	SERPINA6	serpin peptidase inhibitor, clade A (alpha-1 antiproteinase, antitrypsin), member 6
-2.818	212000_at	SFRS14	splicing factor, arginine/serine-rich 14
-2.818	217289_s_at	SLC37A4	solute carrier family 37 (glucose-6-phosphate transporter), member 4
-2.818	214850_at	SMA4	glucuronidase, beta pseudogene
-2.818	207069_s_at	SMAD6	SMAD family member 6
-2.818	201664_at	SMC4	structural maintenance of chromosomes 4
-2.818	218087_s_at	SORBS1	sorbin and SH3 domain containing 1
-2.818	213994_s_at	SPON1	spondin 1, extracellular matrix protein
-2.818	213993_at	SPON1	spondin 1, extracellular matrix protein
-2.818	209436_at	SPON1	spondin 1, extracellular matrix protein
-2.818	203769_s_at	STS	steroid sulfatase (microsomal), isozyme S
-2.818	213971_s_at	SUZ12	suppressor of zeste 12 homolog (Drosophila)
-2.818	213913_s_at	TBC1D30	TBC1 domain family, member 30
-2.818	201447_at	TIA1	TIA1 cytotoxic granule-associated RNA binding protein
-2.818	221951_at	TMEM80	transmembrane protein 80
-2.818	209354_at	TNFRSF14	tumor necrosis factor receptor superfamily, member 14 (herpesvirus entry mediator)
-2.818	201292_at	TOP2A	topoisomerase (DNA) II alpha 170kDa
-2.818	210241_s_at	TP53TG1	TP53 target 1 (non-protein coding)
-2.818	213266_at	TUBGCP4	tubulin, gamma complex associated protein 4

Fold change	Affymetrix ID	Gene symbol	Entrez gene name
-2.818	207559_s_at	ZMYM3	zinc finger, MYM-type 3
-2.818	213269_at	ZNF248	zinc finger protein 248
-2.818	221213_s_at	ZNF280D	zinc finger protein 280D
-2.818	214813_at	ZNF75D	zinc finger protein 75D
-3.020	205969_at	AADAC	arylacetamide deacetylase (esterase)
-3.020	205209_at	ACVR1B	activin A receptor, type IB
-3.020	203609_s_at	ALDH5A1	aldehyde dehydrogenase 5 family, member A1
-3.020	221588_x_at	ALDH6A1	aldehyde dehydrogenase 6 family, member A1
-3.020	211712_s_at	ANXA9	annexin A9
-3.020	218067_s_at	ARGLU1	arginine and glutamate rich 1
-3.020	221656_s_at	ARHGEF10L	Rho guanine nucleotide exchange factor (GEF) 10-like
-3.020	205673_s_at	ASB9	ankyrin repeat and SOCS box-containing 9
-3.020	218857_s_at	ASRGL1	asparaginase like 1
-3.020	203188_at	B3GNT1	UDP-GlcNAc:betaGal beta-1,3-N-acetylglucosaminyltransferase 1
-3.020	203755_at	BUB1B	budding uninhibited by benzimidazoles 1 homolog beta (yeast)
-3.020	221878_at	C2ORF68	chromosome 2 open reading frame 68
-3.020	214475_x_at	CAPN3	calpain 3, (p94)
-3.020	212886_at	CCDC69	coiled-coil domain containing 69
-3.020	207173_x_at	CDH11	cadherin 11, type 2, OB-cadherin (osteoblast)
-3.020	218827_s_at	CEP192	centrosomal protein 192kDa
-3.020	202310_s_at	COL1A1	collagen, type I, alpha 1
-3.020	204136_at	COL7A1	collagen, type VII, alpha 1
-3.020	208835_s_at	CROP	cisplatin resistance-associated overexpressed protein
-3.020	203804_s_at	CROP	cisplatin resistance-associated overexpressed protein
-3.020	204055_s_at	CTAGE5	CTAGE family, member 5
-3.020	219355_at	CXORF57	chromosome X open reading frame 57
-3.020	213378_s_at	DDX11	DEAD/H (Asp-Glu-Ala-Asp/His) box polypeptide 11 (CHL1-like helicase homolog, S. cerevisiae)
-3.020	208159_x_at	DDX11	DEAD/H (Asp-Glu-Ala-Asp/His) box polypeptide 11 (CHL1-like helicase homolog, S. cerevisiae)
-3.020	213279_at	DHRS1	dehydrogenase/reductase (SDR family) member 1
-3.020	213271_s_at	DOPEY1	dopey family member 1

Fold change	Affymetrix ID	Gene symbol	Entrez gene name
-3.020	201025_at	EIF5B	eukaryotic translation initiation factor 5B
-3.020	204143_s_at	ENOSF1	enolase superfamily member 1
-3.020	221884_at	EVI1	ecotropic viral integration site 1
-3.020	204379_s_at	FGFR3	fibroblast growth factor receptor 3
-3.020	222018_at	FKSG17	nascent-polypeptide-associated complex alpha polypeptide pseudogene 1
-3.020	203178_at	GATM	glycine amidinotransferase (L-arginine:glycine amidinotransferase)
-3.020	204836_at	GLDC	glycine dehydrogenase (decarboxylating)
-3.020	204324_s_at	GOLIM4	Golgi integral membrane protein 4
-3.020	210912_x_at	GSTM4	glutathione S-transferase mu 4
-3.020	201036_s_at	HADH	hydroxyacyl-Coenzyme A dehydrogenase
-3.020	207156_at	HIST1H2AK	histone cluster 1, H2ak
-3.020	213931_at	ID2	inhibitor of DNA binding 2, dominant negative helix-loop-helix protein
-3.020	205304_s_at	KCNJ8	potassium inwardly-rectifying channel, subfamily J, member 8
-3.020	218755_at	KIF20A	kinesin family member 20A
-3.020	205235_s_at	KIF20B	kinesin family member 20B
-3.020	205668_at	LY75	lymphocyte antigen 75
-3.020	211042_x_at	MCAM	melanoma cell adhesion molecule
-3.020	206522_at	MGAM	maltase-glucoamylase (alpha-glucosidase)
-3.020	213181_s_at	MOCS1	molybdenum cofactor synthesis 1
-3.020	221965_at	MPHOSPH9	M-phase phosphoprotein 9
-3.020	212095_s_at	MTUS1	mitochondrial tumor suppressor 1
-3.020	213067_at	MYH10	myosin, heavy chain 10, non-muscle
-3.020	210336_x_at	MZF1	myeloid zinc finger 1
-3.020	40569_at	MZF1	myeloid zinc finger 1
-3.020	215434_x_at	NBPF8	neuroblastoma breakpoint family, member 8
-3.020	203245_s_at	NCRNA00094	non-protein coding RNA 94
-3.020	215338_s_at	NKTR	natural killer-tumor recognition sequence
-3.020	202379_s_at	NKTR	natural killer-tumor recognition sequence
-3.020	208343_s_at	NR5A2	nuclear receptor subfamily 5, group A, member 2
-3.020	214130_s_at	PDE4DIP	phosphodiesterase 4D interacting protein

Fold change	Affymetrix ID	Gene symbol	Entrez gene name
-3.020	214129_at	PDE4DIP	phosphodiesterase 4D interacting protein
-3.020	212094_at	PEG10	paternally expressed 10
-3.020	219225_at	PGBD5	piggyBac transposable element derived 5
-3.020	213408_s_at	PI4KA	phosphatidylinositol 4-kinase, catalytic, alpha
-3.020	201927_s_at	PKP4	plakophilin 4
-3.020	205203_at	PLD1	phospholipase D1, phosphatidylcholine-specific
-3.020	206940_s_at	POU4F1	POU class 4 homeobox 1
-3.020	208993_s_at	PPIG	peptidylprolyl isomerase G (cyclophilin G)
-3.020	201213_at	PPP1R7	protein phosphatase 1, regulatory (inhibitor) subunit 7
-3.020	202127_at	PRPF4B	PRP4 pre-mRNA processing factor 4 homolog B (yeast)
-3.020	213521_at	PTPN18	protein tyrosine phosphatase, non-receptor type 18 (brain-derived)
-3.020	204547_at	RAB40B	RAB40B, member RAS oncogene family
-3.020	219222_at	RBKS	ribokinase
-3.020	57540_at	RBKS	ribokinase
-3.020	202449_s_at	RXRA	retinoid X receptor, alpha
-3.020	214402_s_at	SFI1	Sfi1 homolog, spindle assembly associated (yeast)
-3.020	36545_s_at	SFI1	Sfi1 homolog, spindle assembly associated (yeast)
-3.020	214016_s_at	SFPQ	splicing factor proline/glutamine-rich (polypyrimidine tract binding protein associated)
-3.020	64371_at	SFRS14	splicing factor, arginine/serine-rich 14
-3.020	221010_s_at	SIRT5	sirtuin (silent mating type information regulation 2 homolog) 5 (S. cerevisiae)
-3.020	210567_s_at	SKP2	S-phase kinase-associated protein 2 (p45)
-3.020	221572_s_at	SLC26A6	solute carrier family 26, member 6
-3.020	220435_at	SLC30A10	solute carrier family 30, member 10
-3.020	213721_at	SOX2	SRY (sex determining region Y)-box 2
-3.020	213103_at	STARD13	StAR-related lipid transfer (START) domain containing 13
-3.020	222146_s_at	TCF4	transcription factor 4
-3.020	218491_s_at	THYN1	thymocyte nuclear protein 1
-3.020	201446_s_at	TIA1	TIA1 cytotoxic granule-associated RNA binding protein
-3.020	214833_at	TMEM63A	transmembrane protein 63A
-3.020	209917_s_at	TP53TG1	TP53 target 1 (non-protein coding)

Fold change	Affymetrix ID	Gene symbol	Entrez gene name
-3.020	203568_s_at	TRIM38	tripartite motif-containing 38
-3.020	221897_at	TRIM52	tripartite motif-containing 52
-3.020	202242_at	TSPAN7	tetraspanin 7
-3.020	217684_at	TYMS	thymidylate synthetase
-3.020	207245_at	UGT2B17	UDP glucuronosyltransferase 2 family, polypeptide B17
-3.020	218806_s_at	VAV3	vav 3 guanine nucleotide exchange factor
-3.020	212326_at	VPS13D	vacuolar protein sorting 13 homolog D (S. cerevisiae)
-3.020	214567_s_at	XCL2	chemokine (C motif) ligand 2
-3.020	205672_at	XPA	xeroderma pigmentosum, complementation group A
-3.020	203521_s_at	ZNF318	zinc finger protein 318
-3.236	209459_s_at	ABAT	4-aminobutyrate aminotransferase
-3.236	213353_at	ABCA5	ATP-binding cassette, sub-family A (ABC1), member 5
-3.236	218844_at	ACSF2	acyl-CoA synthetase family member 2
-3.236	214261_s_at	ADH6	alcohol dehydrogenase 6 (class V)
-3.236	221569_at	AHI1	Abelson helper integration site 1
-3.236	204551_s_at	AHSG	alpha-2-HS-glycoprotein
-3.236	221589_s_at	ALDH6A1	aldehyde dehydrogenase 6 family, member A1
-3.236	214220_s_at	ALMS1	Alstrom syndrome 1
-3.236	208323_s_at	ANXA13	annexin A13
-3.236	210085_s_at	ANXA9	annexin A9
-3.236	205216_s_at	APOH	apolipoprotein H (beta-2-glycoprotein I)
-3.236	203747_at	AQP3	aquaporin 3 (Gill blood group)
-3.236	221135_s_at	ASTE1	asteroid homolog 1 (Drosophila)
-3.236	208859_s_at	ATRX	alpha thalassemia/mental retardation syndrome X-linked (RAD54 homolog, S. cerevisiae)
-3.236	37547_at	BBS9	Bardet-Biedl syndrome 9
-3.236	214727_at	BRCA2	breast cancer 2, early onset
-3.236	207259_at	C17ORF73	chromosome 17 open reading frame 73
-3.236	219381_at	C5ORF42	chromosome 5 open reading frame 42
-3.236	221427_s_at	CCNL2	cyclin L2
-3.236	202870_s_at	CDC20	cell division cycle 20 homolog (S. cerevisiae)

Fold change	Affymetrix ID	Gene symbol	Entrez gene name
-3.236	205250_s_at	CEP290	centrosomal protein 290kDa
-3.236	219036_at	CEP70	centrosomal protein 70kDa
-3.236	203854_at	CFI	complement factor I
-3.236	215318_at	CG012	hypothetical gene CG012
-3.236	203641_s_at	COBLL1	COBL-like 1
-3.236	220072_at	CSPP1	centrosome and spindle pole associated protein 1
-3.236	211126_s_at	CSRP2	cysteine and glycine-rich protein 2
-3.236	206775_at	CUBN	cubilin (intrinsic factor-cobalamin receptor)
-3.236	212820_at	DMXL2	Dmx-like 2
-3.236	213186_at	DZIP3	DAZ interacting protein 3, zinc finger
-3.236	219833_s_at	EFHC1	EF-hand domain (C-terminal) containing 1
-3.236	201936_s_at	EIF4G3	eukaryotic translation initiation factor 4 gamma, 3
-3.236	214313_s_at	EIF5B	eukaryotic translation initiation factor 5B
-3.236	201024_x_at	EIF5B	eukaryotic translation initiation factor 5B
-3.236	214314_s_at	EIF5B	eukaryotic translation initiation factor 5B
-3.236	216836_s_at	ERBB2	v-erb-b2 erythroblastic leukaemia viral oncogene homolog 2, neuro/glioblastoma derived oncogene homolog (avian)
-3.236	207300_s_at	F7	coagulation factor VII (serum prothrombin conversion accelerator)
-3.236	218248_at	FAM111A	family with sequence similarity 111, member A
-3.236	212991_at	FBXO9	F-box protein 9
-3.236	204988_at	FGB	fibrinogen beta chain
-3.236	205022_s_at	FOXN3	forkhead box N3
-3.236	216733_s_at	GATM	glycine amidinotransferase (L-arginine:glycine amidinotransferase)
-3.236	205505_at	GCNT1	glucosaminyl (N-acetyl) transferase 1, core 2 (beta-1,6-N-acetylglucosaminyltransferase)
-3.236	201056_at	GOLGB1	golgin B1, Golgi integral membrane protein
-3.236	204149_s_at	GSTM4	glutathione S-transferase mu 4
-3.236	210964_s_at	GYG2	glycogenin 2
-3.236	213069_at	HEG1	HEG homolog 1 (zebrafish)
-3.236	201565_s_at	ID2	inhibitor of DNA binding 2, dominant negative helix-loop-helix protein
-3.236	209341_s_at	IKBKB	inhibitor of kappa light polypeptide gene enhancer in B-cells, kinase beta
-3.236	48825_at	ING4	inhibitor of growth family, member 4

Fold change	Affymetrix ID	Gene symbol	Entrez gene name
-3.236	219095_at	JMJD7-PLA2G4B	JMJD7-PLA2G4B readthrough transcript
-3.236	211028_s_at	KHK	ketohexokinase (fructokinase)
-3.236	203276_at	LMNB1	lamin B1
-3.236	215283_at	LOC400642	hypothetical LOC400642
-3.236	200785_s_at	LRP1	low density lipoprotein-related protein 1 (alpha-2-macroglobulin receptor)
-3.236	205698_s_at	MAP2K6	mitogen-activated protein kinase kinase 6
-3.236	214778_at	MEGF8	multiple EGF-like-domains 8
-3.236	217610_at	MGC13098	polymerase (RNA) II (DNA directed) polypeptide J4, pseudogene
-3.236	212023_s_at	MKI67	antigen identified by monoclonal antibody Ki-67
-3.236	212021_s_at	MKI67	antigen identified by monoclonal antibody Ki-67
-3.236	221163_s_at	MLXIPL	MLX interacting protein-like
-3.236	204861_s_at	NAIP	NLR family, apoptosis inhibitory protein
-3.236	201969_at	NASP	nuclear autoantigenic sperm protein (histone-binding)
-3.236	213328_at	NEK1	NIMA (never in mitosis gene a)-related kinase 1
-3.236	213029_at	NFIB	nuclear factor I/B
-3.236	202380_s_at	NKTR	natural killer-tumor recognition sequence
-3.236	208337_s_at	NR5A2	nuclear receptor subfamily 5, group A, member 2
-3.236	219277_s_at	OGDHL	oxoglutarate dehydrogenase-like
-3.236	219236_at	PAQR6	progestin and adipoQ receptor family member VI
-3.236	213227_at	PGRMC2	progesterone receptor membrane component 2
-3.236	209740_s_at	PNPLA4	patatin-like phospholipase domain containing 4
-3.236	210499_s_at	PQBP1	polyglutamine binding protein 1
-3.236	216048_s_at	RHOBTB3	Rho-related BTB domain containing 3
-3.236	212001_at	SFRS14	splicing factor, arginine/serine-rich 14
-3.236	222248_s_at	SIRT4	sirtuin (silent mating type information regulation 2 homolog) 4 (S. cerevisiae)
-3.236	213119_at	SLC36A1	solute carrier family 36 (proton/amino acid symporter), member 1
-3.236	201663_s_at	SMC4	structural maintenance of chromosomes 4
-3.236	213221_s_at	SNF1LK2	salt-inducible kinase 2
-3.236	204067_at	SUOX	sulfite oxidase
-3.236	206546_at	SYCP2	synaptonemal complex protein 2

Fold change	Affymetrix ID	Gene symbol	Entrez gene name
-3.236	213891_s_at	TCF4	transcription factor 4
-3.236	220212_s_at	THADA	thyroid adenoma associated
-3.236	203046_s_at	TIMELESS	timeless homolog (Drosophila)
-3.236	201291_s_at	TOP2A	topoisomerase (DNA) II alpha 170kDa
-3.236	214755_at	UAP1L1	UDP-N-acteylglucosamine pyrophosphorylase 1-like 1
-3.236	213243_at	VPS13B	vacuolar protein sorting 13 homolog B (yeast)
-3.236	201295_s_at	WSB1	WD repeat and SOCS box-containing 1
-3.236	214776_x_at	XYLB	xylulokinase homolog (H. influenzae)
-3.236	212704_at	ZCCHC11	zinc finger, CCHC domain containing 11
-3.236	212655_at	ZCCHC14	zinc finger, CCHC domain containing 14
-3.236	212601_at	ZZEF1	zinc finger, ZZ-type with EF-hand domain 1
-3.467	210377_at	ACSM3	acyl-CoA synthetase medium-chain family member 3
-3.467	209425_at	AMACR	alpha-methylacyl-CoA racemase
-3.467	209521_s_at	AMOT	angiomotin
-3.467	202921_s_at	ANK2	ankyrin 2, neuronal
-3.467	212517_at	ATRN	attractin
-3.467	206913_at	BAAT	bile acid Coenzyme A: amino acid N-acyltransferase (glycine N-choloyltransferase)
-3.467	218471_s_at	BBS1	Bardet-Biedl syndrome 1
-3.467	212744_at	BBS4	Bardet-Biedl syndrome 4
-3.467	207655_s_at	BLNK	B-cell linker
-3.467	218298_s_at	C14ORF159	chromosome 14 open reading frame 159
-3.467	213148_at	C2ORF72	chromosome 2 open reading frame 72
-3.467	220751_s_at	C5ORF4	chromosome 5 open reading frame 4
-3.467	215985_at	C6ORF12	chromosome 6 open reading frame 12
-3.467	210409_at	C6ORF124	chromosome 6 open reading frame 124
-3.467	209031_at	CADM1	cell adhesion molecule 1
-3.467	211890_x_at	CAPN3	calpain 3, (p94)
-3.467	212586_at	CAST	calpastatin
-3.467	220307_at	CD244	CD244 molecule, natural killer cell receptor 2B4
-3.467	203468_at	CDK10	cyclin-dependent kinase 10

Fold change	Affymetrix ID	Gene symbol	Entrez gene name
-3.467	221683_s_at	CEP290	centrosomal protein 290kDa
-3.467	206633_at	CHRNA1	cholinergic receptor, nicotinic, alpha 1 (muscle)
-3.467	206224_at	CST1	cystatin SN
-3.467	203558_at	CUL7	cullin 7
-3.467	205311_at	DDC	dopa decarboxylase (aromatic L-amino acid decarboxylase)
-3.467	220668_s_at	DNMT3B	DNA (cytosine-5-)-methyltransferase 3 beta
-3.467	210656_at	EED	embryonic ectoderm development
-3.467	204797_s_at	EML1	echinoderm microtubule associated protein like 1
-3.467	202177_at	GAS6	growth arrest-specific 6
-3.467	211569_s_at	HADH	hydroxyacyl-Coenzyme A dehydrogenase
-3.467	206194_at	HOXC4	homeobox C4
-3.467	206858_s_at	HOXC6	homeobox C6
-3.467	202390_s_at	HTT	huntingtin
-3.467	207194_s_at	ICAM4	intercellular adhesion molecule 4 (Landsteiner-Wiener blood group)
-3.467	206364_at	KIF14	kinesin family member 14
-3.467	215446_s_at	LOX	lysyl oxidase
-3.467	218437_s_at	LZTFL1	leucine zipper transcription factor-like 1
-3.467	213761_at	MDM1	Mdm1 nuclear protein homolog (mouse)
-3.467	212020_s_at	MKI67	antigen identified by monoclonal antibody Ki-67
-3.467	219703_at	MNS1	meiosis-specific nuclear structural 1
-3.467	218865_at	MOSC1	MOCO sulphurase C-terminal domain containing 1
-3.467	210410_s_at	MSH5	mutS homolog 5 (E. coli)
-3.467	211916_s_at	MYO1A	myosin IA
-3.467	222161_at	NAALAD2	N-acetylated alpha-linked acidic dipeptidase 2
-3.467	209290_s_at	NFIB	nuclear factor I/B
-3.467	209119_x_at	NR2F2	nuclear receptor subfamily 2, group F, member 2
-3.467	222128_at	NSUN6	NOL1/NOP2/Sun domain family, member 6
-3.467	219630_at	PDZK1IP1	PDZK1 interacting protein 1
-3.467	220041_at	PIGZ	phosphatidylinositol glycan anchor biosynthesis, class Z
-3.467	208994_s_at	PPIG	peptidylprolyl isomerase G (cyclophilin G)

Fold change	Affymetrix ID	Gene symbol	Entrez gene name
-3.467	213093_at	PRKCA	protein kinase C, alpha
-3.467	214203_s_at	PRODH	proline dehydrogenase (oxidase) 1
-3.467	201896_s_at	PSRC1	proline/serine-rich coiled-coil 1
-3.467	218700_s_at	RAB7L1	RAB7, member RAS oncogene family-like 1
-3.467	218699_at	RAB7L1	RAB7, member RAS oncogene family-like 1
-3.467	205075_at	SERPINF2	serpin peptidase inhibitor, clade F (alpha-2 antiplasmin,pigment epithelium derived factor), member 2
-3.467	212179_at	SFRS18	splicing factor, arginine/serine-rich 18
-3.467	217226_s_at	SFXN3	sideroflexin 3
-3.467	217538_at	SGSM2	small G protein signaling modulator 2
-3.467	209980_s_at	SHMT1	serine hydroxymethyltransferase 1 (soluble)
-3.467	203625_x_at	SKP2	S-phase kinase-associated protein 2 (p45)
-3.467	205896_at	SLC22A4	solute carrier family 22 (organic cation/ergothioneine transporter), member 4
-3.467	206143_at	SLC26A3	solute carrier family 26, member 3
-3.467	207519_at	SLC6A4	solute carrier family 6 (neurotransmitter transporter, serotonin), member 4
-3.467	215043_s_at	SMA5	glucuronidase, beta pseudogene
-3.467	219695_at	SMPD3	sphingomyelin phosphodiesterase 3, neutral membrane (neutral sphingomyelinase II)
-3.467	204288_s_at	SORBS2	sorbin and SH3 domain containing 2
-3.467	202813_at	TARBP1	TAR (HIV-1) RNA binding protein 1
-3.467	209403_at	TBC1D3	TBC1 domain family, member 3
-3.467	201448_at	TIA1	TIA1 cytotoxic granule-associated RNA binding protein
-3.467	204649_at	TROAP	trophinin associated protein (tastin)
-3.467	211682_x_at	UGT2B28	UDP glucuronosyltransferase 2 family, polypeptide B28
-3.467	218757_s_at	UPF3B	UPF3 regulator of nonsense transcripts homolog B (yeast)
-3.467	222072_at	XPNPEP1	X-prolyl aminopeptidase (aminopeptidase P) 1, soluble
-3.467	221869_at	ZNF512B	zinc finger protein 512B
-3.467	207933_at	ZP2	zona pellucida glycoprotein 2 (sperm receptor)
-3.715	220951_s_at	A1CF	APOBEC1 complementation factor
-3.715	214829_at	AASS	aminoadipate-semialdehyde synthase
-3.715	43427_at	ACACB	acetyl-Coenzyme A carboxylase beta
-3.715	49452_at	ACACB	acetyl-Coenzyme A carboxylase beta

Fold change	Affymetrix ID	Gene symbol	Entrez gene name
-3.715	205364_at	ACOX2	acyl-Coenzyme A oxidase 2, branched chain
-3.715	205942_s_at	ACSM3	acyl-CoA synthetase medium-chain family member 3
-3.715	204694_at	AFP	alpha-fetoprotein
-3.715	204290_s_at	ALDH6A1	aldehyde dehydrogenase 6 family, member A1
-3.715	202888_s_at	ANPEP	alanyl (membrane) aminopeptidase
-3.715	213454_at	APITD1	apoptosis-inducing, TAF9-like domain 1
-3.715	39249_at	AQP3	aquaporin 3 (Gill blood group)
-3.715	210653_s_at	BCKDHB	branched chain keto acid dehydrogenase E1, beta polypeptide
-3.715	220421_at	BTNL8	butyrophilin-like 8
-3.715	219655_at	C7ORF10	chromosome 7 open reading frame 10
-3.715	209032_s_at	CADM1	cell adhesion molecule 1
-3.715	215145_s_at	CNTNAP2	contactin associated protein-like 2
-3.715	213110_s_at	COL4A5	collagen, type IV, alpha 5
-3.715	203139_at	DAPK1	death-associated protein kinase 1
-3.715	205777_at	DUSP9	dual specificity phosphatase 9
-3.715	217838_s_at	EVL	Enah/Vasp-like
-3.715	220326_s_at	FLJ10357	hypothetical protein FLJ10357
-3.715	222274_at	FLJ31568	zinc finger, DHHC-type containing 8 pseudogene
-3.715	213212_x_at	FLJ40113	Golgi autoantigen, golgin subfamily a-like pseudogene
-3.715	218031_s_at	FOXN3	forkhead box N3
-3.715	220506_at	GUCY1B2	guanylate cyclase 1, soluble, beta 2
-3.715	215695_s_at	GYG2	glycogenin 2
-3.715	204569_at	ICK	intestinal cell (MAK-like) kinase
-3.715	201566_x_at	ID2	inhibitor of DNA binding 2, dominant negative helix-loop-helix protein
-3.715	219306_at	KIF15	kinesin family member 15
-3.715	202183_s_at	KIF22	kinesin family member 22
-3.715	213880_at	LGR5	leucine-rich repeat-containing G protein-coupled receptor 5
-3.715	213502_x_at	LOC91316	glucuronidase, beta/ immunoglobulin lambda-like polypeptide 1 pseudogene
-3.715	221834_at	LONP2	lon peptidase 2, peroxisomal
-3.715	203570_at	LOXL1	lysyl oxidase-like 1

Fold change	Affymetrix ID	Gene symbol	Entrez gene name
-3.715	210528_at	MR1	major histocompatibility complex, class I-related
-3.715	203801_at	MRPS14	mitochondrial ribosomal protein S14
-3.715	209120_at	NR2F2	nuclear receptor subfamily 2, group F, member 2
-3.715	220183_s_at	NUDT6	nudix (nucleoside diphosphate linked moiety X)-type motif 6
-3.715	209826_at	PPT2	palmitoyl-protein thioesterase 2
-3.715	220510_at	RHBG	Rh family, B glycoprotein
-3.715	221909_at	RNFT2	ring finger protein, transmembrane 2
-3.715	219482_at	SETD4	SET domain containing 4
-3.715	220736_at	SLC19A3	solute carrier family 19, member 3
-3.715	210677_at	SOAT2	sterol O-acyltransferase 2
-3.715	212386_at	TCF4	transcription factor 4
-3.715	65630_at	TMEM80	transmembrane protein 80
-3.715	221173_at	USH1C	Usher syndrome 1C (autosomal recessive, severe)
-3.715	206366_x_at	XCL1	chemokine (C motif) ligand 1
-3.981	209460_at	ABAT	4-aminobutyrate aminotransferase
-3.981	222362_at	AGFG2	ArfGAP with FG repeats 2
-3.981	222126_at	AGFG2	ArfGAP with FG repeats 2
-3.981	212173_at	AK2	adenylate kinase 2
-3.981	203074_at	ANXA8L2	annexin A8-like 2
-3.981	205108_s_at	APOB	apolipoprotein B (including Ag(x) antigen)
-3.981	209006_s_at	C1ORF63	chromosome 1 open reading frame 63
-3.981	201615_x_at	CALD1	caldesmon 1
-3.981	206878_at	DAO	D-amino-acid oxidase
-3.981	219469_at	DYNC2H1	dynein, cytoplasmic 2, heavy chain 1
-3.981	210220_at	FZD2	frizzled homolog 2 (Drosophila)
-3.981	204973_at	GJB1	gap junction protein, beta 1, 32kDa
-3.981	220085_at	HELLS	helicase, lymphoid-specific
-3.981	217317_s_at	LOC283755	hect domain and RLD 2 pseudogene 3
-3.981	221833_at	LONP2	lon peptidase 2, peroxisomal
-3.981	209348_s_at	MAF	v-maf musculoaponeurotic fibrosarcoma oncogene homolog (avian)

Fold change	Affymetrix ID	Gene symbol	Entrez gene name
-3.981	218440_at	MCCC1	methylcrotonoyl-Coenzyme A carboxylase 1 (alpha)
-3.981	218641_at	MGC3032	hypothetical protein MGC3032
-3.981	210694_s_at	MID1	midline 1 (Opitz/BBB syndrome)
-3.981	215731_s_at	MPHOSPH9	M-phase phosphoprotein 9
-3.981	206964_at	NAT8B	N-acetyltransferase 8B (GCN5-related, putative, gene/pseudogene)
-3.981	213033_s_at	NFIB	nuclear factor I/B
-3.981	214632_at	NRP2	neuropilin 2
-3.981	206623_at	PDE6A	phosphodiesterase 6A, cGMP-specific, rod, alpha
-3.981	205111_s_at	PLCE1	phospholipase C, epsilon 1
-3.981	211341_at	POU4F1	POU class 4 homeobox 1
-3.981	208995_s_at	PPIG	peptidylprolyl isomerase G (cyclophilin G)
-3.981	212805_at	PRUNE2	prune homolog 2 (Drosophila)
-3.981	50965_at	RAB26	RAB26, member RAS oncogene family
-3.981	219864_s_at	RCAN3	RCAN family member 3
-3.981	209441_at	RHOBTB2	Rho-related BTB domain containing 2
-3.981	202976_s_at	RHOBTB3	Rho-related BTB domain containing 3
-3.981	202975_s_at	RHOBTB3	Rho-related BTB domain containing 3
-3.981	221768_at	SFPQ	splicing factor proline/glutamine-rich (polypyrimidine tract binding protein associated)
-3.981	212176_at	SFRS18	splicing factor, arginine/serine-rich 18
-3.981	205097_at	SLC26A2	solute carrier family 26 (sulfate transporter), member 2
-3.981	206535_at	SLC2A2	solute carrier family 2 (facilitated glucose transporter), member 2
-3.981	213364_s_at	SNX1	sorting nexin 1
-3.981	201449_at	TIA1	TIA1 cytotoxic granule-associated RNA binding protein
-3.981	202688_at	TNFSF10	tumor necrosis factor (ligand) superfamily, member 10
-3.981	214329_x_at	TNFSF10	tumor necrosis factor (ligand) superfamily, member 10
-3.981	204391_x_at	TRIM24	tripartite motif-containing 24
-3.981	213301_x_at	TRIM24	tripartite motif-containing 24
-3.981	219632_s_at	TRPV1	transient receptor potential cation channel, subfamily V, member 1
-3.981	212928_at	TSPYL4	TSPY-like 4
-3.981	219740_at	VASH2	vasohibin 2

Fold change	Affymetrix ID	Gene symbol	Entrez gene name
-3.981	211064_at	ZNF493	zinc finger protein 493
-3.981	213659_at	ZNF75D	zinc finger protein 75D
-4.266	213095_x_at	AIF1	allograft inflammatory factor 1
-4.266	218487_at	ALAD	aminolevulinate, delta-, dehydratase
-4.266	203608_at	ALDH5A1	aldehyde dehydrogenase 5 family, member A1
-4.266	219918_s_at	ASPM	asp (abnormal spindle) homolog, microcephaly associated (Drosophila)
-4.266	213143_at	C2ORF72	chromosome 2 open reading frame 72
-4.266	207828_s_at	CENPF	centromere protein F, 350/400ka (mitosin)
-4.266	203642_s_at	COBLL1	COBL-like 1
-4.266	210069_at	CPT1B	carnitine palmitoyltransferase 1B (muscle)
-4.266	206424_at	CYP26A1	cytochrome P450, family 26, subfamily A, polypeptide 1
-4.266	201278_at	DAB2	disabled homolog 2, mitogen-responsive phosphoprotein (Drosophila)
-4.266	214347_s_at	DDC	dopa decarboxylase (aromatic L-amino acid decarboxylase)
-4.266	213645_at	ENOSF1	enolase superfamily member 1
-4.266	220150_s_at	FAM184A	family with sequence similarity 184, member A
-4.266	216238_s_at	FGB	fibrinogen beta chain
-4.266	203632_s_at	GPRC5B	G protein-coupled receptor, family C, group 5, member B
-4.266	204607_at	HMGCS2	3-hydroxy-3-methylglutaryl-Coenzyme A synthase 2 (mitochondrial)
-4.266	219174_at	IFT74	intraflagellar transport 74 homolog (Chlamydomonas)
-4.266	204987_at	ITIH2	inter-alpha (globulin) inhibitor H2
-4.266	205303_at	KCNJ8	potassium inwardly-rectifying channel, subfamily J, member 8
-4.266	203637_s_at	MID1	midline 1 (Opitz/BBB syndrome)
-4.266	214770_at	MSR1	macrophage scavenger receptor 1
-4.266	218966_at	MYO5C	myosin VC
-4.266	209121_x_at	NR2F2	nuclear receptor subfamily 2, group F, member 2
-4.266	215073_s_at	NR2F2	nuclear receptor subfamily 2, group F, member 2
-4.266	213947_s_at	NUP210	nucleoporin 210kDa
-4.266	216945_x_at	PASK	PAS domain containing serine/threonine kinase
-4.266	220954_s_at	PILRB	paired immunoglobin-like type 2 receptor beta
-4.266	205112_at	PLCE1	phospholipase C, epsilon 1

Fold change	Affymetrix ID	Gene symbol	Entrez gene name
-4.266	215807_s_at	PLXNB1	plexin B1
-4.266	218931_at	RAB17	RAB17, member RAS oncogene family
-4.266	219151_s_at	RABL2A	RAB, member of RAS oncogene family-like 2A
-4.266	49306_at	RASSF4	Ras association (RalGDS/AF-6) domain family member 4
-4.266	205933_at	SETBP1	SET binding protein 1
-4.266	212177_at	SFRS18	splicing factor, arginine/serine-rich 18
-4.266	213307_at	SHANK2	SH3 and multiple ankyrin repeat domains 2
-4.266	220413_at	SLC39A2	solute carrier family 39 (zinc transporter), member 2
-4.266	205342_s_at	SULT1C2	sulfotransferase family, cytosolic, 1C, member 2
-4.266	207392_x_at	UGT2B15	UDP glucuronosyltransferase 2 family, polypeptide B15
-4.266	219077_s_at	WWOX	WW domain containing oxidoreductase
-4.266	214823_at	ZNF204	zinc finger protein 204 pseudogene
-4.571	203504_s_at	ABCA1	ATP-binding cassette, sub-family A (ABC1), member 1
-4.571	203756_at	ARHGEF17	Rho guanine nucleotide exchange factor (GEF) 17
-4.571	209693_at	ASTN2	astrotactin 2
-4.571	212672_at	ATM	ataxia telangiectasia mutated
-4.571	222336_at	C4ORF34	chromosome 4 open reading frame 34
-4.571	215785_s_at	CYFIP2	cytoplasmic FMR1 interacting protein 2
-4.571	201280_s_at	DAB2	disabled homolog 2, mitogen-responsive phosphoprotein (Drosophila)
-4.571	220233_at	FBXO17	F-box protein 17
-4.571	214701_s_at	FN1	fibronectin 1
-4.571	213524_s_at	G0S2	G0/G1switch 2
-4.571	219954_s_at	GBA3	glucosidase, beta, acid 3 (cytosolic)
-4.571	219876_s_at	GOLGA2L1	Golgi autoantigen, golgin subfamily a, 2-like 1
-4.571	208798_x_at	GOLGA8A	Golgi autoantigen, golgin subfamily a, 8A
-4.571	220744_s_at	IFT122	intraflagellar transport 122 homolog (Chlamydomonas)
-4.571	204202_at	IQCE	IQ motif containing E
-4.571	206006_s_at	KIAA1009	KIAA1009
-4.571	220393_at	LGSN	lengsin, lens protein with glutamine synthetase domain
-4.571	32062_at	LRRC14	leucine rich repeat containing 14

Fold change	Affymetrix ID	Gene symbol	Entrez gene name
-4.571	210128_s_at	LTB4R	leukotriene B4 receptor
-4.571	212022_s_at	MKI67	antigen identified by monoclonal antibody Ki-67
-4.571	221606_s_at	NSBP1	nucleosomal binding protein 1
-4.571	213046_at	PABPN1	poly(A) binding protein, nuclear 1
-4.571	205380_at	PDZK1	PDZ domain containing 1
-4.571	205697_at	SCGN	secretagogin, EF-hand calcium binding protein
-4.571	212319_at	SGSM2	small G protein signaling modulator 2
-4.571	214719_at	SLC46A3	solute carrier family 46, member 3
-4.571	202761_s_at	SYNE2	spectrin repeat containing, nuclear envelope 2
-4.571	220639_at	TM4SF20	transmembrane 4 L six family member 20
-4.571	218807_at	VAV3	vav 3 guanine nucleotide exchange factor
-4.571	217367_s_at	ZHX3	zinc fingers and homeoboxes 3
-4.898	210962_s_at	AKAP9	A kinase (PRKA) anchor protein (yotiao) 9
-4.898	211298_s_at	ALB	albumin
-4.898	39248_at	AQP3	aquaporin 3 (Gill blood group)
-4.898	219870_at	ATF7IP2	activating transcription factor 7 interacting protein 2
-4.898	210168_at	C6	complement component 6
-4.898	206866_at	CDH4	cadherin 4, type 1, R-cadherin (retinal)
-4.898	205642_at	CEP110	centrosomal protein 110kDa
-4.898	217690_at	ENOSF1	enolase superfamily member 1
-4.898	207981_s_at	ESRRG	estrogen-related receptor gamma
-4.898	208228_s_at	FGFR2	fibroblast growth factor receptor 2
-4.898	213650_at	GOLGA8A	Golgi autoantigen, golgin subfamily a, 8A
-4.898	212906_at	GRAMD1B	GRAM domain containing 1B
-4.898	213359_at	HNRNPD	heterogeneous nuclear ribonucleoprotein D (AU-rich element RNA binding protein 1, 37kDa)
-4.898	205522_at	HOXD4	homeobox D4
-4.898	203153_at	IFIT1	interferon-induced protein with tetratricopeptide repeats 1
-4.898	213832_at	KCND3	potassium voltage-gated channel, Shal-related subfamily, member 3
-4.898	220911_s_at	KIAA1305	KIAA1305
-4.898	209757_s_at	MYCN	v-myc myelocytomatosis viral related oncogene, neuroblastoma derived (avian)

Fold change	Affymetrix ID	Gene symbol	Entrez gene name
-4.898	221207_s_at	NBEA	neurobeachin
-4.898	212151_at	PBX1	pre-B-cell leukaemia homeobox 1
-4.898	213388_at	PDE4DIP	phosphodiesterase 4D interacting protein
-4.898	213431_x_at	SFI1	Sfi1 homolog, spindle assembly associated (yeast)
-5.248	215407_s_at	ASTN2	astrotactin 2
-5.248	220227_at	CDH4	cadherin 4, type 1, R-cadherin (retinal)
-5.248	205046_at	CENPE	centromere protein E, 312kDa
-5.248	205222_at	EHHADH	enoyl-Coenzyme A, hydratase/3-hydroxyacyl Coenzyme A dehydrogenase
-5.248	210425_x_at	GOLGA8A	Golgi autoantigen, golgin subfamily a, 8A
-5.248	204997_at	GPD1	glycerol-3-phosphate dehydrogenase 1 (soluble)
-5.248	219936_s_at	GPR87	G protein-coupled receptor 87
-5.248	213248_at	LOC730101	hypothetical LOC730101
-5.248	206363_at	MAF	v-maf musculoaponeurotic fibrosarcoma oncogene homolog (avian)
-5.248	203636_at	MID1	midline 1 (Opitz/BBB syndrome)
-5.248	212913_at	MSH5	mutS homolog 5 (E. coli)
-5.248	208189_s_at	MYO7A	myosin VIIA
-5.248	209322_s_at	SH2B1	SH2B adaptor protein 1
-5.248	206529_x_at	SLC26A4	solute carrier family 26, member 4
-5.248	215169_at	SLC35E2	solute carrier family 35, member E2
-5.248	206715_at	TFEC	transcription factor EC
-5.248	202687_s_at	TNFSF10	tumor necrosis factor (ligand) superfamily, member 10
-5.623	205043_at	CFTR	cystic fibrosis transmembrane conductance regulator (ATP-binding cassette sub-family C,member 7)
-5.623	221729_at	COL5A2	collagen, type V, alpha 2
-5.623	221730_at	COL5A2	collagen, type V, alpha 2
-5.623	207174_at	GPC5	glypican 5
-5.623	203474_at	IQGAP2	IQ motif containing GTPase activating protein 2
-5.623	217512_at	KNG1	kininogen 1
-5.623	213653_at	METTL3	methyltransferase like 3
-5.623	214241_at	NDUFB8	NADH dehydrogenase (ubiquinone) 1 beta subcomplex, 8, 19kDa
-5.623	213032_at	NFIB	nuclear factor I/B

Fold change	Affymetrix ID	Gene symbol	Entrez gene name
-5.623	205259_at	NR3C2	nuclear receptor subfamily 3, group C, member 2
-5.623	206498_at	OCA2	oculocutaneous albinism II
-5.623	205041_s_at	ORM1	orosomucoid 1
-5.623	205719_s_at	PAH	phenylalanine hydroxylase
-5.623	212148_at	PBX1	pre-B-cell leukaemia homeobox 1
-5.623	210451_at	PKLR	pyruvate kinase, liver and RBC
-5.623	205414_s_at	RICH2	Rho-type GTPase-activating protein RICH2
-5.623	219604_s_at	ZNF3	zinc finger protein 3
-5.623	55872_at	ZNF512B	zinc finger protein 512B
-6.026	206030_at	ASPA	aspartoacylase (Canavan disease)
-6.026	204573_at	CROT	carnitine O-octanoyltransferase
-6.026	221139_s_at	CSAD	cysteine sulfinic acid decarboxylase
-6.026	218858_at	DEPDC6	DEP domain containing 6
-6.026	219612_s_at	FGG	fibrinogen gamma chain
-6.026	207761_s_at	METTL7A	methyltransferase like 7A
-6.026	213040_s_at	NPTXR	neuronal pentraxin receptor
-6.026	222078_at	PKLR	pyruvate kinase, liver and RBC
-6.026	213520_at	RECQL4	RecQ protein-like 4
-6.026	202133_at	WWTR1	WW domain containing transcription regulator 1
-6.457	203505_at	ABCA1	ATP-binding cassette, sub-family A (ABC1), member 1
-6.457	215483_at	AKAP9	A kinase (PRKA) anchor protein (yotiao) 9
-6.457	202920_at	ANK2	ankyrin 2, neuronal
-6.457	201679_at	ARS2	arsenate resistance protein 2
-6.457	214419_s_at	CYP2C9	cytochrome P450, family 2, subfamily C, polypeptide 9
-6.457	203638_s_at	FGFR2	fibroblast growth factor receptor 2
-6.457	220609_at	LOC202181	hypothetical protein LOC202181
-6.457	209519_at	NCBP1	nuclear cap binding protein subunit 1, 80kDa
-6.457	210751_s_at	RGN	regucalcin (senescence marker protein-30)
-6.457	213666_at	SEPT6	septin 6
-6.457	215657_at	SLC26A3	solute carrier family 26, member 3

Fold change	Affymetrix ID	Gene symbol	Entrez gene name
-6.457	205343_at	SULT1C2	sulfotransferase family, cytosolic, 1C, member 2
-6.457	214382_at	UNC93A	unc-93 homolog A (C. elegans)
-6.457	206771_at	UPK3A	uroplakin 3A
-6.918	213411_at	ADAM22	ADAM metallopeptidase domain 22
-6.918	207102_at	AKR1D1	aldo-keto reductase family 1, member D1 (delta 4-3-ketosteroid-5-beta-reductase)
-6.918	213213_at	DIDO1	death inducer-obliterator 1
-6.918	209368_at	EPHX2	epoxide hydrolase 2, cytoplasmic
-6.918	205649_s_at	FGA	fibrinogen alpha chain
-6.918	204515_at	HSD3B1	hydroxy-delta-5-steroid dehydrogenase, 3 beta- and steroid delta-isomerase 1
-6.918	219543_at	PBLD	phenazine biosynthesis-like protein domain containing
-6.918	203895_at	PLCB4	phospholipase C, beta 4
-6.918	204199_at	RALGPS1	Ral GEF with PH domain and SH3 binding motif 1
-6.918	221908_at	RNFT2	ring finger protein, transmembrane 2
-6.918	211470_s_at	SULT1C2	sulfotransferase family, cytosolic, 1C, member 2
-7.413	216661_x_at	CYP2C9	cytochrome P450, family 2, subfamily C, polypeptide 9
-7.413	205650_s_at	FGA	fibrinogen alpha chain
-7.413	220349_s_at	FLJ21865	endo-beta-N-acetylglucosaminidase
-7.413	208476_s_at	FRMD4A	FERM domain containing 4A
-7.413	206005_s_at	KIAA1009	KIAA1009
-7.413	208434_at	MDS1	myelodysplasia syndrome 1
-7.413	209926_at	MEF2B	myocyte enhancer factor 2B
-7.413	210289_at	NAT8	N-acetyltransferase 8 (GCN5-related, putative)
-7.413	217583_at	PAH	phenylalanine hydroxylase
-7.413	212915_at	PDZRN3	PDZ domain containing ring finger 3
-7.413	209568_s_at	RGL1	ral guanine nucleotide dissociation stimulator-like 1
-7.413	215146_s_at	TTC28	tetratricopeptide repeat domain 28
-7.413	215729_s_at	VGLL1	vestigial like 1 (Drosophila)
-7.413	220917_s_at	WDR19	WD repeat domain 19
-7.943	215559_at	ABCC6	ATP-binding cassette, sub-family C (CFTR/MRP), member 6
-7.943	206149_at	CHP2	calcineurin B homologous protein 2

Fold change	Affymetrix ID	Gene symbol	Entrez gene name
-7.943	220999_s_at	CYFIP2	cytoplasmic FMR1 interacting protein 2
-7.943	215014_at	KCND3	potassium voltage-gated channel, Shal-related subfamily, member 3
-7.943	214180_at	MAN1C1	mannosidase, alpha, class 1C, member 1
-7.943	220303_at	PDZD3	PDZ domain containing 3
-7.943	209561_at	THBS3	thrombospondin 3
-7.943	207426_s_at	TNFSF4	tumor necrosis factor (ligand) superfamily, member 4
-8.511	220148_at	ALDH8A1	aldehyde dehydrogenase 8 family, member A1
-8.511	206500_s_at	C14ORF106	chromosome 14 open reading frame 106
-8.511	217558_at	CYP2C9	cytochrome P450, family 2, subfamily C, polypeptide 9
-8.511	214421_x_at	CYP2C9	cytochrome P450, family 2, subfamily C, polypeptide 9
-8.511	220017_x_at	CYP2C9	cytochrome P450, family 2, subfamily C, polypeptide 9
-8.511	216687_x_at	UGT2B15	UDP glucuronosyltransferase 2 family, polypeptide B15
-9.120	220390_at	AGBL2	ATP/GTP binding protein-like 2
-9.120	220084_at	C14ORF105	chromosome 14 open reading frame 105
-9.120	216025_x_at	CYP2C9	cytochrome P450, family 2, subfamily C, polypeptide 9
-9.120	214163_at	HSPB11	heat shock protein family B (small), member 11
-9.772	214420_s_at	CYP2C9	cytochrome P450, family 2, subfamily C, polypeptide 9
-9.772	206643_at	HAL	histidine ammonia-lyase
-9.772	213703_at	LOC150759	hypothetical protein LOC150759
-9.772	205710_at	LRP2	low density lipoprotein-related protein 2
-9.772	214881_s_at	UBTF	upstream binding transcription factor, RNA polymerase I
-10.471	219850_s_at	EHF	ets homologous factor
-10.471	203896_s_at	PLCB4	phospholipase C, beta 4
-10.471	219511_s_at	SNCAIP	synuclein, alpha interacting protein
-10.471	206292_s_at	SULT2A1	sulfotransferase family, cytosolic, 2A, dehydroepiandrosterone (DHEA)-preferring, member 1
-11.220	220622_at	LRRC31	leucine rich repeat containing 31
-11.220	201998_at	ST6GAL1	ST6 beta-galactosamide alpha-2,6-sialyltranferase 1
-11.220	219934_s_at	SULT1E1	sulfotransferase family 1E, estrogen-preferring, member 1
-12.023	210108_at	CACNA1D	calcium channel, voltage-dependent, L type, alpha 1D subunit
-12.023	204307_at	KIAA0329	KIAA0329

Fold change	Affymetrix ID	Gene symbol	Entrez gene name
-12.023	207051_at	SLC17A4	solute carrier family 17 (sodium phosphate), member 4
-12.882	212392_s_at	PDE4DIP	phosphodiesterase 4D interacting protein
-12.882	216228_s_at	WDHD1	WD repeat and HMG-box DNA binding protein 1
-13.804	217904_s_at	BACE1	beta-site APP-cleaving enzyme 1
-13.804	210424_s_at	GOLGA8A	Golgi autoantigen, golgin subfamily a, 8A
-13.804	220385_at	JPH2	junctophilin 2
-13.804	205054_at	NEB	nebulin
-13.804	206293_at	SULT2A1	sulfotransferase family, cytosolic, 2A, dehydroepiandrosterone (DHEA)-preferring, member 1
-14.791	220456_at	SPTLC3	serine palmitoyltransferase, long chain base subunit 3
-15.849	1431_at	CYP2E1	cytochrome P450, family 2, subfamily E, polypeptide 1
-15.849	206963_s_at	NAT8B	N-acetyltransferase 8B (GCN5-related, putative, gene/pseudogene)
-16.982	220679_s_at	CDH7	cadherin 7, type 2
-16.982	204713_s_at	F5	coagulation factor V (proaccelerin, labile factor)
-16.982	40665_at	FMO3	flavin containing monooxygenase 3
-16.982	213241_at	PLXNC1	plexin C1
-18.197	208480_s_at	ABCC6	ATP-binding cassette, sub-family C (CFTR/MRP), member 6
-18.197	211526_s_at	TNFRSF6B	tumor necrosis factor receptor superfamily, member 6b, decoy
-19.498	207487_at	FLJ11996	hypothetical protein FLJ11996
-20.893	218918_at	MAN1C1	mannosidase, alpha, class 1C, member 1
-22.387	208498_s_at	AMY1B	amylase, alpha 1B (salivary)
-23.988	212935_at	MCF2L	MCF.2 cell line derived transforming sequence-like
-25.704	206265_s_at	GPLD1	glycosylphosphatidylinositol specific phospholipase D1
-29.512	220095_at	CNTLN	centlein, centrosomal protein
-29.512	212385_at	TCF4	transcription factor 4
-38.905	204860_s_at	NAIP	NLR family, apoptosis inhibitory protein

9.5 Gene ontology analysis

9.5.1 Down-regulated genes

In the following tables are GO terms, enriched in down-regulated gene list in Caco-2 cells following berry extract treatment. The terms listed are all significantly enriched $p \leq 0.05$ in our gene-list. The tables are organised by GO term categories (i.e. *Molecular function – biological process – cellular component*).

GO term: Molecular function	*p*-value
ion binding	$7.6*10^{-124}$
metal ion binding	$5.7*10^{-121}$
cation binding	$2*10^{-103}$
transition metal ion binding	$5.5*10^{-69}$
zinc ion binding	$2.3*10^{-47}$
calcium ion binding	$1.1*10^{-17}$
transferase activity, transferring one-carbon groups	$7.5*10^{-10}$
microtubule motor activity	$2.6*10^{-9}$
methyltransferase activity	$3.3*10^{-9}$
magnesium ion binding	$3.5*10^{-9}$
iron ion binding	$5*10^{-9}$
motor activity	$1.9*10^{-6}$
S-adenosylmethionine-dependent methyltransferase activity	$4.8*10^{-6}$
hydrolase activity, hydrolyzing O-glycosyl compounds	$5.3*10^{-6}$
lipid transporter activity	$9.2*10^{-6}$
steroid hormone receptor activity	$1.2*10^{-5}$
ligand-dependent nuclear receptor activity	$3.9*10^{-5}$
hydrolase activity, acting on glycosyl bonds	$4.5*10^{-5}$
manganese ion binding	$1.5*10^{-4}$
ligase activity	$3*10^{-4}$
molybdenum ion binding	$4.5*10^{-4}$
cofactor binding	$6.1*10^{-4}$
histone methyltransferase activity	$6.8*10^{-4}$
tetrapyrrole binding	$9.1*10^{-4}$
heme binding	$9.1*10^{-4}$
mannosidase activity	$9.6*10^{-4}$
amylase activity	$1.7*10^{-3}$
alpha-amylase activity	$1.7*10^{-3}$
protein methyltransferase activity	$2*10^{-3}$
DNA (cytosine-5-)-methyltransferase activity	$3.4*10^{-3}$
metalloexopeptidase activity	$3.4*10^{-3}$
biotin binding	$5.5*10^{-3}$
DNA-methyltransferase activity	$5.5*10^{-3}$
carbohydrate kinase activity	$6.2*10^{-3}$
ARF GTPase activator activity	$6.2*10^{-3}$
metallocarboxypeptidase activity	$7*10^{-3}$
vitamin binding	$8.1*10^{-3}$

GO term: Molecular Function	*p*-value
RNA methyltransferase activity	$8.6*10^{-3}$
calcium-dependent phospholipid binding	$8.6*10^{-3}$
histone deacetylase activity	$1*10^{-2}$
protein deacetylase activity	$1*10^{-2}$
ligase activity, forming carbon-carbon bonds	$1.1*10^{-2}$
NAD-dependent histone deacetylase activity	$1.1*10^{-2}$
exopeptidase activity	$1.2*10^{-2}$
NAD binding	$1.3*10^{-2}$
deacetylase activity	$1.5*10^{-2}$
oxygen binding	$1.7*10^{-2}$
coenzyme binding	$1.8*10^{-2}$
chromatin binding	$1.9*10^{-2}$
ligase activity, forming carbon-nitrogen bonds	$1.9*10^{-2}$
transition metal ion transmembrane transporter activity	$2.1*10^{-2}$
carboxypeptidase activity	$2.1*10^{-2}$
phosphoinositide phospholipase C activity	$2.4*10^{-2}$
monooxygenase activity	$2.7*10^{-2}$
ubiquitin-protein ligase activity	$3.3*10^{-2}$
lipase activity	$3.6*10^{-2}$
small protein conjugating enzyme activity	$3.6*10^{-2}$
mannosyl-oligosaccharide mannosidase activity	$3.8*10^{-2}$
phospholipase C activity	$3.8*10^{-2}$
oxidoreductase activity, acting on paired donors, with incorporation or reduction of molecular oxygen	$3.9*10^{-2}$
DNA-directed DNA polymerase activity	$4.1*10^{-2}$
small conjugating protein ligase activity	$4.2*10^{-2}$
cobalt ion binding	$4.3*10^{-2}$
3'-5' exonuclease activity	$4.4*10^{-2}$
acetyl-CoA carboxylase activity	$4.8*10^{-2}$
(S)-limonene 7-monooxygenase activity	$4.8*10^{-2}$
(S)-limonene 6-monooxygenase activity	$4.8*10^{-2}$
4-hydroxyacetophenone monooxygenase activity	$4.8*10^{-2}$
galactokinase activity	$4.8*10^{-2}$
calmodulin binding	$4.8*10^{-2}$
phospholipase activity	$5*10^{-2}$

GO Term: Biological Process	*p*-value
carbohydrate metabolic process	$2.6*10^{-14}$
cellular carbohydrate metabolic process	$2.5*10^{-11}$
cytoskeleton-dependent intracellular transport	$3.7*10^{-10}$
microtubule-based movement	$1.2*10^{-8}$
metal ion homeostasis	$1*10^{-7}$
cellular metal ion homeostasis	$1*10^{-7}$
cellular cation homeostasis	$4.2*10^{-7}$
cation homeostasis	$4.6*10^{-7}$
monosaccharide metabolic process	$8.2*10^{-7}$
calcium ion homeostasis	$1.4*10^{-6}$
cellular calcium ion homeostasis	$1.4*10^{-6}$
cellular di-, tri-valent inorganic cation homeostasis	$1.7*10^{-6}$
microtubule-based process	$1.8*10^{-6}$
di-, tri-valent inorganic cation homeostasis	$1.9*10^{-6}$
alcohol metabolic process	$3.9*10^{-6}$
cellular chemical homeostasis	$4.8*10^{-6}$
cellular ion homeostasis	$4.8*10^{-6}$

GO Term: Biological Process	*p*-value
hexose metabolic process	$1.2*10^{-5}$
ion homeostasis	$1.8*10^{-5}$
carboxylic acid metabolic process	$2.5*10^{-5}$
organic acid metabolic process	$2.8*10^{-5}$
chemical homeostasis	$4.3*10^{-5}$
regulation of biological quality	$4.5*10^{-5}$
mitotic cell cycle	$1*10^{-4}$
catabolic process	$1.4*10^{-4}$
cell cycle phase	$1.7*10^{-4}$
cytoskeleton organisation and biogenesis	$2.1*10^{-4}$
homeostatic process	$2.3*10^{-4}$
regulation of gene expression, epigenetic	$2.4*10^{-4}$
mitosis	$4.4*10^{-4}$
cation transport	$4.4*10^{-4}$
one-carbon compound metabolic process	$4.5*10^{-4}$
M phase of mitotic cell cycle	$4.8*10^{-4}$
metal ion transport	$5.1*10^{-4}$
cellular homeostasis	$6.5*10^{-4}$
regulation of body fluid levels	$8.2*10^{-4}$
monocarboxylic acid metabolic process	$9.2*10^{-4}$
protein amino acid deacetylation	$1.2*10^{-3}$
methylation	$1.3*10^{-3}$
chromosome organisation and biogenesis	$1.5*10^{-3}$
M phase	$1.8*10^{-3}$
amine metabolic process	$1.9*10^{-3}$
biopolymer methylation	$2.1*10^{-3}$
carbohydrate biosynthetic process	$2.2*10^{-3}$
nitrogen compound metabolic process	$2.3*10^{-3}$
blood coagulation	$2.8*10^{-3}$
coagulation	$3.1*10^{-3}$
chromatin modification	$3.7*10^{-3}$
hemostasis	$3.8*10^{-3}$
di-, tri-valent inorganic cation transport	$4.3*10^{-3}$
regulation of ARF GTPase activity	$5.6*10^{-3}$
transition metal ion transport	$6*10^{-3}$
DNA methylation	$7.4*10^{-3}$
DNA alkylation	$7.4*10^{-3}$
glucose metabolic process	$8*10^{-3}$
DNA synthesis during DNA repair	$1.1*10^{-2}$
galactose metabolic process	$1.1*10^{-2}$
anterograde axon cargo transport	$1.1*10^{-2}$
protein ubiquitination	$1.2*10^{-2}$
wound healing	$1.3*10^{-2}$
DNA repair	$1.3*10^{-2}$
DNA modification	$1.4*10^{-2}$
protein modification by small protein conjugation	$1.5*10^{-2}$
glucan metabolic process	$1.6*10^{-2}$
lipid catabolic process	$1.6*10^{-2}$
cellular carbohydrate catabolic process	$1.8*10^{-2}$
response to pH	$1.9*10^{-2}$
gluconeogenesis	$2.2*10^{-2}$
cellular polysaccharide metabolic process	$2.2*10^{-2}$
establishment and/or maintenance of chromatin architecture	$2.2*10^{-2}$

GO Term: Biological Process	*p*-value
regulation of cell adhesion	$2.4*10^{-2}$
polysaccharide metabolic process	$2.4*10^{-2}$
carbohydrate catabolic process	$2.4*10^{-2}$
sequestering of metal ion	$2.8*10^{-2}$
cofactor metabolic process	$2.9*10^{-2}$
tricarboxylic acid cycle intermediate metabolic process	$3*10^{-2}$
pyruvate metabolic process	$3*10^{-2}$
regulation of ARF protein signal transduction	$3.1*10^{-2}$
vitamin metabolic process	$3.2*10^{-2}$
heparan sulfate proteoglycan biosynthetic process	$3.3*10^{-2}$
ARF protein signal transduction	$3.3*10^{-2}$
negative regulation of transcription, DNA-dependent	$3.7*10^{-2}$
chromatin silencing	$3.8*10^{-2}$
dicarboxylic acid metabolic process	$3.8*10^{-2}$
heterochromatin formation	$3.8*10^{-2}$
monosaccharide biosynthetic process	$3.8*10^{-2}$
alcohol biosynthetic process	$3.8*10^{-2}$
iron ion transport	$3.8*10^{-2}$
hexose biosynthetic process	$3.8*10^{-2}$
protein amino acid glycosylation	$3.9*10^{-2}$
biopolymer glycosylation	$4.2*10^{-2}$
axon cargo transport	$4.4*10^{-2}$
glycoprotein metabolic process	$4.6*10^{-2}$
creatine biosynthetic process	$4.8*10^{-2}$
amino acid derivative biosynthetic process	$4.8*10^{-2}$
cyclic nucleotide biosynthetic process	$4.8*10^{-2}$
glycoprotein biosynthetic process	$4.9*10^{-2}$
heparan sulfate proteoglycan metabolic process	$5*10^{-2}$

GO term: Cellular Components	***p*-value**
microtubule associated complex	$2.2*10^{-8}$
microtubule cytoskeleton	$2.4*10^{-5}$
microtubule	$2.8*10^{-5}$
spindle	$4.1*10^{-4}$
kinesin complex	$6.5*10^{-4}$
eSC/e(Z) complex	$1.6*10^{-3}$
PcG protein complex	$2.3*10^{-3}$
endosome	$5.7*10^{-3}$
chromosome	$7.9*10^{-3}$
histone methyltransferase complex	$1.3*10^{-2}$
chromatin silencing complex	$1.3*10^{-2}$
brush border	$1.9*10^{-2}$
integral to Golgi membrane	$1.9*10^{-2}$
microsome	$2*10^{-2}$
midbody	$2.1*10^{-2}$
vesicular fraction	$2.3*10^{-2}$
apical plasma membrane	$3.2*10^{-2}$
microtubule organizing center	$4.4*10^{-2}$
mitochondrial matrix	$4.4*10^{-2}$
mitochondrial lumen	$4.4*10^{-2}$
plus-end kinesin complex	$4.5*10^{-2}$
intrinsic to Golgi membrane	$4.6*10^{-2}$

9.5.2 Up-regulated genes

In the following tables are GO terms, enriched in up-regulated gene list in Caco-2 cells following berry extract treatment. The terms listed are all significantly enriched $p \leq 0.05$ in our gene-list. The tables are organised by GO term categories (Molecular function – biological process – cellular component).

GO term: Molecular Function	*p*- value
transferase activity, transferring glycosyl groups	$4.1*10^{-11}$
UDP-glycosyltransferase activity	$6.8*10^{-11}$
transporter activity	$7.7*10^{-11}$
glucuronosyltransferase activity	$2.6*10^{-10}$
transmembrane transporter activity	$3.6*10^{-10}$
transferase activity, transferring hexosyl groups	$4.9*10^{-10}$
active transmembrane transporter activity	$7.6*10^{-10}$
substrate-specific transporter activity	$1.1*10^{-9}$
GTPase activity	$1.1*10^{-7}$
substrate-specific transmembrane transporter activity	$1.3*10^{-7}$
secondary active transmembrane transporter activity	$2.5*10^{-7}$
symporter activity	$4.7*10^{-7}$
nucleoside-triphosphatase activity	$2.4*10^{-6}$
multidrug transporter activity	$3.3*10^{-6}$
pyrophosphatase activity	$4.6*10^{-6}$
hydrolase activity, acting on acid anhydrides, in phosphorus-containing anhydrides	$5*10^{-6}$
hydrolase activity, acting on acid anhydrides	$6*10^{-6}$
GTP binding	$6.9*10^{-6}$
guanyl ribonucleotide binding	$9*10^{-6}$
guanyl nucleotide binding	$9.2*10^{-6}$
xenobiotic-transporting ATPase activity	$2.6*10^{-4}$
xenobiotic transporter activity	$2.6*10^{-4}$
drug transporter activity	$6.1*10^{-4}$
sugar:hydrogen ion symporter activity	$1.1*10^{-3}$
sugar transmembrane transporter activity	$1.3*10^{-3}$
carbohydrate transmembrane transporter activity	$1.3*10^{-3}$
lipoprotein binding	$2.3*10^{-3}$
ATPase activity, coupled to transmembrane movement of substances	$2.3*10^{-3}$
ATPase activity, coupled to movement of substances	$2.4*10^{-3}$
hydrolase activity, acting on acid anhydrides, catalyzing transmembrane movement of substances	$3*10^{-3}$
P-P-bond-hydrolysis-driven transmembrane transporter activity	$3.5*10^{-3}$
primary active transmembrane transporter activity	$3.5*10^{-3}$
ion transmembrane transporter activity	$3.7*10^{-3}$
low-density lipoprotein receptor activity	$4.6*10^{-3}$
lipoprotein receptor activity	$4.6*10^{-3}$
actin filament binding	$5.1*10^{-3}$
solute:cation symporter activity	$5.5*10^{-3}$
carboxylic acid transmembrane transporter activity	$5.8*10^{-3}$
organic acid transmembrane transporter activity	$6*10^{-3}$

GO term: Molecular Function	*p*- value
anion transmembrane transporter activity	$9.1*10^{-3}$
glucose transmembrane transporter activity	$9.7*10^{-3}$
low-density lipoprotein binding	$9.7*10^{-3}$
hexose transmembrane transporter activity	$1.1*10^{-2}$
monosaccharide transmembrane transporter activity	$1.1*10^{-2}$
voltage-gated ion channel activity	$1.2*10^{-2}$
voltage-gated channel activity	$1.2*10^{-2}$
monocarboxylic acid transmembrane transporter activity	$1.4*10^{-2}$
kinase binding	$1.5*10^{-2}$
enzyme binding	$1.5*10^{-2}$
neurotransmitter:sodium symporter activity	$1.8*10^{-2}$
glutamate-cysteine ligase activity	$1.9*10^{-2}$
voltage-gated potassium channel activity	$1.9*10^{-2}$
protein heterodimerisation activity	$2*10^{-2}$
protein domain specific binding	$2*10^{-2}$
neurotransmitter transporter activity	$2.3*10^{-2}$
passive transmembrane transporter activity	$2.4*10^{-2}$
channel activity	$2.4*10^{-2}$
protein transporter activity	$2.7*10^{-2}$
porin activity	$3.2*10^{-2}$
carbohydrate kinase activity	$3.4*10^{-2}$
protein dimerisation activity	$3.6*10^{-2}$
galactosyltransferase activity	$4.1*10^{-2}$
potassium channel activity	$4.2*10^{-2}$
wide pore channel activity	$4.3*10^{-2}$
secondary active monocarboxylate transmembrane transporter activity	$4.6*10^{-2}$
protein kinase binding	$4.6*10^{-2}$
cation transmembrane transporter activity	$4.8*10^{-2}$

GO term: Biological Process	*p*-value
establishment of localisation	$3.4*10^{-44}$
transport	$1.1*10^{-43}$
localisation	$1.6*10^{-41}$
cellular localisation	$2.3*10^{-16}$
establishment of cellular localisation	$6.1*10^{-16}$
intracellular transport	$4.4*10^{-15}$
establishment of protein localisation	$9.3*10^{-14}$
protein localisation	$9.7*10^{-14}$
vesicle-mediated transport	$1.4*10^{-13}$
protein transport	$4.3*10^{-13}$
macromolecule localisation	$6*10^{-13}$
cellular component organisation and biogenesis	$3.7*10^{-12}$
negative regulation of catalytic activity	$1.2*10^{-10}$
membrane organisation and biogenesis	$4.1*10^{-10}$
negative regulation of kinase activity	$5.2*10^{-10}$
negative regulation of protein kinase activity	$5.2*10^{-10}$
negative regulation of transferase activity	$7.4*10^{-10}$
endocytosis	$3.3*10^{-9}$
membrane invagination	$3.3*10^{-9}$
glucose metabolic process	$5*10^{-9}$
carbohydrate metabolic process	$1.9*10^{-8}$
hexose metabolic process	$2.6*10^{-8}$

GO term: Biological Process	*p*-value
regulation of protein kinase activity	$2.7*10^{-8}$
regulation of a molecular function	$2.7*10^{-8}$
monosaccharide metabolic process	$3.6*10^{-8}$
regulation of kinase activity	$3.8*10^{-8}$
regulation of transferase activity	$5*10^{-8}$
alcohol metabolic process	$6.9*10^{-8}$
response to drug	$2.4*10^{-7}$
regulation of catalytic activity	$2.9*10^{-7}$
negative regulation of MAP kinase activity	$3.4*10^{-7}$
intracellular protein transport	$3.7*10^{-7}$
regulation of transport	$7.1*10^{-7}$
regulation of MAP kinase activity	$1.1*10^{-6}$
cellular carbohydrate metabolic process	$1.2*10^{-6}$
response to xenobiotic stimulus	$4*10^{-6}$
protein targeting	$4.3*10^{-6}$
nuclear import	$5*10^{-6}$
apoptosis	$1.1*10^{-5}$
programmed cell death	$1.3*10^{-5}$
secretion	$1.4*10^{-5}$
negative regulation of transport	$2.1*10^{-5}$
response to chemical stimulus	$2.8*10^{-5}$
death	$3*10^{-5}$
cell death	$3*10^{-5}$
protein import into nucleus	$4.1*10^{-5}$
sterol homeostasis	$4.4*10^{-5}$
lipid homeostasis	$4.4*10^{-5}$
cholesterol homeostasis	$4.4*10^{-5}$
inactivation of MAPK activity	$5.4*10^{-5}$
cell development	$5.7*10^{-5}$
protein kinase cascade	$8.9*10^{-5}$
regulation of protein import into nucleus	$1.2*10^{-4}$
regulation of intracellular protein transport	$1.2*10^{-4}$
lipid transport	$1.4*10^{-4}$
nucleocytoplasmic transport	$1.6*10^{-4}$
nuclear transport	$1.7*10^{-4}$
protein import	$1.8*10^{-4}$
regulation of intracellular transport	$1.9*10^{-4}$
microtubule-based movement	$2*10^{-4}$
intracellular signaling cascade	$2.6*10^{-4}$
regulation of protein transport	$3.2*10^{-4}$
regulation of nucleocytoplasmic transport	$3.7*10^{-4}$
monocarboxylic acid transport	$5*10^{-4}$
cytoskeleton-dependent intracellular transport	$5.3*10^{-4}$
cytoskeleton organisation and biogenesis	$5.5*10^{-4}$
lipid metabolic process	$5.6*10^{-4}$
xenobiotic metabolic process	$5.8*10^{-4}$
microtubule-based process	$6.3*10^{-4}$
ion transport	$6.6*10^{-4}$
digestion	$6.9*10^{-4}$
regulation of apoptosis	$7*10^{-4}$
carbohydrate transport	$7.1*10^{-4}$
protein polymerisation	$7.1*10^{-4}$
regulation of programmed cell death	$7.8*10^{-4}$

GO term: Biological Process	*p*-value
chemical homeostasis	$7.9*10^{-4}$
negative regulation of biological process	$8.2*10^{-4}$
negative regulation of apoptosis	$8.6*10^{-4}$
negative regulation of programmed cell death	$9.4*10^{-4}$
endosome transport	$9.5*10^{-4}$
regulation of blood vessel size	$1*10^{-3}$
regulation of tube size	$1*10^{-3}$
vascular process in circulatory system	$1.1*10^{-3}$
glucose catabolic process	$1.1*10^{-3}$
tube morphogenesis	$1.1*10^{-3}$
secretory pathway	$1.1*10^{-3}$
secretion by cell	$1.1*10^{-3}$
response to hormone stimulus	$1.3*10^{-3}$
monocarboxylic acid metabolic process	$1.3*10^{-3}$
anion transport	$1.4*10^{-3}$
carboxylic acid transport	$1.5*10^{-3}$
organic acid transport	$1.6*10^{-3}$
carbohydrate biosynthetic process	$1.6*10^{-3}$
transcription factor import into nucleus	$1.8*10^{-3}$
regulation of transcription factor import into nucleus	$1.8*10^{-3}$
MAPKKK cascade	$1.9*10^{-3}$
homeostatic process	$1.9*10^{-3}$
hexose catabolic process	$2*10^{-3}$
cell motility	$2*10^{-3}$
localisation of cell	$2*10^{-3}$
monosaccharide catabolic process	$2.1*10^{-3}$
alcohol catabolic process	$2.3*10^{-3}$
negative regulation of cellular process	$2.3*10^{-3}$
gluconeogenesis	$2.4*10^{-3}$
cell migration	$2.7*10^{-3}$
regulation of membrane potential	$2.9*10^{-3}$
regulation of biological quality	$2.9*10^{-3}$
cellular lipid metabolic process	$3*10^{-3}$
pyruvate metabolic process	$3.3*10^{-3}$
peptidoglycan metabolic process	$3.3*10^{-3}$
carboxylic acid metabolic process	$3.5*10^{-3}$
organic acid metabolic process	$3.7*10^{-3}$
membrane depolarisation	$3.9*10^{-3}$
steroid metabolic process	$4.1*10^{-3}$
positive regulation of catalytic activity	$4.3*10^{-3}$
monosaccharide biosynthetic process	$4.4*10^{-3}$
alcohol biosynthetic process	$4.4*10^{-3}$
hexose biosynthetic process	$4.4*10^{-3}$
glycolysis	$4.4*10^{-3}$
protein complex assembly	$4.6*10^{-3}$
glucose transport	$4.8*10^{-3}$
regulation of mitochondrial membrane potential	$4.9*10^{-3}$
cytoplasmic sequestering of transcription factor	$4.9*10^{-3}$
eR to Golgi vesicle-mediated transport	$4.9*10^{-3}$
tube development	$5.1*10^{-3}$
monosaccharide transport	$5.2*10^{-3}$
hexose transport	$5.2*10^{-3}$
cytoplasmic sequestering of protein	$5.9*10^{-3}$

GO term: Biological Process	*p*-value
phagocytosis	$6.7*10^{-3}$
cellular carbohydrate catabolic process	$6.7*10^{-3}$
Golgi vesicle transport	$6.7*10^{-3}$
regulation of nitric oxide biosynthetic process	$7.1*10^{-3}$
response to steroid hormone stimulus	$7.2*10^{-3}$
regulation of cell proliferation	$7.7*10^{-3}$
negative regulation of protein import into nucleus	$8.3*10^{-3}$
negative regulation of transcription factor import into nucleus	$8.3*10^{-3}$
carbohydrate catabolic process	$8.6*10^{-3}$
hormone secretion	$9*10^{-3}$
maintenance of localisation	$9*10^{-3}$
circulatory system process	$9.3*10^{-3}$
blood circulation	$9.3*10^{-3}$
negative regulation of nucleocytoplasmic transport	$9.6*10^{-3}$
anti-apoptosis	$9.9*10^{-3}$
generation of a signal involved in cell-cell signaling	$1*10^{-2}$
negative regulation of protein transport	$1.1*10^{-2}$
protein amino acid glycosylation	$1.3*10^{-2}$
morphogenesis of a branching structure	$1.4*10^{-2}$
biopolymer glycosylation	$1.4*10^{-2}$
positive regulation of protein kinase activity	$1.5*10^{-2}$
positive regulation of cell proliferation	$1.5*10^{-2}$
cholesterol transport	$1.6*10^{-2}$
sterol transport	$1.6*10^{-2}$
glycoprotein biosynthetic process	$1.6*10^{-2}$
positive regulation of kinase activity	$1.7*10^{-2}$
positive regulation of transferase activity	$1.8*10^{-2}$
second-messenger-mediated signaling	$1.8*10^{-2}$
glycosphingolipid metabolic process	$1.9*10^{-2}$
regulation of exocytosis	$1.9*10^{-2}$
protein amino acid autophosphorylation	$1.9*10^{-2}$
positive regulation of apoptosis	$2*10^{-2}$
multicellular organismal protein metabolic process	$2.1*10^{-2}$
multicellular organismal macromolecule catabolic process	$2.1*10^{-2}$
multicellular organismal macromolecule metabolic process	$2.1*10^{-2}$
protein digestion	$2.1*10^{-2}$
multicellular organismal protein catabolic process	$2.1*10^{-2}$
positive regulation of epithelial cell proliferation	$2.1*10^{-2}$
collagen catabolic process	$2.1*10^{-2}$
protein autoprocessing	$2.1*10^{-2}$
positive regulation of programmed cell death	$2.1*10^{-2}$
macromolecule catabolic process	$2.1*10^{-2}$
regulation of hormone secretion	$2.3*10^{-2}$
digestive system process	$2.3*10^{-2}$
multicellular organismal catabolic process	$2.3*10^{-2}$
response to estrogen stimulus	$2.3*10^{-2}$
response to peptide hormone stimulus	$2.3*10^{-2}$
collagen metabolic process	$2.3*10^{-2}$
exocytosis	$2.3*10^{-2}$
lactation	$2.5*10^{-2}$
maintenance of cellular protein localisation	$2.7*10^{-2}$
actin cytoskeleton organisation and biogenesis	$2.7*10^{-2}$
sphingolipid metabolic process	$2.8*10^{-2}$

GO term: Biological Process	*p*-value
cellular chemical homeostasis	$2.8*10^{-2}$
cellular ion homeostasis	$2.8*10^{-2}$
multicellular organismal metabolic process	$2.9*10^{-2}$
maintenance of cellular localisation	$2.9*10^{-2}$
protein oligomerisation	$2.9*10^{-2}$
regulation of secretion	$3*10^{-2}$
maintenance of protein localisation	$3.1*10^{-2}$
nitric oxide metabolic process	$3.1*10^{-2}$
nitric oxide biosynthetic process	$3.1*10^{-2}$
inorganic anion transport	$3.1*10^{-2}$
negative regulation of nitric oxide biosynthetic process	$3.2*10^{-2}$
glycoprotein metabolic process	$3.2*10^{-2}$
monovalent inorganic cation transport	$3.2*10^{-2}$
negative regulation of multicellular organismal process	$3.6*10^{-2}$
actin filament-based process	$3.6*10^{-2}$
regulation of multicellular organismal process	$3.8*10^{-2}$
glycolipid metabolic process	$3.9*10^{-2}$
cytoplasmic sequestering of NF-KappaB	$4.2*10^{-2}$
regulation of mitochondrial depolarisation	$4.2*10^{-2}$
multicellular organism reproduction	$4.2*10^{-2}$
reproductive process in a multicellular organism	$4.2*10^{-2}$
ion homeostasis	$4.2*10^{-2}$
regulation of phosphorylation	$4.5*10^{-2}$
ceramide metabolic process	$4.6*10^{-2}$
cholesterol metabolic process	$4.8*10^{-2}$
leukocyte migration	$4.9*10^{-2}$
metal ion transport	$5*10^{-2}$

GO term: Cellular Component	***p*-value**
cell fraction	$7.9*10^{-19}$
membrane fraction	$5.1*10^{-18}$
cytoplasmic part	$2.4*10^{-14}$
basolateral plasma membrane	$1.9*10^{-8}$
endomembrane system	$1.9*10^{-8}$
microsome	$2.1*10^{-8}$
vesicular fraction	$3*10^{-8}$
organelle membrane	$6.6*10^{-8}$
plasma membrane part	$3.5*10^{-7}$
endoplasmic reticulum	$2.3*10^{-6}$
endosome	$4.3*10^{-6}$
intrinsic to plasma membrane	$6.4*10^{-6}$
Golgi apparatus	$7*10^{-6}$
integral to plasma membrane	$1.4*10^{-5}$
vesicle	$2.1*10^{-5}$
cytoplasmic membrane-bound vesicle	$3.9*10^{-5}$
membrane-bound vesicle	$4.6*10^{-5}$
cytoplasmic vesicle	$6.7*10^{-5}$
Golgi apparatus part	$8.2*10^{-5}$
coated pit	$1.6*10^{-4}$
Golgi membrane	$4.2*10^{-4}$
cytosol	$7.7*10^{-4}$
nuclear envelope	$2.3*10^{-3}$

GO term: Cellular Component	*p*-value
microtubule	$2.3*10^{-3}$
microtubule cytoskeleton	$2.5*10^{-3}$
nuclear pore	$4.7*10^{-3}$
outer membrane	$4.9*10^{-3}$
cytoplasmic vesicle membrane	$5.3*10^{-3}$
cytoplasmic vesicle part	$6.5*10^{-3}$
pore complex	$7.6*10^{-3}$
cell projection	$8.2*10^{-3}$
vesicle membrane	$8.3*10^{-3}$
endosome membrane	$1.1*10^{-2}$
endosomal part	$1.1*10^{-2}$
basal plasma membrane	$1.2*10^{-2}$
voltage-gated potassium channel complex	$1.3*10^{-2}$
basal part of cell	$1.4*10^{-2}$
nuclear membrane part	$1.5*10^{-2}$
late endosome	$1.6*10^{-2}$
glutamate-cysteine ligase complex	$2*10^{-2}$
Golgi stack	$2*10^{-2}$
sarcoplasmic reticulum	$2.2*10^{-2}$
sarcoplasm	$2.2*10^{-2}$
organelle envelope	$2.4*10^{-2}$
envelope	$2.5*10^{-2}$
mitochondrial outer membrane	$3.3*10^{-2}$
late endosome membrane	$3.4*10^{-2}$
perinuclear region of cytoplasm	$3.4*10^{-2}$
soluble fraction	$3.6*10^{-2}$
Golgi trans cisterna	$3.9*10^{-2}$
intercellular canaliculus	$3.9*10^{-2}$
apical plasma membrane	$4.2*10^{-2}$
organelle outer membrane	$4.7*10^{-2}$
nuclear membrane	$4.7*10^{-2}$